2006

# Development and evaluation of test procedures to identify moisture damage prone hot mix asphalt pavements

Andrea Nicole Kvasnak
*Iowa State University*

**Development and evaluation of test procedures to identify moisture damage prone hot mix asphalt pavements**

by

**Andrea Nicole Kvasnak**

A dissertation submitted to the graduate faculty

in partial fulfillment of the requirements for the degree of

DOCTOR OF PHILOSOPHY

Major: Civil Engineering (Civil Engineering Materials)

Program of Study Committee:
R. Christopher Williams, Major Professor
Kejin Wang
Amr Kandil
Charles Jahren
Stephen Vardeman

Iowa State University

Ames, Iowa

2006

# Table of Contents

## List of Figures

# List of Tables

# Chapter 1 Introduction

Pavement engineers have two main purposes: to build satisfactory roads, and to maintain the road network -- all within an established budget. Sustaining the road network requires deciding when to repair or rebuild based upon the condition and given budget. In recent years, the task of meeting the road network needs has become more difficult due to limited resources for transportation facilities (Kvasnak, 2002). Constructing roads that are not only cost effective, but also suitable for the area has become more important with the limited available funds.

There are numerous factors that can cause a road to deteriorate, such as the traffic type, traffic volume, failure of materials used and climatic conditions. All four of the above listed factors can contribute to permanent deformation, commonly called pavement rutting. Most permanent deformation tests and simulation models have concentrated primarily on material properties and traffic loads. The effects of the environmental conditions are often neglected in these models with only a few accounting for climatic effects. The damaging effect of moisture on pavements, specifically hot mix asphalt (HMA), is a significant environmental distress that should be considered. As pavement is subjected to freeze/thaw cycling, the material expands and contracts. During expansion, water can seep into permeable air voids created with the increased volume and freeze. When the material contracts during thawing, the water can propagate cracks created during freezing for further damage in the next freeze cycle, which can weaken the structural strength of a pavement layer. Over time, the repetition of freeze/thaw cycling deteriorates a pavement and can lead to lengthwise indentations in roads appearing as ruts if a moisture susceptible mix is below the surface mix. Surface mixes that are susceptible to moisture damage would experience raveling. Identifying pavements susceptible to moisture damage and the effects of moisture damage on the life of a pavement can reduce maintenance costs accrued with the placement of a poorly performing HMA.

## 1.1 Objectives

Two ways to optimize the usage of the available funds are to conduct laboratory tests related to field performance and to employ simulation models to determine the stresses and life expectancy of an HMA pavement. The initial aim of this dissertation is to determine moisture susceptible mixes and asphalt binders. Once moisture susceptible materials have been distinguished; analysis will commence to determine if certain properties and/or materials are more prone to moisture susceptibility. During this process the advantages of a new method for determining the moisture susceptibility of asphalt binders will be outlined along with newly devised equipment and procedures. The second objective is to discuss the benefits of a device known as the Asphalt Pavement Analyzer (APA) for simulating ruts in HMA prone to moisture saturation and freeze/thaw cycling. A third aim is to outline future goals to facilitate implementation and acceptance of a new moisture susceptibility determination process. Part of this third aim will be the outline of a theoretical framework of a stochastic finite element model. The model will not only account for varying material characteristics throughout the specimen, but also the affect of moisture on a mix. The conditioning will entail water saturation and freeze/thaw cycling. A comparison of an evaluation of conditioned and unconditioned specimens will indicate the extent of moisture damage to determine the adequacy of a given HMA for a region and the life expectancy of the HMA.

This research investigates how moisture damage contributes to permanent deformation for a variety of HMA designs using APA and a modified Dynamic Shear Rheometer (DSR) test results. Data collected from an APA and DSR were analyzed to evaluate the moisture susceptibility of certain pavement materials. The outline of a stochastic finite element model is based on the ability to define probability distribution functions of the material characteristics to develop a random materials structure. The probability distribution functions will be based on data collected from laboratory tests.

## 1.2 Hypotheses

It is anticipated that moisture damage will have a significant effect on permanent deformation and that fine-graded HMAs and low traffic volume designed HMAs will be

more susceptible to moisture damage than coarse-graded HMAs and high traffic HMAs. Past studies have shown that moisture can weaken aggregates and lead to binder detachment. The affect of water on HMA and binders is predominantly related to the chemistry of the materials. The weakening of aggregate could result in aggregates breaking under applied loads thus yielding a weakened pavement. The separation of binders from aggregate can lead to material shifting under applied loads. Coarse-graded HMAs predominantly consists of greater percentage of larger sized aggregates than fine-graded ones consisting of a greater percentage of smaller grained aggregates. The fine-graded mixes thus have more aggregate surface area that can be weakened by the presence of water. The lower traffic designed pavements often contain unmodified asphalt binders that meet the minimum criteria. Modifiers often added to high volume designed HMAs tend to help prevent moisture damage.

## 1.3 Summary of Dissertation

The following chapters describe laboratory work, analysis, and theoretical stochastic finite element model of binders and HMA mixes. Chapter 2 summarizes some of the significant and relevant research in the areas of moisture damage and modeling. Chapter 3 describes the process of establishing the validity of a DSR with modified parts and development of a test procedure. Chapter 4 relates the application of the new test procedure developed in Chapter 3 to field asphalt binders. Chapter 5 explains the process of developing a new moisture damage criterion for asphalt binders. Chapter 6 relates the results of tensile strength testing following AASHTO T-283. Chapter 7 describes the testing and analysis of specimens tested in an APA. A new moisture damage criterion for APA tested specimens is also described in Chapter 7. Chapter 8 relates the theoretical stochastic finite element model of moisture saturated specimens tested in an APA. Chapter 9 summarizes the conclusions and recommendations for this dissertation research. Appendix A contains a list of acronyms and meanings. Appendix B contains additional confidence ellipsoid data.

# Chapter 2 Background

## 2.1 Permanent Deformation

Permanent deformation of pavements is a significant concern. A rut is a longitudinal depression in the wheel path created by the undesired movement of material. There are several factors that can lead to the aggregate and binder movement. Two of the most widely accepted factors involved in rutting are trafficking of material that has been over-compacted and excessive plastic flow due to low shear strength.

### 2.1.1 Over-Compaction

Over-compaction occurs during construction and can be a result of changes in mix properties from the design, more compaction energy than necessary to achieve the target density, or the combination of the two. Over-compaction often occurs after construction in HMA layers due to trafficking. The layer is compacted post construction by repeated trafficking, which can compact the material to between 3-5 percent air voids or even below the desired air voids (Roberts et al., 1996).

### 2.1.2 Plastic Flow

Plastic flow can cause rutting. Excessive binder in an HMA causes the binder to act less like the glue that holds the materials together and more like gelatin, which can move more easily. Major problems occur when excessive binder exists in an HMA pavement during the high temperatures typically encountered during the summer months. The heated binder acts more like a liquid, thus allowing for aggregate to shift with repeated wheel loads. An excess amount of rounded aggregate compounds the problem since round aggregates do not have adequate interlock with one another and are more easily able to "slide" past each other.

## 2.2 Moisture Damage

Several factors can contribute to moisture damage. Stripping is a type of moisture damage that is is the physical deterioration of the bonds between the asphalt binder and the aggregate. Factors leading to poor bonding between aggregate and asphalt binder include hydrophilic aggregate, improperly dried aggregate in the HMA, high content of chemicals easily dispersed by water, and environmental changes associated with freeze/thaw cycling. The first two stripping factors listed are easily remedied by referring to previous experience with local materials and careful construction practices. Chemical analysis of binders can eliminate many moisture prone binders, such as ones with a high carboxylic acid content. Another form of moisture damage is the softening of asphalt binder. Softening occurs when moisture permeates asphalt. The environmental conditions that can lead to moisture damage are not always as easily compensated for, such as subgrade composition and local weather conditions.

Researchers have studied the stresses and strains associated with rutting caused by moisture damage (Lai and Hufferd, 1976). In a study of water stripping and water penetration of asphalt samples were examined with an environmental scanning electron microscope (ESEM) (Williams and Miknis, 1998). The research team conducted two tests. In the first test, aggregate was partially coated with asphalt and submerged in water. During the submersion the partially coated aggregate were subjected to 10 freeze/thaw cycles. Pictures of the microstructure of the partially coated aggregate were taken with an ESEM before the initial freeze and after 4, 5, and 10 freeze/thaw cycles. It was discovered that there is a direct correlation between the aggregate flaking and the number of freeze/thaw cycles. Furthermore, researchers have also observed asphalt binder peeling away from aggregate as the number of freeze/thaw cycles increased. In the second test using an ESEM, the samples were used for testing moisture penetration. Penny sized asphalt samples were made and submerged in water for an initial period of 6 weeks and a total period of 27 weeks. The effect of the water on the asphalt was observed with an ESEM after each time interval. Water did penetrate the samples and was more apparent after 27 weeks. From the results of the study, it is evident from the

results that an ESEM can be used in future research regarding moisture effect on pavements (Williams and Miknis, 1998).

### 2.2.1 Asphalt Binder Moisture Susceptibility

One of the main elements of HMA pavements is asphalt binder. There are numerous sites for obtaining asphalt binders and several methods for processing binders which all contribute to the different chemical components in asphalt binders. As mentioned, moisture susceptibility can originate from the bonding between the aggregate and asphalt binder, within a moisture prone asphalt binder, or an aggregate. In all cases, chemistry is a significant contributor. The following subsections outline how chemical components and bonds can affect the moisture susceptibility of an HMA pavement.

#### 2.2.1.1 Asphalt-Aggregate Interactions

HMA is composed of three main ingredients, asphalt, aggregates, and air voids. Various asphalt binders and aggregates are used, all with unique chemical characteristics. These unique chemical characteristics can lead to both disadvantages and advantages for the completed mix. Most HMAs developed are based on experience in lieu of chemical analysis of the asphalt, aggregate, and asphalt-aggregate interactions.

#### 2.2.1.2 Components of Asphalt

Asphalt is a petroleum byproduct. In general, petroleum is classified as a hydrocarbon, but the percentages of hydrogen and carbon varies for different petroleum sources. Other common principle chemicals found in asphalt are nitrogen, sulfur, oxygen, vanadium, and nickel and like the carbon and hydrogen, the amounts vary depending on the petroleum used (Roberts et al., 1996). The main classifications of asphalt binders are based on carbon structures. Asphalt binders categorized as aliphatic or paraffinic contain chains of carbon atoms, whereas naphthenic and aromic consist of carbon rings. Naphthenic consist of the maximum or saturated amount of hydrogen and carbon in a molecule, while aromatic binders are considered to be unsaturated.

When sulfur, oxygen, and nitrogen attach to the hydrocarbon, the molecules become polar. The polarity of the molecules affects the characteristics of the asphalt binder which in turn affects the performance of the HMA.

#### 2.2.1.3 Bonding

Hydrogen bonds exist within asphalt binders. Electrostatic force attraction is what creates the hydrogen bond between a hydrogen atom and at least one other atom. Hydrogen bonds tend to be weaker than ionic and covalent bonds and prefer certain atom orientations. These weak bonds are easily broken and can lead to dispersion of chemical compounds. Aromatic bonds also exist within asphalt binders.

#### 2.2.1.4 Research on Asphalt-Aggregate Interactions

Much of the limited information available on the interaction between asphalt and aggregates is either empirically based or somewhat speculative. One widely accepted theory relating to asphalt-aggregate interaction is that even with high temperatures the process of asphalt adsorption is a time consuming process. The adsorption process can be decelerated or even ceased by the presence of water since it can act as a desorbing agent for asphalt-aggregate interactions. Several factors, such as temperature and length of time the material is submerged in water, affect the influence of water on the interaction. To investigate how water affects the bonds between asphalt and aggregates, a study was conducted in Wyoming which subjected several specimens to freeze/thaw cycling prior to testing and then examined the material with an infrared spectrometer. The results of the study indicate that sulfoxides and ketones are not displaced by the presence of water, unlike carboxylic acids, implying that moisture damage can be minimized by aging the material (Huang et al., 2005).

Another study was conducted to investigate the affect of water on the bond between asphalt and aggregate. In previous studies it has been found that certain chemicals associated with asphalt binders accumulate on the surface of aggregates. These chemicals include, but are not limited to, carboxylic acids, sulfoxides, and ketones. Carboxylic acids tend to be prevalently adsorbed by aggregates and extremely sensitive

to interactions with water. The water tends to remove the carboxylic acid from the aggregate surface, thus initiating moisture damage in most cases. Sulfoxides react in a similar fashion to water as does carboxylic acids, but on a less significant level (Huang et al., 2005).

Siliceous aggregates tend to be moisture prone. It is believed that the hydroxyl groups located on the surface attract carboxylic acids and water. This attraction introduces a chemical that has bonds with the aggregate which can easily be weakened by the presence of water (Huang et al., 2005).

In the study conducted in Wyoming, looking at SHRP binder AAB-1, the chemical adsorbed the most was ketones. The ketones appeared to not be as moisture susceptible as the other chemicals adsorbed. The moisture resistance of the ketones was contributed to the chemical structure of ketones which allows for multiple bonding sites. The study included the modification of binder by adding either hydrated lime or a siliceous granite. The two aggregates were selected because of their chemical and physical differences. The hydrated lime consists of significant levels of calcium, thus moisture resistance, while the granite is mostly made up of silica, a moisture prone material (Huang et al., 2005).

Tensile strength was used to measure the effect of water on the studied materials. The tensile strength was reduced when asphalt components were displaced by the presence of water. As expected, the granite mixtures were observed to have a much more drastic change in the tensile strength ratio than the limestone mixtures after freeze/thaw conditioning. The results indicated that the aged binder tended to resist moisture damage much better than the original binder after the freeze/thaw conditioning. The researchers hypothesized that either the increased viscosity or more moisture resistant compounds are adsorbed instead of moisture sensitive ones and contributed to the improved results of the aged binders. However, it was noted by the researchers that if the increased viscosity was the cause that the improvement should be uniform for both the limestone and granite when in fact it was not (Huang et al., 2005).

When examining the moisture damage endured by the specimens, the researchers hypothesized why the limestone specimens may have performed better than the granite.

One idea was that the carboxylic acid and calcium react to create salts which resist moisture damage. The other theory was in regards to the hydrogen bonds of the hydroxyl groups found on the surface of the granite being at odds with the water and creating countering adsorption and desorption actions. Surface area dissimilarities along with varying chemical adsorption are also factors considered in determining why the two aggregate types respond differently to the presence of water (Huang et al., 2005).

## 2.3 Asphalt Pavement Analyzer (APA)

The Asphalt Pavement Analyzer (APA) is a type of loaded wheel test. Rutting, moisture susceptibility, and fatigue cracking can all be examined with an APA. The predecessor to an APA is the Georgia Loaded Wheel Tester (GLWT). Similar to the GLWT, an APA can test either cylindrical or rectangular specimens. Using either specimen geometry, the conditioned and unconditioned samples are subjected to a steel wheel that transverses a pneumatic tube, which lies on top of an asphalt sample. As the wheel passes back and forth over the tube, a rut is created in the sample. Numerous passes lead to a more defined rut and eventually, stress fractures can begin to manifest as cracks. Modeling these ruts and cracks helps to predict how different combinations of aggregate and binder for given criteria such as temperature and loading, will react under varying circumstances. The conditioning of the sample is based upon the characteristic an APA is intended to evaluate. One of the main differences between an APA and a GLWT is an APA's ability to test samples under water. Testing submerged samples allows researchers to test for moisture susceptibility (Cooley et al., 2000).

APA test results are comparable to field data. A study that compared WesTrack, a full-scale test track, data with APA results found a strong relationship between the field data and the laboratory performance (Williams and Prowell, 1999). An additional study at the University of Tennessee revealed that an APA sufficiently predicted the potential for rutting of 30 HMAs commonly used in Tennessee (Jackson and Baldwin, 1999).

To test moisture susceptible HMA samples, the specimens are created in the same manner as the specimens for testing rutting potential without moisture. The samples are placed in an APA, which has an inner box which can be filled with water. The samples

are completely submerged at all times during testing; therefore effects of evaporation do not need to be taken into account. The water bath is heated to the desired test temperature and the air in the chamber is also heated to the test temperature.

# Chapter 3 Development of an Asphalt Binder Moisture Susceptibility Procedure with a Dynamic Shear Rheometer

Moisture damage of HMA pavements has been researched extensively resulting in both applicable and ambiguous results (Cheng et al., 2003; Lottman, 1978; Lottman, 1982; Tunnicliff and Root, 1984; Tunnicliff and Root, 1995; Epps et al., 2000; McCann and Sebaaly, 2000). Much of the work conducted to analyze the moisture susceptibility of asphalt binders has centered on the chemistry of asphalt and the interaction effects with fillers. Several studies have investigated the chemical composition via chemical analysis methods to determine which chemical compounds are affected by the presence of moisture. The chemical analysis of asphalt binders has been beneficial in understanding the asphalt-aggregate and asphalt-moisture relationships, but a procedure that could be implemented by owner/agencies to determine the moisture susceptibility of asphalt binder has not evolved from these studies.

A test procedure for examining the moisture damage potential of asphalt binders has recently been developed. Initial results indicate that this new procedure is sensitive to interaction effects between asphalt binders and fillers as well as moisture susceptibility of an asphalt binder.

The new moisture susceptibility testing procedure is similar to the traditional DSR test procedures outlined in AASHTO T-315. The main difference between AASHTO T-315 and the new test procedure is in regards to modifications to the base plate and spindle. Instead of the asphalt interacting with a stainless steel interface, a new base plate and spindle were devised that allowed for a ceramic interface with the asphalt binder. The stainless steel interface was deemed an unrealistic material for simulating in-situ conditions. Previous studies also identified the disadvantage of using stainless steel (Scholz and Brown, 1996; Rottermond, 2004). The ceramic material used was the same utilized by Youtcheff in developing a moisture sensitivity test of asphalt binder via a pneumatic pull-off test (Youtcheff and Aurilio, 1997). A modification was deemed necessary to simulate moisture accessibility to asphalt binder. The stainless steel

interface not only was an unrealistic representation of field conditions, but also does not allow for water to interact at the top and bottom of a specimen (asphalt-aggregate interface). Figures 3.1 through 3.3 depict the alterations to the DSR parts incorporated into the new test procedure for determining moisture susceptibility. The modification to the DSR allows for any material to be used as an interface with asphalt as long as it meets the geometric dimensions of the space allowed for the disc. A manufactured ceramic disc was selected as the interface to reduce the variability contributed by an aggregate with possible material variations. An additional modification was incorporated into the spindle to allow for moisture to penetrate the asphalt via the ceramic disc. Three holes 120˚ apart were created in the spindle head. It should be noted that if more than three holes were added specimens would be exposed to greater amounts of water flowing through a ceramic disc. Testing with three holes in a water bath indicated that a ceramic disc is exposed to enough water over an extended amount of time to saturate a disc. If more holes were added, it is hypothesized that the disc would saturate faster.

**Figure 3.1 Modified DSR Base plate**

**Figure 3.2 Modified DSR Spindle**

**Figure 3.3 Modified DSR Spindle with Three Holes**

## 3.1 Dynamic Shear Rheometer

The DSR is used to determine the complex shear modulus and phase angle of asphalt binders. Traditionally, a small disc shaped specimen is placed in between a steel base plate and spindle. The base plate remains stationary while the spindle oscillates back and forth. The frequency at which the spindle oscillates back and forth can be varied depending on the type of test being conducted. Another factor of the test that can vary is whether or not the material is tested in water or in air.

One of the disadvantages of the current procedure is the use of stainless steel as the material surrounding the asphalt specimen under examination. A stainless steel surface is less porous than an aggregate based surface and offers a different friction factor.

One of the goals of the dissertation was to alter the existing test equipment to better represent the conditions in the field. Modifications were made to a base plate and spindle to allow for an aggregate-type interface with the asphalt binder. The purpose of the aggregate-type interface was to allow water to permeate the binder from multiple directions.

### 3.1.1 Modified Base Plate and Spindle

The objectives outlined for the modified spindle were to allow for an aggregate type interface and entrance of water from both above and below a test specimen. The aggregate interface was desired to better simulate the moisture conditions in the field. As mentioned earlier, the stainless steel surface is not an adequate representation of the material in contact with the asphalt binder when in the field. The minimal porosity of the stainless steel parts prevents water contact at the top of an asphalt binder specimen. The allowance of water to saturate a specimen from above and below was preferred for moisture susceptibility testing.

The final modification allowed for a disc of any material type to be placed within the base plate and spindle. Set screws are used to hold the disc in place for both the base plate and the spindle. The set screws are at 120˚ intervals as are the holes through the top of the spindle. Figure 3.3 illustrates the placement of the holes that allow for water flow from the top down. Figure 3.4 illustrates the dimensions and modifications of a modified spindle.

Asphalt binder and filler were heated prior to mixing. Once the materials were heated the filler was added to obtain a pre-specified percentage by weight of the total mastic (binder and filler). The percentages used were 5%, 10%, and 20%. When the filler was completely mixed with the asphalt binder, a 25mm sample was poured into a mold and allowed to rest for 10 minutes. Specimens were tested in either the water bath

or temperature controlled air chamber. After initial testing with the DSR, specimens with ceramics discs were carefully removed from the spindle and base plate and placed in a water bath for 24 hours to allow for moisture saturation. The specimens were then retested in the DSR with the appropriate temperature control apparatus; either the water bath or temperature controlled air chamber. In other words, a specimen originally tested in the water bath for the unconditioned specimen was again tested in the water bath after saturation.

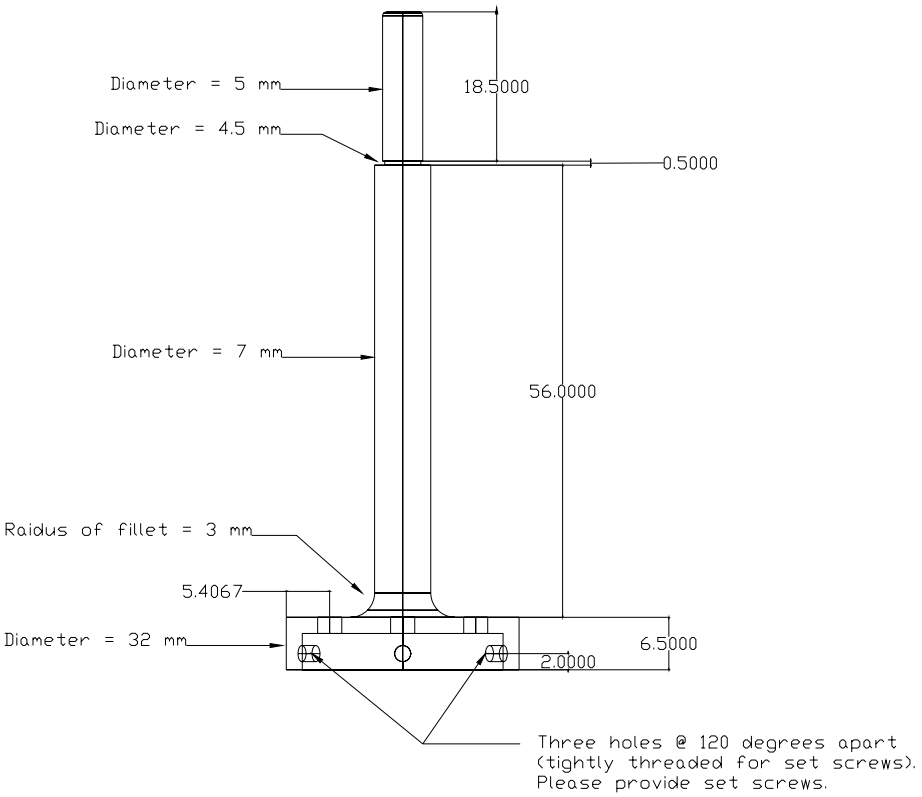


**Figure 3.4 Dimensions of Modified Spindle (Bausano, 2004)**

## 3.2 Experimental Plans

Two experimental plans were executed. The first set of experiments determined which testing conditions should be employed in the final testing procedure. Testing of the hypothesis that an aggregate type material would yield significantly different results than a steel interface was conducted.

Two types of discs were employed to determine if the hypothesis of the material interface would yield a significant difference. The control disc was stainless steel. The selection of the aggregate type of material was a bit more complex than the selection for the control disc. The material desired was an aggregate type, but a neutral material to reduce inconsistencies from a source was coveted. Manufactured ceramic discs were selected as the neutral aggregate type disc for testing.

### 3.2.1 Gap Size and Interface Selection

Since it was only thought that ceramic discs would be a better interface for moisture susceptibility testing of asphalt binders, the hypothesis needed to be tested. Both ceramic and stainless steel interfaces were tested using the AAA-1 and AAM-1 asphalt binders, from the Materials Reference Library (MRL), at different gap sizes. The gap sizes evaluated were 200µm, 300µm, 500µm, and 1000µm for both binders and interface types.

Statistical analyses were employed to answer the following questions:

1. Is there a significant difference in G* values obtained from a stainless steel interface versus those obtained from a ceramic interface?
2. When using a modified base plate and spindle, what is the appropriate gap size to use if variability is to be low?
3. Do any of the examined gap sizes offer a precision similar to a traditional DSR grading test? The precision for a traditional DSR grading test is a coefficient of variation of G* for a single operator of 3.4% (ASTM D 7175).
4. What is an appropriate gap size for a binder with filler tested using a modified spindle and base plate while maintaining a low variability and similar precision as outlined in ASTM D 7175?
5. Is a DSR with modified base plate and spindle sensitive to fillers added to a binder?
6. Is a DSR with modified base plate and spindle sensitive to different types of fillers added to a binder?

Multi-way ANOVAs were employed to answer the above questions, along with coefficients of variation. ANOVAs aided in determining if there were significant differences in G* values between gap sizes and interface material (ceramic or stainless steel). Coefficients of variation of G* were calculated for combination of gap size and interface material. These coefficients of variation were compared to a coefficient of variation of 3.4%, which is the precision outlined in ASTM D7175 for a single operator testing original binders.

It has been hypothesized by some researchers that a smaller gap size would yield more reliable results since a small gap size would be closer to the actual film thickness found in pavements. However, the issue found with the smaller gap size was not repeatable results. Table 3.1 summarizes the repeatability analysis performed on the 200µm and 300µm gap size. Cells labeled "Yes" are results that were repeatable, whereas ones labeled "No" were not repeatable. It can be seen that over half of the tests conducted were unrepeatable. The lack of repeatability indicates that a different gap size should be considered. The issue with the smaller gap size is associated with parallel plate theory, which the DSR and the calculation of G*/sin(δ) are based upon. Smaller gap sizes are more sensitive to plates that are not parallel, whereas any small deviation from parallelism with a larger gap size becomes less sensitive.

**Table 3.1 Repeatability of 200µm and 300µm Gap Size**

| Complex Modulus | | | | | | | | | |
|---|---|---|---|---|---|---|---|---|---|
| Binder | Bath | Original Binder | | | | RTFO Aged Binder | | | |
| | | 200 micrometer | | 300 micrometer | | 200 micrometer | | 300 micrometer | |
| | | Stainless Steel | Ceramic | Stainless Steel | Ceramic | Stainless Steel | Ceramic | Stainless Steel | Ceramic |
| AAA-1 | Water | No | Yes | No | No | No | No | Yes | No |
| AAA-1 | Air | Yes | No | No | No | Yes | No | No | Yes |
| AAM-1 | Water | Yes | Yes | Yes | No | Yes | No | Yes | Yes |
| AAM-1 | Air | No | Yes | No | No | No | Yes | Yes | No |

The 200µm and 300µm gap sizes, 500µm and 1000µm were evaluated for repeatability. It should be noted that 1000µm is the current standard gap size for unaged binders tested using the Superpave system. Both the 500µm and 1000µm were statistically viable gap sizes for the unaged original binders. 500µm and 1000µm were used to test asphalt binders AAA-1 and AAM-1 with 3 percentage levels of 2 fillers.

During the testing with the fillers, it was discovered that some of binders with silica could not be measured for complex shear modulus and phase angle at a gap size of 500μm. Further difficulties were faced with the 500μm gap with some silica modified binders that yielded unrepeatable results. These issues were not observed with the 1000μm, hence the selection of a 1000μm gap size for testing with the modified DSR parts.

Comparisons between the stainless steel and ceramic interfaces yielded varying results based on the gap size. No statistical difference was observed for the complex shear modulus and phase angle results obtained with either a stainless steel or ceramic interface for 200μm and 300μm. The inability of the test to distinguish between the two interfaces could be associated with the high level of variability of measurements acquired at these smaller gap sizes. There were differences between the gap sizes for the 500μm and 1000μm gaps. Gap size selection was based on the precision statement in ASTM D 7175. The precision statement in ASTM D 7175 stipulates that the coefficient of variation for a single operator for $G^*/\sin(\delta)$ not exceed 3.4%. The data collected for specimens tested at the 200μm and 300μm yielded coefficient of variation values greater than 3.4%, thus eliminating these two gap sizes for further testing.

The second set of tests evaluated only the 500μm and 1000μm gap sizes. The test set consisted of examining the effects of filler in a binder and the sensitivity of the modified DSR to the differences in filler type. The analysis for this test set consisted of applying the ASTM D 7175 precision statement and statistical evaluation. The statistical evaluation included mean comparisons and analysis of variance (ANOVA).

The third set of tests for the SHRP binders evaluated the effects of conditioning on a specimen. This set of tests was conducted only for one gap size and with ceramic discs in a water bath. Three specimen conditions were examined using original binders, binders with hydrated lime (at 5%, 10%, and 20% by weight), and silica (at 5%, 10%, and 20% by weight). The analysis consisted of ANOVA.

The final section of this chapter summarizes the results and the testing procedure selected for testing field binders.

### 3.2.2 Testing Procedure for AAA-1 and AAM-1 Asphalt Binders

The initial binders used to test the applicability of the new modified spindle for moisture susceptibility testing were MRL binders AAM-1 and AAA-1, collected during the original Strategic Highway Research Program (SHRP). These two binders were selected for the availability of data collected and stored in the materials reference library. The choice of AAA-1 and AAM-1 was based on work conducted by Rottermond (Rottermond, 2004) on a similar modified spindle and base plate. The SHRP binders were used to determine which testing phases should be incorporated when testing asphalt binders for moisture susceptibility.

Table 3.2 outlines the tests conducted using the SHRP asphalt binders. Testing consisted of evaluation of material within a water environment using ceramic and stainless steel discs. In addition, specimens tested with ceramic discs were also examined after 24 hours of water saturation. The 24 hour saturation period occurred in a distilled water bath at 25˚C. The stainless steel discs were not used since stainless steel is not permeable. The moisture saturation was used to saturate the surface of binders. If a stainless steel disc was used, then the surface of the binder in contact with a stainless steel disc would not be exposed to moisture and limit exposure to the horizontal perimeter of a specimen.

Hydrated lime and silica were used as the mastic material added to the asphalt binders to examine the interaction with aggregates. Both the hydrated lime and silica passed the #200 sieve. Prior to mixing the mastic into the binder, both the binder and mastic were heated. Each mastic was added by weight and stirred into the binder until it appeared homogenous.

All samples were poured into standard 25mm molds in conjunction with the DSR. Each specimen rested for a minimum of 10 minutes prior to testing. In all cases, the discs were screwed into the base plate and spindle prior to initiation of testing. Once the DSR was zeroed, the spindle was raised to enable the application of the asphalt binder sample. The spindle was then lowered to a gap of 1050µm. If the sample required trimming it occurred at this point and then the spindle was lowered to 1000µm. Testing did not initiate until the water bath once again reached the desired testing temperature. After

testing, the set screws in the modified spindle were unscrewed and then the spindle raised. The base plate with the specimen was then removed from the DSR. The specimen was then removed from the base plate by unscrewing the set screws holding the bottom of the specimen.

The samples tested with the ceramic discs were examined with the DSR three times. The first examination occurred with unconditioned samples. After the first test, the disc and binder sample were placed in a water bath with distilled 25˚C water for a period of 24 hours. After 24 hours of saturation, the specimens were retested as conditioned specimens. After the second round of testing, the specimen was wrapped in cellophane and placed in a freezer for 24 hours. The temperature in the freezer was -18 ± 3˚C. A specimen's time in a freezer was selected based on current practices for mixes according to AASHTO T-283. After 24 hours in a freezer, the specimen was returned to the water bath to thaw for another 24 hours. One the specimen had thawed it was retested.

### 3.2.2.1 Testing Results for AAA-1 and AAM-1

Statistical analyses were conducted to determine which factors significantly affected complex shear modulus results when using modified DSR parts. The main type of analysis used was ANOVA with a 95% level of confidence. P-values from ANOVA tables will be presented. A low (in this case below 0.05) indicates a significant factor, while a high p-value is associated with an insignificant factor.

#### *3.2.2.1.1 Gap Size and Interface Selection Analysis*

It was hypothesized that ceramic discs would be a better interface for moisture susceptibility testing of asphalt binders, and thus the hypothesis needed to be tested. Both ceramic and stainless steel interfaces were tested using AAA-1 and AAM-1 asphalt binders at different gap sizes. As mentioned earlier, original binders were used for all gap size tests while binders with fillers were only used for testing with a 500µm and

1000µm gap. The gap sizes evaluated were 200µm, 300µm, 500µm, and 1000µm for both binders and interface types.

**Table 3.2 Experimental Plan for AAA-1 and AAM-1 Asphalt Binders**

| Test Condition | | | | | | AAA-1 | AAM-1 |
|---|---|---|---|---|---|---|---|
| Environment | Disk | Saturation | Freeze/Thaw | Mastic | Percent | | |
| Water | Ceramic | Unconditioned | No | Hydrated Lime | 5 | XXX | XXX |
| | | | | | 10 | XXX | XXX |
| | | | | | 20 | XXX | XXX |
| | | | | Silica | 5 | XXX | XXX |
| | | | | | 10 | XXX | XXX |
| | | | | | 20 | XXX | XXX |
| | | | | None | 0 | XXX | XXX |
| | | Conditioned | No | Hydrated Lime | 5 | XXX | XXX |
| | | | | | 10 | XXX | XXX |
| | | | | | 20 | XXX | XXX |
| | | | | Silica | 5 | XXX | XXX |
| | | | | | 10 | XXX | XXX |
| | | | | | 20 | XXX | XXX |
| | | | | None | 0 | XXX | XXX |
| | | | Yes | Hydrated Lime | 5 | XXX | XXX |
| | | | | | 10 | XXX | XXX |
| | | | | | 20 | XXX | XXX |
| | | | | Silica | 5 | XXX | XXX |
| | | | | | 10 | XXX | XXX |
| | | | | | 20 | XXX | XXX |
| | | | | None | 0 | XXX | XXX |
| | Steel | Unconditioned | No | Hydrated Lime | 5 | XXX | XXX |
| | | | | | 10 | XXX | XXX |
| | | | | | 20 | XXX | XXX |
| | | | | Silica | 5 | XXX | XXX |
| | | | | | 10 | XXX | XXX |
| | | | | | 20 | XXX | XXX |
| | | | | None | 0 | XXX | XXX |

ANOVAs were employed to determine which factors significantly contribute to different complex shear modulus values. The main effects considered were binder type (AAA-1 or AAM-1), filler type (hydrated lime or silica), percent level (5%, 10%, or 20%), disc material (stainless steel or ceramic), gap size (500µm or 1000µm), and testing environment (water bath or air chamber). Table 3.3 summarizes the calculated p-values obtained from an ANOVA. All of the main effects considered were deemed statistically significant. This implies that each of these factors contributed to changes in complex shear modulus readings. Interaction effects were also considered within this ANOVA. Interestingly, the interaction between binder type and filler type was not considered a significant contributor to the complex shear modulus variability. It has been hypothesized that chemical interactions between binders and fillers would results in

significantly different complex shear modulus values. It is hypothesized that certain levels of filler accounts for significant levels of complex shear modulus variability. It should be noted that the interaction between binder and percent level does not distinguish between hydrated lime and silica. Additional analysis will be presented that examines this more complex relationship. The interaction between binder type and disc type was also regarded as significant with respect to complex shear modulus variability. The precise reasoning for this interaction is not clear, but it is thought that either absorption of binder into a disc or friction created between a disc and binder results in different complex shear modulus readings. Since filler and disc interactions do not have an effect on complex shear modulus variability, friction may not be the cause of low p-values for binder and disc interactions. Based on filler and disc not being a cause, it is more likely that the absorption of the binder into a disc results in a low p-value. Another surprising relationship that did not significantly affect complex shear modulus measurements was the interaction between binder type and environmental testing condition.

#### *3.2.2.1.2 Saturation Effects on Asphalt Binders*

Saturation and freeze/thaw effects were analyzed by testing unsaturated, saturated, saturated plus one freeze/thaw cycle specimens. For this testing only ceramic insets were used in the modified DSR parts. Analyses were conducted to determine if saturation or saturation plus one freeze/thaw cycle has an effect on complex shear modulus values. According to the analysis, there is a significant difference between unsaturated and saturated specimens. However, there is no statistical difference between saturation plus one freeze/thaw versus either unsaturated or saturated specimens. This would indicate that it is sufficient to test just unsaturated and saturated specimens. The effects of multiple freeze/thaw cycles could be examined, but to remain consistent with current freeze/thaw testing procedures for HMA mix, only one freeze/thaw was considered.

The viscous and elastic moduli results were examined next. For the AAA-1 binder, it was found that the viscous modulus changed much more than the elastic modulus when comparing between unsaturated, saturated, and saturated plus one freeze/thaw cycle. The significant difference between viscous moduli for AAM-1 asphalt binders was less than

that of AAA-1. Both AAA-1 and AAM-1 yielded statistically different elastic moduli values for saturated and unsaturated specimens. Both binders also found that the elastic moduli values for saturated and saturated plus one freeze/thaw were statistically equivalent. The analysis shows that the viscous component of asphalt binders changes the most with saturation in comparison to the elastic component. In general, saturation caused the complex shear modulus to decrease for the original binders. Tukey's mean comparisons were in agreement with the results found in Table 3.4.

**Table 3.3 P-Values of Main and Interaction Effects on Complex Shear Modulus Results**

| Effect | P-Values |
|---|---|
| ***binder*** | <.0001 |
| ***filler*** | <.0001 |
| ***percent*** | <.0001 |
| ***disc*** | 0.0003 |
| ***gap*** | <.0001 |
| ***bath*** | <.0001 |
| ***binder*filler*** | 0.3524 |
| ***binder*percent*** | 0.0229 |
| ***binder*disc*** | 0.0033 |
| ***filler*percent*** | 0.0041 |
| ***filler*disc*** | 0.6379 |
| ***filler*bath*** | 0.3286 |
| ***filler*gap*** | <.0001 |
| ***binder*bath*** | 0.4009 |

**Table 3.4 P-Values of Condition Comparisons of Original Binders**

| Binder | Condition Comparison | Elastic Modulus | Viscous modulus |
|---|---|---|---|
| *AAA-1* | *Saturated vs Unsaturated* | 0.0006 | 0.0002 |
| | *Saturated vs Saturated Plus Freeze-Thaw* | 0.1526 | 0.0018 |
| | *Unsaturated vs Saturated Plus Freeze-Thaw* | 0.1530 | 0.0020 |
| *AAM-1* | *Saturated vs Unsaturated* | 0.0007 | 0.0006 |
| | *Saturated vs Saturated Plus Freeze-Thaw* | 0.6172 | 0.0304 |
| | *Unsaturated vs Saturated Plus Freeze-Thaw* | 0.0262 | 0.0031 |

### *3.2.2.1.3 Conditioning Time Effects on Asphalt Binders*

Some of the modified binders were used to see if there was any effect on the specimens due to conditioning time. The time intervals considered were 0, 5, 10, and 20 minutes. Binders were tested at their high PG temperature. Both stainless steel and ceramic discs were employed in determining time conditioning effects on complex shear modulus values. Comparisons were made between complex shear modulus values at different conditioning times. Table 3.5 summarizes the results of these comparisons. According to the results, there is no significant statistical difference in testing a specimen that has been in a water bath anywhere from 0 to 20 minutes. Tukey's mean comparisons on these means also revealed no significant differences.

**Table 3.5 P-Values Comparing Conditioning Times**

| Time Comparison (minutes) | P-value |
|---|---|
| ***0 vs 5*** | 0.8697 |
| ***0 vs 10*** | 0.9158 |
| ***0 vs 20*** | 0.5386 |
| ***5 vs 10*** | 0.9740 |
| ***5 vs 20*** | 0.4639 |
| ***10 vs 20*** | 0.5330 |

### 3.2.2.2 AAA-1 and AAM-1 Testing Parameter Conclusions

A new moisture susceptibility test was developed using modified DSR parts. Testing was conducted to determine if material interface affects complex shear modulus results. It was determined that material interface does affect complex shear modulus results. Hence, for the new test protocol, ceramic discs would be used to allow for water to access the top and bottom of a binder sample in addition to the circumference of a sample. Further testing was conducted to establish an appropriate gap size for a new testing procedure. The gap size selected was 1000µm. Subsequent testing indicated that the new test procedure is sensitive to binder type and addition of filler. The test also appears to be able to distinguish between filler type. Additional testing indicated that statistically different complex shear modulus results were obtained from unsaturated asphalt binder samples versus saturated specimens. However, no additional differences were observed with the samples were moisture saturated and had endured one freeze/thaw cycle. There were also no statistical differences in complex shear modulus readings when leaving a specimen in a heated water bath anywhere from 0 to 20 minutes prior to testing.

Based on laboratory testing and statistical analysis a new test procedure was established in this chapter. Specimens would be tested first unsaturated with ceramic discs at a gap of 1000µm. Second the specimens would soak in a water bath for a period of 24 hours at 25˚C. After 24 hours of soaking, specimens would be tested again in a

DSR using ceramic discs. Table 3.4 summarized results from an ANOVA indicating that binder type, filler type, percent of filler, disc material, gap size, testing environment, interaction between binder type and percent of filler, interaction between binder type and disc material, and interaction between filler type and gap size were all deemed significant factors contributing to complex shear modulus dispersion.

# Chapter 4 Evaluating Asphalt Binders with the Developed Moisture Susceptibility Test Procedure

Twenty-one binders were collected from paving construction sites around the state of Michigan. The binders collected varied in performance grade. Table 4.1 summarizes the binders tested. The testing procedure developed in the previous chapter was used to evaluate the moisture susceptibility of the field binders. Several binders contained polymers, however the nature and amount of the polymer was unknown to the researchers.

**Table 4.1 Summary of Binders Tested**

| Site | PG High Temperature | PG Low Temperature | Polymer | Polymer Percent | Asphalt Source |
|---|---|---|---|---|---|
| Ann Arbor | 70 | -22 | Cellulose Fibers | 0.3 | T & M Oil |
| Battle Creek | 64 | -28 | None | - | Michigan Paving and Materials |
| Brighton | 58 | -22 | None | - | Marathon Detroit |
| Clarkston | 70 | -22 | Modifier | Unknown | Marathon Detroit |
| Detroit | 70 | -22 | Modifier | Unknown | Marathon Detroit |
| Dundee 12.5mm NMAS | 64 | -28 | None | - | MTM Oil |
| Dundee 19mm NMAS | 64 | -28 | None | - | Marathon Detroit |
| Grand Rapids I-196 | 64 | -22 | None | - | Michigan Paving and Materials |
| Grand Rapids M-45 | 58 | -28 | Antistrip | 0.3 | T & M Oil |
| Hartland | 64 | -22 | None | - | Marathon Detroit |
| Howell | 70 | -28 | Modifier | Unknown | Michigan Paving and Materials |
| Levering | 58 | -28 | None | - | British Petroleum |
| Michigan Ave 12.5mm NMAS | 70 | -22 | Modifier | Unknown | Marathon Detroit |
| Michigan Ave 19mm NMAS | 58 | -28 | None | - | Marathon Detroit |
| Michigan International Speedway | 64 | -28 | None | - | Marathon Detroit |
| Owosso | 64 | -28 | None | - | Michigan Paving and Materials |
| Pinckney | 64 | -22 | None | - | Marathon Detroit |
| Saginaw | 58 | -28 | None | - | Marathon Detroit |
| St. Johns | 58 | -22 | None | - | Michigan Paving and Materials |
| Toledo | 70 | -22 | Modifier | Unknown | 6505 MPM Oil |
| Van Dyke | 64 | -22 | None | - | Marathon Detroit |

As with the SHRP MRL binders, binders collected from Michigan were mixed with hydrated lime and silica. The hydrated lime and silica used for creating mastics was the same for both the SHRP MRL binders and Michigan binders. Mixing of the fillers with binders was conducted in the same manner as outlined previously for the SHRP MRL mastics. Once mastics had been procured, 25mm specimens were made with standard 25mm molds and allowed to rest for the required 10 minutes prior to testing.

Specimen attachment and DSR zeroing was conducted in the same manner as was done for AAA-1 and AAM-1 binder testing.

The samples tested with ceramic discs were examined with a DSR twice. The first examination occurred with unconditioned samples. After the first test, the disc and binder cylinder were placed in a water bath with distilled 25˚C water for a period of 24 hours. After 24 hours of saturation, the specimens were retested as conditioned specimens. Both testing procedures were tested utilizing a water bath and an air chamber separately. Table 4.2 summarizes the different testing conditions employed for each binder. As the table indicates, 28 different scenarios were conducted for each binder, yielding 588 scenarios for all 21 binders.

## 4.1 Materials for Field Binder Testing

The binders selected for analysis were collected from the field and encompassed a range of Performance Grades (PG). Three categories of PG high temperature were available for analysis: PG 58, 64, and 70. Binders were tested at the high temperature (e.g. 58˚C or 64˚C) with exception of the binders with a high temperature of 70, these were tested at 64˚C. The discrepancy in test temperature for the PG 70-X binders was based on the knowledge that the PG 70-X was only used to allow for better rutting performance in the field where high traffic volumes were expected. Some of the binders contained polymers while others were neat or unmodified. Two fillers, the same ones used in modifying AAA-1 and AAM-1, were selected based on moisture susceptibility: a hydrated lime and a silica. Both fillers passed the #200 sieve (0.075mm). Table 4.3 summarizes the number of tests conducted for each condition state and filler-binder combination.

**Table 4.2 Testing Plan for One Michigan Binder**

| Binder | Environment | Mastic | Percentage of Mastic | Unconditioned | Conditioned |
|---|---|---|---|---|---|
| 1 | Water | Lime | 5 | XXX | XXX |
| | | | 10 | XXX | XXX |
| | | | 20 | XXX | XXX |
| | | Silica | 5 | XXX | XXX |
| | | | 10 | XXX | XXX |
| | | | 20 | XXX | XXX |
| | | None | 0 | XXX | XXX |
| | Air | Lime | 5 | XXX | XXX |
| | | | 10 | XXX | XXX |
| | | | 20 | XXX | XXX |
| | | Silica | 5 | XXX | XXX |
| | | | 10 | XXX | XXX |
| | | | 20 | XXX | XXX |
| | | None | 0 | XXX | XXX |

**Table 4.3 Samples Tested**

| | | Water Bath | | | Air Chamber | | |
|---|---|---|---|---|---|---|---|
| | | Performance High Grade | | | Performance High Grade | | |
| | | *58* | *64* | *70* | *58* | *64* | *70* |
| Original Binder | Unconditioned | 18 | 27 | 18 | 18 | 27 | 18 |
| | Saturated | 18 | 27 | 18 | 18 | 27 | 18 |
| 5% Hydrated Lime | Unconditioned | 18 | 27 | 18 | 18 | 27 | 18 |
| | Saturated | 18 | 27 | 18 | 18 | 27 | 18 |
| 10% Hydrated Lime | Unconditioned | 18 | 27 | 18 | 18 | 27 | 18 |
| | Saturated | 18 | 27 | 18 | 18 | 27 | 18 |
| 20% Hydrated Lime | Unconditioned | 18 | 27 | 18 | 18 | 27 | 18 |
| | Saturated | 18 | 27 | 18 | 18 | 27 | 18 |
| 5% Silica | Unconditioned | 18 | 27 | 18 | 18 | 27 | 18 |
| | Saturated | 18 | 27 | 18 | 18 | 27 | 18 |
| 10% Silica | Unconditioned | 18 | 27 | 18 | 18 | 27 | 18 |
| | Saturated | 18 | 27 | 18 | 18 | 27 | 18 |
| 20% Silica | Unconditioned | 18 | 27 | 18 | 18 | 27 | 18 |
| | Saturated | 18 | 27 | 18 | 18 | 27 | 18 |

## 4.2 Statistical and Graphical Results of Michigan Binder Tests

Statistical analyses were conducted to determine statistically significant factors and moisture susceptible binders upon the conclusion of testing all 588 scenarios. All of the statistical analyses used a level of confidence of 95% for evaluating statistical significance.

### 4.2.1 Statistical and Graphical Comparisons of All Michigan Binders

The initial set of statistical analysis examined all of the data prior to categorizing the DSR test results by possible significant factors. Figure 4.1 displays the data collected from the modified DSR spindle and base plate configuration, and is difficult to distinguish a trend using all the data. Several mean comparisons and ANOVAs were employed to help ascertain important information. Table 4.4 summarizes the results of mean comparisons calculated to obtain significant information. An "Accept" indicates that the means were deemed statistically similar, while a "Reject" indicates that the means were considered statistically different.

#### 4.2.1.1 Effects of Moisture on Original Binder

The focus of the analysis was the affects of moisture on the rutting potential of an asphalt binder. The statistical evaluation of the data was grouped by individual filler-asphalt combinations and then comparisons between the groups were made. In all cases where hypothesis testing was conducted a level of significance of 5% was used.

Part of the analysis conducted was determining if any of the binders failed the Superpave criterion that $G^*/\sin(\delta)$ be greater than 1.0 kPa for unaged binders. It was hypothesized that if moisture softened the binder, the performance grade rating would change. It should be noted that this criteria was established for stainless steel and not for a ceramic interfaces for grading binders. Comparisons between the stainless steel interface and ceramic interface have revealed that the specimens tested with ceramic tend to give a slightly lower $G^*/\sin(\delta)$ value than those tested with a stainless steel interface

for unsaturated specimens. The saturated specimens tend to yield greater differences between the two interfaces for G*/sin(δ) values.

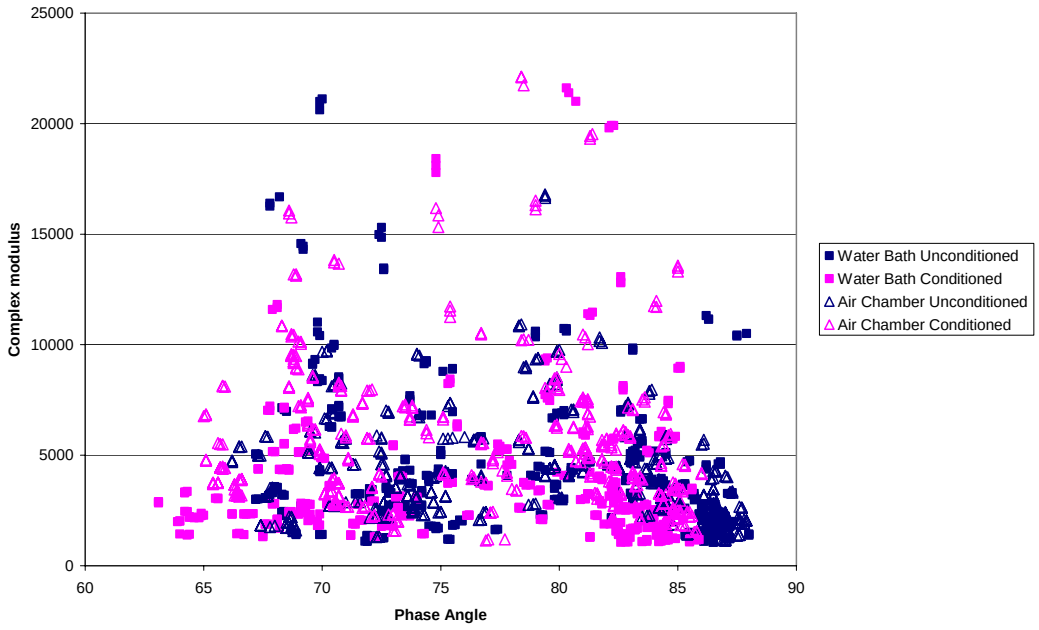


**Figure 4.1 Graphical Comparison of Environmental Testing Conditions for All Data**

**Table 4.4 Results of Original Binder Mean Comparisons**

| | Unconditioned Water | | Unconditioned | | Saturated Water | | Unconditioned Air | | Saturated Water | |
|---|---|---|---|---|---|---|---|---|---|---|
| | Complex Shear Modulus | G*/ sin(δ) | Complex Shear Modulus | G*/ sin(δ) | Complex Shear Modulus | G*/ sin(δ) | Complex Shear Modulus | G*/ sin(δ) | Complex Shear Modulus | G*/ sin(δ) |
| Ann Arbor | Not Rejected | Not Rejected | *Reject* | *Reject* | *Reject* | *Reject* | *Reject* | *Reject* | *Reject* | *Reject* |
| Battle Creek | *Reject* | *Reject* | *Reject* | *Reject* | *Reject* | *Reject* | *Reject* | *Reject* | *Reject* | *Reject* |
| Brighton | Not Rejected | Not Rejected | *Reject* | *Reject* | *Reject* | *Reject* | *Reject* | *Reject* | *Reject* | *Reject* |
| Clarkston | *Reject* | *Reject* | *Reject* | *Reject* | *Reject* | *Reject* | *Reject* | *Reject* | *Reject* | *Reject* |
| Detroit | *Reject* | *Reject* | *Reject* | *Reject* | *Reject* | *Reject* | *Reject* | *Reject* | *Reject* | *Reject* |
| Dundee 12.5mm NMAS | Not Rejected | Not Rejected | *Reject* | *Reject* | *Reject* | *Reject* | Not Rejected | Not Rejected | *Reject* | *Reject* |
| Dundee 19.0mm | *Reject* | *Reject* | *Reject* | *Reject* | *Reject* | *Reject* | *Reject* | *Reject* | *Reject* | *Reject* |
| Grand Rapids I-196 | *Reject* | *Reject* | *Reject* | *Reject* | *Reject* | *Reject* | *Reject* | *Reject* | *Reject* | *Reject* |
| Grand Rapids M-45 | *Reject* | *Reject* | *Reject* | *Reject* | *Reject* | *Reject* | *Reject* | *Reject* | *Reject* | *Reject* |
| Hartland | *Reject* | *Reject* | *Reject* | *Reject* | *Reject* | *Reject* | *Reject* | *Reject* | *Reject* | *Reject* |
| Howell | *Reject* | *Reject* | *Reject* | *Reject* | *Reject* | *Reject* | *Reject* | *Reject* | *Reject* | *Reject* |
| Levering | Not Rejected | Not Rejected | *Reject* | *Reject* | *Reject* | *Reject* | *Reject* | *Reject* | *Reject* | *Reject* |
| Michigan Ave 12.5mm NMAS | *Reject* | *Reject* | *Reject* | *Reject* | *Reject* | *Reject* | *Reject* | *Reject* | *Reject* | *Reject* |
| Michigan Ave 19.0mm NMAS | *Reject* | *Reject* | *Reject* | *Reject* | *Reject* | *Reject* | *Reject* | *Reject* | *Reject* | *Reject* |
| Michigan International Speedway | *Reject* | *Reject* | *Reject* | *Reject* | *Reject* | *Reject* | *Reject* | *Reject* | *Reject* | *Reject* |
| Owosso | *Reject* | *Reject* | *Reject* | *Reject* | *Reject* | *Reject* | *Reject* | *Reject* | *Reject* | *Reject* |
| Pinckney | *Reject* | *Reject* | *Reject* | *Reject* | *Reject* | *Reject* | *Reject* | *Reject* | *Reject* | *Reject* |
| Saginaw | *Reject* | *Reject* | *Reject* | *Reject* | *Reject* | *Reject* | *Reject* | *Reject* | *Reject* | *Reject* |
| St. Johns | *Reject* | *Reject* | *Reject* | *Reject* | *Reject* | *Reject* | *Reject* | *Reject* | *Reject* | *Reject* |
| Toledo | *Reject* | *Reject* | *Reject* | *Reject* | *Reject* | *Reject* | *Reject* | *Reject* | *Reject* | *Reject* |
| VanDyke | *Reject* | *Reject* | *Reject* | *Reject* | *Reject* | *Reject* | *Reject* | *Reject* | *Reject* | *Reject* |

The initial analysis examined the effects of moisture on the original binders. The null hypothesis for the following comparisons states that there is no statistical difference between the rheological measurements of two original binder data sets examined. Table 4.5 summarizes the results of comparisons conducted to determine if there are significant differences between the testing conditions for original binders. It can be seen that most of the comparisons indicated that there are statistical differences between the testing conditions; this however does not mean that all of the original binders with statistical differences will be moisture susceptible. It is expected that the varying testing conditions may yield different G* values. However, drastic changes in G* could be indicative of a moisture prone binder. In most cases, the phase angles were statistically equivalent, indicating that a closer examination of the results is needed to determine which binders are moisture susceptible.

The following analysis summarized in Table 4.5 examined whether the varying G* and G*/sin(δ) values would result in a revised binder high temperature grade. If different testing conditions result in a new grade, then the binder will be marked as moisture susceptible. The Superpave specification requirement is that G*/sin(δ) is at least 1.0 kPa at the given test temperature. All of the original binders tested within the varying environmental conditions pass the Superpave requirements, however there were several binders after moisture saturation that barely met the 1.0 kPa requirement. The original binders that were close to the 1.0 kPa requirement will be monitored closely for changes with the fillers.

**Table 4.5 Comparison of Testing Conditions for All Data**

| | | ALL | |
|---|---|---|---|
| | | Hydrated Lime | Silica |
| Unconditioned Water Bath Vs. Conditioned Water Bath | Complex Modulus | *Reject* | *Reject* |
| | Phase Angle | *Reject* | *Reject* |
| | G*/ sin(δ) | *Reject* | *Reject* |
| Unconditioned Water Bath Vs. Unconditioned Air Chamber | Complex Modulus | *Reject* | Not Rejected |
| | Phase Angle | *Reject* | Not Rejected |
| | G*/ sin(δ) | *Reject* | Not Rejected |
| Conditioned Water bat Vs. Conditioned Air Chamber | Complex Modulus | *Reject* | *Reject* |
| | Phase Angle | Not Rejected | Not Rejected |
| | G*/ sin(δ) | *Reject* | *Reject* |
| Unconditioned Air Chamber Vs. Conditioned Air Chamber | Complex Modulus | *Reject* | *Reject* |
| | Phase Angle | *Reject* | *Reject* |
| | G*/ sin(δ) | *Reject* | *Reject* |

**Table 4.6 Comparison of Environmental Testing Conditions and Specimen Condition**

| Site | Water Bath Unconditioned vs Water Bath Conditioned | | Water Bath Unconditioned vs Air Chamber Unconditioned | | Water Bath Conditioned vs Air Chamber Conditioned | | Air Chamber Unconditioned vs Air Chamber Conditioned | |
|---|---|---|---|---|---|---|---|---|
| | Complex Modulus | G*/ sin(δ) | Complex Modulus | G*/ sin(δ) | Complex Modulus | G*/ sin(δ) | Complex Modulus | G*/ sin(δ) |
| Pinckney | Accept | Accept | Accept | Accept | Reject | Reject | Accept | Accept |
| VanDyke | Accept | Accept | Reject | Reject | Reject | Accept | Reject | Reject |
| St. Johns | Reject | Reject | Reject | Reject | Reject | Reject | Reject | Reject |
| Grand Rapids M-45 | Accept | Accept | Accept | Accept | Reject | Reject | Reject | Reject |
| Saginaw | Accept | Accept | Reject | Accept | Reject | Reject | Reject | Reject |
| Michigan Ave 19.0mm NMAS | Reject | Reject | Accept | Accept | Reject | Reject | Reject | Reject |
| Levering | Reject | Reject | Reject | Reject | Reject | Reject | Reject | Reject |
| Ann Arbor | Accept | Accept | Accept | Accept | Reject | Reject | Accept | Accept |
| Detroit | Reject | Reject | Reject | Reject | Reject | Reject | Reject | Reject |
| Toledo | Reject | Reject | Reject | Reject | Reject | Reject | Reject | Reject |
| Hartland | Reject | Reject | Reject | Reject | Accept | Accept | Reject | Reject |
| MIS | Accept | Accept | Accept | Accept | Reject | Reject | Accept | Accept |
| Battle Creek | Reject | Reject | Accept | Accept | Reject | Reject | Accept | Accept |
| Howell | Reject | Reject | Reject | Reject | Reject | Reject | Reject | Reject |
| Clarkston | Accept | Accept | Accept | Accept | Reject | Reject | Reject | Reject |
| Owosso | Reject | Reject | Reject | Reject | Reject | Reject | Accept | Accept |
| Dundee 19.0mm NMAS | Reject | Reject | Reject | Reject | Accept | Accept | Reject | Reject |
| Brighton | Reject | Reject | Accept | Accept | Reject | Reject | Reject | Reject |
| Michigan Ave 12.5mm NMAS | Reject | Reject | Accept | Accept | Reject | Reject | Reject | Reject |
| Grand Rapids I-196 | Reject | Reject | Accept | Accept | Reject | Reject | Accept | Accept |
| Dundee 12.5mm NMAS | Accept | Accept | Reject | Reject | Reject | Reject | Accept | Accept |

### 4.2.2 Statistical and Graphical Results of Michigan Binders Categorized by Mastic Type

Moisture damage issues can arise in HMA pavements even if the asphalt binder has not been found to be moisture susceptible. The moisture susceptibility could be caused by either the aggregate or the interaction between the aggregate and asphalt binder. Two fillers and their interactions with asphalt binders were examined as part of this dissertation. Three percentages by weight were examined to see if different levels of each filler had dissimilar results. The fillers considered were hydrated lime and silica, both passing the #200 sieve. The following analysis explored the affects of each filler associated with the 21 asphalt binders sampled.

In Table 4.7, comparisons are grouped by filler type and percentage level of filler. Not pooling the data allows certain trends to be observed. G*/sin(δ) values tend to be deemed statistically similar for comparison of specimens tested in a water bath or unconditioned. Differences begin to arise with an increased level of filler. G*/sin(δ)

comparisons are also dissimilar when comparing conditioned specimens or ones tested in an air chamber.

**Table 4.7 Results of Comparing Environmental Testing Conditions by Mastic Percentage Level**

| | | 5% Hydrated Lime | 5% Silica | 10% Hydrated Lime | 10% Silica | 20% Hydrated Lime | 20% Silica |
|---|---|---|---|---|---|---|---|
| Unconditioned Water Bath Vs. Conditioned Water Bath | Complex Modulus | Not Rejected | Not Rejected | Not Rejected | ***Reject*** | ***Reject*** | ***Reject*** |
| | Phase Angle | ***Reject*** | ***Reject*** | ***Reject*** | ***Reject*** | ***Reject*** | ***Reject*** |
| | G*/ sin(δ) | Not Rejected | Not Rejected | Not Rejected | ***Reject*** | ***Reject*** | Not Rejected |
| Unconditioned Water Bath Vs. Unconditioned Air Chamber | Complex Modulus | Not Rejected | Not Rejected | Not Rejected | Not Rejected | Not Rejected | Not Rejected |
| | Phase Angle | Not Rejected | Not Rejected | Not Rejected | Not Rejected | ***Reject*** | ***Reject*** |
| | G*/ sin(δ) | Not Rejected | Not Rejected | Not Rejected | Not Rejected | ***Reject*** | Not Rejected |
| Conditioned Water Bath Vs. Conditioned Air Chamber | Complex Modulus | ***Reject*** | ***Reject*** | Not Rejected | ***Reject*** | ***Reject*** | ***Reject*** |
| | Phase Angle | Not Rejected | Not Rejected | ***Reject*** | Not Rejected | ***Reject*** | Not Rejected |
| | G*/ sin(delta) | ***Reject*** | ***Reject*** | Not Rejected | ***Reject*** | ***Reject*** | ***Reject*** |
| Unconditioned Air Chamber Vs. Conditioned Air Chamber | Complex Modulus | ***Reject*** | ***Reject*** | ***Reject*** | ***Reject*** | Not Rejected | ***Reject*** |
| | Phase Angle | ***Reject*** | ***Reject*** | ***Reject*** | ***Reject*** | ***Reject*** | ***Reject*** |
| | G*/ sin(δ) | ***Reject*** | ***Reject*** | ***Reject*** | ***Reject*** | ***Reject*** | ***Reject*** |
| Conditioned Water Bath Vs. Unconditioned Air Chamber | Complex Modulus | ***Reject*** | ***Reject*** | ***Reject*** | ***Reject*** | ***Reject*** | ***Reject*** |
| | Phase Angle | ***Reject*** | ***Reject*** | ***Reject*** | ***Reject*** | ***Reject*** | ***Reject*** |
| | G*/ sin(δ) | ***Reject*** | ***Reject*** | ***Reject*** | ***Reject*** | ***Reject*** | ***Reject*** |

### 4.2.2.1 Effects of Hydrated Lime

Extensive research has been conducted analyzing the advantages of using hydrated lime in binders to resist moisture damage. Since past research has shown that hydrated lime is moisture resistant and aids in preventing moisture damage within HMA, the current research used hydrated lime as a mineral filler to prevent moisture damage. Table 4.8 outlines the results of comparisons conducted to determine if there is a statistical difference between testing conditions results within a certain percentage of filler. The

comparisons with the unconditioned samples tested in the water bath for both 5% and 10% of hydrated lime yield statistically equivalent results with conditioned specimens tested in a water bath and unconditioned specimens tested in an air chamber. However, comparisons between conditioned specimens tested in the water bath and unconditioned specimens tested in the air chamber were statistically different for both G* and G*/sin(δ) implying that there is a shift in the distributions' location, with respect to the unconditioned air chamber specimens, for G* and G*/sin(δ) after water saturation. In general, binders with 20% hydrated lime are statistically different when comparing environmental test conditions.

**Table 4.8 Results of Hydrated Lime Comparisons Grouped by Percentage of Filler**

| | | 5% Lime | 10% Lime | 20% Lime |
|---|---|---|---|---|
| **Unconditioned Water Bath Vs. Conditioned** | **Complex Modulus** | Not Rejected | Not Rejected | ***Reject*** |
| | **G*/ sin(δ)** | Not Rejected | Not Rejected | ***Reject*** |
| **Unconditioned Water Bath Vs. Unconditioned** | **Complex Modulus** | Not Rejected | Not Rejected | Not Rejected |
| | **G*/ sin(δ)** | Not Rejected | Not Rejected | ***Reject*** |
| **Conditioned Water Bath Vs. Conditioned** | **Complex Modulus** | ***Reject*** | Not Rejected | ***Reject*** |
| | **G*/ sin(δ)** | ***Reject*** | Not Rejected | ***Reject*** |
| **Unconditioned Air Chamber Vs. Conditioned** | **Complex Modulus** | ***Reject*** | ***Reject*** | Not Rejected |
| | **G*/ sin(δ)** | ***Reject*** | ***Reject*** | ***Reject*** |
| **Conditioned Water Bath Vs. Unconditioned** | **Complex Modulus** | ***Reject*** | ***Reject*** | ***Reject*** |
| | **G*/ sin(δ)** | ***Reject*** | ***Reject*** | ***Reject*** |

Table 4.9 summarizes the results of comparisons by site, filler type, and percentage of filler. As with the comparisons for the original binders by site, most of the

results indicate that the environmental testing conditions yield different G* and G*/sin(δ) measurements.

Since the comparisons indicate that there are significant statistical differences between test condition measurements of G* and G*/sin(δ), the raw data was examined to determine if the addition of hydrated lime was beneficial, detrimental, or had little affect on the G* and G*/sin(δ) measurements. This was a twofold process where the minimum Superpave requirements were applied and then a comparison between the original binder results and hydrated lime results commenced.

All of the binders with hydrated lime met the Superpave minimum requirement for G*/sin(δ). However, G*/sin(δ) values did tend to increase for the binders with hydrated lime. The increase in G*/sin(δ) could mean the filler changes to a higher temperature grade, thus enabling the binder to perform better in summer months. Also, a higher G*/sin(δ) for the materials tested in the water bath and/or saturated indicates that the hydrated lime is preventing moisture damage.

Table 4.10 displays the results of calculating the G*/sin(δ) ratio of hydrated lime to original binders. The values close to 1 indicate that little change occurred and is neither beneficial nor detrimental. Values less than 1, displayed in bold in the table, indicate binders that performed poorly with the hydrated lime when compared with the performance of the binder without hydrated lime. In most cases, the values were greater than 1, which indicates that the hydrated lime improved the performance and resistance to moisture damage. The ratio increases with an increasing percentage of hydrated lime for all but four binders. This increase in the ratio indicates that the hydrated lime is improving the rut resistance of a binder.

## Table 4.9 Results of Hydrated Lime Comparing Testing Conditions

| | | | Unconditioned Water Bath vs Saturated Water Bath | | Unconditioned Water Bath vs Unconditioned Air Chamber | | Saturated Water Bath vs Saturated Air Chamber | | Unconditioned Air Chamber vs Saturated Air Chamber | | Saturated Water Bath vs Unconditioned Air Chamber | |
|---|---|---|---|---|---|---|---|---|---|---|---|---|
| Site | Mastic | Percentage | Complex Modulus | G*/ sin(delta) | Complex Modulus | G*/ sin(delta) | Complex Modulus | G*/ sin(delta) | Complex Modulus | G*/ sin(delta) | Complex Modulus | G*/ sin(delta) |
| Ann Arbor | Lime | 5 | Reject | Reject | Reject | Reject | Reject | Reject | Reject | Reject | Reject | Reject |
| Battle Creek | Lime | 5 | Reject | Reject | Reject | Reject | Reject | Reject | Reject | Reject | Not Rejected | Not Rejected |
| Brighton | Lime | 5 | Reject | Reject | Reject | Reject | Reject | Reject | Reject | Reject | Reject | Reject |
| Clarkston | Lime | 5 | Reject | Reject | Reject | Reject | Reject | Reject | Reject | Reject | Reject | Reject |
| Detroit | Lime | 5 | Reject | Reject | Reject | Reject | Reject | Reject | Reject | Reject | Reject | Not Rejected |
| Dundee 19.0mm NMAS | Lime | 5 | Reject | Reject | Reject | Reject | Reject | Reject | Reject | Reject | Reject | Reject |
| Dundee 12.5mm NMAS | Lime | 5 | Reject | Reject | Reject | Reject | Reject | Reject | Reject | Reject | Reject | Reject |
| Grand Rapids M-45 | Lime | 5 | Reject | Reject | Reject | Reject | Reject | Reject | Reject | Reject | Reject | Reject |
| Grand Rapids I-196 | Lime | 5 | Reject | Reject | Reject | Reject | Reject | Reject | Reject | Reject | Reject | Reject |
| Hartland | Lime | 5 | Reject | Reject | Reject | Reject | Reject | Reject | Reject | Reject | Reject | Reject |
| Howell | Lime | 5 | Reject | Reject | Reject | Reject | Reject | Reject | Reject | Reject | Reject | Reject |
| Levering | Lime | 5 | Reject | Reject | Reject | Reject | Reject | Reject | Reject | Reject | Reject | Reject |
| Michigan Ave 19.0mm NMAS | Lime | 5 | Reject | Reject | Reject | Reject | Reject | Reject | Reject | Reject | Reject | Reject |
| Michigan Ave 12.5mm NMAS | Lime | 5 | Reject | Reject | Reject | Reject | Reject | Reject | Reject | Reject | Reject | Reject |
| Michigan International Speedway | Lime | 5 | Reject | Reject | Reject | Reject | Reject | Reject | Reject | Reject | Reject | Reject |
| Owosso | Lime | 5 | Reject | Reject | Reject | Reject | Reject | Reject | Reject | Reject | Reject | Reject |
| Pinckney | Lime | 5 | Reject | Reject | Not Rejected | Not Rejected | Reject | Reject | Reject | Reject | Reject | Reject |
| Saginaw | Lime | 5 | Reject | Reject | Reject | Reject | Reject | Reject | Reject | Reject | Reject | Reject |
| St. Johns | Lime | 5 | Reject | Reject | Reject | Reject | Reject | Reject | Reject | Reject | Reject | Reject |
| Toledo | Lime | 5 | Reject | Reject | Reject | Reject | Reject | Reject | Reject | Reject | Reject | Not Rejected |
| Van Dyke | Lime | 5 | Reject | Reject | Reject | Reject | Reject | Reject | Reject | Reject | Reject | Reject |
| Ann Arbor | Lime | 10 | Reject | Reject | Reject | Reject | Reject | Reject | Reject | Reject | Reject | Reject |
| Battle Creek | Lime | 10 | Reject | Reject | Reject | Reject | Reject | Reject | Reject | Reject | Reject | Reject |
| Brighton | Lime | 10 | Reject | Reject | Reject | Reject | Reject | Reject | Reject | Reject | Reject | Reject |
| Clarkston | Lime | 10 | Reject | Reject | Reject | Reject | Reject | Reject | Reject | Reject | Reject | Not Rejected |
| Detroit | Lime | 10 | Reject | Reject | Reject | Reject | Reject | Reject | Reject | Reject | Reject | Reject |
| Dundee 19.0mm NMAS | Lime | 10 | Not Rejected | Not Rejected | Reject | Reject | Reject | Reject | Reject | Reject | Reject | Reject |
| Dundee 12.5mm NMAS | Lime | 10 | Reject | Reject | Reject | Reject | Reject | Reject | Reject | Reject | Reject | Reject |
| Grand Rapids M-45 | Lime | 10 | Reject | Reject | Reject | Reject | Not Rejected | Not Rejected | Reject | Reject | Reject | Reject |
| Grand Rapids I-196 | Lime | 10 | Reject | Reject | Reject | Reject | Reject | Reject | Reject | Reject | Reject | Reject |
| Hartland | Lime | 10 | Reject | Reject | Reject | Reject | Reject | Reject | Reject | Reject | Reject | Reject |
| Howell | Lime | 10 | Reject | Reject | Reject | Reject | Reject | Reject | Reject | Reject | Reject | Reject |
| Levering | Lime | 10 | Reject | Reject | Reject | Reject | Reject | Reject | Reject | Reject | Reject | Reject |
| Michigan Ave 19.0mm NMAS | Lime | 10 | Reject | Reject | Reject | Reject | Reject | Reject | Reject | Reject | Reject | Reject |
| Michigan Ave 12.5mm NMAS | Lime | 10 | Reject | Reject | Reject | Reject | Reject | Reject | Reject | Reject | Reject | Reject |
| Michigan International Speedway | Lime | 10 | Reject | Reject | Reject | Reject | Reject | Reject | Reject | Reject | Reject | Reject |
| Owosso | Lime | 10 | Reject | Reject | Reject | Reject | Reject | Reject | Reject | Reject | Reject | Reject |
| Pinckney | Lime | 10 | Reject | Reject | Reject | Reject | Reject | Reject | Reject | Reject | Reject | Reject |
| Saginaw | Lime | 10 | Reject | Reject | Not Rejected | Not Rejected | Reject | Reject | Reject | Reject | Reject | Reject |
| St. Johns | Lime | 10 | Reject | Reject | Reject | Reject | Reject | Reject | Reject | Reject | Reject | Reject |
| Toledo | Lime | 10 | Reject | Reject | Reject | Reject | Reject | Reject | Reject | Reject | Reject | Reject |
| Van Dyke | Lime | 10 | Reject | Reject | Reject | Reject | Reject | Reject | Reject | Reject | Reject | Reject |
| Ann Arbor | Lime | 20 | Reject | Reject | Reject | Reject | Reject | Reject | Reject | Reject | Reject | Reject |
| Battle Creek | Lime | 20 | Reject | Reject | Reject | Reject | Reject | Reject | Reject | Reject | Reject | Reject |
| Brighton | Lime | 20 | Not Rejected | Not Rejected | Reject | Reject | Reject | Reject | Reject | Reject | Reject | Reject |
| Clarkston | Lime | 20 | Reject | Reject | Reject | Reject | Reject | Reject | Reject | Reject | Reject | Reject |
| Detroit | Lime | 20 | Reject | Reject | Reject | Reject | Reject | Reject | Reject | Reject | Reject | Reject |
| Dundee 19.0mm NMAS | Lime | 20 | Reject | Reject | Reject | Reject | Reject | Reject | Reject | Reject | Reject | Reject |
| Dundee 12.5mm NMAS | Lime | 20 | Reject | Reject | Reject | Reject | Reject | Reject | Reject | Reject | Reject | Reject |
| Grand Rapids M-45 | Lime | 20 | Reject | Reject | Reject | Reject | Reject | Reject | Reject | Reject | Reject | Reject |
| Grand Rapids I-196 | Lime | 20 | Reject | Reject | Reject | Reject | Reject | Reject | Reject | Reject | Reject | Reject |
| Hartland | Lime | 20 | Reject | Reject | Reject | Reject | Reject | Reject | Reject | Reject | Reject | Reject |
| Howell | Lime | 20 | Reject | Reject | Reject | Reject | Reject | Reject | Reject | Reject | Reject | Reject |
| Levering | Lime | 20 | Reject | Reject | Reject | Reject | Reject | Reject | Reject | Reject | Reject | Reject |
| Michigan Ave 19.0mm NMAS | Lime | 20 | Reject | Reject | Reject | Reject | Reject | Reject | Reject | Reject | Reject | Reject |
| Michigan Ave 12.5mm NMAS | Lime | 20 | Reject | Reject | Reject | Reject | Reject | Reject | Reject | Reject | Reject | Reject |
| Michigan International Speedway | Lime | 20 | Reject | Reject | Not Rejected | Not Rejected | Reject | Reject | Reject | Reject | Reject | Reject |
| Owosso | Lime | 20 | Reject | Reject | Reject | Reject | Reject | Reject | Reject | Reject | Reject | Reject |
| Pinckney | Lime | 20 | Reject | Reject | Reject | Reject | Reject | Reject | Reject | Reject | Reject | Reject |
| Saginaw | Lime | 20 | Reject | Reject | Reject | Reject | Reject | Reject | Reject | Reject | Reject | Reject |
| St. Johns | Lime | 20 | Reject | Reject | Reject | Reject | Reject | Reject | Reject | Reject | Reject | Reject |
| Toledo | Lime | 20 | Reject | Reject | Reject | Reject | Reject | Reject | Reject | Reject | Reject | Reject |
| Van Dyke | Lime | 20 | Reject | Reject | Reject | Reject | Not Rejected | Not Rejected | Reject | Reject | Reject | Reject |

## Table 4.10 Ratio G*/sin(δ) of Hydrated Lime to Original Binder

| | | | Averages Ratio of Hydrated Lime:Original Binder | | | |
|---|---|---|---|---|---|---|
| Site | Mastic | Percentage | WC | AC | WO | AO |
| Ann Arbor | Lime | 5 | 1.65 | 1.74 | 2.57 | 1.46 |
| Ann Arbor | Lime | 10 | 7.99 | 2.51 | 3.39 | 2.06 |
| Ann Arbor | Lime | 20 | 3.66 | 2.79 | 3.95 | 2.09 |
| Battle Creek | Lime | 5 | 1.74 | 2.51 | 2.05 | **1.03** |
| Battle Creek | Lime | 10 | 1.67 | 3.22 | 2.16 | **0.92** |
| Battle Creek | Lime | 20 | 1.69 | 3.64 | 9.41 | 2.93 |
| Brighton | Lime | 5 | **0.60** | **0.89** | **0.69** | **0.87** |
| Brighton | Lime | 10 | **0.60** | **0.64** | **0.95** | 1.09 |
| Brighton | Lime | 20 | 1.31 | 1.03 | 1.32 | 1.83 |
| Clarkston | Lime | 5 | **0.86** | 5.00 | 2.42 | 1.31 |
| Clarkston | Lime | 10 | 1.02 | 2.42 | 2.41 | 1.33 |
| Clarkston | Lime | 20 | 1.58 | 3.39 | 5.02 | 2.61 |
| Detroit | Lime | 5 | 1.55 | 2.29 | 2.57 | 1.97 |
| Detroit | Lime | 10 | 1.82 | 2.71 | 3.27 | 2.96 |
| Detroit | Lime | 20 | 2.50 | 3.97 | 4.44 | 3.85 |
| Dundee 19.0mm NMAS | Lime | 5 | 3.97 | **0.86** | 1.88 | 1.11 |
| Dundee 19.0mm NMAS | Lime | 10 | **0.97** | 1.22 | 1.30 | 1.44 |
| Dundee 19.0mm NMAS | Lime | 20 | 1.61 | 1.61 | 1.93 | 2.56 |
| Dundee 12.5mm NMAS | Lime | 5 | **0.73** | 1.16 | 1.27 | 1.18 |
| Dundee 12.5mm NMAS | Lime | 10 | 1.19 | 2.42 | **0.97** | 1.95 |
| Dundee 12.5mm NMAS | Lime | 20 | 2.25 | 3.97 | 2.11 | 3.30 |
| Grand Rapids M-45 | Lime | 5 | **0.79** | **0.74** | 1.10 | **0.82** |
| Grand Rapids M-45 | Lime | 10 | **0.99** | **0.34** | 1.59 | **0.68** |
| Grand Rapids M-45 | Lime | 20 | 3.02 | **0.86** | 8.11 | 1.08 |
| Grand Rapids I-196 | Lime | 5 | 1.16 | 1.19 | 1.20 | **0.92** |
| Grand Rapids I-196 | Lime | 10 | 1.60 | 1.39 | 1.52 | 1.28 |
| Grand Rapids I-196 | Lime | 20 | 2.84 | 2.69 | 3.29 | 1.96 |
| Hartland | Lime | 5 | 2.80 | 1.65 | 1.63 | 2.20 |
| Hartland | Lime | 10 | 5.13 | 1.52 | 2.30 | 2.62 |
| Hartland | Lime | 20 | 18.39 | 2.33 | 3.41 | 4.52 |
| Howell | Lime | 5 | **0.66** | 1.18 | 1.68 | **0.93** |
| Howell | Lime | 10 | 1.07 | 1.19 | 0.88 | 1.06 |
| Howell | Lime | 20 | 1.39 | 2.17 | 4.37 | 1.91 |
| Levering | Lime | 5 | 2.04 | **0.73** | 1.67 | 1.83 |
| Levering | Lime | 10 | **0.71** | 1.93 | 2.42 | 2.31 |
| Levering | Lime | 20 | 1.66 | 2.28 | 3.41 | 2.97 |
| Michigan Ave 19.0mm NMAS | Lime | 5 | **0.70** | **0.74** | 1.17 | 1.19 |
| Michigan Ave 19.0mm NMAS | Lime | 10 | 1.05 | 1.47 | 1.37 | 2.04 |
| Michigan Ave 19.0mm NMAS | Lime | 20 | 2.02 | 0.94 | 1.66 | 2.54 |
| Michigan Ave 12.5mm NMAS | Lime | 5 | **0.42** | **0.66** | **0.20** | **0.67** |
| Michigan Ave 12.5mm NMAS | Lime | 10 | **0.57** | 1.10 | **0.29** | **0.79** |
| Michigan Ave 12.5mm NMAS | Lime | 20 | **0.50** | 1.35 | **0.36** | 1.26 |
| Michigan International Speedway | Lime | 5 | **0.73** | **0.91** | 2.04 | 2.48 |
| Michigan International Speedway | Lime | 10 | **0.88** | 1.40 | 3.19 | 2.31 |
| Michigan International Speedway | Lime | 20 | 2.96 | 1.55 | 4.71 | 3.82 |
| Owosso | Lime | 5 | 1.45 | 1.15 | **0.75** | 1.50 |
| Owosso | Lime | 10 | 1.45 | 1.19 | 1.17 | 2.82 |
| Owosso | Lime | 20 | 1.27 | 1.74 | 1.67 | 3.30 |
| Pinckney | Lime | 5 | 2.71 | 5.61 | 3.37 | 2.88 |
| Pinckney | Lime | 10 | 2.93 | 2.30 | 4.24 | 2.88 |
| Pinckney | Lime | 20 | 2.92 | **0.57** | 5.55 | 5.92 |
| Saginaw | Lime | 5 | 1.06 | **0.56** | 2.20 | 1.16 |
| Saginaw | Lime | 10 | 3.21 | **0.77** | 2.63 | 2.37 |
| Saginaw | Lime | 20 | **0.62** | **0.42** | 4.08 | 4.05 |
| St. Johns | Lime | 5 | 5.04 | 1.06 | **0.59** | 1.71 |
| St. Johns | Lime | 10 | 4.18 | 2.09 | 1.30 | 1.22 |
| St. Johns | Lime | 20 | 3.26 | 2.40 | 2.18 | 1.96 |
| Toledo | Lime | 5 | 2.27 | 1.76 | 2.69 | 2.16 |
| Toledo | Lime | 10 | 1.25 | 2.74 | 3.23 | 3.19 |
| Toledo | Lime | 20 | 4.82 | 3.00 | 6.36 | 3.77 |
| VanDyke | Lime | 5 | 3.67 | 1.37 | 2.41 | 1.92 |
| VanDyke | Lime | 10 | 18.18 | 1.73 | 3.50 | 3.52 |
| VanDyke | Lime | 20 | 5.25 | 2.34 | 6.14 | 4.46 |

WC= Conditioned Water Bath Specimens, WO= Unconditioned Water Bath Specimens,
AC= Conditioned Air Chamber Specimens, AO=Unconditioned Air Chamber Specimens

### 4.2.2.2 Effects of Silica

The second filler selected for determining the sensitivity of the new moisture susceptibility test was silica since siliceous materials are known to be moisture prone. The analysis conducted for the binders with hydrated lime were repeated for the binders with silica, as previously described in section 3.2.2.

Table 4.11 summarizes the results of comparisons conducted to determine if G* and G*/sin(δ) are statistically different when measured in dissimilar testing environments. As the table relates, almost all of the comparisons indicate that G* and G*/sin(δ) are not the same with the exception of the comparison between the unconditioned water bath and unconditioned air chamber. The results indicate that water saturation has a significant impact on G* and G*/sin(δ).

**Table 4.11 Results of Comparing Testing Conditions for Binders with Silica**

| | | 5% Silica | 10% Silica | 20% Silica |
|---|---|---|---|---|
| Unconditioned Water Bath Vs. Conditioned | Complex Modulus | Not Rejected | ***Reject*** | ***Reject*** |
| | G*/ sin(δ) | Not Rejected | ***Reject*** | Not Rejected |
| Unconditioned Water Bath Vs. Unconditioned | Complex Modulus | Not Rejected | Not Rejected | Not Rejected |
| | G*/ sin(δ) | Not Rejected | Not Rejected | Not Rejected |
| Conditioned Water Bath Vs. Conditioned | Complex Modulus | ***Reject*** | ***Reject*** | ***Reject*** |
| | G*/ sin(δ) | ***Reject*** | ***Reject*** | ***Reject*** |
| Unconditioned Air Chamber Vs. Conditioned | Complex Modulus | ***Reject*** | ***Reject*** | ***Reject*** |
| | G*/ sin(δ) | ***Reject*** | ***Reject*** | ***Reject*** |
| Conditioned Water Bath Vs. Unconditioned | Complex Modulus | ***Reject*** | ***Reject*** | ***Reject*** |
| | G*/ sin(δ) | ***Reject*** | ***Reject*** | ***Reject*** |

The comparison results between environmental testing condition measurements for G* and G*/ sin(δ) are displayed in Table 4.12. It can be seen that very few of the comparisons yield statistically equivalent results.

G*/ sin(δ) ratios of binders with silica to original binders were computed to determine any trends. The computed ratios are displayed in Table 4.13. Unlike the ratios computed with the hydrated lime filler, many of the binders with silica make only a small advantageous contribution if any at all. There are quite a few more silica results with a lower G*/ sin(δ) in comparison to the original binder G*/ sin(δ). Less than half of the binders exhibit an increasing ratio with increasing silica amounts.

All of the binders with silica met the minimum Superpave requirement of 1.0 kPa, but there were several that barely passed. A few of the binders that barely passed were originally well above the minimum requirement, thus indicating that attention should be paid to the interaction between aggregates and binders to prevent moisture damage.

A further analysis of the affects of silica on the moisture susceptibility of asphalt binders was conducted by comparing G*/sin(δ) of specific groupings. The first set of groupings compared conditioned specimens to unconditioned specimens within silica percentage, testing environment, and temperature. The ratio of G*/sin(δ) was used to determine the loss, if any, of G*/sin(δ) of moisture saturated specimens.

Table 4.14 summarizes the results of this first set of analyses. It can be seen that several groups exhibit a loss of G*/sin(δ) after moisture saturation, to ascertain whether or not the change is due to a viscous or elastic loss, G* and δ of the respective groups were examined. In all of the cases where there is a loss of G*/sin(δ) with moisture saturation, the viscous component decreases the most in comparison to the elastic component. The decrease in viscosity was the most extreme for the groups containing 10% silica. The loss in elasticity was only apparent in about half of the groups and was slight. Binders with 20% and 5% silica exhibited the greatest decrease in elasticity.

**Table 4.12 Results of Comparing Testing Conditions of Binders with Silica by Site**

| | | | Unconditioned Water Bath vs. Conditioned Water Bath | | Unconditioned Water Bath vs. Unconditioned Air Chamber | | Conditioned Water Bath vs. Conditioned Air Chamber | | Unconditioned Air Chamber vs. Conditioned Air Chamber | | Conditioned Water Bath vs. Unconditioned Air Chamber | |
|---|---|---|---|---|---|---|---|---|---|---|---|---|
| Site | Mastic | Percentage | Complex Modulus | G*/ sin(δ) | Complex Modulus | G*/ sin(delta) | Complex Modulus | G*/ sin(delta) | Complex Modulus | G*/ sin(delta) | Complex Modulus | G*/ sin(delta) |
| Ann Arbor | Silica | 5 | Reject | Reject | Reject | Reject | Reject | Reject | Reject | Reject | Reject | Reject |
| Battle Creek | Silica | 5 | Reject | Reject | Reject | Reject | Reject | Reject | Reject | Reject | Reject | Reject |
| Brighton | Silica | 5 | Reject | Reject | Reject | Reject | Reject | Reject | Reject | Reject | Reject | Reject |
| Clarkston | Silica | 5 | Reject | Reject | Reject | Reject | Reject | Reject | Reject | Reject | Reject | Reject |
| Detroit | Silica | 5 | Reject | Reject | Reject | Reject | Reject | Reject | Reject | Reject | Reject | Not Rejected |
| Dundee 19.0mm NMAS | Silica | 5 | Reject | Reject | Reject | Reject | Reject | Reject | Reject | Reject | Reject | Reject |
| Dundee 12.5mm NMAS | Silica | 5 | Reject | Reject | Reject | Reject | Reject | Reject | Reject | Reject | Reject | Reject |
| Grand Rapids M-45 | Silica | 5 | Reject | Reject | Reject | Reject | Not Rejected | Not Rejected | Reject | Reject | Reject | Reject |
| Grand Rapids I-196 | Silica | 5 | Reject | Reject | Not Rejected | Not Rejected | Reject | Reject | Reject | Reject | Reject | Reject |
| Hartland | Silica | 5 | Reject | Reject | Reject | Reject | Reject | Reject | Reject | Reject | Reject | Reject |
| Howell | Silica | 5 | Reject | Reject | Reject | Reject | Reject | Reject | Reject | Reject | Reject | Reject |
| Levering | Silica | 5 | Reject | Reject | Reject | Reject | Reject | Reject | Reject | Reject | Reject | Reject |
| Michigan Ave 19.0mm NMAS | Silica | 5 | Reject | Reject | Reject | Reject | Reject | Reject | Reject | Reject | Reject | Reject |
| Michigan Ave 12.5mm NMAS | Silica | 5 | Reject | Reject | Reject | Reject | Reject | Reject | Reject | Reject | Reject | Reject |
| Michigan International Speedway | Silica | 5 | Reject | Reject | Reject | Reject | Reject | Reject | Reject | Reject | Reject | Reject |
| Owosso | Silica | 5 | Reject | Reject | Not Rejected | Not Rejected | Reject | Reject | Not Rejected | Not Rejected | Reject | Reject |
| Pinckney | Silica | 5 | Reject | Reject | Reject | Reject | Reject | Reject | Reject | Reject | Reject | Reject |
| Saginaw | Silica | 5 | Reject | Reject | Reject | Reject | Reject | Reject | Reject | Reject | Reject | Reject |
| St. Johns | Silica | 5 | Reject | Reject | Reject | Reject | Reject | Reject | Reject | Reject | Reject | Reject |
| Toledo | Silica | 5 | Reject | Reject | Reject | Reject | Not Rejected | Not Rejected | Reject | Reject | Reject | Reject |
| Van Dyke | Silica | 5 | Reject | Reject | Reject | Reject | Reject | Reject | Reject | Reject | Reject | Reject |
| Ann Arbor | Silica | 10 | Reject | Reject | Reject | Reject | Reject | Reject | Reject | Reject | Reject | Reject |
| Battle Creek | Silica | 10 | Reject | Reject | Reject | Reject | Reject | Reject | Reject | Reject | Reject | Reject |
| Brighton | Silica | 10 | Reject | Not Rejected | Reject | Reject | Reject | Reject | Reject | Reject | Reject | Reject |
| Clarkston | Silica | 10 | Reject | Reject | Reject | Reject | Reject | Reject | Reject | Reject | Reject | Reject |
| Detroit | Silica | 10 | Reject | Not Rejected | Reject | Not Rejected | Reject | Reject | Reject | Reject | Reject | Reject |
| Dundee 19.0mm NMAS | Silica | 10 | Reject | Reject | Reject | Reject | Reject | Reject | Reject | Reject | Reject | Reject |
| Dundee 12.5mm NMAS | Silica | 10 | Reject | Reject | Reject | Reject | Reject | Reject | Reject | Reject | Reject | Reject |
| Grand Rapids M-45 | Silica | 10 | Reject | Reject | Reject | Reject | Reject | Reject | Reject | Reject | Reject | Reject |
| Grand Rapids I-196 | Silica | 10 | Reject | Reject | Reject | Reject | Reject | Reject | Reject | Reject | Reject | Reject |
| Hartland | Silica | 10 | Reject | Reject | Reject | Reject | Reject | Reject | Reject | Reject | Reject | Reject |
| Howell | Silica | 10 | Reject | Reject | Reject | Reject | Reject | Reject | Reject | Reject | Reject | Reject |
| Levering | Silica | 10 | Reject | Reject | Reject | Reject | Reject | Reject | Reject | Reject | Reject | Reject |
| Michigan Ave 19.0mm NMAS | Silica | 10 | Reject | Reject | Reject | Reject | Reject | Reject | Reject | Reject | Reject | Reject |
| Michigan Ave 12.5mm NMAS | Silica | 10 | Reject | Reject | Reject | Reject | Reject | Reject | Reject | Reject | Reject | Reject |
| Michigan International Speedway | Silica | 10 | Reject | Reject | Reject | Reject | Reject | Reject | Reject | Reject | Not Rejected | Not Rejected |
| Owosso | Silica | 10 | Reject | Reject | Reject | Reject | Reject | Reject | Not Rejected | Reject | Reject | Reject |
| Pinckney | Silica | 10 | Reject | Reject | Reject | Reject | Reject | Reject | Reject | Reject | Reject | Reject |
| Saginaw | Silica | 10 | Reject | Reject | Reject | Reject | Reject | Reject | Reject | Reject | Reject | Reject |
| St. Johns | Silica | 10 | Reject | Reject | Reject | Reject | Reject | Reject | Reject | Reject | Reject | Reject |
| Toledo | Silica | 10 | Reject | Not Rejected | Reject | Reject | Reject | Reject | Reject | Reject | Reject | Reject |
| Van Dyke | Silica | 10 | Reject | Reject | Not Rejected | Not Rejected | Reject | Reject | Reject | Reject | Reject | Reject |
| Ann Arbor | Silica | 20 | Reject | Reject | Reject | Reject | Reject | Reject | Not Rejected | Not Rejected | Reject | Reject |
| Battle Creek | Silica | 20 | Reject | Reject | Reject | Reject | Reject | Reject | Reject | Reject | Reject | Reject |
| Brighton | Silica | 20 | Reject | Reject | Reject | Reject | Reject | Reject | Reject | Reject | Reject | Reject |
| Clarkston | Silica | 20 | Reject | Reject | Reject | Reject | Reject | Reject | Reject | Reject | Reject | Reject |
| Detroit | Silica | 20 | Reject | Reject | Reject | Reject | Reject | Reject | Reject | Reject | Reject | Reject |
| Dundee 19.0mm NMAS | Silica | 20 | Reject | Reject | Reject | Reject | Reject | Reject | Reject | Reject | Reject | Reject |
| Dundee 12.5mm NMAS | Silica | 20 | Reject | Reject | Reject | Reject | Reject | Reject | Reject | Reject | Reject | Reject |
| Grand Rapids M-45 | Silica | 20 | Reject | Reject | Reject | Reject | Reject | Reject | Reject | Reject | Reject | Reject |
| Grand Rapids I-196 | Silica | 20 | Reject | Reject | Not Rejected | Not Rejected | Reject | Reject | Reject | Reject | Reject | Reject |
| Hartland | Silica | 20 | Reject | Reject | Reject | Reject | Reject | Reject | Reject | Reject | Reject | Reject |
| Howell | Silica | 20 | Not Rejected | Not Rejected | Reject | Reject | Reject | Reject | Reject | Reject | Reject | Reject |
| Levering | Silica | 20 | Reject | Reject | Reject | Reject | Reject | Reject | Reject | Reject | Reject | Reject |
| Michigan Ave 19.0mm NMAS | Silica | 20 | Reject | Reject | Reject | Reject | Reject | Reject | Reject | Reject | Reject | Reject |
| Michigan Ave 12.5mm NMAS | Silica | 20 | Reject | Reject | Reject | Reject | Reject | Reject | Reject | Reject | Reject | Reject |
| Michigan International Speedway | Silica | 20 | Reject | Reject | Reject | Reject | Reject | Reject | Reject | Reject | Reject | Reject |
| Owosso | Silica | 20 | Reject | Reject | Reject | Reject | Reject | Reject | Reject | Reject | Reject | Reject |
| Pinckney | Silica | 20 | Reject | Reject | Not Rejected | Not Rejected | Reject | Reject | Reject | Reject | Reject | Reject |
| Saginaw | Silica | 20 | Reject | Reject | Reject | Reject | Reject | Reject | Reject | Reject | Reject | Reject |
| St. Johns | Silica | 20 | Reject | Reject | Reject | Reject | Reject | Reject | Reject | Reject | Reject | Reject |
| Toledo | Silica | 20 | Reject | Reject | Reject | Reject | Reject | Reject | Reject | Reject | Reject | Reject |
| Van Dyke | Silica | 20 | Reject | Reject | Reject | Reject | Reject | Reject | Reject | Reject | Reject | Reject |

## Table 4.13 G*/sin(δ) Ratio of Silica to Original Binder

| | | | Averages Ratio of Silica:Original Binder | | | |
|---|---|---|---|---|---|---|
| Site | Mastic | Percentage | WC | AC | WO | AO |
| *Ann Arbor* | *Silica* | *5* | 1.36 | 2.80 | 2.27 | 1.54 |
| *Ann Arbor* | *Silica* | *10* | 2.42 | 3.04 | 4.12 | 3.50 |
| *Ann Arbor* | *Silica* | *20* | 2.79 | 3.02 | 1.85 | 2.67 |
| *Battle Creek* | *Silica* | *5* | 1.29 | 2.08 | 1.90 | 1.93 |
| *Battle Creek* | *Silica* | *10* | 1.47 | 1.77 | 2.19 | 1.72 |
| *Battle Creek* | *Silica* | *20* | 1.99 | 2.15 | 2.63 | 2.16 |
| *Brighton* | *Silica* | *5* | **0.91** | **0.40** | **0.90** | **0.93** |
| *Brighton* | *Silica* | *10* | **0.64** | **0.65** | **0.67** | **0.89** |
| *Brighton* | *Silica* | *20* | **0.70** | **0.80** | **0.77** | **0.84** |
| *Clarkston* | *Silica* | *5* | **0.76** | 1.19 | **0.82** | **0.60** |
| *Clarkston* | *Silica* | *10* | 1.02 | 1.08 | **0.98** | 1.19 |
| *Clarkston* | *Silica* | *20* | 1.29 | 1.40 | **0.93** | 1.01 |
| *Detroit* | *Silica* | *5* | 1.53 | 1.79 | 6.40 | 1.97 |
| *Detroit* | *Silica* | *10* | 2.51 | 2.02 | 10.24 | 2.29 |
| *Detroit* | *Silica* | *20* | 1.80 | 2.36 | 2.82 | 2.71 |
| *Dundee 19.0mm NMAS* | *Silica* | *5* | **0.96** | **0.87** | **0.93** | 1.33 |
| *Dundee 19.0mm NMAS* | *Silica* | *10* | 1.14 | **0.92** | **0.98** | 1.08 |
| *Dundee 19.0mm NMAS* | *Silica* | *20* | 1.32 | 1.12 | 1.18 | 1.42 |
| *Dundee 12.5mm NMAS* | *Silica* | *5* | **0.78** | 3.68 | **0.65** | 1.53 |
| *Dundee 12.5mm NMAS* | *Silica* | *10* | 1.07 | 1.34 | **0.93** | 1.40 |
| *Dundee 12.5mm NMAS* | *Silica* | *20* | 1.47 | 1.12 | 1.11 | 1.62 |
| *Grand Rapids M-45* | *Silica* | *5* | 1.90 | **0.67** | **0.99** | **0.66** |
| *Grand Rapids M-45* | *Silica* | *10* | **0.78** | 1.05 | 1.01 | **0.68** |
| *Grand Rapids M-45* | *Silica* | *20* | **0.84** | **0.54** | **0.98** | 1.38 |
| *Grand Rapids I-196* | *Silica* | *5* | 1.14 | 3.82 | 1.39 | **0.94** |
| *Grand Rapids I-196* | *Silica* | *10* | 1.69 | 1.45 | 7.43 | 1.02 |
| *Grand Rapids I-196* | *Silica* | *20* | 1.89 | 1.57 | 2.33 | 1.62 |
| *Hartland* | *Silica* | *5* | 9.80 | 2.30 | 2.00 | 2.53 |
| *Hartland* | *Silica* | *10* | 2.44 | 2.49 | 1.05 | 2.43 |
| *Hartland* | *Silica* | *20* | 2.60 | 1.61 | 1.89 | 2.95 |
| *Howell* | *Silica* | *5* | **0.85** | 1.04 | 2.63 | **0.85** |
| *Howell* | *Silica* | *10* | **0.60** | **0.91** | 1.51 | 1.01 |
| *Howell* | *Silica* | *20* | **0.65** | 1.03 | **0.86** | 1.20 |
| *Levering* | *Silica* | *5* | 1.05 | **0.75** | 1.87 | 1.53 |
| *Levering* | *Silica* | *10* | 1.41 | **0.80** | 1.98 | 1.96 |
| *Levering* | *Silica* | *20* | 1.34 | **0.56** | 2.00 | 1.72 |
| *Michigan Ave 19.0mm NMAS* | *Silica* | *5* | **0.75** | **0.68** | **0.92** | 1.35 |
| *Michigan Ave 19.0mm NMAS* | *Silica* | *10* | **0.65** | **0.41** | **0.80** | 1.27 |
| *Michigan Ave 19.0mm NMAS* | *Silica* | *20* | **0.87** | 1.29 | 1.21 | 1.56 |
| *Michigan Ave 12.5mm NMAS* | *Silica* | *5* | **0.41** | **0.58** | **0.18** | **0.68** |
| *Michigan Ave 12.5mm NMAS* | *Silica* | *10* | **0.36** | **0.80** | **0.21** | **0.76** |
| *Michigan Ave 12.5mm NMAS* | *Silica* | *20* | **0.55** | **0.78** | **0.28** | **0.88** |
| *Michigan International Speedway* | *Silica* | *5* | **0.67** | 1.01 | 2.04 | 2.46 |
| *Michigan International Speedway* | *Silica* | *10* | 1.68 | 1.49 | 7.17 | 2.89 |
| *Michigan International Speedway* | *Silica* | *20* | **0.83** | 2.81 | 2.47 | 4.16 |
| *Owosso* | *Silica* | *5* | **0.88** | 1.00 | 1.06 | 1.78 |
| *Owosso* | *Silica* | *10* | **0.96** | 1.51 | 1.10 | 2.70 |
| *Owosso* | *Silica* | *20* | 1.07 | 2.16 | 1.02 | 3.07 |
| *Pinckney* | *Silica* | *5* | 4.30 | 2.02 | 8.77 | 2.16 |
| *Pinckney* | *Silica* | *10* | 3.70 | 1.95 | 3.65 | 4.02 |
| *Pinckney* | *Silica* | *20* | 6.03 | 7.71 | 3.57 | 3.12 |
| *Saginaw* | *Silica* | *5* | 1.01 | 1.66 | 2.18 | 2.25 |
| *Saginaw* | *Silica* | *10* | 1.79 | **0.47** | 2.87 | 3.04 |
| *Saginaw* | *Silica* | *20* | 1.16 | **0.70** | 2.99 | 3.76 |
| *St. Johns* | *Silica* | *5* | **0.92** | 1.91 | 1.02 | 0.99 |
| *St. Johns* | *Silica* | *10* | 1.73 | 1.95 | 1.11 | 0.88 |
| *St. Johns* | *Silica* | *20* | 1.82 | 3.09 | 1.36 | 3.61 |
| *Toledo* | *Silica* | *5* | 2.13 | 1.50 | 2.74 | 2.23 |
| *Toledo* | *Silica* | *10* | 2.53 | 2.15 | 2.39 | 2.68 |
| *Toledo* | *Silica* | *20* | 2.66 | 2.44 | 3.78 | 3.16 |
| *VanDyke* | *Silica* | *5* | 5.49 | 2.26 | 1.87 | 2.38 |
| *VanDyke* | *Silica* | *10* | 2.09 | 2.00 | 2.83 | 3.25 |
| *VanDyke* | *Silica* | *20* | 11.79 | 2.20 | 3.17 | 3.45 |

The second set of analyses examining the ratio of G*/sin(δ) compared environmental testing conditions. G*/sin(δ) computed from specimens tested in a water bath were divided by G*/sin(δ) values determined from specimens tested in an air chamber. The results of these comparisons are displayed in Table 4.14. The comparisons indicate that in most cases G*/sin(δ) measured from specimens tested in a water bath are less than those measured in an air chamber. The groupings exhibiting a loss in G*/sin(δ) were further investigated to determine if the decrease is due to a loss in the viscous or elastic component. In almost all cases where G*/sin(δ) decreases, the loss of elasticity is greater than the loss of viscosity. The viscosity decrease was greater than the elasticity loss for binders with 10% and 20% silica conditioned tested at 64˚C and 5% and 20% silica unconditioned tested at 58˚C.

**Table 4.14 Ratio of G*/sin(δ) Conditioned to Unconditioned Specimens**

| Percentage of Silica | Test Environment | Temperature | G*/sin(δ) Conditoned: Unconditioned |
|---|---|---|---|
| 5 | Air Chamber | 58 | 1.36 |
| | | 64 | 1.25 |
| | | All | 1.28 |
| | Water Bath | 58 | ***0.76*** |
| | | 64 | 1.06 |
| | | All | ***0.99*** |
| | All | All | 1.15 |
| 10 | Air Chamber | 58 | 2.71 |
| | | 64 | 1.36 |
| | | All | 1.65 |
| | Water Bath | 58 | ***0.84*** |
| | | 64 | ***0.71*** |
| | | All | ***0.73*** |
| | All | All | 1.14 |
| 20 | Air Chamber | 58 | 1.63 |
| | | 64 | 1.08 |
| | | All | 1.19 |
| | Water Bath | 58 | ***0.90*** |
| | | 64 | ***0.51*** |
| | | All | ***0.57*** |
| | All | All | ***0.84*** |

The most extreme comparison case for relating moisture damage was between the unconditioned air chamber samples and conditioned water bath samples. The G*/sin(δ) ratio computed for the extreme case are outlined in Table 4.16. The ratio analysis indicates that there is a loss of G*/sin(δ) after moisture saturation and water bath testing

for all classifications. In all cases the decrease in viscosity was greater than the reduction of elasticity. Proportionally, binders with 10% silica exhibited the greatest decline in viscosity compared to elasticity, followed by binders with 20% silica. The loss in viscosity indicates that the binder is more prone to causing rutting issues in HMA pavements. Determining which binders will exhibit a drastic change in viscosity in advance of its use allows for owner/agencies to replace the binder with a more moisture resistant binder, which is likely less expensive than adjusting the aggregate.

**Table 4.15 Ratio of G*/sin(δ) of Specimens Tested in a Water Bath to Those Tested in an Air Chamber**

| Percentage of Silica | Condition State | Temperature | G*/sin(δ) Water Bath: Air Chamber |
|---|---|---|---|
| 5 | Conditioned | 58 | *0.37* |
| | | 64 | *0.66* |
| | | All | *0.58* |
| | Unconditioned | 58 | *0.66* |
| | | 64 | *0.78* |
| | | All | *0.75* |
| 10 | Conditioned | 58 | *0.31* |
| | | 64 | *0.68* |
| | | All | *0.55* |
| | Unconditioned | 58 | 1.01 |
| | | 64 | 1.31 |
| | | All | 1.24 |
| 20 | Conditioned | 58 | *0.52* |
| | | 64 | *0.66* |
| | | All | *0.62* |
| | Unconditioned | 58 | *0.94* |
| | | 64 | 1.40 |
| | | All | 1.31 |

**Table 4.16 Ratio of G*/sin(δ) for Conditioned Water Bath Specimens Versus Unconditioned Air Chamber Specimens with Silica**

| Percentage of Silica | Temperature | G*/sin(δ) Conditioned Water Bath: Unconditioned Air Chamber |
|---|---|---|
| 5 | 58 | *0.85* |
| | 64 | *0.93* |
| | All | *0.91* |
| 10 | 58 | *0.84* |
| | 64 | *0.72* |
| | All | *0.74* |
| 20 | 58 | *0.50* |
| | 64 | *0.83* |
| | All | *0.74* |

### 4.2.2.3 Comparison of Hydrated Lime to Silica

The previous sections outlined the advantages and disadvantageous of the fillers detected by the new test method. This section summarizes a comparison of the sensitivity of the new test methods to the selected fillers. Figure 4.2 displays the variability of G*/sin(δ) with the data grouped by environmental testing condition (water bath or air chamber), condition status (unconditioned or saturated), filler percentage, and filler. The variability of the original binders is rather slight in comparison to many of the mastics.

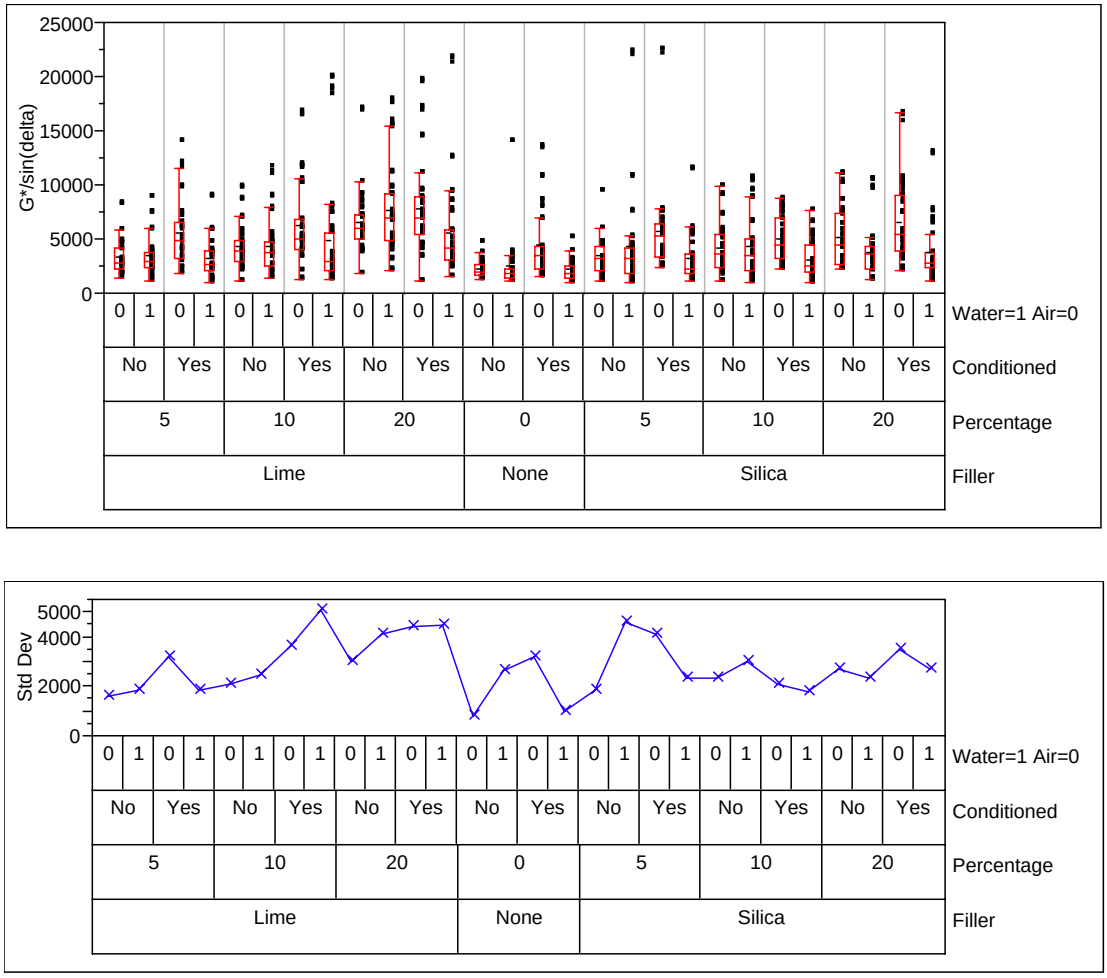


**Figure 4.2 Variability Plot of G*/sin(δ)**

Figure 4.3 illustrates the difference in mean G*/sin(δ) values for original binders grouped by testing environment and condition status. The mean G*/sin(δ) for unconditioned specimens tested in air is almost the same as the conditioned specimens tested in water. The unconditioned specimens tested in water were only slightly greater than the unconditioned specimens tested in air on average. The greatest difference can be seen with the conditioned specimens tested in air.

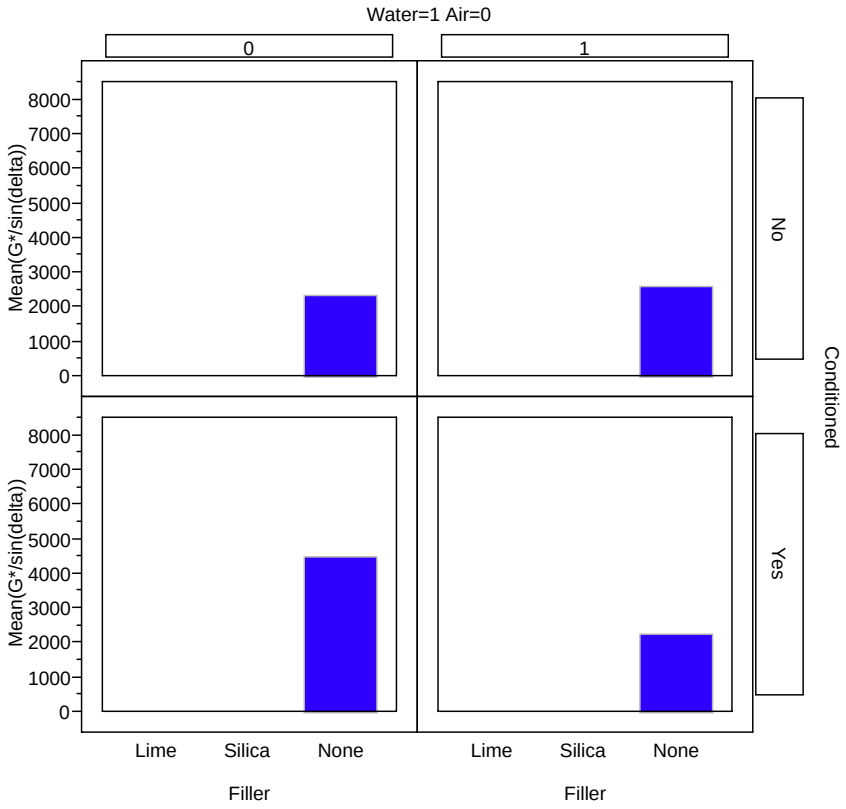


**Figure 4.3 Chart of Mean G*/sin(δ) for Neat Binders**

Figure 4.4 relates the G*/sin(δ) means for binders with 5% filler grouped by testing environment and condition status. Once again the unconditioned specimens tested in air and conditioned specimens tested in water yielded equivalent G*/sin(δ) means. Interestingly, the binders with silica yielded almost the same mean G*/sin(δ) as the binders with hydrated lime. As with the original binders, the conditioned specimens tested in air yielded the greatest average G*/sin(δ) values. Another possibility is that the saturation process leached out the lighter components of the asphalt binder. Specimens tested after conditioning were exposed to temperatures close to the PG high temperature for longer periods of time due to two test cycles in comparison to the unconditioned test specimens which only endure one test cycle. The difference between the air chamber conditioned specimens and the water bath conditioned specimens could be attributed to the water bath specimens not having an opportunity for the water logged specimens to

dry out, thus the moisture was allowed to soften the binder making it more prone to rutting. The most significant difference between mean G*/sin(δ) values for hydrated lime and silica occurs with the unconditioned specimens tested in water.

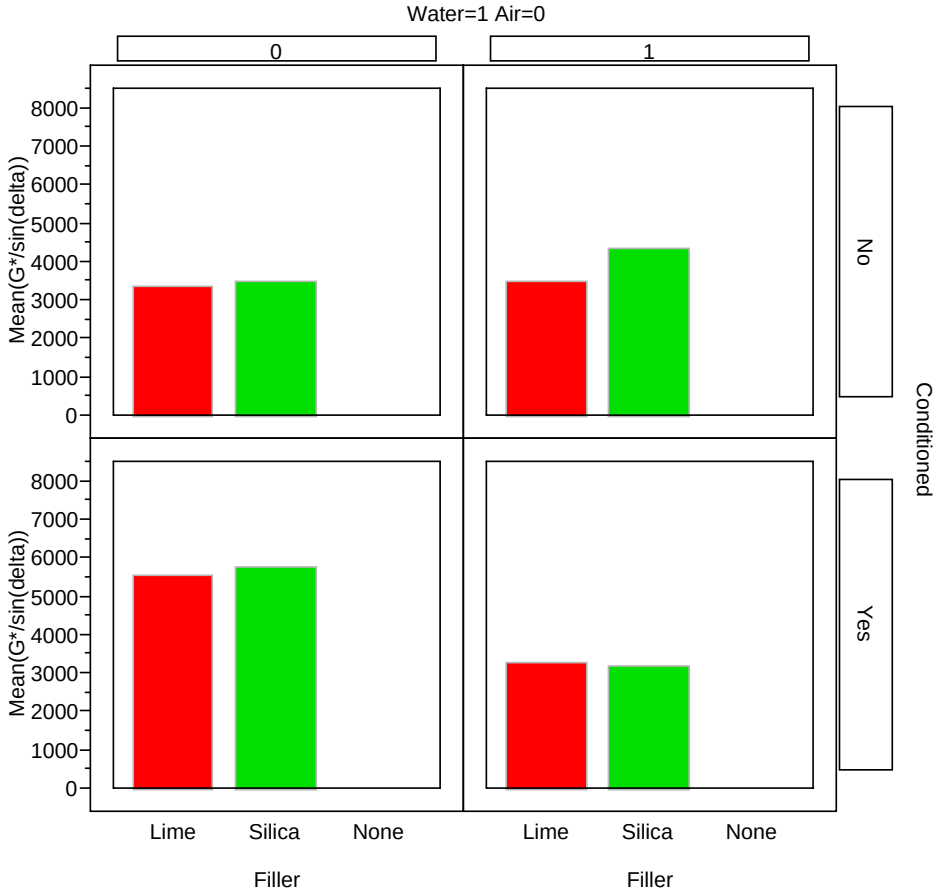


**Figure 4.4 Chart of Mean G*/sin(δ) of Binders with 5% Filler**

Figure 4.5 graphically summarizes the mean G*/sin(δ) values for binders with 10% filler grouped by testing environment and condition status. With 10% filler, on average, hydrated lime and silica unconditioned specimens tested in water or air are equivalent indicating that at 10% neither filler has a significant effect on the binders prior to moisture saturation. Substantial differences between hydrated lime and silica at 10% are seen for the conditioned specimens tested in either water or air.

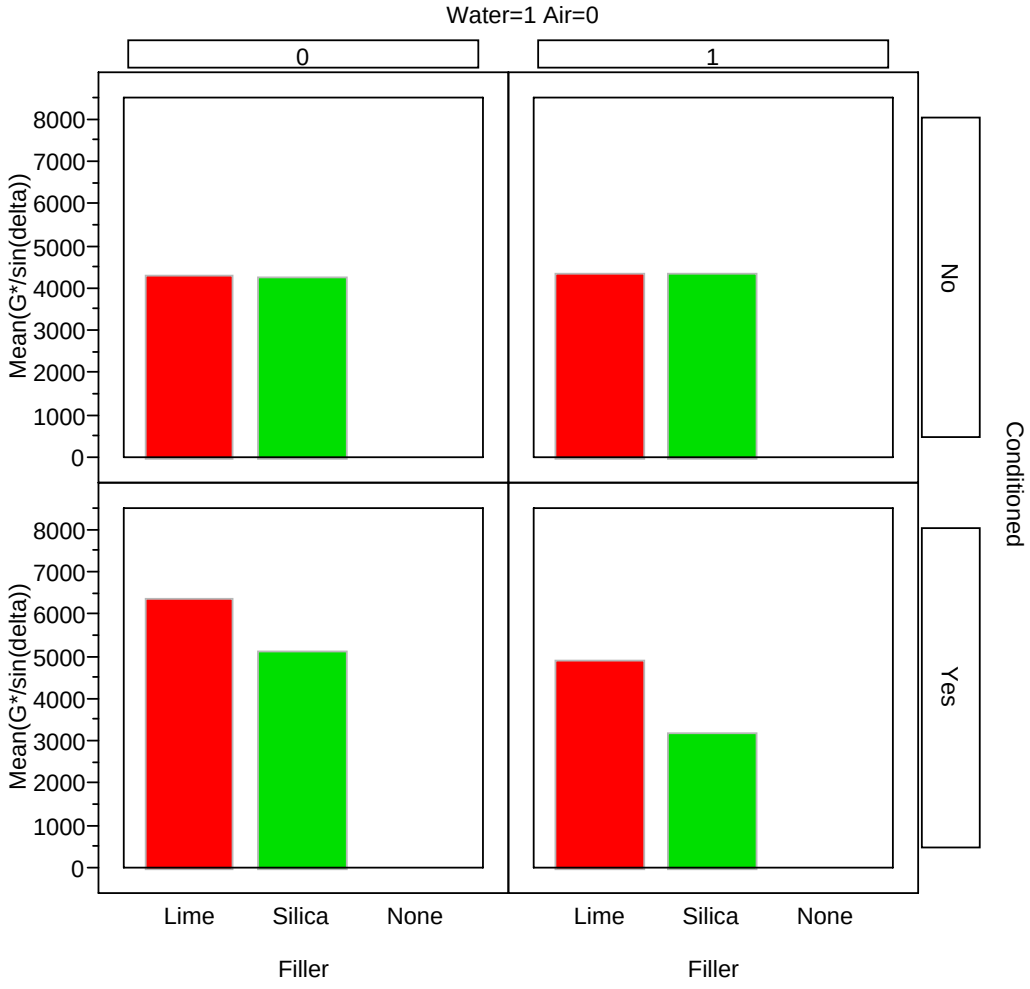


**Figure 4.5 Chart of Mean G*/sin(δ) of Binders with 10% Filler**

Figure 4.6 illustrates the mean G*/sin(δ) values for binders with 20% filler grouped by condition status and testing environment. It can be seen that for all four testing environment and conditioning combinations, on average, the hydrated lime specimens perform better than the binders with silica. The greatest difference occurs with the unconditioned specimens tested in water.

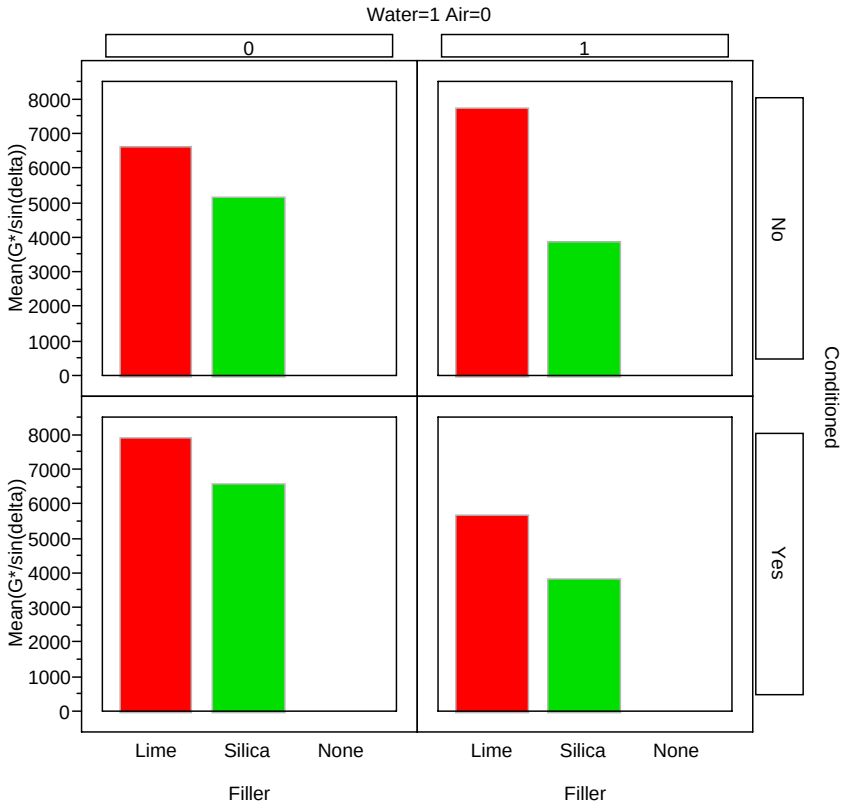


**Figure 4.6 Chart of Mean G*/sin(δ) of Binders with 20% Filler**

In general, Figures 4.4 through 4.6 relate that as the amount of filler increases the difference in G*/sin(δ) values between the two fillers becomes more pronounced. In comparing Figure 4.3, that of the original binders, to Figure 4.4 through Figure 4.6, it can also be seen that the addition of binder tends to slightly increase the G*/sin(δ) value in most cases, which reiterates what was seen in Table 4.10 and Table 4.13 where most of the ratios were greater than 1 for both fillers.

An Analysis of Variance (ANOVA) was conducted to determine which factors may be significant. Several variable combinations were examined, altering the variable entered into the analysis first. The analysis indicated that filler type, filler percentage, testing condition, and specimen conditioning are all significant factors contributing to changes in G*/sin(δ).

#### 4.2.2.4 Conclusions about Filler Effects

A new test method for determining moisture susceptibility was developed and this dissertation outlines the results of fillers on binders tested using the new method. The new method appears to be sensitive to the addition of fillers in binders and is able to distinguish between moisture susceptible fillers and non-moisture susceptible fillers. Interestingly, binders with hydrated lime did not always perform the best. This would indicate that hydrated lime cannot be used for all binders to deter moisture damage. Hydrated lime may not be chemically compatible with all binders for resisting moisture damage.

None of the binders examined in this dissertation failed the Superpave minimum criteria of $G^*/\sin(\delta)$ being at least 1.0 kPa, however several of the binders did exhibit degradation during testing. During the saturation process many of the binders maintained the original shape prior to saturation, however there were a few binders that tended to spread and even experienced the loss of small sections of binder. The binders which did tend to creep during saturation also emitted a visible oil sheen. Specimens displaying creep and oil sheens tended to yield $G^*/\sin(\delta)$ close to the Superpave minimum of 1.0 kPa indicating that perhaps the criteria should be re-evaluated if used for moisture susceptibility testing.

# Chapter 5 Development of Moisture Susceptibility Criterion for Asphalt Binders

Several moisture susceptibility tests exist for HMA pavements. For example, the modified Lottman test is often used to determine the moisture susceptibility of a mix. Unfortunately, attempts at establishing a moisture susceptible test for asphalt binders have been limited. Some studies have examined the moisture susceptibility of asphalt binders by determining chemical compositions that are known to be moisture prone (Roberts, 1991); however a definitive test based on these chemical analysis techniques has not evolved.

Research on the moisture susceptibility of binders has concentrated on chemical analysis, but there have been several tests adapted from other fields. Youtcheff and Aurilio (Youtcheff and Aurilio, 1997) adapted a procedure for a pneumatic adhesion tensile tester to test the bond strength of binders. The analysis of the results consists of observations of the amount of binder remaining on a substrate. Surface energies of binders have been evaluated by Cheng et al. (Cheng et al., 2002) using a universal sorption device and a Wilhelmy plate.

In a previous chapter, a new test method to determine the moisture susceptibility of asphalt binders was presented. In this chapter, a criterion for the newly developed test procedure with the modified DSR is presented. The binders selected were based on obtaining a variety of mixes used for the Northern Midwest climate. Two binders from SHRP were used in conjunction with the field obtained binders to establish a new criterion for asphalt binders using a modified DSR.

The proceeding sections outline a preliminary moisture susceptibility criterion for the newly developed moisture susceptibility test for asphalt binders. The proposed moisture criteria should be verified with field performance data prior to including in a test protocol.

## 5.1 Hypotheses

It was initially hypothesized that specimens tested in a water bath would yield differing asphalt binder measurements than those tested in a temperature controlled air chamber. Conditioned specimens were predicted to generate dissimilar asphalt binder measurements than unconditioned specimens. Since differences in asphalt binder measurements were anticipated, it was decided that specimens would not be identified as moisture susceptible simply because of divergences in asphalt binder readings for water bath tested, temperature controlled air chamber tested, unconditioned, or conditioned specimens. It was realized that a guideline for categorizing asphalt binders as either moisture susceptible or moisture resistant was needed that considered more than a difference between asphalt binder measurements. The following sections outline the development of a moisture susceptibility criterion for asphalt binders tested using a modified base plate and spindle in a DSR.

## 5.2 Asphalt Binder Criteria

When researchers established criteria for asphalt binder tests incorporated in the Superpave system a consensus of asphalt binder minimums was reached by an Expert Task Group. The minimum proposed by the Expert Task Group was verified by subsequent testing (Dongre, 2006). There was an initial inclination to only examine the change in the viscous component, but it was realized that the elastic component should be incorporated in the criteria system. The inclusion of both elastic and viscous components prompted the use of $G^*/\sin(\delta)$ in the Superpave criteria (Petersen et al., 1994). The minimum criterion established for unaged binders is that $G^*/\sin(\delta)$ exceeds 1.0 kPa.

The performance grade specification associated with the Superpave system was adapted for establishing a specification for surface treatments. Numerous Texas Department of Transportation (TxDOT) agencies completed surveys on distresses identified for surface treatments and rated the successfulness of certain surface treatments in the field. The information collected from the cooperating TxDOT agencies was used in conjunction with laboratory tests to altar the performance grade system established in Superpave (Barcena et al., 2002). Unfortunately, there is no available field data for the

materials researched for this study. However, the goal of was to base a criterion on material properties. The validity of the criterion should be evaluated with field data in the future.

## 5.3 Application of Superpave Asphalt Binder Criterion

The initial inclination was to determine if moisture was detrimental enough to change the performance grade of an asphalt binder. Since all of the binders tested with the modified DSR parts were unaged, the criterion that G*/sin(δ) exceed 1.0 kPa was applied to all binders tested. Original binders, hydrated lime treated binders, and silica treated binders all passed the minimum criterion that G*/sin(δ) surpass 1.0 kPa. It was noted however, that several of the filler treated binders were close to not meeting the minimum criterion.

Since the Superpave criterion for unaged binders did not identify moisture susceptible binders, another criterion was sought. It was concluded that a criterion similar to the Superpave system should be utilized. Thus, subsequent methods were employed to establish a new minimum criterion for binders established with modified DSR parts. Visual observations had indicated which asphalt binders were severely affected by moisture, but this only indicated that the Superpave criterion was not a satisfactory measure and a new guideline needed to be established.

## 5.4 Asphalt Binder Absorption Analysis

The next attempt at establishing a minimum criterion evaluated the amount of water absorbed by an asphalt binder. A ranking system would be established to rate the moisture attraction of an asphalt binder. All hydrated lime modified and silica modified binders were examined for water absorption tendency. The filler modified binders were used in lieu of original binders to analyze if more water is absorbed for binders with silica than those with hydrated lime.

### 5.4.1 Absorption Evaluation Procedure

The 25mm DSR molds were used for making asphalt binder specimens since the original binders tested employed 25mm molds. Binders were poured into molds and allowed to

rest for 10 minutes. After 10 minutes, an asphalt specimen was placed on a piece of plastic wrap to prevent a sample from sticking to the water bath. The weight of the plastic wrap and asphalt specimen was recorded. The sample was then placed in a 25˚C water bath. Glass rods were placed on the plastic wrap to keep the asphalt binder submerged. Care was taken to ensure the glass rod did not come in contact with an asphalt binder specimen. After 2 minutes, 3 minutes, 24 hours, and 48 hours, asphalt binder specimens were weighed and weights recorded. Three replicate samples were used for each binder, filler, and filler percentage.

### 5.4.2 Absorption Evaluation Results

Data collected pertained to the weight of each specimen after four soak time intervals. Each saturation weight was divided by the original weight to yield a percent difference in weight (PDW). The PDWs within a binder group were compared to determine if there were significant differences between the four soak times. Tukey's was used to compare the mean weights with a confidence level of 95%. Three-way ANOVA was conducted to evaluate the recorded weights of the binder specimens. The ANOVA indicated that filler percentage and soak time affect the weight of a specimen while filler type has no significant effect.,

Twenty of the original twenty-one binders were evaluated. Both silica and hydrated lime binders were utilized in the water absorption testing. The majority of binders gained a significant amount of weight after 48 hours of saturation in comparison to 2 minutes of saturation. However, 17 of the binders did not exhibit significant weight gain after 48 hours of saturation. Table 5.1 summarizes the mean comparisons of weight data. Six binders retained their initial weights with both filler blends. These binders were not affected by the moisture prone silica, thus implying that these binders would be durable in an area with a significant amount of moisture. These six binders are Ann Arbor, Brighton, Clarkston, Dundee 12.5mm NMAS, Levering, and Van Dyke

**Table 5.1 Mean Comparison of Specimen Weights after Saturation**

| Binder | Filler | Saturation Time | | | | Moisture Susceptible |
|---|---|---|---|---|---|---|
| | | 2 Minutes | 3 Minutes | 24 Hours | 48 Hours | |
| Ann Arbor | *Silica* | A B | A | B | A B | **No** |
| | *Hydrated Lime* | A | A | A | A | **No** |
| Battle Creek | *Silica* | B | B | A | A | Yes |
| | *Hydrated Lime* | B | B | A | A | Yes |
| Brighton | *Silica* | A | A | A | A | **No** |
| | *Hydrated Lime* | A | A | A | A | **No** |
| Clarkston | *Silica* | A B | A | B | A B | **No** |
| | *Hydrated Lime* | A B | A | A B | A | **No** |
| Detroit | *Silica* | B | B | B | A | Yes |
| | *Hydrated Lime* | B | B | B | A | Yes |
| Dundee 19.0mm NMAS | *Silica* | A | A | A | A | **No** |
| | *Hydrated Lime* | B | A B | A B | A | Yes |
| Dundee 12.5mm NMAS | *Silica* | A | A | A | A | **No** |
| | *Hydrated Lime* | A | A | A | A | **No** |
| Grand Rapids M-45 | *Silica* | B | A B | A B | A | Yes |
| | *Hydrated Lime* | B | A B | A B | A | Yes |
| Hartland | *Silica* | B | B | A | A | Yes |
| | *Hydrated Lime* | B | B | A | A | Yes |
| Howell | *Silica* | B | B | A B | A | Yes |
| | *Hydrated Lime* | B | B | A | A | Yes |
| Levering | *Silica* | A B | A | B | A B | **No** |
| | *Hydrated Lime* | A | A | A | A | **No** |
| Michigan Ave 19.0mm NMAS | *Silica* | B | B | B | A | Yes |
| | *Hydrated Lime* | B | A B | A | A B | **No** |
| Michigan Ave 12.5mm NMAS | *Silica* | B | B | B | A | Yes |
| | *Hydrated Lime* | B | B | B | A | Yes |
| Michigan International Speedway US-12 | *Silica* | B | A B | B | A | Yes |
| | *Hydrated Lime* | A | A | A | A | **No** |
| Owosso | *Silica* | B | B | B | A | Yes |
| | *Hydrated Lime* | B | B | B | A | Yes |
| Pinckney | *Silica* | B | B | A | B | **No** |
| | *Hydrated Lime* | B | B | B | A | Yes |
| Saginaw | *Silica* | B | B | B | A | Yes |
| | *Hydrated Lime* | A B | A B | B | A | **No** |
| St Johns | *Silica* | B | B | A | A | Yes |
| | *Hydrated Lime* | B | A B | A B | A | Yes |
| Toledo | *Silica* | B | B | A | A | Yes |
| | *Hydrated Lime* | B | B | A | A | Yes |
| Van Dyke | *Silica* | A | A | A | A | **No** |
| | *Hydrated Lime* | A | A | A | A | **No** |

.

### 5.4.3 Water Absorbed Standard Deviation Analysis

The previous subsections summarized individual results of mean comparisons which related absorbing or weight loss tendencies of various asphalt binders. The significance of these differences will be examined in this section, using a Tukey's mean comparison and one standard deviation as criteria. Two methods were examined to see if significant

differences arise. For Tukey's mean comparison, if the mean weight of binder samples is significantly different after 48 hours in comparison to after 2 minutes, a binder will be considered prone to moisture absorption. If data is outside of one standard deviation it will be deemed moisture prone while data within one standard deviation will indicate a binder that does not tend to absorb water. Since the majority of significant weight gains were found after 24 and 48 hours of saturation, only those time intervals will be considered in this section. The data analyzed was the 24 and 48 hour weights divided by the original weight of the asphalt sample. A standard deviation of 0.02 was used for determining the significance of water absorbed.

Mean comparisons using Tukey's method were conducted on data grouped by site, filler type, and filler percentage. A confidence level of 95% was assumed. Many binder sample groups did not have statistically different weights at 48 hours and 2 minutes of soak time. However, there were a few that did increase in weight as the soak time increased. The results of mean comparisons are displayed in Table 5.2. Binders with 10% silica tended to be the most prone to moisture absorption. Binders with either 20% silica or hydrated lime were the least prone to moisture absorption. The addition of hydrated lime to binder is known to aid in moisture resistance, therefore a low number of binders with hydrated lime prone to moisture absorption was expected. Since some binders gained significant weight at certain filler levels and not at others within a filler group another method for labeling moisture absorption was evaluated.

The second method considered for rating a binder's potential to gain a significant amount of weight was based on a universal standard deviation. Only one binder presented data outside of one standard deviation after 24 hours of saturation. There were several binders that were marginally contained within the one standard deviation limit. Oddly, the one binder that failed the criterion after 24 hours of saturation was the Ann Arbor binder with 5% silica. This was found to be peculiar since the Ann Arbor binders all passed the criterion after 48 hours of saturation. Possibly, the release of light ends after 48 hours of saturation was enough to lower the weight to within one standard deviation offsetting moisture absorption.

**Table 5.2 Summary of Mean Comparisons of Binder Weights**

| | 5% Silica | 10% Silica | 20% Silica | 5% Hydrated Lime | 10% Hydrated Lime | 20% Hydrated Lime |
|---|---|---|---|---|---|---|
| **Ann Arbor** | No Difference | No Difference | No Difference | No Difference | No Difference | No Difference |
| **Battle Creek** | No Difference | **Difference** | **Difference** | No Difference | **Difference** | No Difference |
| **Brighton** | No Difference | No Difference | No Difference | No Difference | No Difference | **Difference** |
| **Clarkston** | No Difference | No Difference | No Difference | No Difference | No Difference | **Difference** |
| **Detroit** | No Difference | No Difference | No Difference | **Difference** | No Difference | No Difference |
| **Dundee 19.0mm NMAS** | No Difference | No Difference | No Difference | **Difference** | No Difference | No Difference |
| **Dundee 12.5mm NMAS** | No Difference | No Difference | **Difference** | No Difference | No Difference | - |
| **Grand Rapids I-196** | - | No Difference | No Difference | - | No Difference | - |
| **Grand Rapids M-45** | No Difference | No Difference | No Difference | **Difference** | No Difference | No Difference |
| **Hartland** | No Difference | **Difference** | No Difference | **Difference** | No Difference | No Difference |
| **Howell** | No Difference | **Difference** | No Difference | **Difference** | No Difference | No Difference |
| **Levering** | No Difference | **Difference** | - | No Difference | **Difference** | - |
| **Michigan Ave 19.0mm NMAS** | **Difference** | **Difference** | No Difference | No Difference | No Difference | No Difference |
| **Michigan Ave 12.5mm NMAS** | **Difference** | **Difference** | No Difference | **Difference** | No Difference | No Difference |
| **Michigan International Speedway US-12** | No Difference | **Difference** | - | No Difference | - | - |
| **Owosso** | **Difference** | **Difference** | No Difference | No Difference | **Difference** | No Difference |
| **Pinckney** | No Difference | No Difference | No Difference | **Difference** | - | **Difference** |
| **Saginaw** | **Difference** | **Difference** | **Difference** | No Difference | No Difference | No Difference |
| **St. Johns** | **Difference** | No Difference | No Difference | No Difference | No Difference | No Difference |
| **Toledo** | No Difference | **Difference** | No Difference | No Difference | **Difference** | No Difference |
| **VanDyke** | No Difference | No Difference | No Difference | No Difference | No Difference | No Difference |

After 48 hours of saturation, nine binders exhibited data outside of one standard deviation. Like the analysis for the 24 hour saturation data, there were several binders that marginally met the one standard deviation criterion to be labeled as not prone

to significant water absorption. Table 5.3 summarizes the categorization of binders based on one standard deviation for data obtained after 48 hours of saturation.

**Table 5.3 Summary of Weights after 48 Hours of Soaking Within One Standard Deviation**

| All Data Within 1 Standard Deviation | All Data Not Within 1 Standard Deviation |
|---|---|
| Ann Arbor | Battle Creek |
| Clarkston | Brighton |
| Dundee 12.5mm NMAS | Detroit |
| Grand Rapids M-45 | Dundee 19.0mm NMAS |
| Michigan Ave 19.0mm NMAS | Hartland |
| Michigan Ave 12.5mm NMAS | Howell |
| Owosso | Levering |
| Saginaw | Michigan International Speedway |
| St. Johns | Pinckney |
| Toledo | |
| Vandyke | |

### 5.4.4 Water Absorption Conclusions

The previous subsections outlined the significance of mean weight gained by asphalt samples. The trends identified during mean weight comparisons offered useful information to understanding why some binders seemed to perform better than others during the DSR testing. It is felt that this particular method should not be used as a sole criterion for establishing the moisture susceptibility of a binder, but used in conjunction with other methods. This process is helpful in identifying binders that may be prone to absorbing water.

## 5.5 Viscous and Elastic Component Analysis

The final method used in conjunction with the previously mentioned methods in establishing a criterion for asphalt binders tested with modified DSR parts was an analysis of the change in viscous and elastic components of asphalt binders based on the different testing conditions.

The initial analysis only considered original binders. For each binder the viscous and elastic components were computed for unconditioned air chamber, unconditioned water bath, conditioned air chamber, and conditioned air chamber specimens. Viscous and elastic components were computed by using G* and δ data. The relationship between the viscous component, elastic component and G* can be illustrated as a right triangle. Figure 5.1 illustrates the relationships with reference to the complex shear modulus. Knowing this relationship allowed for basic geometry and trigonometry to be used to calculate the viscous and elastic components.

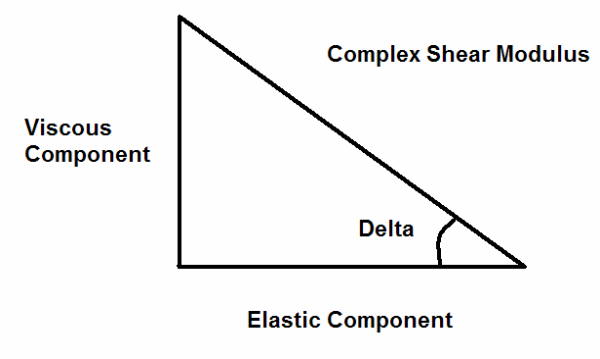


**Figure 5.1 Complex Shear Modulus**

The main difference considered was a contrast between conditioned water bath and unconditioned air chamber specimens. Differences were divided by an unconditioned air chamber sample to yield a percent change. Figure 5.2 illustrates the dispersion of the percent change of the viscous to elastic components for the comparison of unconditioned air chamber specimens to conditioned water bath specimens. Based on the dispersion, a four category ranking system was developed. Each section of a graph was labeled quandrant I, II, III, or IV. Quadrant I is the upper right corner where both the elastic and viscous components are positive. Quadrant II is the upper left corner. Quadrant III is the lower left corner. Quadrant IV is the lower right corner.

Binders in quadrant I were given a rank of 1, implying the most favorable asphalt binders since both the elastic and viscous properties increased with conditioning. Binders in quadrant II were ranked 2, these binder demonstrated a loss in the viscous component, but an improvement in elasticity. Quadrant III binders were given the rank of 3, these

binders exhibited a loss in both viscous and elastic properties. The level 3 binders were deemed the least favorable, fortunately only two original binders fell into this category. There were no data points in quadrant IV, loss in elastic component and gain in viscous component. The grey dashed lines represent one standard deviation above and below the normalized mean. The grey dotted line is the standard deviation limits for normalized viscous differences. The grey dashed and dotted line represents the standard deviation limits for normalized elastic differences. The standard deviations for normalized viscous and elastic components were calculated by pooling all of the data together.

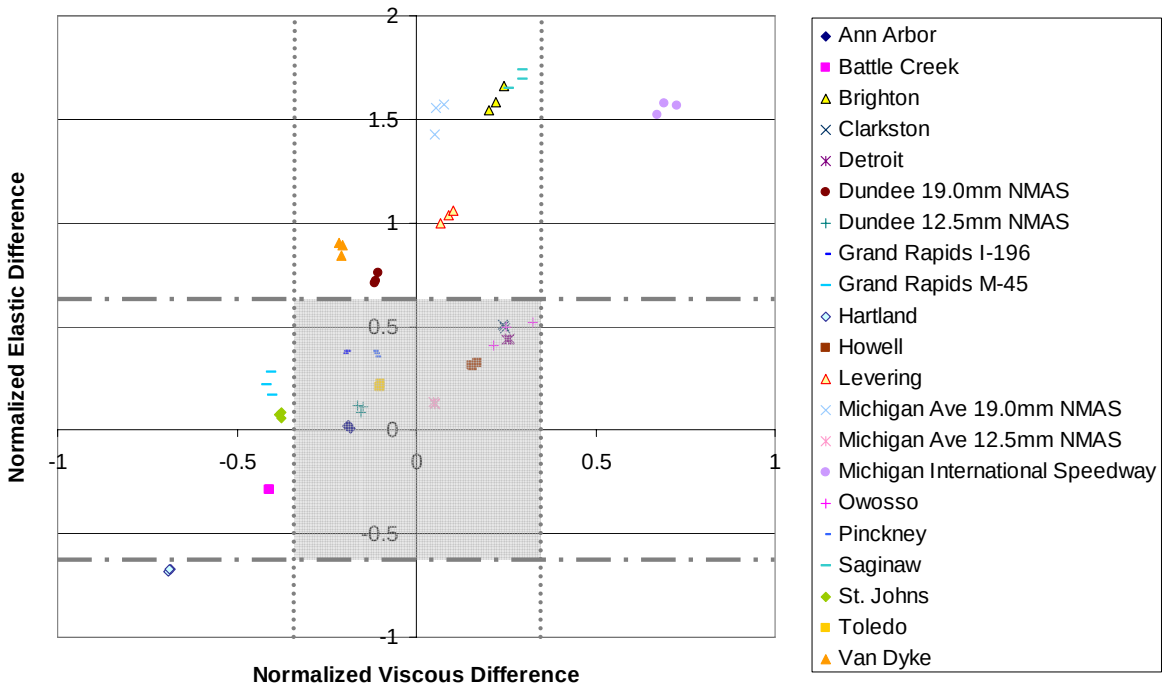


**Figure 5.2 Comparison of Elastic and Viscous Percent Changes for Original Binders**

Table 5.4 summarizes the binders which exist within one standard deviation, outside one standard deviation, and marginally within one standard deviation. Examining binders within one standard deviation allowed for the identification of binders which yielded drastic changes in elastic and viscous components. The marginal binders are binders that were either located on top of a standard deviation line or relatively close to one. From the table, it can be seen that about half of the binders responded quite differently than the other half. After examining the wide range in normalized elastic and viscous component

differences it was concluded that additional analysis was required to understand these differences.

**Table 5.4 Normalized Viscous and Component of Original Binders Standard Deviation Analysis Summary**

| Within 1 Standard Deviation | Marginal Binders | Outside 1 Standard Deviation |
|---|---|---|
| Ann Arbor | Clarkston | Brighton |
| Battle Creek | Dundee 19.0mm NMAS | Detroit |
| Dundee 12.5mm NMAS | Howell | Michigan Ave 19.0mm NMAS |
| Grand Rapids I-196 | Levering | Michigan Ave 12.5mm NMA |
| Grand Rapids M-45 | Owosso | Saginaw |
| Hartland | | VanDyke |
| Michigan International Speedway | | |
| Pinckney | | |
| Saginaw | | |
| St. Johns | | |
| Toledo | | |

An additional method of evaluating the normalized difference was employed to account for statistical noise associated with the data collected. Confidence ellipsoids were defined at a level of 95% for the normalized elastic and viscous component differences of each original binder. If the confidence ellipsoid existed completely in quadrant I and II, that binder would be considered not significantly affected by moisture. If the ellipsoid was in quadrant III, viscous and elastic components both decreased in value, then the binder was considered prone to moisture affects.

### 5.5.1 Ann Arbor

Figure 5.3 illustrates the relationship between the normalized differences for the elastic and viscous components. The confidence ellipsoid for Ann Arbor spans quadrants II and III. Since the ellipsoid overlaps into quadrant III, the binder collected from Ann Arbor is considered possibly prone to moisture susceptibility. The correlation between the elastic and viscous components is negative but strong, with a value of -0.8889. Figure 5.4 displays the dispersion of the elastic and viscous components by filler. The normalized component values increase drastically with increasing hydrated lime levels.

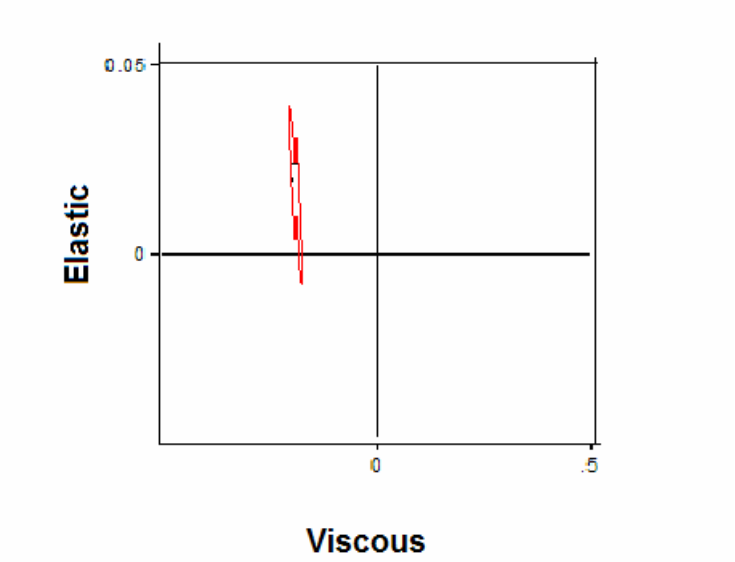


**Figure 5.3 Ann Arbor Confidence Ellipsoid**

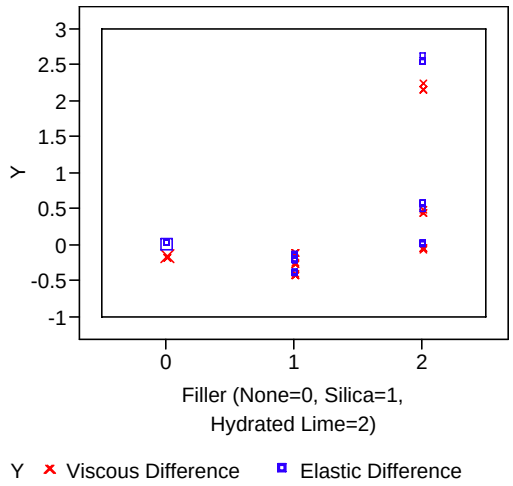


**Figure 5.4 Plot of Normalized Elastic and Viscous Differences**

### 5.5.2 Battle Creek

The confidence ellipsoid for the viscous and elastic components of the Battle Creek binder were extremely small since the changes in elastic and viscous components with

conditioning were small. Figure 5.5 illustrates the confidence ellipsoid obtained for the normalized differences of elastic and viscous components for Battle Creek. The correlation between the differences in elastic and viscous components was -0.9779. Figure 5.6 illustrates the range in normalized difference measurements. The original binder normalized differences are close fitting with little dispersion. Binder specimens with hydrated lime display the greatest dispersion, however hydrated lime modified binders are the only specimens which should show improvement with conditioning.

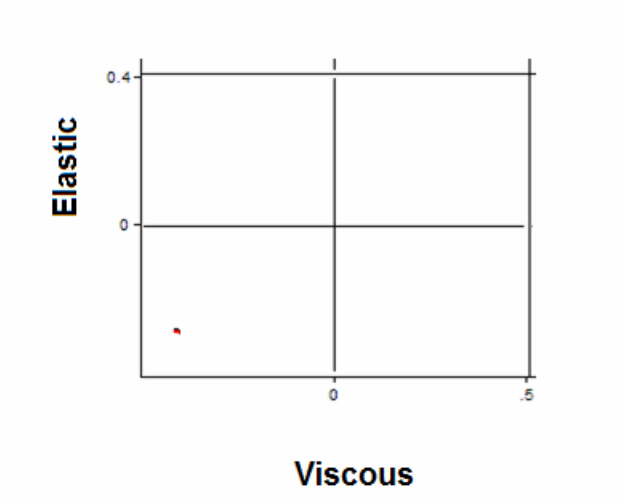


**Figure 5.5 Confidence Ellipsoid for Battle Creek Original Binder**

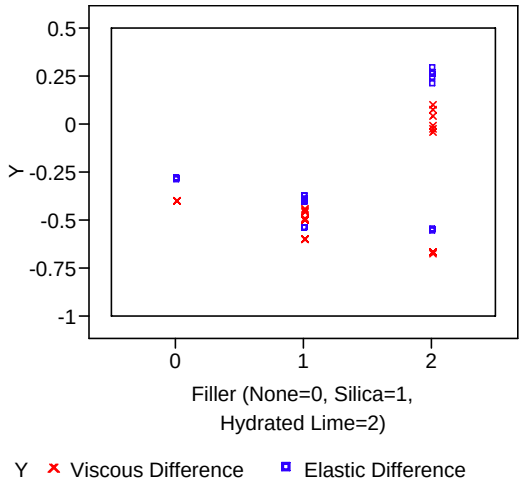


**Figure 5.6 Plot of Normalized Viscous and Elastic Differences for Battle Creek**

### 5.5.3 Brighton

The normalized elastic and viscous component differences are graphed along with a confidence ellipsoid in Figure 5.7. The figure showed that there is no overlap into an adjacent quadrant at a confidence level of 95%. The correlation between the normalized viscous and elastic differences is 0.9892. The range of values for the calculated normalized viscous and elastic component differences are displayed in Figure 5.8. The elastic component for original binders improves significantly, as can be seen in Figure 5.7.

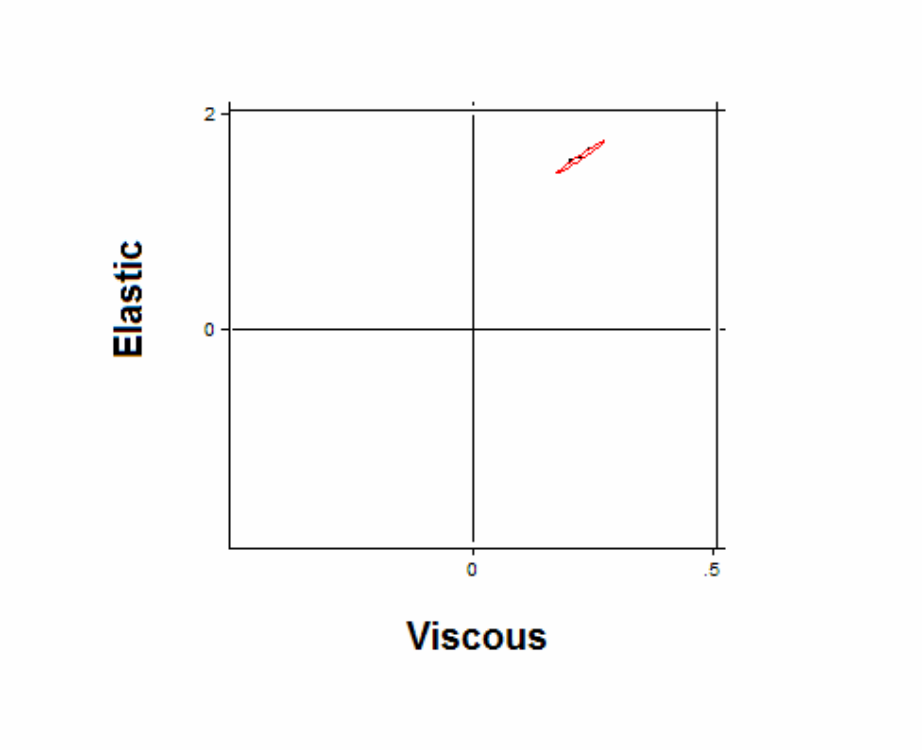


**Figure 5.7 Confidence Ellipsoid of Normalized Elastic and Viscous Differences of Brighton Original Binder**

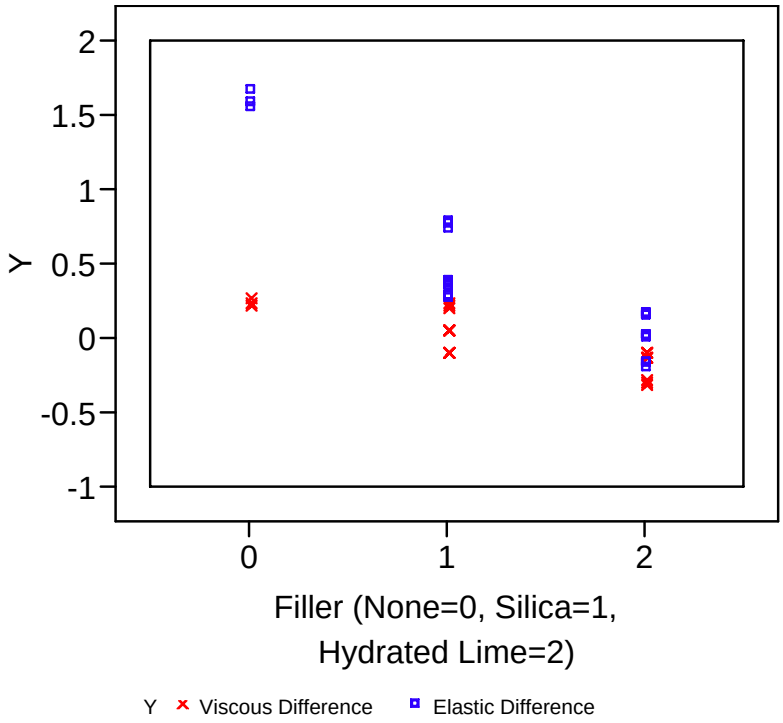


**Figure 5.8 Plot of Viscous and Elastic Component Normalized Differences for Brighton**

### 5.5.4 Clarkston

The differences in the elastic and viscous components were rather precise, thus resulting in rather small confidence ellipsoids. The confidence ellipsoids for viscous and elastic differences of original binder obtained from Clarkston can be seen in Figure 5.9. From the figure, it can be seen that the region of 95% confidence limit is rather small, but all contained within quadrant I. Despite the small confidence ellipsoid, the data clearly falls within quadrant I therefore it is not deemed a binder prone to moisture damage. The correlation between the two normalized component differences is -0.9826. Figure 5.10 displays the diverse values for the normalized components.

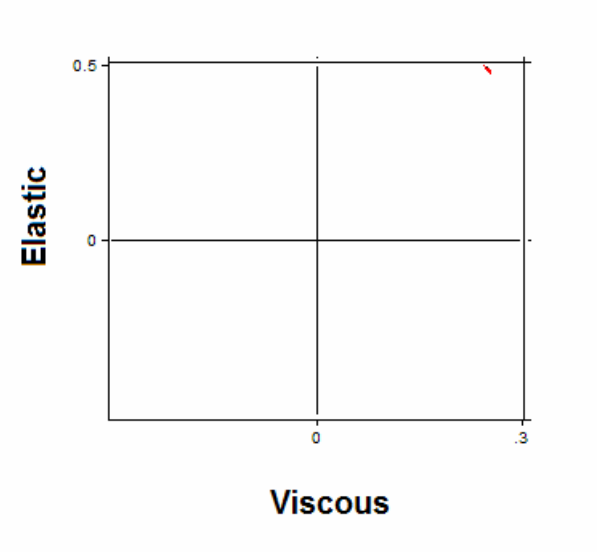


**Figure 5.9 Confidence Ellipsoid for Elastic and Viscous Component Differences of Clarkston Original Binder**

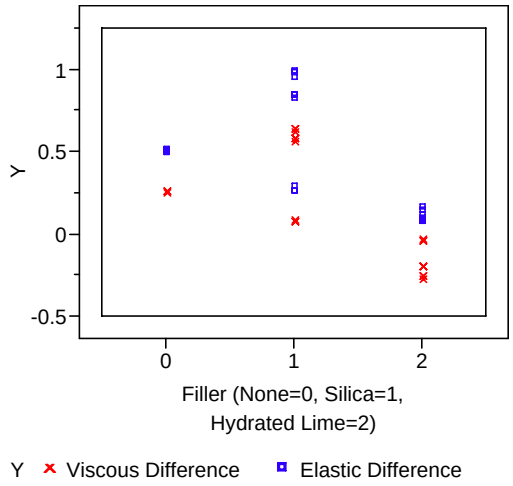


**Figure 5.10 Plot of Normalized Elastic and Viscous Component Differences for Clarkston**

### 5.5.5 Detroit

The confidence ellipsoids based on the normalized elastic and viscous component differences are illustrated in Figure 5.11. The confidence ellipsoid is clearly in quadrant I, thus implying that it is not a binder prone to moisture damage. The correlation between the normalized elastic and viscous component differences is 0.1286. The range of

differences for original binder, binder with silica, and binder with hydrated lime is shown in Figure 5.12. It would appear that the addition of filler actually has a negative effect on this binder's ability to resist moisture absorption. This would indicate that the addition of hydrated lime does not always aid in improving a binder's resistance to moisture damage. In other words, the practice of adding hydrated lime to any binder to improve the moisture resistance should be reevaluated.

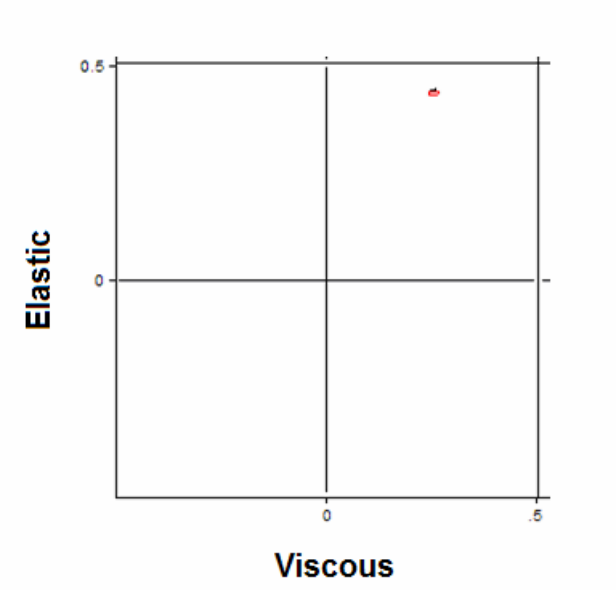


**Figure 5.11 Confidence Ellipsoid of Normalized Elastic and Viscous Differences of Original Binder from Detroit**

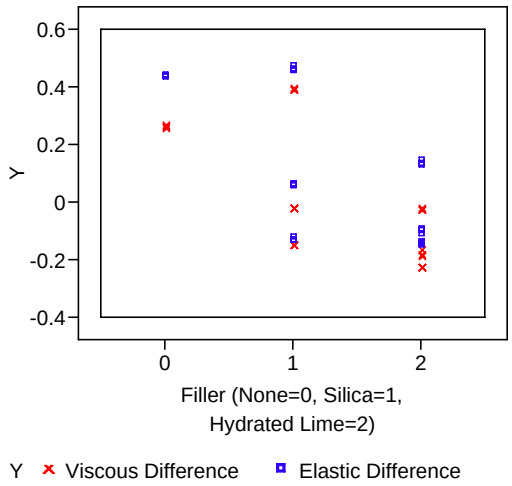


**Figure 5.12 Plot of Normalized Elastic and Viscous Component Differences for Detroit Binder**

### 5.5.6 Dundee 19.0mm NMAS

The confidence ellipsoid for Dundee 19.0mm NMAS original binder is completely in quadrant II as can be seen in Figure 5.13. The correlation between the normalized elastic and viscous component differences is 0.9739. The dispersion in the normalized differences for original binder, binder with silica, and binder with hydrated lime specimens can be seen in Figure 5.14. The improvement in the elastic and viscous components occurred with the higher percentages of filler in the binder.

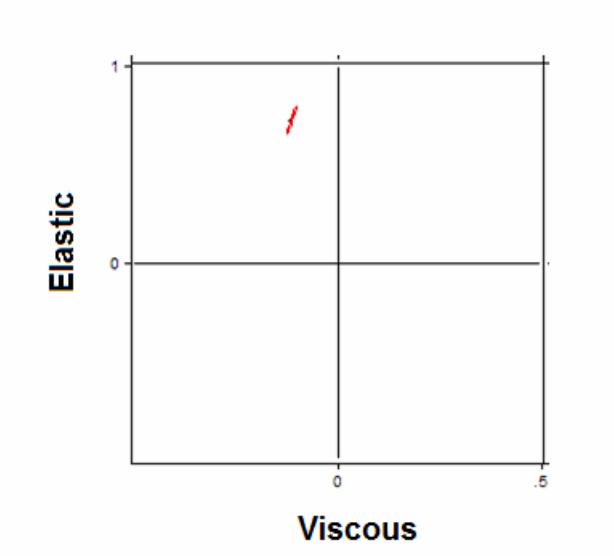


**Figure 5.13 Confidence Ellipsoid for Original Binder Dundee 19.0mm NMAS**

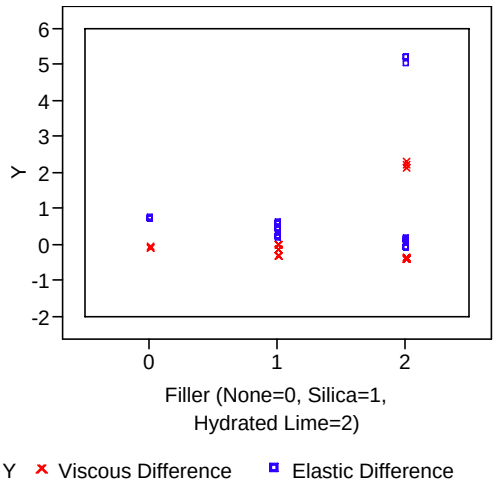


**Figure 5.14 Plot of Normalized Elastic and Viscous Component Differences for Dundee 19.0mm NMAS Binder**

### 5.5.7 Dundee 12.5mm NMAS

The confidence ellipsoid of normalized elastic and viscous component differences of Dundee 12.5mm NMAS original binder exist completely in quadrant II, which can be seen in Figure 5.15. Existence in quadrant II implies that the elastic component is increasing while the viscous component is decreasing with moisture conditioning. The correlation between the two normalized component differences is -0.2617. The range of values for normalized difference is displayed in Figure 5.16. Silica has the greatest negative effect on the normalized elastic and viscous components, which can be seen in Figure 5.16.

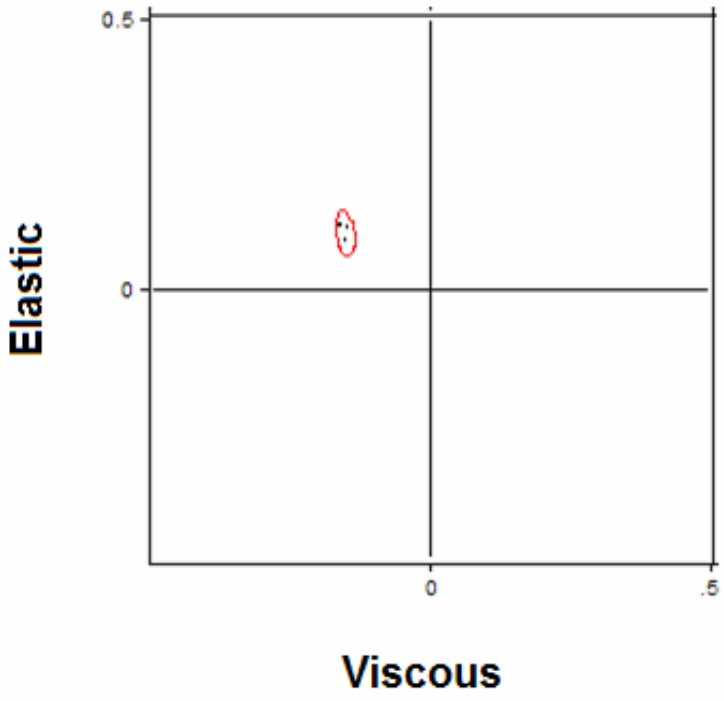


**Figure 5.15 Confidence Ellipsoid of Dundee 12.5mm NMAS Original Binder**

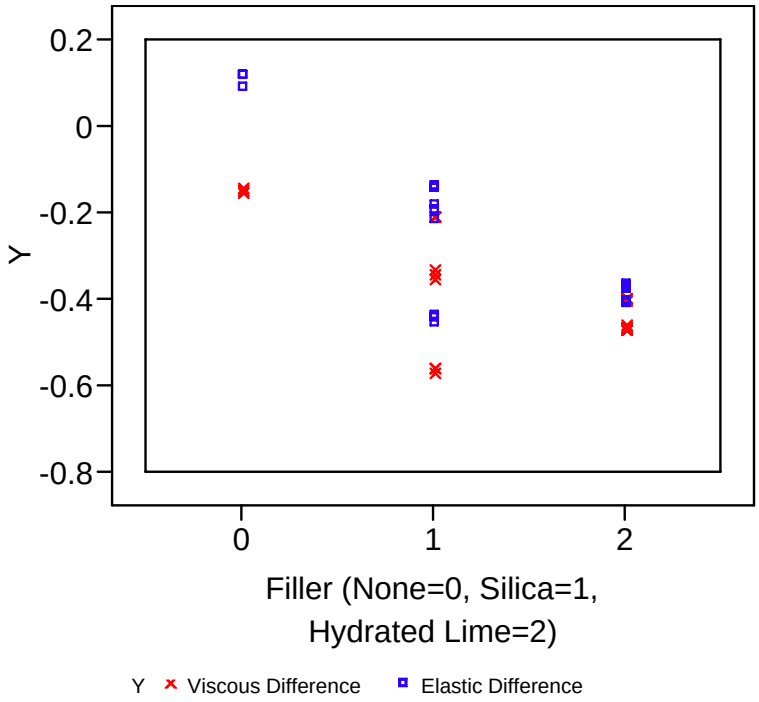


**Figure 5.16 Plot of Normalized Elastic and Viscous Component Differences for Dundee 12.5mm NMAS Binder**

### 5.5.8 Grand Rapids I-196

The confidence ellipsoid for the elastic and viscous component differences of the Grand Rapids I-196 original binder exists completely in quadrant II, as can be seen in Figure 5.17. The correlation between the normalized elastic and viscous component differences is 1, thus implying that the component differences are strongly related. Figure 5.18 illustrates the dispersion associated with normalized differences for binder from Grand Rapids I-196. As can be seen, the binder improves the most with the increased levels of hydrated lime.

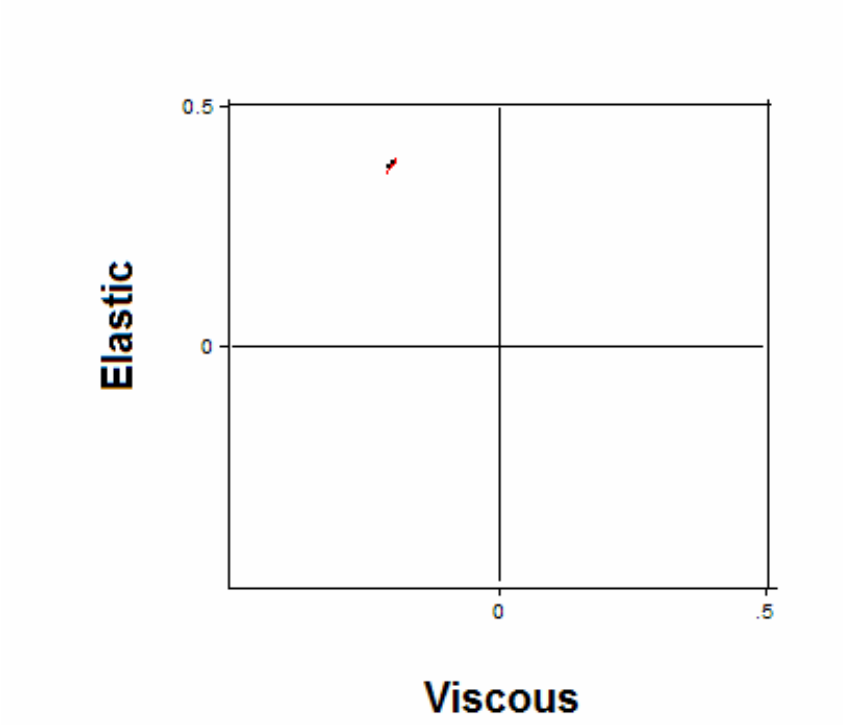


**Figure 5.17 Confidence Ellipsoid of Grand Rapids I-196 Original Binder**

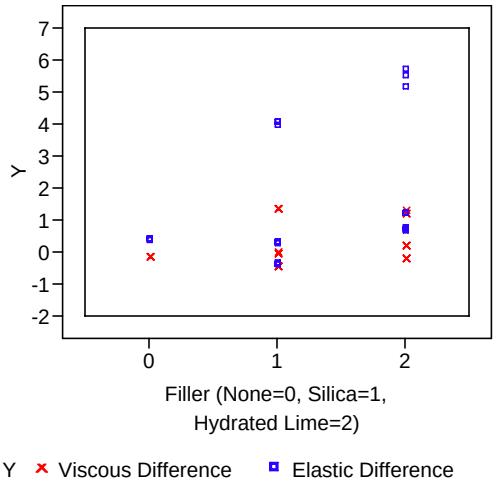


**Figure 5.18 Plot of Normalized Elastic and Viscous Component Differences for Grand Rapids I-196 Binder**

### 5.5.9 Grand Rapids M-45

Quadrant II surrounds the confidence ellipsoid for the Grand Rapids M-45 original binder normalized elastic and viscous component differences. The confidence ellipsoid is displayed in Figure 5.19. The correlation between the normalized elastic and viscous component differences is -0.0938. Figure 5.20 illustrates the range of values of the normalized differences. The greatest improvements come with the addition of silica, followed closely by hydrated lime.

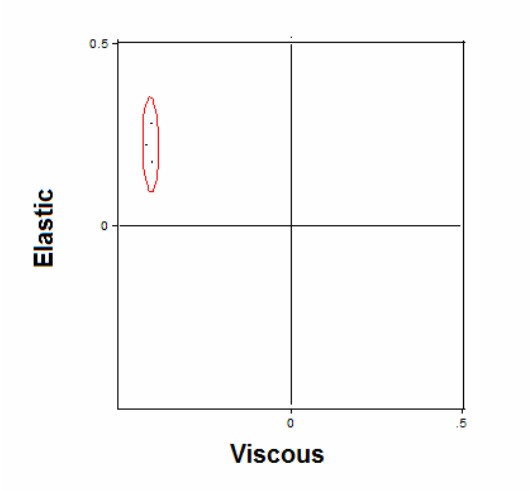


**Figure 5.19 Confidence Ellipsoid for Grand Rapids M-45 Original Binder**

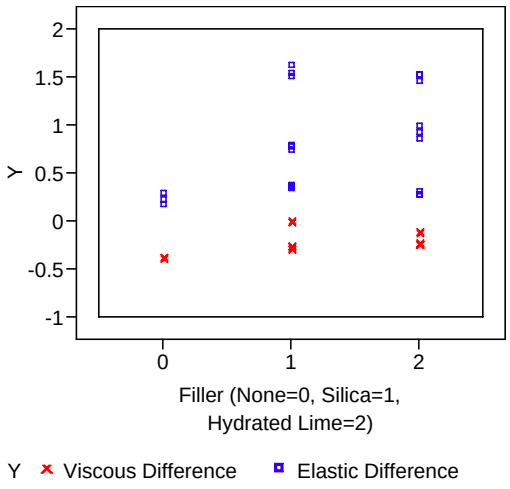


**Figure 5.20 Plot of Normalized Elastic and Viscous Component Differences for Grand Rapids M-45 Original Binder**

### 5.5.10 Hartland

The Hartland confidence ellipsoid based on normalized elastic and viscous component differences exists only in quadrant III. Figure 5.21 illustrates the confidence ellipsoids location in quadrant III. The correlation between the normalized elastic and viscous component differences is 0.7904. Normalized elastic and viscous component differences for the Hartland binder are displayed in Figure 5.22.

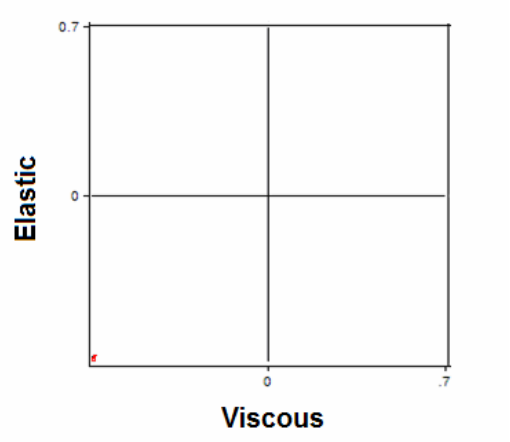


**Figure 5.21 Confidence Ellipsoid for Hartland Original Binder**

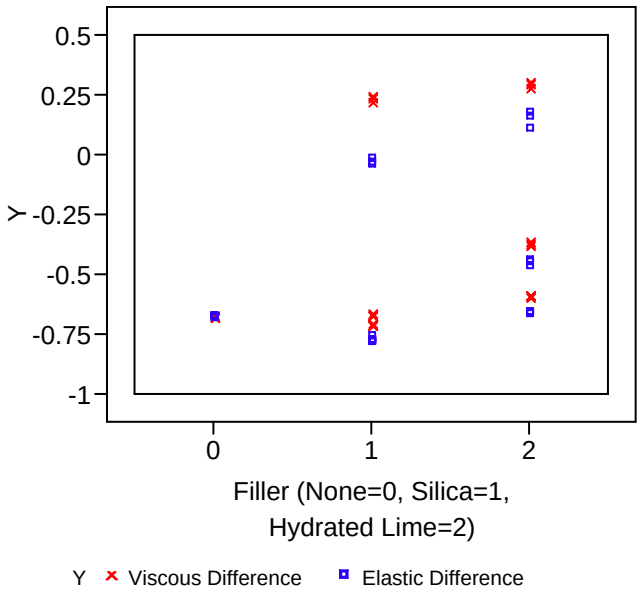


**Figure 5.22 Plot of Normalized Elastic and Viscous Component Differences for Hartland Binder**

### 5.5.11 Howell

Figure 5.23 illustrates the placement of the confidence ellipsoid for Howell original binder in quadrant I. The correlation between the normalized elastic and viscous component differences is 0.6988. Figure 5.24 illustrates the range of differences for the normalized elastic and viscous components of Howell binder specimens. The binder performs well without filler. The addition of silica and hydrated lime actually deteriorate the binder's resistance to moisture.

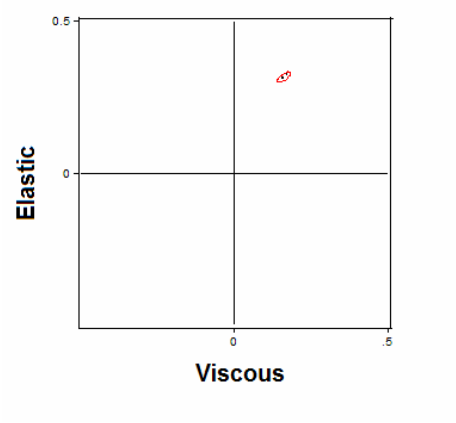


**Figure 5.23 Confidence Ellipsoid for Howell Original Binder**

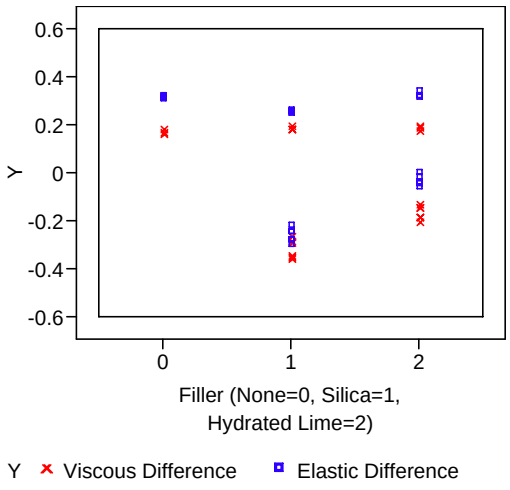


**Figure 5.24 Plot of Normalized Elastic and Viscous Component Differences for Howell Binder**

### 5.5.12 Levering

The confidence ellipsoid for the Levering original binder is located in quadrant I, as can be seen in Figure 5.25. The correlation between the normalized elastic and viscous component differences is 1, implying that there is an extremely strong relationship between the normalized differences. Figure 5.26 displays the range of values obtained for the normalized elastic and viscous component differences.

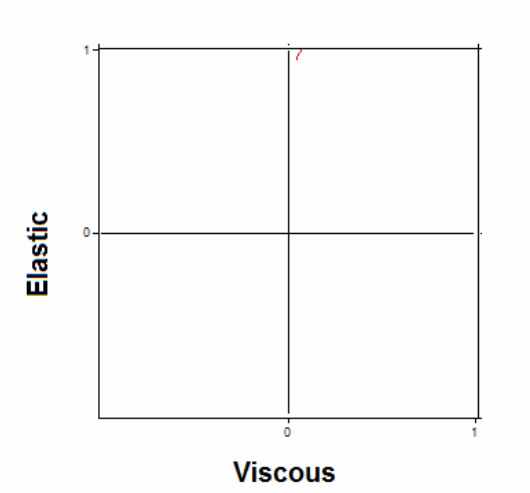


**Figure 5.25 Confidence Ellipsoid for Levering Original Binder**

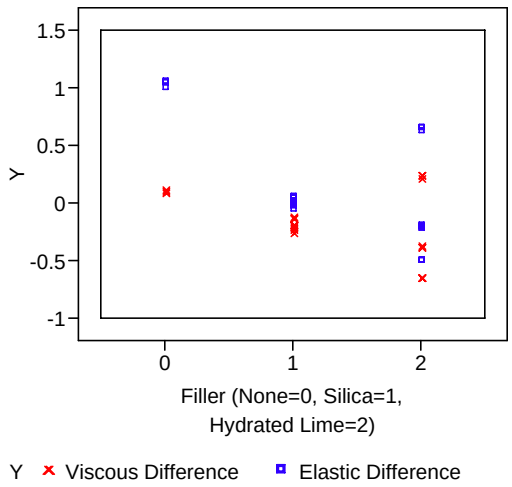


**Figure 5.26 Plot of Normalized Elastic and Viscous Component Differences for Levering Binder**

### 5.5.13 Michigan Ave 19.0mm NMAS

Figure 5.27 illustrates the placement of the confidence ellipsoid of the normalized elastic and viscous component differences for Michigan Ave. 19.0mm NMAS original binder. The correlation between the two component differences is 0.6684. The range of normalized component differences can be seen in Figure 5.28.

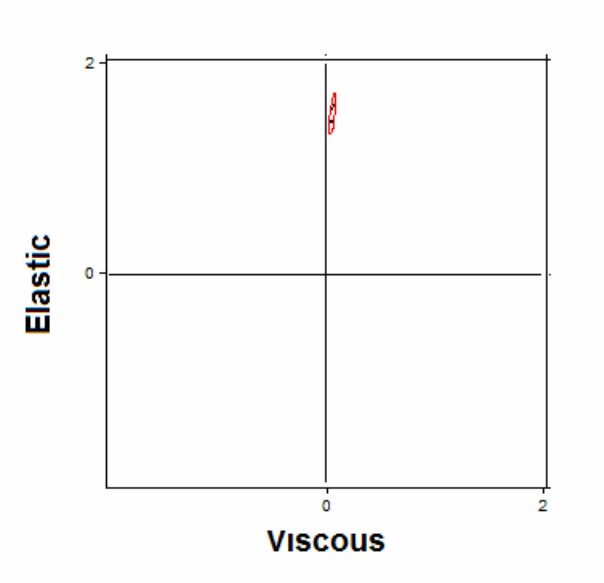


**Figure 5.27 Confidence Ellipsoid for Michigan Ave 19.0mm NMAS Original Binder**

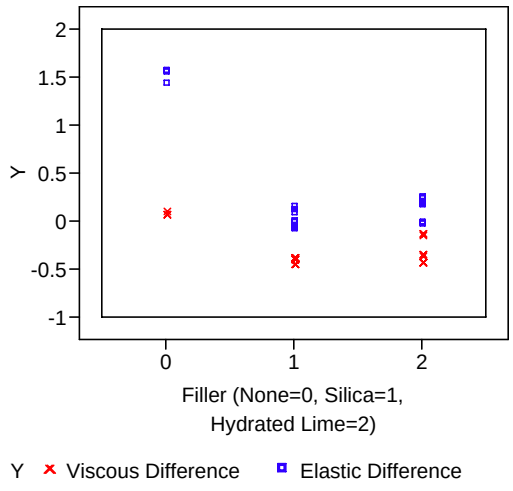


**Figure 5.28 Plot of Normalized Elastic and Viscous Component Differences for Michigan Ave 19.0mm NMAS Binder**

### 5.5.14 Michigan Ave 12.5mm NMAS

The confidence ellipsoid for the normalized elastic and viscous component differences lies completely in quadrant I, as shown in Figure 5.29. This indicates that this binder is not prone to moisture damage. The correlation between the two normalized components is -0.8426. From Figure 5.30, it can be seen that the improvement of the binder with either filler for resisting moisture effects is minimal if at all.

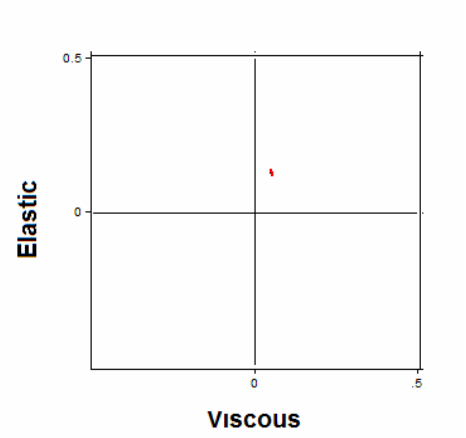


**Figure 5.29 Confidence Ellipsoid for Michigan Avenue 12.5mm NMAS Original Binder**

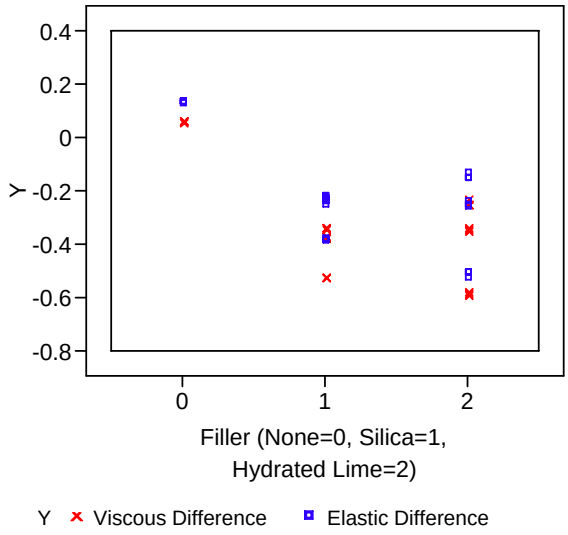


**Figure 5.30 Overlay Plot of Normalized Elastic and Viscous Component Differences for Michigan Avenue 12.5mm NMAS Binder**

### 5.5.15 Michigan International Speedway US-12

Quadrant I completely encompasses the confidence ellipsoid of the normalized elastic and viscous component differences for the original binder from Michigan International Speedway. An ellipse completely encompassed by quadrant I imples that the binder is not prone to moisture damage. The correlation between the two normalized component differences is 0.6614. The range of values obtained for the differences can be seen in Figure 5.32. The addition of filler hinders the binder's ability to resist moisture damage.

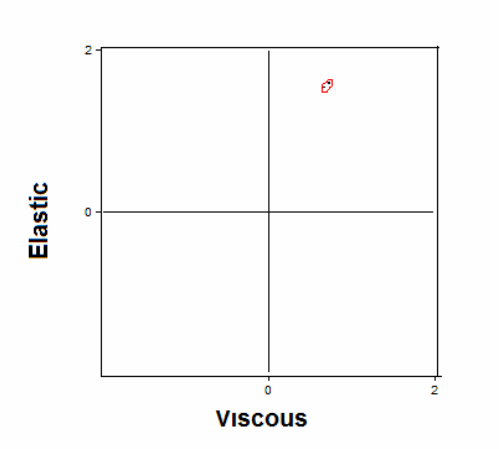


**Figure 5.31 Confidence Ellipsoid for Michigan International Speedway US-12 Original Binder**

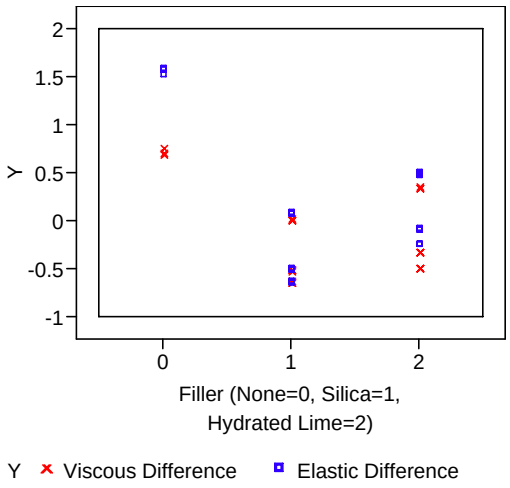


**Figure 5.32 Overlay Plot of Normalized Elastic and Viscous Component Differences for Michigan International Speedway US-12 Binder**

### 5.5.16 Owosso

The confidence ellipsoid of the elastic and viscous component differences for the original binder from Owosso exists completely in quadrant I, seen in Figure 5.33. The correlation between the two normalized components is 0.8680. The range of values obtained when finding the difference between normalized components can be seen in Figure 5.34. As the amount of filler was added to the binder, the moisture resistance increased.

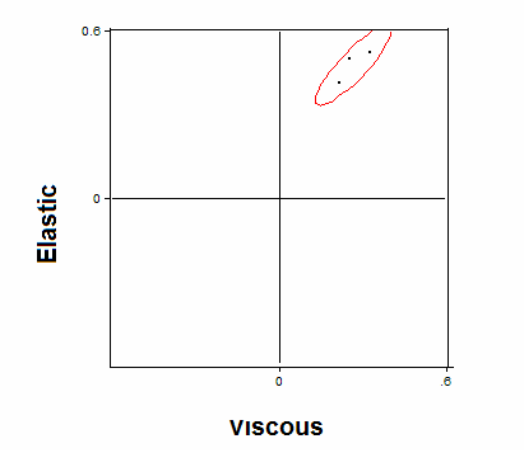


**Figure 5.33 Confidence Ellipsoid for Owosso Original Binder**

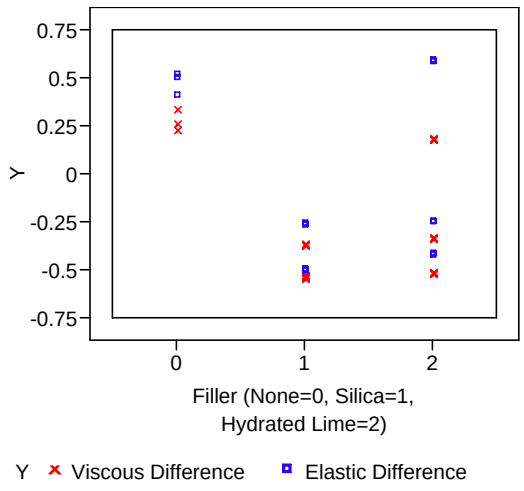


**Figure 5.34 Overlay Plot of Normalized Elastic and Viscous Component Differences for Owosso Binder**

### 5.5.17 Pinckney

The confidence ellipsoid for the normalized elastic and viscous component differences lies completely in quadrant II, see Figure 5.35, indicating that the elastic component increased and the viscous component decreased. The correlation between the two normalized differences is -0.8513. The range in difference values obtained can be seen in Figure 5.36. The addition of silica improves the moisture resistance and performance of the binder.

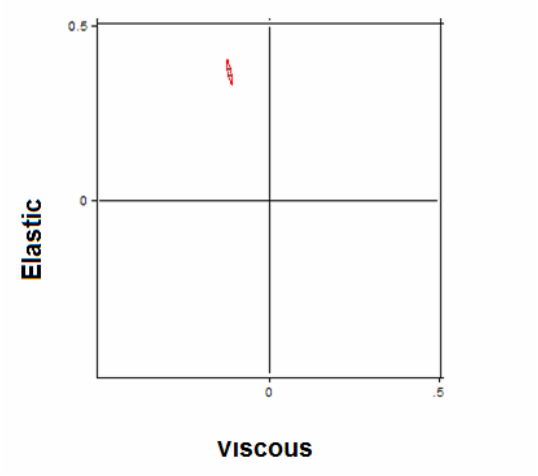


**Figure 5.35 Confidence Ellipsoid for Pinckney Original Binder**

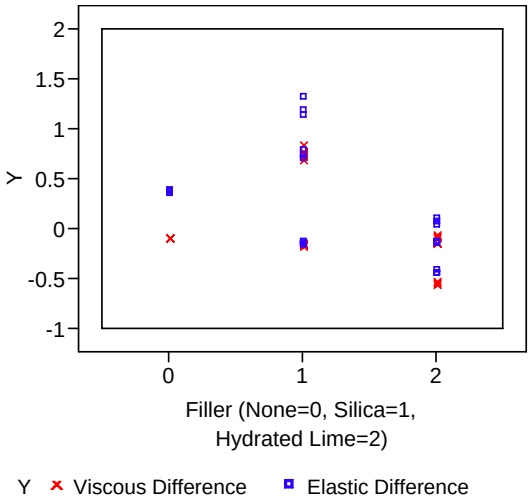


**Figure 5.36 Overlay Plot of Normalized Elastic and Viscous Component Differences for Pinckney Binder**

### 5.5.18 Saginaw

The confidence ellipsoid for the Saginaw original binder exists completely in quadrant I, as seen in Figure 5.37. Since the data falls in quadrant I, the binder is deemed moisture damage resistant. The correlation between the normalized elastic and viscous component differences is 0.8530. The range of normalized difference values can bee observed in Figure 5.38. The binder performs best without fillers.

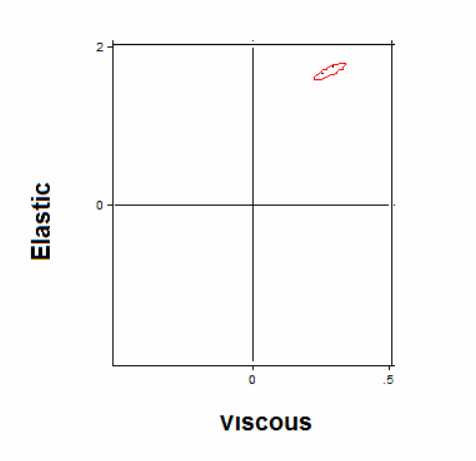


**Figure 5.37 Confidence Ellipsoid for Saginaw Original Binder**

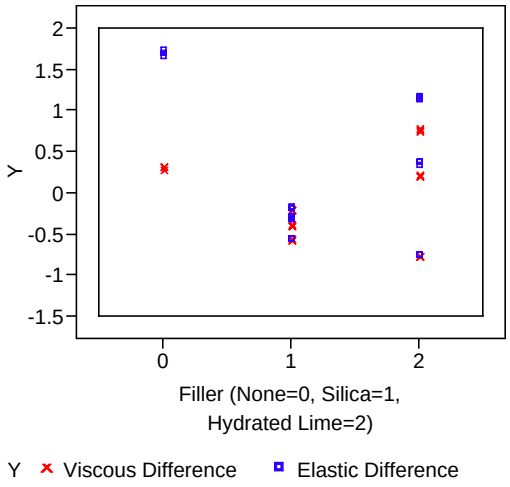


**Figure 5.38 Overlay Plot of Normalized Elastic and Viscous Component Differences for Saginaw Binder**

### 5.5.19 St. Johns

Figure 5.39 illustrates that the confidence ellipsoid for St. Johns of the normalized elastic and viscous component differences lies completely in quadrant II. The correlation between the two normalized component differences is -0.4764. The range of difference values can be seen in Figure 5.40. The binder performs best with hydrate lime followed by silica.

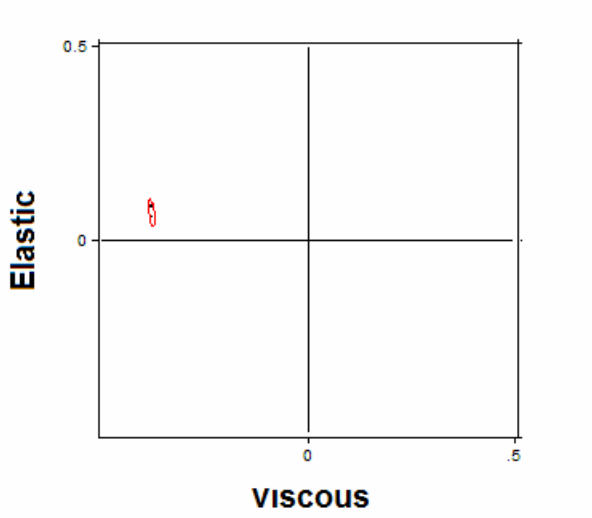


**Figure 5.39 Confidence Ellipsoid of St. Johns Original Binder**

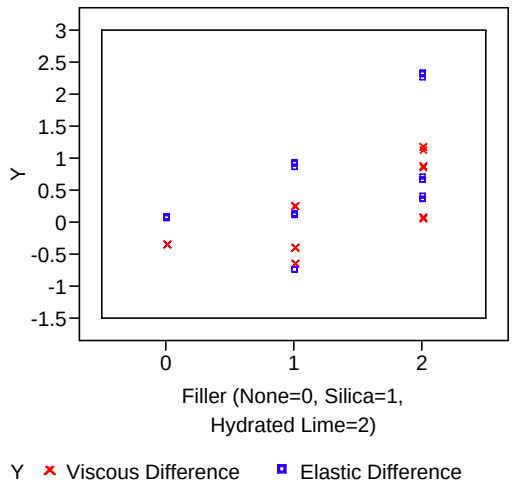


**Figure 5.40 Overlay Plot of Normalized Elastic and Viscous Component Differences for St. Johns Binder**

### 5.5.20 Toledo

Figure 5.41 displays the confidence ellipsoid of the normalized elastic and viscous component differences in quadrant II. The correlation between the two component differences is 0.3777. The range of difference values can be seen in Figure 5.42. The binder performs best with the addition of hydrated lime followed closely by the original binder.

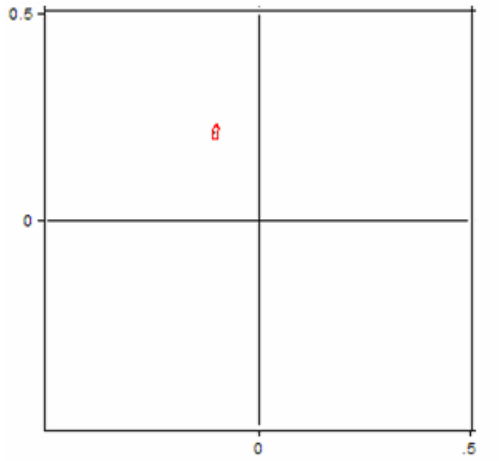


**Figure 5.41 Confidence Ellipsoid for Toledo Original Binder**

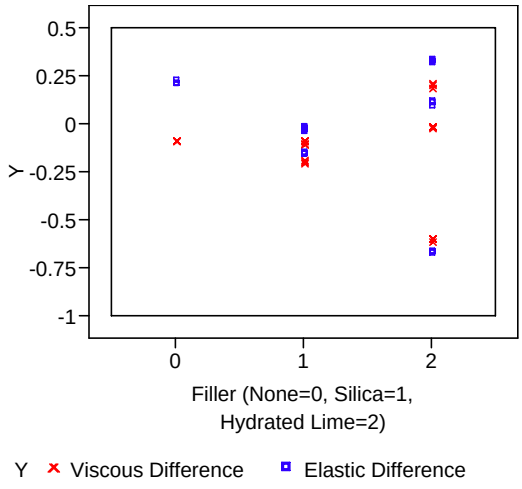


**Figure 5.42 Overlay Plot of Normalized Elastic and Viscous Component Differences for Toledo Binder**

### 5.5.21 Van Dyke

Figure 5.43 illustrates the placement of the confidence ellipsoid in quadrant II. The correlation between the normalized elastic and viscous component differences is -0.1733. The range of difference values for original binder and binder with filler can be seen in Figure 5.44. The binder performs best with higher levels of hydrated lime.

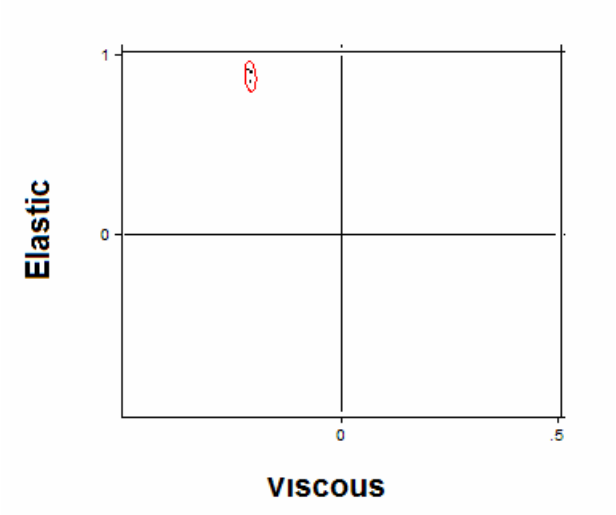


**Figure 5.43 Confidence Ellipsoid of Van Dyke Original Binder**

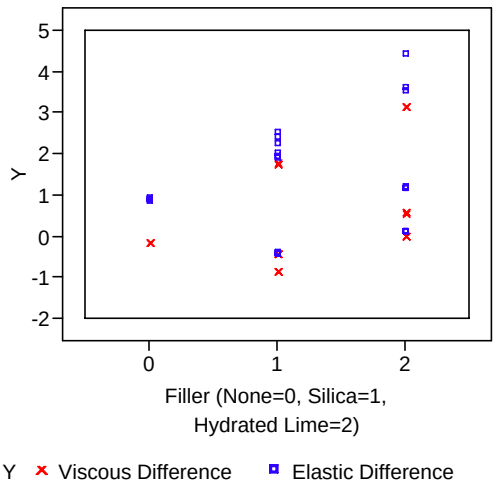


**Figure 5.44 Overlay Plot of Normalized Elastic and Viscous Component Differences for Van Dyke Binder**

### 5.5.22 Summary of Statistical Noise

Confidence ellipsoids were employed to evaluate the noise associated with the data obtained from the DSR testing. Evaluating whether or not all of the recorded data and confidence region lies completely encompassed in one quadrant aided in defining the moisture susceptibility of a binder. Confidence ellipsoids account for the confidence regions of both the elastic and viscous normalized component differences. The confidence ellipsoids are based on a confidence level of 95%. Table 5.5 summarizes the locations of the various confidence ellipsoids. The only binder that spanned multiple quadrants was Ann Arbor. The binders completely contained in quadrant I improved in both elastic and viscous properties, thus indicating that moisture does not have a damaging effect on these binders. Binders completely in quadrant II exhibited increasing values for the elastic component, but decreasing values for the viscous component. These binders are slightly effected by moisture, but since the elastic component increased the affect is not considered significant. An increased elastic component indicated that a binder recovers better after a load application than prior to an elastic component increase. Binders in quadrant III were considered prone to moisture damage since both the elastic and viscous components decreased. Confidence ellipsoids of binders with filler can be found in Appendix B.

**Table 5.5 Location of Confidence Ellipsoids**

| Quadrant I | Quadrant II | Quadrant III |
|---|---|---|
| Brighton, Clarkston, Detroit, Howell, Levering, Michigan Avenue 19.0mm NMAS, Michigan Avenue 12.5mm NMAS, Michigan International Speedway, Owosso, Saginaw | Ann Arbor, Dundee 19.0mm NMAS, Dundee 12.5mm NMAS, Grand Rapids I-196, Grand Rapids M-45, Pinckney, St. Johns, Toledo, VanDyke | Ann Arbor, Battle Creek, Hartland |

### 5.5.23 Summary of Correlation of Normalized Component Differences

Normalized elastic and viscous components were computed to evaluate the affect of moisture on these components. The correlation of the difference between normalized

components was computed to determine if the changes caused by moisture on each component was related. For negative and positive correlations, absolute values between 0 and 0.5 were considered low, while values between 0.5 and 0.75 were deemed moderate, and all above 0.75 labeled as high. Table 5.6 summarizes the results of categorizing the correlations. Most of the binders have a strong (labeled as high) relationship, the difference is whether or not it is positive or negative. Strong relationships between the normalized components were considered auspicious. If the two components change with respect to one another as a result of moisture exposure, defining a relationship of how moisture affects binders will be much easier than if there was no relationship between the two normalized components.

**Table 5.6 Correlation Ratings of Normalized Viscous and Elastic Component Differences**

| | Low | Moderate | High |
|---|---|---|---|
| **Positive** | Detroit, Dundee 12.5mm NMAS, Toledo | Howell, Michigan Ave 19.0mm NMAS | Brighton, Dundee 19.0mm NMAS, Grand Rapids I-196, Hartland, Levering, Michigan International Speedway, Owosso, Saginaw |
| **Negative** | Grand Rapids M-45, St. Johns, VanDyke | | Ann Arbor, Battle Creek, Clarkston, Michigan Ave 12.5mm NMAS, Pinckney |

## 5.6 Comparison of Moisture Saturation and Modified DSR Testing

This summarizes the comparisons between binders tested with a modified DSR versus the water absorption specimens. The first comparison examined whether or not all of the binders in a particular quadrant for the normalized component analysis were related to significant weight increases. Table 5.7 summarizes the quadrant location for each binder by filler type. Only binders with fillers are listed in the table since original binders were not tested using the absorption test. Comparisons of Table 5.7 with Table 5.2 indicate

that there is no significant relationship between quadrant location and significant weight gain.

**Table 5.7 Location of Normalized Elastic and Viscous Component for DSR Tested Binders with Fillers**

| | 5% Silica | 10% Silica | 20% Silica | 5% Hydrated Lime | 10% Hydrated Lime | 20% Hydrated Lime |
|---|---|---|---|---|---|---|
| Ann Arbor | III | III | III | II | I | I |
| Battle Creek | III | III | III | II | I | III |
| Brighton | I | II | I | II | III | II |
| Clarkston | I | I | I | II | I | II |
| Detroit | II | I | III | II | III | III |
| Dundee 19.0mm NMAS | II | II | II | I | II | III |
| Dundee 12.5 mm NMAS | III | III | III | III | III | III |
| Grand Rapids I-196 | I | II | III | II | I | I |
| Grand Rapids M-45 | II | II | II | II | II | II |
| Hartland | IV | III | III | III | III | I |
| Howell | I | III | III | III | I | I |
| Levering | II | III | II | I | III | III |
| Michigan Ave 19.0mm NMAS | III | II | III | II | III | II |
| Michigan Ave 12.5mm NMAS | III | III | III | III | III | III |
| Michigan International Speedway | III | II | III | III | III | I |
| Owosso | III | III | III | I | III | III |
| Pinckney | I | III | I | III | II | III |
| Saginaw | III | III | III | I | I | III |
| St. Johns | II | I | III | I | I | I |
| Toledo | III | III | III | II | III | I |
| VanDyke | II | III | I | I | I | II |

The next comparison examined whether there is a relationship between significant G*/sin(δ) changes and asphalt binder specimen weight gain. To determine significant changes in G*/sin(δ), unconditioned and conditioned specimens tested in a water bath were compared. Table 5.8 summarizes the results of comparisons between complex shear modulus values of unconditioned and conditioned specimens tested in a water bath. Only five binders did not yield statistically different complex shear modulus values after moisture saturation. These same binders also did not gain a significant amount of weight during the absorption testing. However, there were other binders that also did not gain weight but were deemed statistically different when comparing complex shear modulus values of specimens tested in a water bath.

**Table 5.8 Comparison Summary Comparing Conditioned and Unconditioned Specimens Tested in a Water Bath**

| | 5% Silica | 10% Silica | 20% Silica | 5% Hydrated Lime | 10% Hydrated Lime | 20% Hydrated Lime |
|---|---|---|---|---|---|---|
| Ann Arbor | Reject | Reject | Reject | Reject | Reject | Reject |
| Battle Creek | Reject | Reject | Reject | Reject | Reject | Reject |
| Brighton | Reject | Reject | Not Rejected | Reject | Reject | Reject |
| Clarkston | Reject | Reject | Reject | Reject | Reject | Reject |
| Detroit | Reject | Reject | Reject | Reject | Reject | Reject |
| Dundee 19.0mm NMAS | Reject | Not Rejected | Reject | Reject | Reject | Reject |
| Dundee 12.5 mm NMAS | Reject | Reject | Reject | Reject | Reject | Reject |
| Grand Rapids I-196 | Reject | Reject | Reject | Reject | Reject | Reject |
| Grand Rapids M-45 | Reject | Reject | Reject | Reject | Reject | Reject |
| Hartland | Reject | Reject | Reject | Reject | Reject | Reject |
| Howell | Reject | Reject | Reject | Reject | Reject | Not Rejected |
| Levering | Reject | Reject | Reject | Reject | Reject | Reject |
| Michigan Ave 19.0mm NMAS | Reject | Reject | Not Rejected | Reject | Reject | Reject |
| Michigan Ave 12.5mm NMAS | Reject | Reject | Reject | Reject | Reject | Reject |
| Michigan International Speedway | Reject | Reject | Reject | Reject | Reject | Reject |
| Owosso | Reject | Reject | Reject | Reject | Reject | Reject |
| Pinckney | Reject | Reject | Reject | Not Rejected | Reject | Reject |
| Saginaw | Reject | Reject | Reject | Reject | Reject | Reject |
| St. Johns | Reject | Reject | Reject | Reject | Reject | Reject |
| Toledo | Reject | Reject | Reject | Reject | Reject | Reject |
| Van Dyke | Reject | Reject | Reject | Reject | Reject | Reject |

Examining the binders from the absorption testing that gained a significant amount of weight to DSR results indicated a loose trend. The majority of binders with either silica or hydrated lime that demonstrated a significant amount of weight gain resulted in decreased complex shear modulus values after moisture saturation. This decrease in complex shear modulus values could be attributed to moisture penetration.

## 5.7 Recommended Moisture Susceptibility Criterion

This test criterion is based on data obtainable from DSR testing software and water absorption. As previously mentioned, this criterion is based on theory and has been applied to laboratory results, but still needs to be verified with field results. It is recommended that binders are tested with a DSR using a modified spindle and base plate. The binder that should be tested is original binder and binder with a filler. A binder with filler should be tested to allow for breaks in an asphalt binder specimen membrane surface, which enables water to permeate a specimen faster than a specimen without

surface breaks. Surface breaks occur in pavements; therefore inducing breaks by adding a filler simulates, to an extent, reality.

Both of the original binder and binder with filler should be tested as unsaturated and saturated. The saturation should occur for a minimum of 24 hours in a 25˚C water bath. An evaluation of the change in viscous and elastic components should be conducted, as outlined in this chapter. Confidence ellipsoids should be developed to account for noise associated with data readings. The rating used in this chapter should be followed.

In conjunction with DSR testing results, specimens should be evaluated to determine water absorbing tendencies, following steps outlined in this chapter. If a binder exhibits an confidence ellipsoid that is close to crossing over into another quadrant, the water absorption test results should be consulted. This method should be validated with field data once the pavements where the material was collected from have aged properly and performance data has been collected.

# Chapter 6 Tensile Strength Testing and Evaluation

Current HMA moisture susceptibility tests outline procedures for determining the tensile strength ratio (TSR) via AASHTO T-283. TSRs are calculated by dividing the wet tensile strength by the dry tensile strength. The common bisecting value for identifying moisture susceptible mixes is 80%. The TSR method was employed to determine a moisture prone and a moisture resistant mix from the field sampled mixes examined in this project. Two mixes identified by the TSR moisture susceptible test procedure were then used to establish the subsequent test conditions to be evaluated for all 21 mixes utilizing an Asphalt Pavement Analyzer.

## 6.1 AASHTO T-283

The current standard for evaluating the moisture susceptibility of an HMA pavement is outlined in AASHTO T-283. The basic premise of AASHTO T-283 consists of testing specimens unconditioned and conditioned. The conditioning consists of saturating a specimen to within 70-80% saturation and then subjecting specimens to one freeze/thaw cycle. The testing evaluates the tensile strength of a mix. Once unconditioned and conditioned specimens have been tested, a ratio is calculated. The ratio is made by dividing the tensile strength of the conditioned specimens by the tensile strength of the unconditioned specimens. If the ratio is greater than 80%, the mix is deemed not moisture susceptible. If the mix is less than 80%, the mix is considered moisture susceptible.

The current issue under debate is whether or not AASHTO T-283 as it is outlined now is appropriate for Superpave mixes. The original inception of AASHTO T-283 was based on research conducted on Marshall compacted mixes. Standard specimens made with a Marshall hammer are 100mm in diameter. Standard specimens made by a Superpave gyratory compactor are 150mm in diameter. The mechanistic process of compacting a specimen also differs. A Marshall hammer places a repeated load on a specimen perpendicular to the ground. Specimens procured using the Superpave system

are subjected to loading at an angle. It should be noted that most states have switched from using the Marshall method to the Superpave system.

In this dissertation, the use of an APA to identify moisture prone mixes is explored. The appropriateness of using AASHTO T-283 was evaluated along with the relationship between APA moisture testing and AASHTO T-283.

## 6.2 Testing Procedure

Specimens were procured using a Superpave Gyratory Compactor. Four specimen groups were established. The first group was saturated just prior to testing. The second group was saturated prior to enduring one freeze/thaw cycle prior to testing. A third group was saturated prior to being subjected to two freeze/thaw cycles before being tested. A final group was moisture saturated before undergoing three freeze/thaw cycles prior to testing.

## 6.3 Results

The variety of HMAs examined are outlined below in Table 6.1. Different mix types, aggregate sources, and conditioning approaches were considered. A sensitivity study on the effects of specimen size and compaction method was conducted on a limited number of mixes to determine the amount of conditioning that should be sustained by the larger Superpave compacted specimens.

**Table 6.1 Experimental Plan for Mix and Aggregate Types**

| | | Traffic Level Equivalent Single Axle Loads (ESAL's) | |
|---|---|---|---|
| | NMAS (mm) | < 3,000,000 | > 3,000,000 |
| Mix Size | 25 or 19 | Limestone Gravel | Limestone |
| | 12.5 or 9.5 | Limestone Gravel | Limestone Slag |

## 6.4 Analysis

A statistical analysis of the effect of aggregate source, NMAS, gradation, traffic level, compaction type, and number of freeze/thaw cycles was conducted to assist in evaluating the appropriateness of AASHTO T-283 for moisture susceptibility testing. These results will later be compared to APA testing results in Chapter 7. The following sections summarize the statistical significance of each factor affecting the moisture susceptibility criterion.

### 6.4.1 Statistical

The first type of statistical test used was ANOVA of 100mm Marshall to 100mm and 150mm Superpave specimens. The goal of this test procedure is to determine the number of freeze/thaw cycles required to attain an equivalent amount of damage to one freeze/thaw cycle for the 100mm Marshall specimens. The compaction method, number of freeze/thaw cycles, and the change in size of the specimens will be taken into account.

The average lowest TSR was obtained with the 100mm Marshall compacted specimens. In general, 100mm Superpave specimens had the highest TSR. The method and specimens with the lowest standard deviation were the 150mm Superpave specimens. Interestingly, the 100mm Superpave specimens had the highest level of variability. These results indicate that the 150mm Superpave specimens are more precise, the data is less spread out, than both the TSR values for the Marshall and 100mm Superpave specimens. The coefficient of variation supports the concept of the TSR results being less dispersed for the 150 mm Superpave specimens. However, the TSRs for Marshall specimens were lower than those for Superpave compacted specimens, indicating that perhaps the moisture criterion outlined for Marshall procured specimens is not appropriate for Superpave procured specimens.

As suspected, the TSR is lowest on average once the specimens endured three freeze/thaw cycles and the highest TSRs occurred after only one freeze/thaw cycle. The coefficients of variation indicate that for all three compaction and size categories, three freeze/thaw cycles led to less precise TSR values, while the most precise values are

obtained after one freeze/thaw for Marshall and 150mm Superpave and two freeze/thaw cycles for 100mm Superpave specimens.

Several ANOVAs were conducted to examine whether or not there were significant statistical differences in the TSR results between number of freeze/thaw cycles and also compaction and diameter size. The ANOVAs conducted grouped the data by NMAS and gradation. Table 6.2 outlines the results of comparing the TSR values between freeze/thaw cycles when categorized by NMAS. The ANOVA for the data categorized by NMAS hypothesized that there was no significant statistical difference between the TSR values obtained from the two freeze/thaw cycles of interest. The type classification in the table refers to the compaction method and diameter of the specimens tested. Type S100 and S150 represent the 100mm and 150mm Superpave specimens, respectively, and Type M100 signifies the 100mm Marshall specimens. The conclusions gleaned from these ANOVAs were:

- Freeze/thaw cycling has a significant affect on 9.5mm NMAS TSR values;
- TSR values obtained after one and two freeze/thaws for all 9.5mm NMAS specimens are equivalent regardless of compaction method and specimen diameter;
- Superpave compacted 100mm specimens with a 19.0mm NMAS yield statistically equivalent TSR values for all three freeze/thaw cycles;
- Marshall compacted 100mm specimens with a 12.5mm NMAS yield statistically equivalent TSR values for all three freeze/thaw cycles;
- Marshall compacted 100mm specimens with a 19.0mm NMAS yield statistically different TSR values for all three freeze/thaw cycles; and
- Almost all of the TSR values compared for one and three freeze/thaw cycles were statistically different.

**Table 6.2 Results of ANOVAs Comparing TSR within NMAS for the Freeze/thaw Cycle Levels**

| | | Freeze Thaw Comparisons | | |
|---|---|---|---|---|
| **NMAS** | **Type** | **1 vs 2** | **1 vs 3** | **2 vs 3** |
| **19mm** | **S100** | Not Rejected | Not Rejected | Not Rejected |
| | **S150** | ***Reject*** | Not Rejected | Not Rejected |
| | **M100** | ***Reject*** | ***Reject*** | ***Reject*** |
| **12.5mm** | **S100** | Not Rejected | ***Reject*** | ***Reject*** |
| | **S150** | Not Rejected | ***Reject*** | ***Reject*** |
| | **M100** | Not Rejected | Not Rejected | Not Rejected |
| **9.5mm** | **S100** | Not Rejected | ***Reject*** | ***Reject*** |
| | **S150** | ***Reject*** | ***Reject*** | ***Reject*** |
| | **M100** | ***Reject*** | ***Reject*** | Not Rejected |

S100= 100mm Superpave Specimens; S150= 150mm Superpave Specimens; M100= 100mm Marshall Specimens

Table 6.3 outlines the results of the ANOVAs performed to compare compaction method and diameter of specimen within NMAS level and freeze/thaw cycle. The null hypothesis employed was there is no significant statistical difference between TSR values within a freeze/thaw cycle level for two different combinations of compaction and specimen diameter. The results, based on 95% confidence, indicate that:

- TSR values obtained from 100mm Marshall and 150mm Superpave specimens for all NMAS levels are statistically equivalent when comparing data collected after only one freeze/thaw cycle; and
- TSR values obtained from the 100mm Superpave and 100mm Marshall specimens for all NMAS levels are statistically distinct when comparing data collected after two freeze/thaw cycles.

**Table 6.3 Comparison of TSR Values for Compaction Method and Diameter Within NMAS and Freeze/Thaw Cycle Using ANOVAs**

| | S100 vs S150 | | | S100 vs M100 | | | S150 vs M100 | | |
|---|---|---|---|---|---|---|---|---|---|
| NMAS | TSR1 | TSR 2 | TSR3 | TSR1 | TSR 2 | TSR3 | TSR1 | TSR 2 | TSR3 |
| 19.0mm | Not Rejected | Not Rejected | Not Rejected | Not Rejected | **Reject** | **Reject** | Not Rejected | **Reject** | **Reject** |
| 12.5mm | **Reject** | **Reject** | Not Rejected | Not Rejected | **Reject** | Not Rejected | Not Rejected | Not Rejected | Not Rejected |
| 9.5mm | **Reject** | **Reject** | **Reject** | **Reject** | **Reject** | **Reject** | Not Rejected | **Reject** | Not Rejected |

S100= 100mm Superpave; S150= 150mm Superpave; M100= 100mm Marshall

Table 6.4 summarizes the results of the ANOVAs grouping TSR values by gradation. The null hypotheses for this table was that no significant difference in TSR values existed between freeze/thaw cycles within a gradation type for a given compaction and diameter size. The results of the ANOVA indicate that:

- For both fine and coarse-graded mixes, the TSR values are statistically dissimilar when comparing one and three freeze/thaw cycles;
- TSR values obtained from the coarse 100mm Marshall specimens are statistically different when comparing all freeze/thaw cycles;
- Both fine and coarse-graded mixes have statistically diverse TSR values when comparing one and two freeze/thaw cycles for 150mm Superpave specimens; and
- Both fine and coarse-graded mixes have statistically different TSR values when comparing one and two freeze/thaw cycles for 100mm Marshall specimens.

**Table 6.4 Results of ANOVA Comparing TSR Values Between Freeze/Thaw Cycles Within Gradation**

| | | Freeze Thaw Comparisons | | |
|---|---|---|---|---|
| Gradation | Type | 1 vs 2 | 1 vs 3 | 2 vs 3 |
| Coarse | S100 | Not Rejected | **Reject** | Not Rejected |
| | S150 | **Reject** | **Reject** | Not Rejected |
| | M100 | **Reject** | **Reject** | **Reject** |
| Fine | S100 | Not Rejected | **Reject** | **Reject** |
| | S150 | **Reject** | **Reject** | **Reject** |
| | M100 | **Reject** | **Reject** | Not Rejected |

S100= 100mm Superpave; S150= 150mm Superpave; M100= 100mm Marshall

Table 6.5 encapsulates the results of ANOVAs comparing TSR values within a gradation and one freeze/thaw cycle. The null hypothesis for these tests states that there is no significant statistical difference between compaction method and diameter combinations within a gradation and freeze/thaw cycle. The conclusions obtained from these ANOVAs were:

- No statistical difference exists when comparing TSR values for coarse-graded Superpave 100 and 150mm specimens for all freeze/thaw cycles;
- TSR values are statistically equivalent when comparing fine-graded 150 mm Superpave and 100 mm Marshall specimens for all freeze/thaw values;
- After three freeze/thaw cycles, TSR values are statistically similar for 100mm and 150mm Superpave coarse- and fine-graded mixes;
- After one freeze/thaw cycle, TSR values are statistically similar for 150mm Superpave and 100mm Marshall coarse- and fine-graded specimens; and
- After two freeze/thaw cycles, TSR values are statistically different for 100mm Superpave and Marshall coarse- and fine-graded specimens.

**Table 6.5 Results of ANOVA Comparing TSR Values within Gradation and Freeze/Thaw Cycle**

| | S100 vs S150 | | | S100 vs M100 | | | S150 vs M100 | | |
|---|---|---|---|---|---|---|---|---|---|
| **Gradation** | **TSR1** | **TSR 2** | **TSR3** | **TSR1** | **TSR 2** | **TSR3** | **TSR1** | **TSR 2** | **TSR3** |
| **Coarse** | Not Rejected | Not Rejected | Not Rejected | Not Rejected | **Reject** | **Reject** | Not Rejected | **Reject** | **Reject** |
| **Fine** | **Reject** | **Reject** | Not Rejected | **Reject** | **Reject** | Not Rejected | Not Rejected | Not Rejected | Not Rejected |

S100= 100mm Superpave; S150= 150mm Superpave; M100= 100mm Marshall

After examining ANOVAs of NMAS and gradation categorized TSR values, correlation analysis was conducted. The correlation analysis investigated the factors that could be related to wet strength after one, two, and three freeze/thaw cycles. It was revealed that polymer modification, NMAS, and dry strength are all directly related to wet strength. Traffic level, gradation, compaction method, and diameter were not directly related wet strength. Interestingly, aggregate type was not considered

statistically related to wet strength for one and two freeze/thaw cycles, but was directly related for three freeze/thaw cycles.

## 6.5 Conclusions

Several statistical methods were used to determine the significant factors affecting and related to the specimen wet strength. The main statistical conclusions reached were:

- The most precise TSR data was obtained from the 150mm Superpave specimens indicating that the specimens were more consistent using the diameter of 150mm and SGC.
- There is a direct moderate relationship between polymer modification type and wet strength and a strong direct relationship between both NMAS and dry strength with wet strength, based on correlation analysis.
- For 150mm Superpave gyratory compacted specimens, to obtain an equivalent amount of damage as occurs in 100mm Marshall compacted specimens, specimens need to endure three freeze/thaw cycles.

The difference in damage caused to Marshall specimens in comparison to Superpave specimens indicate that the current AASHTO T-283 standards are not appropriate for identifying the moisture susceptibility of Superpave mixes. If the current standard is not appropriate then a new standard for testing the moisture susceptibility of Superpave compacted specimens should be developed. The new standard could either be a revised AASHTO T-283 standard or a new test procedure, such as one with an APA, could be developed to identify moisture prone mixes.

# Chapter 7 Moisture Susceptibility Testing with the Asphalt Pavement Analyzer

The asphalt pavement analyzer (APA) has been used for years to rank the rutting potential of HMA mixes. Several studies have concluded that the APA adequately ranks the rutting susceptibility of an HMA mix. One objective of this dissertation was to determine if the APA could be used to rank not only the rutting potential of a mix, but also the moisture susceptibility of a mix. The Hamburg wheel tracker has been used to rank the moisture susceptibility of mixes in various studies. One study concluded that the APA and Hamburg do an adequate job of ranking (West et al., 2004), while another concluded that the two were too severe (Cooley et al., 2000).

## 7.1 Asphalt Pavement Analyzer Moisture Susceptibility Test Procedure

HMA was compacted using a Superpave Gyratory Compactor (SGC). Once the specimens were made, volumetric testing and properties were obtained. A preliminary study on two mixes was conducted to determine which testing conditions should be employed for all 21 mixes. The selection of the two mixes was based on moisture susceptibility testing which evaluated the tensile strength ratio of several mixes. Testing conditions evaluated with the two mixes were unconditioned submerged in water, unconditioned in air, one freeze/thaw condition submerged in water, and one freeze/thaw condition in air. Three cylindrical specimens were subjected to APA testing for each condition. The unconditioned specimens were tested in accordance with guidelines established by the APA's User Manual (APA, 2002). The freeze/thaw conditioned specimens were prepared in accordance with the conditioning process outlined in AASHTO T283. HMAs with a high temperature grade of 58 or 64 were tested at their respective high temperature. The polymer modified mixes with a high temperature grade of 70 were also tested at 64, since this was the prescribed field temperature; the higher grade of 70 provides improved rutting resistance. The samples were heated to the high

temperature (either 58 or 64˚C) since permanent deformation typically occurs during the warm months when the binder is more fluid or less viscous.

## 7.2 Sensitivity Study

Two mixes were used to establish testing conditions for moisture susceptibility evaluation using the APA. The two mixes selected were based on TSR results. One of the mixes was deemed moisture resistant while the other was considered to be moisture susceptible based on a TSR criterion of 80% retained tensile strength.

Four condition states were considered for moisture susceptibility evaluation. The first condition state consisted of unconditioned specimens tested in air. The second condition state encompassed unconditioned specimens tested in water. A third condition state consisted of moisture saturated specimens that had endured one freeze/thaw cycle prior to testing in air. The final condition considered moisture saturated specimens that had undergone one freeze/thaw cycle prior to testing in water.

Mean comparisons were conducted to determine if the different condition states yielded statistically different mean rut depths. The mean comparisons indicated that no statistical differences existed between the four condition states when comparing mean rut depths. Since a statistical difference in mean rut depths was not detected, it was concluded that not all four condition states would be required for testing the remaining 19 field mixes. The condition state selected for the study were a control state (unconditioned specimens tested in air), and two condition states of moisture saturated specimens that had endured one freeze thaw cycle with one set tested in air and another in water.

## 7.3 APA Testing of Field Sampled HMA

As mentioned, 21 HMA mixes were collected from the field. Two of the 21 mixes were evaluated during the Sensitivity study to determine the testing conditions to be considered when examining the moisture damage of HMA with the APA. The 19 HMA mixes not evaluated during the Sensitivity study were tested under three condition states. Previously mentioned in the last subsection, the three condition states considered were:

1. Unconditioned tested in air (control set),

2. Moisture saturated and one freeze/thaw cycle tested in air (condition state 2), and
3. Moisture saturated and one freeze/thaw cycle tested in water (condition state 3).

### 7.3.1 Conditioning of the HMA Specimens for APA Testing

All specimens were cut to the appropriate height (75mm) for circular specimens using a circular saw. New geometries of the specimens were recorded after sawing along with new bulk specific gravity measurements using the saturated surface dry method. Specimens were grouped into sets of three based on bulk specific gravity measurements.

Control specimens were preheated at the high performance grade for a minimum time of 6 hours in accordance with the APA testing guidelines. After preheating, a pneumatic tube and steel wheel were lowered over the central axis of each specimen and an APA was set to run 8,000 cycles. As mentioned previously, a cycle is equivalent to a wheel passing one time forward and back to its starting position over the test specimen. Once the inner chamber of the APA reheated to the appropriate testing temperature a test was initiated. The reheating usually took less than 2 minutes, since the chamber was heated to the appropriate test temperature prior to the placement of specimens. The reheating was necessary since there was some heat loss upon the opening of the APA doors to install the specimens locked inside the molds. After a completion of 8,000 cycles, test data was automatically transferred to a spreadsheet file and saved for future analysis.

Specimens in either the condition state 2 or 3 were prepared in the same manner, except the specimens which were moisture saturated and endured one freeze/thaw cycle prior to testing. These specimens were moisture saturated to a maximum of 80% air voids filled with water. Specimens were wrapped in Glad Press n' Seal® with ends of the wrap taped down with packing tape. Wrapped specimens and 10mL of water were placed inside a plastic freezer bag labeled with mix information, specimen number, and condition state group. Specimens inside the freezer bags were then placed in a freezer for a period of 24 hours. To minimize the amount of heat entering the freezer, all specimens

in a particular group were prepared first and then placed into the freezer at the same time instead of individually. After 24 hours, specimens were placed in a 60˚C water bath to thaw. Once thawing was complete, specimens were preheated to the appropriate APA testing temperature for the 6 hour minimum time. Specimens tested in air were placed in an air chamber for preheating, while those to be tested in water were placed in a water bath for preheating. After the allotted 6 hours of preheating, specimens were placed in an APA for testing. Specimens tested in air were placed in an APA and a steel wheel lowered on top of a pneumatic tube and the APA chamber was allowed to re-establish the test temperature prior to the initiation of 8,000 cycles. Specimens tested in water were placed in an APA chamber and the doors sealed shut. Once the APA doors were shut, a metal box elevated to surround the APA molds. Once the metal box had reached its highest point, water heated to the appropriate temperature flowed into the chamber to fill the metal box. The heated water at all times kept specimens completely immersed. Once the metal box was filled and the water and test chamber re-established the appropriate test temperature, 8,000 cycles commenced. Data from both condition states 2 and 3 were automatically transferred to a spreadsheet file to be saved and analyzed later.

### 7.3.2 APA Test Results for Field Sampled HMA

Mean comparisons and dispersion analysis were employed to evaluate data collected from APA testing. A significance level of 0.05% was assumed for all evaluations. Data from each mix was analyzed along with all of the data combined.

#### 7.3.2.1 Analysis of All APA Data

Analysis of data combined indicated that the significant factors affecting rut depths were condition state, PG high temperature, NMAS, and aggregate passing the #4, #8, #50, #100 sieves. Mean comparisons of the main effects were conducted using the Tukey method to determine whether or not means of different groups are statistically equivalent. Tables 7.1 through 7.6 outline the results of the mean comparisons. Effect levels considered statistically equivalent share the same group letter. Two group letters appear if an effect level is statistically similar to more than one group.

Table 7.1 summarizes comparisons of mean rut depths grouped by condition state. Condition states 1 (unconditioned) and 3 are considered statistically equivalent. Condition state 2 differed from the rut depth means of the two other groups. The average rut depth for condition state 2 specimens was about 6mm while condition states 1 and 3 were 8.5mm and 9.5mm, respectively. It would appear that condition state 2 specimens performed better than condition state 1 and 3. It is hypothesized that the specimens stiffened during the combined freeze/thaw cycle and preheating for APA testing which resulted in the condition state 2 specimens performing better. Condition state 1 was only preheated and condition state 3 was preheated in a water bath not an air chamber.

**Table 7.1 Mean Comparison by Condition State**

| Condition | Group |
|---|---|
| Unconditioned Tested in Air | A |
| Conditioned, One Freeze-Thaw Tested in Air | B |
| Conditioned, One Freeze-Thaw Tested in Water | A |

Table 7.2 compared average rut depths of specimens grouped by PG high temperature. Mixes with PG 58 and PG 64 binders were found statistically equivalent and PG 70 mixes differed. The rut depth for PG 70 mixes was 1.3mm and 3.4mm less than PG 64 and PG 58 mixes, respectively. It is hypothesized that the PG 70 mixes performed better since these mixes were tested at 64˚C instead of at 70˚C. It should be remembered that mixes with PG 70 binders were used in lieu of PG 64 binders to realize better performance for certain mixes; therefore, these mixes were tested at 64˚C to observe the improved performance if any.

**Table 7.2 Mean Comparison by PG High Temperature**

| PG High Temperature | Group |
|---|---|
| PG 58 | A |
| PG 64 | A |
| PG 70 | B |

Table 7.3 summarizes the results of a rut depth mean comparison between specimens tested at 64˚C and 58˚C. The specimens tested at 64˚C performed better than

the ones tested at 58˚C. It is hypothesized that the 64˚C specimens performed better since the PG 70 binders were included in this group.

**Table 7.3 Mean Comparisons by Test Temperature**

| Test Temperature | Group |
|---|---|
| 58˚C | A |
| 64˚C | B |

Table 7.4 summarizes a rut depth mean comparison grouping the specimens by NMAS. 19.0mm NMAS and 12.5mm NMAS were deemed statistically equivalent. 12.5mm NMAS and 9.5mm NMAS were found to be statistically equivalent. 19.0mm NMAS and 9.5mm NMAS differed statistically. 9.5mm NMAS specimens yielded the lowest rut depth while 19.0mm NMAS specimens yielded the deepest ruts.

**Table 7.4 Mean Comparisons by NMAS**

| NMAS | Group |
|---|---|
| 19.0mm | A |
| 12.5mm | A B |
| 9.5mm | B |

Table 7.5 summarizes rut depth mean comparisons grouped by ESAL level. ESAL levels 3 (3 million ESALs) and 10 (10 million ESALs) were deemed statistically equivalent and 10 million ESALs and 30 million ESALs were also found to be statistically equivalent. Mixes made for 30 million ESALs performed the best and 1 million ESAL specimens performed the worst.

**Table 7.5 Mean Comparisons by ESAL Level**

| ESAL | Group |
|---|---|
| 1 | A |
| 3 | B |
| 10 | B C |
| 30 | C |

Table 7.6 summarizes a rut depth mean comparison by gradation. The mean rut depths for the two gradations were considered statistically similar.

**Table 7.6 Mean Comparisons by Gradation**

| Gradation | Group |
|---|---|
| Fine | B |
| Coarse | B |

### 7.3.2.2 Analysis By Field Mix

Material collected from Ann Arbor was tested at 64˚C since the asphalt binder used in the mix had a PG high temperature of 70. An ANOVA table indicated that there is no significant difference between the three condition states.

Material collected from Battle Creek was tested at 64˚C since the asphalt binder used in the mix had a PG high temperature of 64˚C. Variance analysis indicated that there is a significant difference between the three condition states. Further analysis revealed that no difference exists between unconditioned samples and condition state 3 samples of this set. However, condition state 2 of this set differed from both the unconditioned and condition state 3.

Material collected from Brighton was tested at 58˚C since the asphalt binder used in the mix had a PG high temperature of 58˚C. No significant statistical difference was found between the three condition states.

Material collected from Detroit was tested at 64˚C since the asphalt binder used in the mix had a PG high temperature of 70˚C. Variance and mean analysis indicated that there is a significant difference between the three condition states. Further analysis revealed that no difference exists between unconditioned samples and condition state 3 samples of this set. However, condition state 2 of this set differed from the unconditioned and condition state 3 specimens.

Material collected from Dundee with an 19.0mm NMAS was tested at 64˚C since the asphalt binder used in the mix had a PG high temperature of 64˚C. Based on the

analysis conducted on rut depth data, the 3 condition states are statistically different. Condition states 1 (unconditioned) and 2 were statistically different. Condition states 2 and 3 are marginally equivalent.

Material collected from Dundee with an 12.5mm NMAS was tested at 64˚C since the asphalt binder used in the mix had a PG high temperature of 64˚C. Rut depths created at the three different test conditions were statistically equivalent.

Material obtained from Grand Rapids with an 19.0mm NMAS was tested at 58˚C since the asphalt binder used in the mix had a PG high temperature of 58˚C. The rut depths at all condition levels were considered statistically equivalent with the other condition levels.

Material obtained from Hartland was tested at 58˚C since the asphalt binder used in the mix had a PG high temperature of 58˚C. No significant statistical difference was found between the three condition states.

Material obtained from Howell was tested at 64˚C since the asphalt binder used in the mix had a PG high temperature of 70˚C. Based on the analysis conducted on rut depth data, the 3 condition states are statistically different. Condition states 1 (unconditioned) and 2 were statistically different. Condition states 2 and 3 are marginally equivalent.

Material obtained from Levering was tested at 58˚C since the asphalt binder used in the mix had a PG high temperature of 58˚C. No significant statistical difference was found between the three condition states.

Material obtained from Michigan Ave with a 19.0mm NMAS was tested at 58˚C since the asphalt binder used in the mix had a PG high temperature of 58˚C. No significant statistical difference was found between the three condition states.

Material obtained from Michigan Ave with a 12.5mm NMAS was tested at 64˚C since the asphalt binder used in the mix had a PG high temperature of 70˚C. Based on the analysis conducted on rut depth data, the 3 condition states are statistically different. The unconditioned specimens in this set yielded statistically different rut depths than those for both condition states 2 and 3.

Material obtained from US-12 was tested at 64˚C since the asphalt binder used in the mix had a PG high temperature of 64˚C. No significant statistical difference was found between the three condition states.

Material collected from Owosso was tested at 64˚C since the asphalt binder used in the mix had a PG high temperature of 64˚C. The levels of condition were deemed significant factors for affecting rut depths. Further analysis indicated that specimens tested in condition state 3 differed from both those tested in condition state 1 (unconditioned) and condition state 2.

Material obtained from Pinckney was tested at 64˚C since the asphalt binder used in the mix had a PG high temperature of 64˚C. No significant statistical difference was found between the three condition states.

Material obtained from Saginaw was tested at 58˚C since the asphalt binder used in the mix had a PG high temperature of 58˚C. No significant statistical difference was found between the three condition states.

Material collected from St. Johns was tested at 58˚C since the asphalt binder used in the mix had a PG high temperature of 58˚C. Statistical differences were found between condition state 1 and condition state 3 specimens.

Material collected from Toledo was tested at 64˚C since the asphalt binder used in the mix had a PG high temperature of 70˚C. The levels of condition were deemed significant factors for affecting rut depths. Further analysis indicated that specimens tested in condition state 3 differed from both those tested in condition state 1 (unconditioned) and condition state 2.

Material collected from Van Dyke was tested at 64˚C since the asphalt binder used in the mix had a PG high temperature of 64˚C. The levels of condition were deemed significant factors for affecting rut depths. Further analysis indicated that specimens tested in condition state 2 differed from both those tested in condition state 1 (unconditioned) and condition state 3.

Table 7.7 summarizes the results of the rut depth mean comparisons conducted on the APA Data. It can be seen that many of the mixes yielded statistically equivalent rut depths for the different combinations of testing environment and specimen conditioning.

**Table 7.7 Summary of Rut Depth Mean Comparison**

| | Condition State | | |
|---|---|---|---|
| Mix | 1 | 2 | 3 |
| Ann Arbor | A | A | A |
| Battle Creek | A | B | A |
| Brighton | A | A | A |
| Clarkston | A | A | A |
| Detroit | A | B | A |
| Dundee 19.0mm NMAS | A | B | B C |
| Dundee 12.5mm NMAS | A | A | A |
| Grand Rapids I-196 | A | A | A |
| Grand Rapids M-45 | A | A | A |
| Hartland | A | A | A |
| Howell | A | B | B C |
| Levering | A | A | A |
| Michigan Ave 19.0mm NMAS | A | A | A |
| Michigan Ave 12.5mm NMAS | A | B | B |
| Michigan International Speedway US-12 | A | A | A |
| Owosso | A | A | B |
| Pinckney | A | A | A |
| Saginaw | A | A | A |
| St. Johns | A | A | A |
| Toledo | A | A | B |
| Van Dyke | A | A | B |

### 7.3.3 General Linear Model Analysis of APA Data

General linear models (GLMs), ANOVA and stepwise regression, were used to evaluate the significance of several factors affecting the rut depth of a specimen. The first set of analyses evaluated all of the data without grouping by a factor. Table 7.8 summarizes the conclusions gleaned from the ANOVA. Dots in a cell indicate that a factor is deemed significant based on a level of significance of 0.05. The sum of squares associated with each factor was evaluated. Sum of squares relate how the variability of a factor affects a model. Type I sum of squares calculates a factor's effect with regards to the preceding

factors have already been entered into a model. Factor order is not an issue for Type III sum of squares, which account for a factor's variation assuming that all factors have been entered into a model. According to the Type I sum of squares, the factors with a significant affect on rut depth are site, condition, high PG temperature, test temperature, material retained on a 19mm sieve, material obtained on a 9.5mm sieve, and binder content. Type III sum of squares only identifies two factors as significantly affecting rut depth, test temperature and material retained on a 9.5mm sieve. From this analysis, it can be seen that conservatively speaking, test temperature and material retained on a 9.5mm sieve are significant factors. Closer examination indicates that overall, specimens tested at 64˚C exhibited lower rut depths, especially those with a high PG temperature of 70˚C.

**Table 7.8 Summary of ANOVA for All of the APA data**

| Factor | Type I Sum of Squares Significance | Type III Sum of Squares Significance |
|---|---|---|
| Site | • | |
| Condition | • | • |
| High PG Temp | • | |
| Test Temperature | | |
| 25mm | | |
| 19mm | | |
| 12.5mm | | |
| 9.5mm | • | |
| 4.75mm | • | |
| 2.36mm | • | |
| 1.18mm | | |
| 0.60mm | | |
| 0.30mm | • | |
| 0.15mm | | |
| 0.075mm | | |
| Binder Modification | | |
| RAP | | |
| Binder Content | | |
| Fines/Binder | • | |
| NMAS | • | |
| ESAL | | |
| Gradation | | |
| Angularity | | |

Regression analysis was employed to evaluate the nature of the relationship of a factor and a model. Stepwise selection was used to develop a model. Table 7.9 summarizes the results of the regression analysis based on stepwise selection. The model selected consisted of six factors. The $R^2$, which quantitatively describes how well rut depth is predicted by a model, was 0.9982. Another statistical tool used to evaluate the regression model selected via stepwise selection was Mallow's Cp. Mallow's Cp is a statistical tool used to select an appropriate model. A propitious model will have a Cp value close to the number of variables in the model plus 1. Mallow's Cp is calculated as follows:

$$Cp = \frac{SSE}{MSE} - N + 2 \bullet p \quad \textbf{Equation 7.1}$$

where:

SSE= Residual sum of squares,

MSE= Mean sum of squares,

N= Number of observations, and

p=Number of factors +1.

Mallow's Cp for the selected regression model was 10.0917. The best value for this model would have been 7 since there are six factors; however a value of 10 is not a sign of a poorly fit model. The parameter estimates are the coefficients associated with each factor. A large parameter estimate indicates that a relationship is strong. The measure of significance is related in the column labeled Pr > F.

The next set of ANOVA and regression analyses grouped the data by condition state. The first condition state explored was the condition state 1 (the control set). The first GLM analysis evaluated was the ANOVA table for condition state 1. Table 7.10 summarizes the results of the ANOVA for condition state rut depth data. As with the previous ANOVA table analysis, information about Type I and Type III sum of squares is provided. The level of significance was $\alpha$=0.05. The dots in the table indicate that a factor is significant. Nine factors were considered significant for Type I sum of squares, however no factors were considered significant for Type III sum of squares. The factors

deemed significant by Type I sum of squares included site, high PG temperature, several sieve sizes, and the fines to binder ratio.

**Table 7.9 Regression Parameter Estimated for All APA Data**

| Factor | Parameter Estimate | Pr > F |
|---|---|---|
| Intercept | 775.15666 | <0.0001 |
| Site | 0.32019 | 0.0001 |
| Condition | 0.52751 | 0.0287 |
| High PG Temp | 1.5151 | 0.0462 |
| Test Temperature | -2.17985 | 0.0093 |
| 25mm | | |
| 19mm | -7.33037 | <0.0001 |
| 12.5mm | 1.67161 | <0.0001 |
| 9.5mm | -1.31011 | <0.0001 |
| 4.75mm | | |
| 2.36mm | | |
| 1.18mm | | |
| 0.60mm | 0.38679 | <0.0001 |
| 0.30mm | | |
| 0.15mm | -1.27069 | 0.0006 |
| 0.075mm | | |
| Binder Modification | -5.42499 | 0.0134 |
| RAP | | |
| Binder Content | | |
| Fines/Binder | | |
| NMAS | 4.70714 | 0.0005 |
| ESAL | | |
| Gradation | | |
| Angularity | -1.36009 | <0.0001 |

**Table 7.10 Summary of ANOVA for Condition State 1 APA Data**

| Factor | Type I Sum of Squares Significance | Type III Sum of Squares Significance |
|---|---|---|
| Site | • | |
| Condition | | |
| High PG Temp | • | |
| Test Temperature | | |
| 25mm | | |
| 19mm | • | |
| 12.5mm | | |
| 9.5mm | • | |
| 4.75mm | • | |
| 2.36mm | • | |
| 1.18mm | | |
| 0.60mm | | |
| 0.30mm | • | |
| 0.15mm | • | |
| 0.075mm | | |
| Binder Modification | | |
| RAP | | |
| Binder Content | | |
| Fines/Binder | • | |
| NMAS | | |
| ESAL | | |
| Gradation | | |
| Angularity | | |

The second set of analysis conducted for condition state 1 was regression analysis to evaluate the nature of the factor relationships. Table 7.11 summarizes the results of the regression analysis for condition state 1 APA rut depth data. The $R^2$ for the condition state 1 regression model was 0.7797 and Mallow's Cp was 22.5524. The model would be considered good based on the $R^2$ and Mallow's Cp. An excellent model would have yielded a higher $R^2$ and lower Mallow's Cp. Outside of the intercept, the fines to binder ratio has the largest parameter estimate indicating that the rut depth of the control specimens is strongly related to the fines to binder ratio.

**Table 7.11 Regression Parameter Estimates for Condition State 1 APA Rut Depth Data**

| Factor | Parameter Estimate | Pr > F |
|---|---|---|
| Intercept | 369.62144 | 0.009 |
| Site | -0.15442 | 0.0005 |
| Condition | | |
| High PG Temp | | |
| Test Temperature | -0.2361 | 0.0226 |
| 25mm | | |
| 19mm | -3.29513 | 0.0031 |
| 12.5mm | | |
| 9.5mm | | |
| 4.75mm | -0.4561 | <0.0001 |
| 2.36mm | | |
| 1.18mm | | |
| 0.60mm | | |
| 0.30mm | 0.32202 | 0.0600 |
| 0.15mm | 1.7956 | 0.0036 |
| 0.075mm | | |
| Binder Modification | | |
| RAP | 0.12625 | 0.0756 |
| Binder Content | | |
| Fines/Binder | -15.43404 | <0.0001 |
| NMAS | 4.04996 | <0.0001 |
| ESAL | | |
| Gradation | -8.39689 | <0.0001 |
| Angularity | | |

After evaluating the data from condition state 1, condition state 2 was evaluated (moisture saturation plus one freeze/thaw cycle tested in air). Table 7.12 summarizes the ANOVA results of condition state 2 rut depth data obtained from APA testing. Nine factors were deemed significant based on Type I sum of squares. The factors deemed statistically significant for condition state 2 are not the same as the factors deemed statistically significant for condition state 1 ruts. Both condition state ruts were affected by site, high PG temperature, and the fines to binder ratio. However, condition state 2 ruts were also affected by binder modification. There were also several differences in which sieve sizes affected the ruts.

**Table 7.12 Summary of ANOVA for Condition State 2 APA Rut Depth Data**

| Factor | Type I Sum of Squares Significance | Type III Sum of Squares Significance |
|---|---|---|
| Site | • | |
| Condition | | |
| High PG Temp | • | |
| Test Temperature | | |
| 25mm | | |
| 19mm | • | |
| 12.5mm | • | |
| 9.5mm | | |
| 4.75mm | | |
| 2.36mm | • | |
| 1.18mm | | |
| 0.60mm | • | |
| 0.30mm | | |
| 0.15mm | • | |
| 0.075mm | | |
| Binder Modification | • | |
| RAP | | |
| Binder Content | | |
| Fines/Binder | • | |
| NMAS | | |
| ESAL | | |
| Gradation | | |
| Angularity | | |

Regression analysis was conducted after evaluating the ANOVA table for condition state 2. Table 7.13 summarizes the parameter estimates for condition state 2 rut depth data. Disregarding the intercept, gradation exhibits the largest parameter estimate, indicating that gradation (fine or coarse) is strongly related to rut depths of condition state 2 specimens.

**Table 7.13 Regression Parameter Estimates for Condition State 2 APA Rut Depth Data**

| Factor | Parameter Estimate | Pr > F |
|---|---|---|
| Intercept | 354.05987 | <0.0001 |
| Site | 0.11773 | 0.0314 |
| Condition | | |
| High PG Temp | -0.14946 | 0.0127 |
| Test Temperature | | |
| 25mm | | |
| 19mm | -3.00001 | <0.0001 |
| 12.5mm | | |
| 9.5mm | | |
| 4.75mm | -0.38694 | <0.0001 |
| 2.36mm | 0.59923 | 0.0003 |
| 1.18mm | | |
| 0.60mm | | |
| 0.30mm | | |
| 0.15mm | | |
| 0.075mm | -0.78474 | 0.0220 |
| Binder Modification | | |
| RAP | | |
| Binder Content | | |
| Fines/Binder | | |
| NMAS | | |
| ESAL | | |
| Gradation | 6.65655 | 0.0017 |
| Angularity | -0.92217 | <0.0001 |

The final condition state to be evaluated was condition state 3 (moisture saturation plus one freeze/thaw cycle tested in water). Table 7.14 summarizes the ANOVA conclusions for condition state 3 rut depth data. Evaluation of condition state 3 ANOVA indicates that six factors were deemed statistically significant for Type I sum of squares. Like condition states 1 and 2, condition state 3 Type I sum of squares indicated that high PG temperature and fines to binder ratio are significant factors. No factors were deemed statistically equivalent for Type III sum of squares.

**Table 7.14 Summary of ANOVA for Condition State 3 APA Rut Depth Data**

| Factor | Type I Sum of Squares Significance | Type III Sum of Squares Significance |
|---|---|---|
| Site | | |
| Condition | | |
| High PG Temp | • | |
| Test Temperature | | |
| 25mm | | |
| 19mm | • | |
| 12.5mm | | |
| 9.5mm | • | |
| 4.75mm | • | |
| 2.36mm | | |
| 1.18mm | | |
| 0.60mm | | |
| 0.30mm | | |
| 0.15mm | • | |
| 0.075mm | | |
| Binder Modification | | |
| RAP | | |
| Binder Content | | |
| Fines/Binder | • | |
| NMAS | | |
| ESAL | | |
| Gradation | | |
| Angularity | | |

Once the ANOVA evaluation was completed, regression analysis was used to evaluate the nature of the relationships of the factors affecting condition state 3 rut depths. Table 7.15 displays the parameter estimates for the regression model selected based on condition state 3 rut depth data. Disregarding the intercept, the 19mm sieve yields the largest parameter estimate. Interestingly, in the stepwise regression model selected, the fines to binder ratio is marginally significant.

**Table 7.15 Regresion Parameter Estimates for Condition State 3 APA Rut Depth Data**

| Factor | Parameter Estimate | Pr > F |
|---|---|---|
| Intercept | 680.98121 | <0.0001 |
| Site | | |
| Condition | | |
| High PG Temp | | |
| Test Temperature | -0.29178 | 0.0679 |
| 25mm | | |
| 19mm | -6.26604 | <0.0001 |
| 12.5mm | | |
| 9.5mm | | |
| 4.75mm | -0.75907 | <0.0001 |
| 2.36mm | 0.58732 | 0.0042 |
| 1.18mm | | |
| 0.60mm | 0.28329 | 0.1102 |
| 0.30mm | | |
| 0.15mm | | |
| 0.075mm | | |
| Binder Modification | | |
| RAP | | |
| Binder Content | -4.32343 | 0.0034 |
| Fines/Binder | -5.57584 | 0.0538 |
| NMAS | 4.98947 | <0.0001 |
| ESAL | | |
| Gradation | | |
| Angularity | | |

Evaluation of the data grouped by condition state offered some useful insight. According to the ANOVAs, there are several factors that consistently affect the rut depth of APA tested specimens. Those factors are high PG temperature, fines to binder ratio, and the sieve sizes 19mm and 0.15mm. The regression analysis differed between the three condition states. The factor exhibiting the largest parameter estimate was not consistent for all three condition states. This indicates that not only does testing environment, but also condition may be affecting the final rut depth created by an APA. Further inspection of the high PG temperature groupings revealed that the PG 70-X binders performed the best, smallest rut depths. The mixes with a PG 70-X binders were tested at 64˚C and performed better than the other mixes. Most likely these mixes performed better since the binders were less fluid during testing. Binders that tend to be

fluid easily move with the application of a load. Aggregates can also move when the binders are moving during this fluid state. Shifting of material in a specimen in the presence of water can allow for breaks in a binder membrane thus enabling the penetration of moisture. Once moisture penetrates a binder it tends to soften a binder making it less resistant to moisture damage.

#### 7.3.3.1 APA Analysis Summary

The analysis conducted on rut depth obtained from APA testing was outlined in the above sections summarizing ANOVA table results and mean comparison results. Interestingly for the majority of comparisons where there were differences between the condition effect levels, the unconditioned and condition state 3 specimens were usually deemed statistically equivalent while condition state 2 was deemed statistically different from both. However, only 8 mixes were affected statistically different by the condition state. The majority of mixes yielded statistically equivalent rut depths for all three condition states. A second observation that is intriguing is that there is no statistical difference between the rut depths of coarse-graded and fine-graded mixes.

### 7.3.4 APA Moisture Criteria

A moisture criterion for APA testing was developed based on ratio of the rut depths. The ratio consisted of condition state 3 divided by condition state 1. Any value less than 1± 0.05 was considered not prone to moisture damage. Values greater than 1± 0.05 were deemed moisture damage prone. The assumption for this criterion is that as mix ages it becomes stiffer therefore the specimens that endured longer heating times are aged more than the unconditioned specimens. Condition state 2 and 3 specimens therefore should be stiffer than condition state 1 specimens. Stiffer binders are less prone to rutting. The ratio of condition state 2 to condition state 1 should also be determined to see if the freeze/thaw cycle has an affect on rut depth results. Table 7.16 summarizes the results of applying the two criteria. It appears that the majority of mixes fail both the freeze/thaw and moisture criteria. This is possible, however, these results should be compared to

field cores to better refine both criteria. It is suspected that the criterion is on the conservative side.

**Table 7.16 Summarized Results of Field Mixes Based on Freeze/thaw and Moisture Criteria**

| | Moisture Damage Prone | Moisture Damage Resistant |
|---|---|---|
| **Freeze-Thaw Damage Prone** | Grand Rapids M-45, Hartland | MIS US12, Pinckney |
| **Freeze-Thaw Damage Resistant** | Battle Creek, Detroit, Dundee 19.0mm NMAS, Dundee 12.5mm NMAS, Howell, Levering, Michigan Ave 19.0mm NMAS, Owosso, Saginaw, St. Johns, Toledo, Vandyke | Ann Arbor, Michigan Ave 4, Brighton |

Rutting results at WesTrack were compared to APA results (Epps Martin and Park, 2003). In the study, a rut of 12.5mm was considered dangerous and used as a failure marker. Tests with the APA of the same mixes yielded ruts of 9.1mm on average. The rut depth of 9.1mm created by the APA was then deemed the failure point for the mixes. Until field data can be acquired to relate APA results to Michigan mixes, a value of 9.1mm should be used as the failure criteria. The 9.1mm criteria was used to improve the criterion based on the ratio of the conditioned water tested specimens divided by the control specimens. Several specimen groups yielded high ratios which would be deemed moisture prone, however the rut depths were very small. Setting a failure rut depth and then calculating the ratio alleviates the issue of specimens with small rut depths being labeled as moisture prone. Table 7.17 summarizes which conditions groups within a mix failed the rut depth criterion of 9.1mm. It can be seen that most of the specimens from condition state 2 (moisture saturation plus one freeze/thaw tested in air) specimens did not fail the rut depth criterion. Seven of the control groups failed and nine of the condition state 3 groups failed.

A further analysis was conducted to determine if these failure groups failed due to moisture damage or if the mix is merely susceptible to rutting. For this analysis, the ratio method of dividing water tested conditioned specimen rut depth values by control specimen rut depth values was implemented. If the ratio is greater than 1 the mix is considered moisture prone; whereas if the ratio is less than one it is not considered moisture prone. Table 7.18 summarizes the rut depth ratios of the mixes that failed the maximum rut depth criterion of 9.1mm. All of the mixes actually yielded lower rut depths for conditioned specimens tested in water except for the two mixes from Grand Rapids.

**Table 7.17 Summary of Rut Depth Failure for all Three Condition States**

| Site | Control | Saturated and Freeze/Thaw Tested in Air | Saturated and Freeze/Thaw Tested in Water |
|---|---|---|---|
| Ann Arbor | Pass | Pass | Pass |
| Battle Creek | **Fail** | Pass | **Fail** |
| Brighton | Pass | Pass | Pass |
| Clarkston | Pass | Pass | Pass |
| Detroit | Pass | Pass | Pass |
| Dundee 19.0mm NMAS | **Fail** | Pass | **Fail** |
| Dundee 12.5mm NMAS | Pass | Pass | Pass |
| Grand Rapids I-196 | **Fail** | **Fail** | **Fail** |
| Grand Rapids M-45 | **Fail** | **Fail** | **Fail** |
| Hartland | Pass | Pass | Pass |
| Howell | **Fail** | Pass | **Fail** |
| Levering | **Fail** | **Fail** | **Fail** |
| Michigan Ave 19.0mm NMAS | Pass | Pass | **Fail** |
| Michigan Ave 12.5mm NMAS | Pass | Pass | Pass |
| Michigan International Speedway | Pass | Pass | Pass |
| Owosso | **Fail** | Pass | Pass |
| Pinckney | Pass | Pass | Pass |
| Saginaw | Pass | Pass | Pass |
| St. Johns | Pass | Pass | **Fail** |
| Toledo | Pass | Pass | Pass |
| Van Dyke | Pass | Pass | **Fail** |

**Table 7.18 Rut Depth Ratios of Mixes that Failed the Rut Depth Maximum Criterion**

| Site | Ratio of Conditioned Specimens Tested in Water by Control Specimens |
|---|---|
| Battle Creek | 0.42 |
| Dundee 19.0mm NMAS | 0.62 |
| Grand Rapids I-196 | **1.05** |
| Grand Rapids M-45 | **1.07** |
| Howell | 0.66 |
| Levering | 0.84 |
| Michigan Ave 19.0mm NMAS | 0.90 |
| St. Johns | 0.76 |
| Van Dyke | 0.53 |

## 7.4 Comparison between AASHTO T-283 and APA Results

In the previous chapter, the factors affecting TSR were examined. This section will examine whether or not those same factors that affect TSR also affect APA results along with identifying if there is a relationship between the two test methods. Table 7.19 summarizes which mixes were found to be prone to moisture damage and which ones were resistant. Table 7.20 summarizes the results of AASHTO T-283 testing. The specimens tested using an APA endured only one freeze/thaw cycle, while the TSR specimens endured three freeze/thaw cycles. Interestingly, none of the mixes fail the TSR criterion until after three freeze/thaw cycles when specimens are procured with a Superpave gyratory compactor to 150mm in diameter. The results obtained from the TSR tests after three freeze/thaw cycles are analogous to the results of the APA testing after one freeze/thaw cycle. The question arises, is the relationship between the two tests of significance? The mix identified by both the APA and TSR, after three freeze/thaw cycles, test results as moisture susceptible is also identified by the traditional TSR method using Marshall compacted specimens. However, the Dundee mix was also identified as moisture susceptible by the traditional TSR test procedure but not by the APA or TSR after three freeze/thaw cycles of 150mm specimens. Evaluating the results

for Dundee obtained for SGC specimens indicates that neither test procedure was close to identifying Dundee as a moisture prone mix. Identifying which test method is more appropriate for identifying the moisture susceptibility cannot be completed until after field data is compared to the laboratory test results. For now, the agreement of moisture susceptibility results on six of the seven mixes is considered favorable.

**Table 7.19 APA Moisture Damage Testing Results**

| Site | Moisture Damage |
|---|---|
| Dundee | Resistant |
| Howell | Resistant |
| Owosso | Resistant |
| Brighton | Resistant |
| Grand Rapids I-196 | **Prone** |
| Clarkston | Resistant |
| St. Johns | Resistant |

**Table 7.20 TSR Moisture Damage Testing Results**

| | Average TSR for 100mm Superpave | | | Average TSR for 100mm Marshall | | | Average TSR for 150mm Superpave | | |
|---|---|---|---|---|---|---|---|---|---|
| | TSR 1F/T | TSR 2F/T | TSR 3F/T | TSR 1F/T | TSR 2F/T | TSR 3F/T | TSR 1F/T | TSR 2F/T | TSR 3F/T |
| Dundee | **Prone** | Resistant | **Prone** | Resistant | **Prone** | **Prone** | Resistant | Resistant | Resistant |
| Howell | Resistant | Resistant | Resistant | Resistant | Resistant | Resistant | Resistant | Resistant | Resistant |
| Owosso | Resistant | Resistant | Resistant | Resistant | Resistant | Resistant | Resistant | Resistant | Resistant |
| Brighton | Resistant | Resistant | Resistant | Resistant | Resistant | **Prone** | Resistant | Resistant | Resistant |
| Grand Rapids I-196 | Resistant | **Prone** | **Prone** | **Prone** | **Prone** | **Prone** | Resistant | Resistant | **Prone** |
| Clarkston | Resistant | Resistant | Resistant | Resistant | Resistant | Resistant | Resistant | Resistant | Resistant |
| St. Johns | Resistant | Resistant | Resistant | Resistant | Resistant | **Prone** | Resistant | Resistant | Resistant |

### 7.4.1 Factors Affecting Moisture Damage Test Results

ANOVA and Regression analyses of the seven mixes used for evaluating AASHTO T-283 procedure were conducted on the APA test results for those mixes. The ANOVA indicated that the only significant factor was the performance grade for all three testing conditions. The factors affecting tensile strength according to a regression analysis are

compaction method and diameter of specimen. Obviously, the factors affecting the test results of these two tests are different. An additional analysis was conducted by evaluating factors affecting TSR within a compaction method and diameter grouping. Table 7.21 summarizes the factors significantly affecting TSR for Marshall 100mm specimens.

Table 7.22 summarizes the factors significantly affecting TSR for Superpave 150mm specimens. The dry strength has a shared significant factor with the APA results, binder PG. Upon closer examination of the binder PG factor for wet strength and tensile strength, most of the p-values marginally failed to be insignificant. This revelation indicates that binder PG effects should be researched more to observe the effects on moisture susceptibility testing.

**Table 7.21 Factors Affecting TSR of Marshall 100mm Specimens**

| Factor | Dry Strength | Wet Strength | Tensile Strength Ratio |
|---|---|---|---|
| PG | | | |
| 25.0mm | | | |
| 19.0mm | • | | • |
| 12.5mm | | | • |
| 9.5mm | | | |
| 4.75mm | • | • | |
| 2.36mm | | | |
| 1.18mm | | | |
| 0.600mm | | | |
| 0.300mm | | | |
| 0.150mm | | | |
| 0.075mm | | | |
| Polymer | | | |
| Binder Content | | | |
| Fines/Binder | | | |
| NMAS | | | |
| ESAL | | | |
| Gradation | | | |
| Angularity | | | |

**Table 7.22 Factors Affecting TSR of Superpave 150mm Specimens**

| Factor | Dry Strength | Wet Strength | Tensile Strength Ratio |
|---|---|---|---|
| PG | • | | |
| 25.0mm | | | |
| 19.0mm | • | | • |
| 12.5mm | • | | • |
| 9.5mm | • | | • |
| 4.75mm | • | • | • |
| 2.36mm | | | |
| 1.18mm | | | |
| 0.600mm | | | |
| 0.300mm | | | |
| 0.150mm | | | |
| 0.075mm | | | |
| Polymer | | | |
| Binder Content | | | |
| Fines/Binder | | | |
| NMAS | | | |
| ESAL | | | • |
| Gradation | | | |
| Angularity | | | |

Regression analysis was conducted on the TSR obtained after three freeze/thaw cycles for 150mm Superpave specimens. The analysis concentrated on 150mm Superpave specimens to allow for a comparison between the APA rut depth data for the same seven mixes. Stepwise selection was employed to develop a regression model to evaluate the nature of the relationships affecting rut depth. Table 7.23 summarizes the parameter estimates for TSRs obtained after three freeze/thaw cycles for 150mm Superpave specimens. Binder content exhibits the largest parameter estimate indicating that binder content has a strong relationship with TSR values. Table 7.24 summarizes the results of regression analysis of APA tested specimens made from mixes also used for TSR evaluation. The factor with the largest parameter estimate was binder content. Both the TSR after three freeze/thaw cycles and APA testing data indicated that binder content has a strong relationship with the test output (strength for TSR or rut depth for APA).

**Table 7.23 Regression Parameter Estimates for 150mm Superpave TSR Data After Three Freeze/Thaw Cycles**

| Factor | Parameter Estimate | Pr > F |
|---|---|---|
| Intercept | 233.47892 | 0.0020 |
| Site | | |
| Condition | | |
| High PG Temp | | |
| Test Temperature | | |
| 25mm | | |
| 19mm | | |
| 12.5mm | | |
| 9.5mm | | |
| 4.75mm | | |
| 2.36mm | | |
| 1.18mm | | |
| 0.60mm | | |
| 0.30mm | | |
| 0.15mm | | |
| 0.075mm | -8.55387 | 0.0020 |
| Binder Modification | -0.10745 | 0.0453 |
| RAP | | |
| Binder Content | -14.24302 | 0.0020 |
| Fines/Binder | | |
| NMAS | -4.64588 | 0.0020 |
| ESAL | -1.98402 | 0.0020 |
| Gradation | | |
| Angularity | | |

**Table 7.24 Regression Parameter Estimates for APA Data of Mixes Used for TSR Evaluation**

| Factor | Parameter Estimate | Pr > F |
|---|---|---|
| Intercept | 66.34154 | <0.0001 |
| Site | | |
| Condition | | |
| High PG Temp | 0.14813 | 0.1192 |
| Test Temperature | | |
| 25mm | | |
| 19mm | | |
| 12.5mm | | |
| 9.5mm | | |
| 4.75mm | | |
| 2.36mm | | |
| 1.18mm | | |
| 0.60mm | | |
| 0.30mm | | |
| 0.15mm | 1.96252 | 0.0012 |
| 0.075mm | | |
| Binder Modification | | |
| RAP | | |
| Binder Content | -13.97035 | <0.0001 |
| Fines/Binder | | |
| NMAS | | |
| ESAL | | |
| Gradation | | |
| Angularity | | |

### 7.4.2 Summary of TSR and APA Comparison

Comparing factors that affect moisture damage test results and mixes deemed moisture prone for TSR and APA testing resulted in finding no relationship between the two test methods. Very few of the mixes were considered moisture damage susceptible by both test procedures. The same factors were considered for regression analysis with the exception of compaction and diameter, which were only accounted for in the TSR analysis. There were no similar factors affecting the results of these two tests. When the TSR values were grouped by compaction method and diameter it could be seen that binder PG was the one shared factor that may be affecting the moisture susceptibility.

## 7.5 Comparison of Moisture Susceptibility Testing of HMA Mixes and Asphalt Binders

One part of this research was developing and applying a moisture susceptibility test for asphalt binders. A second portion was examining the use of an APA for moisture susceptibility testing of HMA mixes. In this section data obtained during this research is evaluated to determine if there is a relationship between results obtained for mixes and asphalt binders. Regression analysis was employed to evaluate the relationship between mixes and binders in term of moisture susceptibility. The regression analysis indicated that there is a relationship between the APA, DSR, and water absorbed data. According to the analysis the weight of a binder specimen after 3 minutes and 48 hours has a significant effect on the rut depth of a moisture conditioned specimen tested in water. This indicates that changes in weight due to moisture saturation have an effect on rut depth. Other variables deemed significant were polymer modification, binder content percent, gradation, and aggregate angularity.

Table 7.25 summarizes the materials deemed moisture susceptible by the three different procedures. The solid dots indicate that material collected from that location was deemed moisture susceptible. The strongest agreement occurs between the water absorbed procedure and APA test results. However, material from two sites, Battle Creek and Hartland, were deemed moisture susceptible by three procedures; thus indicating that there is a very strong possibility that these two mixes will be prone to rutting caused by moisture damage.

**Table 7.25 Moisture Susceptible Comparison**

| Site | Water Absorbed | Dynamic Shear Rheometer | Asphalt Pavement Analyzer Based on Ratio | Asphalt Pavement Analyzer Based on Ratio and Maximum Allowable Rut Depth |
|---|---|---|---|---|
| Ann Arbor | | | | |
| Battle Creek | • | • | • | |
| Brighton | • | | | |
| Clarkston | | | | |
| Detroit | • | | • | |
| Dundee 19.0mm NMAS | • | | • | |
| Dundee 12.5mm NMAS | | | • | |
| Grand Rapids I-196 | | | • | • |
| Grand Rapids M-45 | | | • | • |
| Hartland | • | • | • | |
| Howell | • | | • | |
| Levering | • | | • | |
| Michigan Ave 19.0mm NMAS | | | • | |
| Michigan Ave 12.5mm NMAS | | | | |
| Michigan International Speedway | • | | | |
| Owosso | | | • | |
| Pinckney | • | | | |
| Saginaw | | | • | |
| St. Johns | | | • | |
| Toledo | | | • | |
| Van Dyke | | | • | |

## 7.6 APA Conclusions

In this chapter the use of an APA to evaluate the moisture susceptibility of HMA was explored. The criterion developed to determine whether or not a mix is moisture susceptible indicated that 2 of the 21 mixes were moisture susceptible. Further analysis revealed that there is a strong relationship between water absorbed data and APA test data. There, however is not a strong relationship between DSR and APA test results, nor is there a strong relationship between TSR results and APA test results. It is recommended that if a loaded wheel tester is to be used for moisture susceptibility testing that more than three specimens be tested. The variability of the rut depth data was rather high and it is believed that additional specimens tested would yield data less affected by outliers.

# Chapter 8 Proposed Future Work

## 8.1 Model to Predict Rutting Caused by Moisture Damage

Several models exist to relate the potential of a pavement to rut. The work conducted in this dissertation could be used to develop a model that predicts rutting caused by moisture damage. The following sections outline a brief literature review on the current HMA rutting models and a framework for developing a stochastic finite element model based on testing conducted for this dissertation.

### 8.1.1 Forecasting Techniques

Many techniques have been employed over the years in an attempt to simulate stresses HMA experiences in the field in-situ. The main advantage of stress simulation is the determination of the deterioration rate in a cost effective manner. Permanent deformation is one of the significant asphalt distresses researchers attempt to model. Different types of permanent deformation models have employed the use of either laboratory or field data. The analysis methods include regression analysis, linear multilayer analysis, and finite element analysis (FEA). FEA has recently gained popularity in transportation materials modeling.

Most of the rutting models developed account for two factors that significantly attribute to rutting: traffic load and material properties. A third significant factor is the effects of the environmental conditions. Some of the identified factors that indirectly contribute to rutting are disproportionate asphalt content, fine-grained aggregate, natural sand, aggregate shape, and moisture. Varied ranges in temperature from the surrounding environment can also accelerate the deterioration process. All of these factors are encompassed within the Marshall Stability, complex shear modulus, resilient modulus, and deflection measurements; therefore, these measurements are often included in prediction models. Layer thickness in the field is frequently a result of the predicted traffic; therefore, using traffic loads and layer thickness from field data could lead to multicollinearity problems (a statistical weakness that results from counting at least one effect more than once in a statistical model) in a regression model. A drawback associated with many models is that experimental data may not decay at the same rate as

field data. However, the experimental data can establish relationships between factors involved in the rutting process (Jackson and Baldwin, 1999).

#### 8.1.1.1 Regression Based Forecasting Models

A common model basis, developed via regression analysis, relates plastic strain to loads or stresses.

$$\varepsilon_p = aN^b \qquad \textbf{Equation 8.1}$$

In the generic model, N is the number of stressors or loads and *a* and *b* are coefficients of the stressors or loads. Several variations of the equation have been recognized for rut depth prediction. One developed by Kenis (Rauhut et al., 1976; Uzan, 2004), multiplies the right side of the equation by the elastic strain and uses deflection coefficients for *a* and *b*. The Texas Flexible Pavements Systems developed a model concurring with Kenis's model with a slight variation, the Texas Flexible Pavements model assumes that elastic strain is constant (Uzan, 2004).

A concave shape for rut depth develops from numerous loads. Unfortunately, in the past many of the models developed are based on data that have been linear rather than polynomial. Another drawback of these linear models is that environmental effects are often ignored (Uzan, 2004). A pavement surface model developed by Thompson and Nauman (Thompson and Nauman, 1993) related rutting rate to rut depth divided by the number of loads applied to a pavement's surface. The model was the basis for another model developed by Achilla et al. (Achilla and Madanat, 2000). One of the differences between the two models was the use of rutting rate. The model developed by Achilla equated rutting depth to the rut depth following construction plus the pavement characteristic coefficient multiplied by the number of loads applied to a surface to the power of some coefficient *b,* which is determined by a pavement characteristic. The value for N was determined directly from laboratory experiments, but calculating N from the AASHO test road data required some mathematical manipulation (Achilla and Madanat, 2000).

Achilla et al. (Achilla and Madanat, 2000) created an equation to relate pavement strength in terms of rutting, RN, which sums over the layer thicknesses multiplied by coefficients. The coefficient *a* from the general equation can be determined using RN.

$$a_i = \beta_4 * e^{-RN} \quad \textbf{Equation 8.2}$$

The environmental effect was accounted for by a Thaw Index (TI). The TI was computed by multiplying the summed temperatures of freeze cycles by the maximum of the mean maximum temperature for two weeks (Achilla and Madanat, 2000).

A nonlinear viscous steady-state deformation model was developed by Deshpande and Cebon (Deshpande and Cebon, 2004) based on idealized asphalt assuming a half space. The volumetric and deviatoric strains were ascertained from triaxial compression tests. The tests indicated that the hydrostatic and deviatoric stresses influenced the deformation of the asphalt. It was found that the relationship between the load and deformation of the asphalt is nonlinear. Agreement between the model predictions and measurements was obtained (Deshpande and Cebon, 2004).

As mentioned, development of a permanent deformation model must address the complexities of a flexible pavement structure, such as the complicated nonlinear relationships that exist between the materials within the structure; small correlation between loose material and time of loading or load duration while there is a strong correlation between asphalt concrete and load duration; and the variation of temperature and moisture throughout the structure and time. The Shell Method (Claessen et al., 1977) and the Asphalt Institute Method (Shook et al., 1982) are two mechanistic-empirical models that restrict the vertical strain of the subgrade to prevent rutting. Since the effect of the pavement layers on permanent deformation is not accounted for in the restricted subgrade strain models, other methods are often utilized. Monismith (Monismith et al., 1977), Kenis (Kenis, 1977), and NCHRP employ linear response methods. Linear elasticity is assumed for linear response methods. Other factors that should be considered, which have also been employed in the past, are material properties, loading and environmental conditions (Uzan, 2004).

### 8.1.1.2 Multi-Layered Models

Uzan (Uzan, 2004) computed the rut depth by integrating the rate of rutting over time, in lieu of the more popular approach of summing the strains in the layers under the load. Three scenario types are facilitated within Uzan's model. The three scenarios are changing environmental conditions, fluctuating traffic conditions, and constant environmental and traffic conditions. In all three scenarios, moisture content is assumed to be constant. Repetitive loading and dynamic modulus tests were used to ascertain the resilient and permanent deformation for the model analysis. The calculation of the resilient and permanent deformations varied with aggregate type. The multilayer linear elastic program JULEA was used to compute the stresses and deformation in the pavement caused by loading. The layers of the pavement were subdivided into horizontal layers. The modulus can differ between the subdivided layers, but it cannot differ within one of the subdivided layers. After establishing the parameters within each scenario, a sensitivity analysis was conducted by varying temperature and load factors. The analysis indicated that a thicker pavement resists rutting more than a thinner one and the number of subdivided layers needs to be varied for different materials (Uzan, 2004). This model accounts for some of the variability found in pavement materials but does not account for variability found within a layer.

General Analysis of Multi-layered Elastic Systems (GAMES) is a pavement analysis software developed as an alternative to 3-D Finite Element Analysis (FEA) for roads and runways (Maina and Matsui, 2004). Linear analysis is used in lieu of non-linear analysis to simplify the demands on the user. Within the software analysis module, the pavement surface, base, subbase, and subgrade are divided into several horizontal layers, a maximum of 10 layer divisions is allowed. The number of layer divisions is dependent upon the pavement layer thicknesses. The layer divisions are assumed to be homogeneous and isotropic. The loads are programmed as horizontal circular forces. Measurement points are located throughout each layer division. GAMES can handle up to 10,000 measurement points for an entire model (Lytton, 2000). As with the previous multilayer models, the assumption of pavement materials being homogenous and isotropic is unrealistic.

### 8.1.1.3 Finite Element Analysis (FEA) Models

A FEA model is a computer simulation of the stresses and strains associated with an object. The object is divided into a mesh consisting of 2- or 3-dimensional triangles or rectangles. Within each triangle or rectangle the material properties are defined. Once the material properties have been defined for each subsection of the object a force is applied to induce stress on the object. The changes that occur in the object are measured within each one of the subsections. Nonlinear 3-D finite element model of the response of pavement was deemed the most appropriate model by Lytton et al. in 1993 (Lytton et al., 1993).

FEA has been employed in HMA analyses of several characteristics. In the past, regression analysis of field data has been used to determine the effective temperature of an HMA structure. Recently at Tung Nan Institute of Technology in Taiwan, FEA, viscoelastic theory, and falling weight deflectometer (FWD) were combined to develop a material model that can reveal the effective temperature of the HMA structure (Lee, 2004). A study in the Netherlands investigated the effects of triaxial strains on fatigue cracking at the top of an HMA layer utilizing an FEA model that the research team developed (Scarpas et al., 1997). FEA has also been used to analyze the effects of moving loads, which can cause permanent deformation, in HMA (Olsson, 2004). One of the commercial FEM software packages available for pavements is ABAQUS. ABAQUS is able to analyze linear, nonlinear, viscoelastic, and viscoplastic characteristics of HMA (Sadd, 2003).

Even though HMA research using FEA has existed for more than a decade, the HMA analysis of field data has not yet fully adopted 3-D FEA. The common reasons for not using FEA are the complex mathematics required to establish an FEM, lack of computing power, and cost. However, in many cases the FEMs developed by researchers have been thoroughly tested and include extensive parameter information to allow for analysis of many of the popular HMA designs. The programs with vast databases allow usage without understanding the full implications of the mathematics behind the analysis. Workstations are no longer required for running an FEM as several programs have been developed for personal computers (PCs). A high powered PC can be purchased at a

relatively low cost (Lytton, 1993). The cost of these programs is negligible compared to the cost of constructing an improper HMA that requires removal or extensive maintenance to meet the satisfactory performance criteria in a region.

Zaghloul and White (Zaghloul and White, 1993) at Purdue University developed a 3-D dynamic finite element model (DFEM) of HMA. The data used in the model was collected from the field and the pavement structure was defined with infinite boundaries. The wheel load was simulated by a rectangular force with two semicircles. The material properties were constant within each layer. The models sensitivity was measured against data collected from Canada. It was concluded that the model did an adequate job in testing the real world deformation (Lytton et al., 1993).

A 2-dimensional finite element model of asphalt materials was developed using a model of load transfer among cemented particles (Dvorkin et al., 1994). Instead of modeling the hot mix asphalt as a homogenous material, the researchers utilized a lattice network that connected aggregate elements with rectangular asphalt links. An approximate elasticity solution was used to develop the stiffness matrix, which was based on asphalt moduli, aggregate location, aggregate size, and location of asphalt and aggregate elements. The load transfer model was incorporated in the asphalt binder links that connected the aggregate elements to one another. The aggregate elements were modeled as either ellipses or circles of varying sizes. It was assumed that the asphalt binder links were less stiff than the aggregate elements and that the asphalt thickness was consistent throughout the model. Ishikawa et al. (1986) developed a damage mechanics theory that was applied to the asphalt to account for the softening and inelasticity of the asphalt binder. The softening criteria applied to the damage mechanics methodology varied throughout the model of the specimen. The elastic moduli employed in the model were based on experimental data. The softening criteria were based on either previous studies or adjusted to make the model work properly.

#### 8.1.1.4 Stochastic Finite Element Models

There is uncertainty in structures associated with the geometry, material properties, and applied load. To address the uncertainty a probabilistic finite element model can be

developed incorporating random fields to represent the distributions associated with the geometry, material properties, and applied loads found throughout the structure. There are several categories of stochastic finite element models; perturbation, first and second-order reliability, and expansion simulation methods (Liu et al., 1995). Parvini and Stolle (Parvini and Stolle, 1996) employed Taylor's expansion in the perturbation method of the stochastic finite element model of pavement deflection. In the model, the elastic modulus, $e$, was defined as a random variable. The equilibrium equation was defined as:

$$K(b)q(b) = Q(b) \qquad \textbf{Equation 8.3}$$

where:

K(b)= stiffness matrix,

Q(b)= applied load,

q(b)= displacement, and

b= random parameter.

Parvini defined the modulus of elasticity as the sum of the expected value of $e$, $e_0$, and perturbation caused by the randomness of $e$, $\Delta e$. Applying a second order Taylor's expansion of the equilibrium equation at $e_0$ generated:

$$(K_0 + K'\Delta e + \frac{K''}{2!}\Delta e^2)(q_0 + q'\Delta e + \frac{q''}{2!}\Delta e^2) = (Q_0 + Q'\Delta e + \frac{Q''}{2!}\Delta e^2) \qquad \textbf{Equation 8.4}$$

The values for $q, q', and\ q''$ are determined by grouping like terms. Then to calculate the expected response of the deflection, the product of the Taylor expansion of the deformation and the probability density function of $e$ are integrated over the range between positive and negative infinity. The following estimation was obtained by Parvini and Stolle (Parvini and Stolle, 1996):

$$E(q) = q_0 + \frac{q''}{2!}\mathrm{var}(e) \qquad \textbf{Equation 8.5}$$

Rearranging the above equation and integrating the product of the equation squared and the probability density function of $e$ from positive to negative infinity allowed Parvini and Stolle to determine the variance associated with the deflection by the yielded equation:

$$\mathrm{var}(q) = (q')^2 \,\mathrm{var}(e) \qquad \textbf{Equation 8.6}$$

For equations 2.4 through 2.6 listed above, the perturbation is assumed to be small and the random variable probability distribution function is not defined. Parvini and Stolle merely determined the mean and dispersion of each random variable and inserted the values after the simplification. For the case where perturbation is large, Parvini and Stolle discovered that the higher order terms of the Taylor's expansion would need to be incorporated along with statistical moments of higher order for the estimation and variance of the deformation calculations.

The covariance matrix was included in Parvini and Stolle's stochastic finite element models when multiple random variables existed in the problem. The inclusion would change the estimation of the deformation to the following:

$$E(q) = q_0 + \frac{1}{2}\sum_{i=1}^{p}\sum_{i=1}^{p} s_{ij}\,\mathrm{cov}(e_i, e_j) \qquad \textbf{Equation 8.7}$$

The dispersion is then reported as the covariance instead of the variance using the following equation:

$$\mathrm{cov}(q) = A\,\mathrm{cov}(e)A^T \qquad \textbf{Equation 8.8}$$

where

$$s_{ij} = (K_0^{-1}K_{,e_i})(K_0^{-1}K_{,e_j})q_0 \qquad i, j = 1,\ldots, p \qquad \textbf{Equation 8.9}$$

and matrix A is defined by the vectors

$$a_i = -K_0^{-1} K_{,e_i} q_0 \qquad i = 1,..., p \qquad \textbf{Equation 8.10}$$

The estimation of the deflection and the covariance matrix are used in lieu of deterministic values in the finite element model. Aside from employing the statistical moments for values, the stochastic finite element model is solved similar to a non-stochastic finite element model (Parvini and Stolle, 1996).

High reliabilities are often employed to meet factors of safety in civil engineering structures; therefore the probabilities of failure are very small regions towards the ends of distribution curves. To ascertain information from the tail regions of the probability distributions about such response variables as material properties and load, Der Kiureghian and Ke (Der Kiureghian and Ke, 1985) suggest employing not only a first-order reliability method, but also integrating that process with response surface analysis, statistical modeling, and simulations.

Within the first-order reliability analysis, Der Kiureghian and Ke (Der Kiureghian and Ke, 1985) assume a vector of random variables characterized by the state of the structure and only safe and failure states exist. The limit state surface ( $g(s) = 0$ ) is defined as the boundary between the safe state ( $g(s) > 0$ ) and the failure state ( $g(s) \le 0$ ). The probability of failure of the structure is based on the probability distribution functions of the stresses and deformations, defined mathematically as:

$$p_f = \int_{g(s)\le 0} f_s(s)ds \qquad \textbf{Equation 8.11}$$

where:

$f_s(s)ds$ =probability density function S, and

**S**=vector of stresses and deformation effects.

The finite element method is employed to compensate for the lack of statistical information concerning certain response variables, such as load effects.

Random variables, such as load, material properties, and member sizes were defined as vector **X** with a defined probability distribution function, $f_x = (x)$. The load space is ascertained by the outcome space of **X**. A mechanical transformation connects vectors **S** and **X** as denoted below.

**S=S(X)** **Equation 8.12**

A probabilistic transformation is used to map X onto the standard normal space via

**Y=Y(X)** **Equation 8.13**

where,

**Y**=Vector of standard normal elements

The limit state surface ( $g(s) = 0$ ) is far from the mean of the distribution since civil engineering materials are typically constructed with an extremely low probability of failure. Transforming the limit state surface to a standard normal space enables good estimations, since distances between points and the mean increase exponentially for standard normal space; i.e. distances extremely far from the mean prior to the transformation are no longer as far and points within the probability of success are fit closely to the origin. Another benefit of examining the analysis in standard normal space is the accessibility of probability information for simple subsets in arbitrary dimensions. To transform the limit state to the standard normal space to take advantage of the above benefits, Der Kiureghian and Ke (1985) used the following probability transformation:

$g(s) = g(s(x(y))) \equiv G(y) = 0$ **Equation 8.14**

The first-order reliability estimation of the probability of failure in the standard normal space used in Der Kiureghian and Ke (Der Kiureghian and Ke, 1985) was:

$p_{f_1} = \Phi(-\beta)$ **Equation 8.15**

where:

$\Phi(y)$ = cumulative probability of the standard normal, and

$\beta$ = reliability index.

A constrained optimization problem is employed to find the minimum distance points in which the absolute value of *y* is minimized with the constraint that the standard normal limit state is equal to 0. The gradient of the limit state is often used to facilitate the convergence of the optimization problem.

Developing the finite element portion of the analysis requires establishment of which points within the standard normal optimization problems are of interest. Once the points have been selected, the load effects for established points need to be calculated. The inverse of the probability transformation is employed in the finite element analysis of these points. An additional step in the development of the finite element model is the calculation of the mechanical transformation Jacobian, which enables the efficient convergence of the standard normal optimization problem and definition of the stress field. Discrete random fields are employed to represent the varying structural properties and loads. Two meshes were created, one for the FEA and a second for discrete random fields by Der Kiureghian and Ke (Der Kiureghian and Ke).

Liu and Der Kiureghian (Liu and Der Kiureghian, 1989) developed a finite element reliability model for geometrically nonlinear materials that exhibit an elastic behavior. The random variables, such as loading, material properties, and geometry of the structure, were denoted by the vector **V**. The load effects were represented by the vector **S**. The variables that compiled to create vector **S** were related to stresses and deformations. Liu and Der Kiureghian (Liu and Kiureghian, 1989) defined the relationship between **S** and **V** as:

$S = S(V)$ **Equation 8.16**

The limit state function, $g(v,s)$, was used to define the limit state surface, $g(v,s) = 0$, the safe state, $g(v,s) > 0$, and the failure state, $g(v,s) \le 0$.

The probability of failure of the system was described as

$$p_f = \int_{g(v,s)\le 0} f_v(v)dv \qquad \textbf{Equation 8.17}$$

where, the joint probability density function of **V** is symbolized by $f_v(v)$. **V** was then transformed into the standard normal space following the method developed by Der Kiureghian and Ke (Der Kiureghian and Ke, ) earlier.

Liu and Der Kiureghian (Liu and Der Kiureghian, 1989) defined the equilibrium state of a static elastic material as:

$R(X,U,D) = F(X,U,P)$ **Equation 8.18**

where:

**R**= resisting nodal forces,

**F**= external nodal forces,

**X**= undeformed nodal coordinates,

**U**= nodal displacement,

**D**= constitutive restriction, and

**P**= loading restriction.

The explicit functions of **V** are **X**, **D**, and **P**. The implicit function of **X**, **D**, and **P** is **U**. The Jacobian is determined from the derivative of the equilibrium equation with respect to **V**. The Newton method is employed to solve the derivation of the equilibrium equation. The chain rule was utilized for the components of the stress and strain gradients. Liu and Der Kiureghian's computations reduce the calculations for the gradients of linear and nonlinear elastic materials. Since this is not a perturbation method there are no affects of numerical instability (Liu and Der Kiureghian, 1989).

Weissman et al. (Weissman et al., 1999) developed 2-D and 3-D finite element models to analyze the rutting and fatigue of different laboratory specimens given certain stress-strain model criteria and comparisons with previous models. One of the main aspects of the research was establishing the proper size specimen for each test. The researchers looked at the representative volume element (RVE) as a means of quantifying their conclusions. The size of the RVE was based on the smallest division that would be of a homogenous material. To determine the RVE, digitized pictures of specimen slices were produced. An equal sized grid was constructed over the photographs and each element of the grid was color coded based on the dominating material property. The grid and color scheme were then used for a 2-D finite element mesh for simulations of an axial compression test. The RVE length was then related to the stiffness of the specimen. From the RVE analysis it was determined that testing in the laboratory should either consist of numerous small samples or several larger samples (Weismann et al., 1999).

Probabilistic finite element models have been used to account for airfield uncertainties such as environmental conditions, loading, material properties, and geometry. In the probabilistic finite element model developed by Lua and Sues (Lua and Sues, 1996) the material property was characterized by independent homogenous Gaussian random fields. The material property of interest to Lua and Sues was the elastic modulus, but multiple material properties could be examined. The size of the mesh was primarily based on the variation in the structure. In general, the size of the mesh elements were ½ *to* ⅓ of the correlation length. To determine the variability Lua and

Sues calculated the correlation lengths; which is the interval that will yield a correlation of less than $e^{-1}$. If the correlation lengths were short a fine mesh was used since the variability was high. Lua and Sues (Lua and Sues, 1996) used Liu and Der Kiureghian's (Liu and Der Kiureghian, 1989) Gaussian correlation function:

$$\rho(x_i, x_j) = \exp\left(-\frac{|x_i - x_j|^2}{b^2}\right) \qquad \textbf{Equation 8.19}$$

where:

$x_i$, $x_j$ =points within the structure, and

$b$ =correlation length.

The development of the discrete random field was based on a combination of the midpoint method and the spectral-decomposition method. The advantage of an additional step of incorporating the spectral-decomposition method is the reduction of random variables within the model (Weissman et al., 1999).

Lua and Sues opted to use the expansion simulation method for the probabilistic aspect of the probability finite element model. Since pavements can exhibit high levels of variability and are not constructed at high levels of reliability, the perturbation and reliability based methods were deemed inappropriate by the research team. Lua and Sues also employed a nested simulation to account for the joint statistical distribution of the elastic modulus and pavement thickness to compensate for the lack of explicit definition for the two distributions (Lua and Sues, 1996).

The mesh developed by Lua and Sues was fine near the wheel path and coarse elsewhere. It was assumed that the material variability away from the wheel path has little effect on the response of the pavement and therefore a single random variable was adequate for those areas (Lua and Sues, 1996). The methodology developed by Lua and Sues is depicted in **Error! Reference source not found.**.

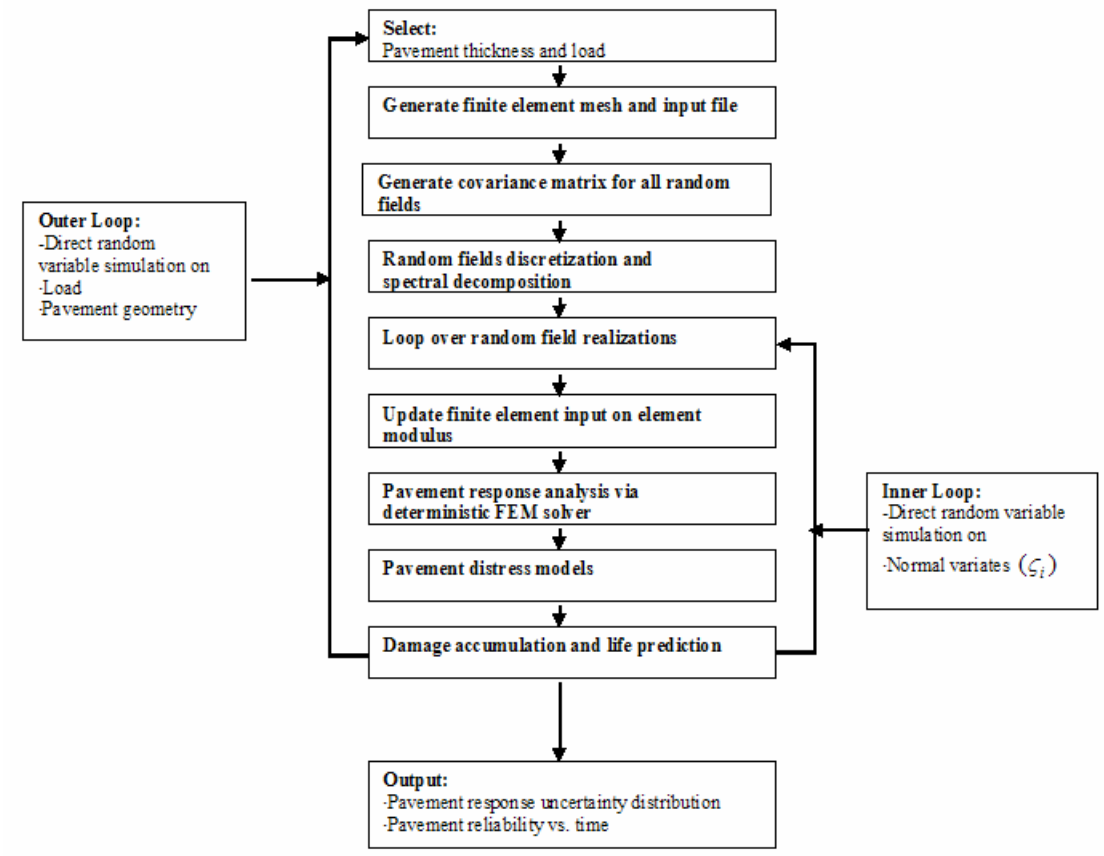


**Figure 8.1 Components of PFEM Methodology (Lua and Sues, 1996)**

Rutting and fatigue models were used to calculate the accrued damage over the life span of the pavement (Lua and Sues, 1996).

Another stochastic finite element method is a variation of the Neumann expansion as it uses the Karhunen-Loeve expansion within the Galerkin formulation. Its advantage over the ordinary use of the Neumann expansion is it lends itself to automation easily (Ghanem and Spanos, 1991).

The two major differences between the proposed research and past FEMs is the use of probability distributions in lieu of constant material characteristic values for APA results and concentration on the effects of moisture on HMA rutting created by an APA. Many past permanent deformation models have used constant material properties either throughout the object or, in the case of multilayer elastic analysis, within a layer. Stochastic finite element models have been applied to numerous civil engineering fields,

but has yet to be applied to laboratory scale testing using loaded wheel testers. Using a probability distribution instead of a constant material value allows for the model to account for material variation throughout the specimen created by binder variation and a variety of aggregate properties. Variation can occur from non-homogeneity, variation within material used, or user variation. Moisture damage is a significant concern especially in Northern regions with freeze/thaw cycling, thus a simulation based on laboratory results could be a cost effective way to determine moisture prone material.

### 8.1.2 Finite Element and Reliability Interface

The reliability analysis conducted on the significant factors will be integrated with the finite element model of the HMA laboratory specimen. A finite element code developed by Pacific Earthquake Engineering Research Center known as OpenSees (Open System for Earthquake Engineering Simulation) encompasses an interface between a reliability algorithm and finite element compiler. The code is an object-oriented program. The user defines the random variables, which includes statistical moment information. A limit-state function is evaluated several times varying the values for the random variables. Information about the response of the random variables is extracted from the finite element analysis. The random variables within the finite element model receive information from the reliability analysis and the reliability analysis obtains information pertinent to the limit-state function. When building the finite element model, each random variable is linked to an object within the model. **Error! Reference source not found.** depicts the communication process between the finite element model and the reliability analysis.

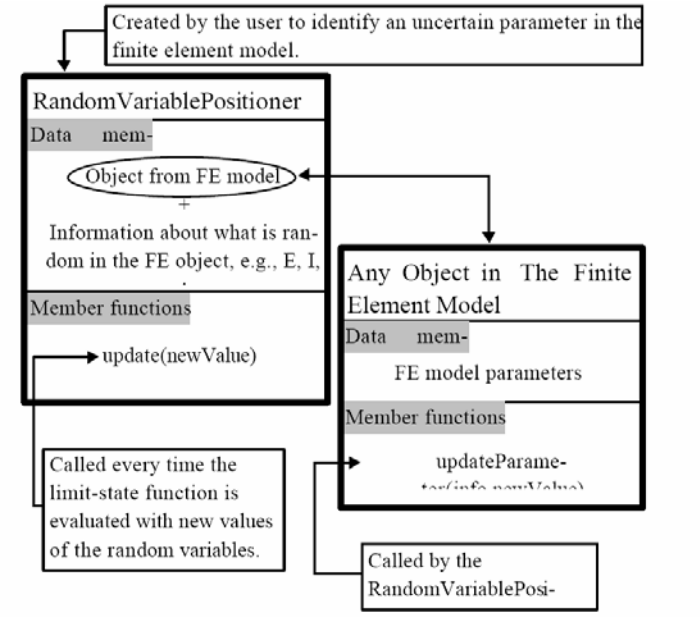


**Figure 8.2 Flowchart Illustrating Interface Between the Reliability Analysis and the Finite Element Model (Haukaas and Der Kiureghian, 2001)**

### 8.1.3 Monte Carlo Simulation

Reliability analysis, also known as risk analysis, has been utilized for centuries in scientific research. The use of reliability in HMA analysis however is relatively new. There are several areas of the HMA design process that could benefit from the power of reliability analysis. Risk analysis can be used to evaluate proposed HMA designs or models (Pendelton, 1994; Kulkarni, 1994; White, 1998).

Risk analysis evaluates the potential consequences associated with each possible scenario. There is no risk associated with past events since there is no uncertainty. Using existing data to hypothesize future behavior of a product or process can provide a good estimation of what could happen in the future, but it is not exact. The risk is the uncertainty associated with the forecast.

A decision model is employed in determining the risk associated with a product or process. A decision model consists of an objective function, decision variables, decision outcomes, the effects and probabilities of the decision outcomes and effect of the decision

variables. The objective function defines the desired result based on decision variables. The decision outcomes are the events that occur due to a choice made by the user.

Several techniques exist for performing risk analysis, one of which is Monte Carlo Simulation (MCS). MCS generates data for uncertain variables. Information about the variable such as distribution type, mean, and standard deviation are input along with a seed value. The seed value is an educated guess of a variable value for the model. Several different seed values can be tested. Each seed value undergoes the various scenarios allowed within the model. The coefficient of variation is used as a bias factor in determining the uncertainty associated with the forecast. The consequences are calculated for each scenario. Experience has shown that the MCS is the paramount method for risk analysis. However, the ability to employ the MCS is not always feasible. Classic MCS is computationally intensive for accurate results. Several other methods in the past have been implemented in place of Classic MCS when the resources are not available, such as the Point-Estimate method and the MCS with Latin Hypercube Sampling (LHS). Usually, the scenario with the least amount of uncertainty is the selected method (Williams et al., 2004).

Random sampling, either Monte Carlo Simulation with Monte Carlo Sampling (MCSMCS) or Monte Carlo Simulation with Latin Hypercube Sampling (MCSLHS), is used to select a value between 0 and 1. Once a number is chosen, the cumulative probability distribution is employed to determine the field sample value associated with the probability randomly selected. Weights are not affiliated with any of the values in the MCSMCS. The lack of bias can cause clustering when a low number of iterations are employed. MCSLHS accounts for the tendency for values to be drawn to certain points within the range of possible values. MCSLHS sampling divides the cumulative probability distribution into several sections, called stratification, and one number selection is made from each section to determine the risk. The number of partitions made is based upon the designated number of iterations. The time required to converge is generally shorter for simulations employing MCSLHS than MCSMCS, due to the stratification used in MCSLHS.

The objective function for each of the decision models will analyze the probability of a certain material characteristic occurring. A different decision model will be developed for each type of material characteristic; i.e. there will be one decision model for determining Poisson's ratio, another for the modulus of elasticity, etc.

This study will incorporate an FEA model to simulate the stresses occurring in a moisture damaged pavement subjected to varying traffic volumes. Instead of employing constant material properties across the whole HMA sample like past models, a distribution of HMA properties will be used based on laboratory measurements. Reliability analysis will be employed to select the material properties for each individual pavement subsection.

A similar method was developed to study the factor of safety for pillars in the Feng Huangshan copper mine located in China. The researchers used Monte Carlo simulation (MCS) to determine the probability of occurrence and artificial neural networks (ANN) to define relationships between concrete pillar characteristics (i.e. Poisson's ratio and elasticity) and the compressive strength. The relationships were then employed to define the parameters of a finite element model (Liu et al., 1995).

## 8.2 Outline for the Development of a Stochastic Finite Element Model

The following sections outline a theoretical stochastic finite element model approach of HMA specimens tested in an APA. One of the recommendations originating from previous research is that a stochastic finite model be developed to use in lieu of excessive laboratory testing. It is believed that a computer simulation of the effect of moisture on asphalt pavement would likely be more cost effective and timely than procuring and testing specimens.

The method described below could be adopted by any agency and use an off the shelf finite element software package, such as ABAQUS or FEMLAB. The material characteristics used in the model will need to be obtained, but in most cases the material properties of interest are already collected.

### 8.2.1 Aggregate Shape and Size

At the University of Hong Kong, a random aggregate structure was developed for a three phase finite element model of concrete (Wang et al., 1999). Aggregate was defined as either gravel or crushed aggregates. Gravel was defined as rounded aggregates which would have a spherical or cubical shape. Crushed aggregates were defined as polygonal aggregates with sharp edges. Two formulas were developed to generate different shaped aggregates. Both formulas utilize random number generation and polar coordinates (Wang et al., 1999). The formula for gravel was:

$$r = r(\theta) = A_0 + \sum_{j=1}^{m} A_j \cos(j\theta + \alpha_j) \quad \textbf{Equation 8.20}$$

*where*:

$A_o$ = Average radius,

$A_j$ = Amplitude of Fourier frequencies, and

$\alpha_j$ = Phase angles.

For simplification, phase angles should range between 0 and 2π and selected randomly from a uniform distribution. The formula for crushed aggregates is based on elongation of an aggregate. The polar coordinates are treated as random variables. Below is the formula for crushed aggregates (Wang et al., 1999).

$$\theta = \eta_i \times 2\pi \quad \textbf{Equation 8.21}$$

*where*:

$\eta_i$ = Random number between 0 and 1

$$r_i = A_0 + (2\nu - 1) \times A_1 \quad \textbf{Equation 8.22}$$

*where*:

$A_0$ = Average value of $r_i$,

$A_1$ = Maximum value of $r_i$, *and*

$\nu_i$ = Ranges between 0 and 1; normally distributed random number.

The particle size distribution was based on the gradation of several concrete mixes. Particle sizes were determined in terms of sieve sizes, percent retained. A

gradation was divided into subcategories, several sieve sizes were assigned to each subcategory. The number of aggregates assigned to each subcategory was calculated based on percent volume. The shapes of these aggregates for each subcategory were generated using either the gravel or crushed aggregate formula.

### 8.2.2 Specimen Geometry

The finite element model will be based upon cylindrical APA test specimens. The height of a specimen is 75mm and with a diameter of 150mm. A specimen is constrained on all sides except for the top by a device that holds a specimen in place during testing.

### 8.2.3 Material Distribution

Several APA test specimens made from each mix will be evaluated to determine material distribution. Each untested specimen will be sliced width wise in 30mm intervals. An imaging process similar to what has been used in Texas (Masad and Somadevan, 2002) will be adopted. The sliced faces will be photographed with a digital camera and transferred to a computer for image processing. There is an imaging processing technique which will color code material based upon pixel intensity using a grey scale. Each shade of grey is associated with a numerical value utilizing discriminate analysis. Masad and Somadevan (2002) used this technique to identify aggregates of similar size in an image. Aggregates of similar size would be shaded the same grey and labeled with a numerical value. A grid with 0.30mm x 0.30mm sections will be superimposed onto each image. Each section in the grid will have a unique label. For each image, a material will be assigned to each grid. The material selection identification will be based on the grey scale image processing conducted. The information for each grid will relate the likelihood of a particular material existing at that location.

Wang et al. developed a random aggregate structure. The largest aggregates were generated first. As aggregates were generated, the generated shape was placed into the model using the Monte Carlo random sampling technique. The placement of these

aggregates was based on the polar coordinates that were randomly generated (Wang et al. 1999).

Once the random aggregate structure was developed, the inclusion of mortar was considered. The mortar thickness was based on the aggregate size and distribution. Determination of mortar thickness was a trial and error process, starting with the highest possible mortar thickness in a realistic concrete. Once all of the aggregates and appropriate amount of mortar was placed within the boundaries of the model, a concrete specimen without overlapping and extruding aggregates was created, a finite mesh was developed. Three meshes in all were developed; one for aggregates, another for mortar, and a final one for the interface between aggregates and mortar. The advancing front approach was used to generate a triangle element mesh for aggregates and one for mortar. The mesh for the interface was developed first and composed of Goodman type elements with four nodes (Wang et al., 1999).

Each mix has a job mix formula (JMF). JMFs list information about a mix including aggregate size and percent of certain aggregate sizes in a mix. It will be assumed that the percentages of aggregates of varying sizes in a mix will be the same for a specimen in a mix. In other words, it is assumed a mix consisted of material evenly distributed and that this was not affected during handling and compaction of a mix.

Combining the image processing data and JMF information material assignment to different locations throughout a specimen can be conducted. For example if a mix consists of 50% of material A, then material A can only be assigned to 50% of the locations. Selection of which locations will be based on the imaging processes conducted which yielded data that could relate the likelihood of a certain material occurring in an area.

### 8.2.4 Specimen Material Properties

The current issue that many asphalt pavement modelers encounter is how to represent the varying material properties that exist throughout a pavement. Several techniques have been employed.

The material properties in stochastic finite element models are defined by indefinite parameters. The structural response is revealed through the computation of the gradients with respect to the material property parameters. Computations of the gradients are complex for both linear and non-linear material. Hisada et al. (Hisada et al., 1991) outline a method for non-linear dynamic response gradients to be determined. Hisada et al. defined the tangent stiffness matrix, K, as the sum of the nonlinear and linear strain. Integrating the tangent stiffness matrix multiplied by the displacement derivate will yield the final applied force for the given path.

A 2-dimensional finite element model of asphalt materials was developed using Dvorkin et al.'s (Dvorkin et al., 1994) model of load transfer among cemented particles. Instead of modeling HMA as a homogenous material, the researchers utilized a lattice network that connected aggregate elements with rectangular asphalt links. The approximate elasticity solution developed by Dvorkin et al. (Dvorkin et al., 1994) was used to develop the stiffness matrix, which was based on asphalt moduli, aggregate location, aggregate size, and location of asphalt and aggregate elements. The load transfer model was incorporated in the asphalt binder links that connected the aggregate elements to one another. The aggregate elements were modeled as either ellipses or circles of varying sizes. It was assumed that the asphalt binder links were less stiff than the aggregate elements and that the asphalt thickness was consistent throughout the model. Ishikawa et al. (Ishikawa et al., 1986) developed a damage mechanics theory that was applied to the asphalt to account for the softening and inelasticity of the asphalt binder. The softening criteria applied to the damage mechanics methodology varied throughout the model of the specimen. The elastic moduli employed in the model were based on experiments. The softening criteria were based on either previous studies or adjusted to make the model work properly (Sadd et al., 2004).

Several factors that affect the microstructure of HMA are aggregate-asphalt bond, gradation, air void distribution, air void interconnectivity, and aggregate orientation. The material classification of HMA originates with the linear elastic nature of the aggregate and viscoelastic quality of asphalt binder. Mixture theory has been used to model the conglomeration of asphalt and aggregate with their varying material characteristics.

Recently, a model was developed that applied a volume fraction mixture theory to some field mixes. X-ray tomography was used to nondestructively obtain a spatial image of the materials in a specimen. For simplification purposes the asphalt binder and aggregate were modeled as one element. Air was the second element in the mixture theory model. 1-D and 2-D models were developed to illustrate the spatial gradient and void volume fraction (Wang et al., 2004).

A micromechanical model of HMA was developed that accounts for the gradation of a mix (Li et al., 1999). The model divides a specimen into asphalt coated aggregate and asphalt. The elastic modulus is then computed for each component using the theory of elasticity. A modulus of elasticity is defined for the aggregate, aggregate-asphalt interface, and the asphalt.

A piece of aggregate coated in asphalt is simulated as a circular plane. The displacements at interfaces and boundaries can be determined by using the theory of elasticity developed by Timoshenko and Goodier in 1970. It was assumed that there was no gap between either the asphalt and asphalt-aggregate matrix or the asphalt-aggregate matrix and asphalt. It was also assumed that within a circular plane (microscopic level; one piece of aggregate) the strain energy was constant.

### 8.2.5 Moisture Saturation Element

Material properties obtained during laboratory testing will be used. Asphalt binder material properties will be obtained from DSR testing. DSR tests relate G* and phase angle of a binder. Data from several tests on the same binder will be used to define material properties. The moisture affect will be accounted for by obtaining binders tested with and without moisture saturation. Sadd et al. (Sadd et al., 2004) developed a method to incorporate a softening criteria, this method will be employed to account for moisture damage. Binders affected by moisture are softened, G* decreases, thus testing moisture saturated asphalt binder specimens will yield data that can be incorporated as a softening element. The criteria for establishing a material that has failed due to softening will have to be established based on a linkage to field data.

### 8.2.6 Load Application

The load applied to a specimen is created by a steel wheel rolling over a pressurized pneumatic tube. It will be assumed that the load is uniform across the specimen. A steel wheel in an APA applies 100 ± 5 lbs to a specimen and a tube has a pressure of 100 ± 5 psi. A study of the stress distribution associated with APAs was conducted at the University of Florida. It was found that the vertical stress induced by the pneumatic tube and steel wheel is not constant across a cylindrical specimen. The average vertical stress, based on data collected from a sensor mat, was 64.9 psi. During this study, the contact area of the pressurized hose with a specimen was 1.54 $in^2$ (Drakos, 2003).

### 8.2.7 Theoretical Stochastic Finite Element Framework Summary

The theoretical stochastic finite element framework will be a conglomeration of previous models with adaptations to account for material variability and asphalt properties. The material properties will be obtained from laboratory testing. Material distribution will be conducted using the method employed by Wang et al. for portland cement concrete. The imaging process used by Masad et al. will also be used to determine aggregate settlement and asphalt film thickness trends. Since the random aggregate structure will be based on a JMF for each mix, material property distributions will be used to account for variability. It is suggested that OpenSEES be used to define material probability distributions for both properties and locations. OpenSEES has been used successfully in other stochastic finite element models.

# Chapter 9 Conclusions

Moisture can infiltrate a pavement and cause damage. In this dissertation the effects of moisture on binder and on HMA were examined. Evaluation of the affect of moisture on binder included the development of new test equipment, procedure, and criterion. It is believed that the new method for examining the moisture susceptibility of a binder is one that could easily be adopted by owner/agencies. The evaluation of mix was conducted using an APA. A new criterion for determining whether or not a mix is moisture prone was developed. The new criterion uses information already collected during APA testing, rut depth information. For both of these new test criteria field validation will need to be conducted once field data is available.

A theoretical stochastic finite element framework was developed. The elements of the stochastic framework incorporate elements developed in a variety of areas. It is felt that additional work should be conducted to implement the model described. Implementing a computer simulation would be advantageous in regards to financial and time savings. Once the model is validated and calibrated for laboratory specimens, an additional module would be to develop a relationship between field and laboratory results.

In all, moisture damage will continue to plague pavements until realistic test procedures are implemented and calibrated with field results. The test procedures and criteria outlined in this dissertation would aid in reducing the number of mixes used that are moisture prone.

## 9.1 Summary of Developed Moisture Damage Susceptibility Test for Asphalt Binders

A new moisture susceptibility test was developed using modified DSR parts. Testing was conducted to determine if material interface affects complex shear modulus results. It was determined that material interface does affect complex shear modulus results. Hence, for the new test protocol, ceramic discs would be used to allow for water to access

the top of a binder sample in addition to the circumference of a sample. Further testing was conducted to establish an appropriate gap size for a new testing procedure. The gap size selected was 1000-µm. Subsequent testing indicated that the new test procedure is sensitive to binder type and addition of filler. The test also appears to be able to distinguish between filler type. Additional testing indicated that statistically different complex shear modulus results were obtained from unsaturated asphalt binder samples versus saturated specimens. However, no additional differences were observed with the samples were moisture saturated and had endured one freeze/thaw cycle. There were also no statistical differences in complex shear modulus readings when leaving a specimen in a heated water bath anywhere from 0 to 20 minutes prior to testing.

Based on laboratory testing and statistical analysis a new test procedure was established in Chapter 3. Specimens would be tested first unsaturated with ceramic discs at a gap of 1000µm. Second the specimens would soak in a water bath for a period of 24 hours at 25˚C. After 24 hours of soaking, specimens would be tested again in a DSR using ceramic discs. Table 3.4 summarized results from an ANOVA indicating that binder type, filler type, percent of filler, disc material, gap size, testing environment, interaction between binder type and percent of filler, interaction between binder type and disc material, and interaction between filler type and gap size were all deemed significant factors contributing to complex shear modulus dispersion. The new method appears to be sensitive to the addition of fillers in the binders and is able to distinguish between moisture susceptible fillers and non-moisture susceptible fillers.

None of the binders examined in this dissertation failed the Superpave minimum criteria of $G^*/\sin(\delta)$ being at least 1.0 kPa at their original performance grade , however several of the binders did exhibit degradation during testing. During the saturation process many of the binders maintained the original shape prior to saturation, however there were a few binders that tended to spread and even lose small sections of the binder. The binders which did tend to creep during saturation also emitted a visible oil sheen. Specimens displaying creep and oil sheens tended to yield $G^*/\sin(\delta)$ close to the Superpave minimum of 1.0 kPa indicating that perhaps the criteria should be re-evaluated if used for moisture susceptibility testing.

## 9.2 Development of a Moisture Susceptibility Criterion for Asphalt Binders

A water absorption procedure was conducted to determine weight gain after saturation. The trends identified during mean weight comparisons offered useful information to understanding why some binders seemed to perform better than others during the DSR testing. It is felt that this particular method should not be used as a sole criterion for establishing the moisture susceptibility of a binder, but used in conjunction with other methods. This process is helpful in identifying binders that may be prone to absorbing water.

Analysis of elastic and viscous components of binders tested with a modified DSR was conducted. Binders with decreased elastic and viscous component values were deemed moisture susceptible. The relationship between the moisture absorption analysis and complex shear modulus values was weak. It is believed that additional information is needed to relate the two tests.

## 9.3 Summary of Moisture Damage Susceptibility Testing via AASHTO T-283

Several statistical methods were used to determine the significant factors affecting and related to the specimen wet strength. The main statistical conclusions reached were:

- The most precise TSR data was obtained from the 150mm Superpave specimens indicating that the specimens were more consistent using the diameter of 150mm and SGC.
- There is a direct moderate relationship between polymer modification type and wet strength and a strong direct relationship between both NMAS and dry strength with wet strength, based on correlation analysis.

## 9.4 Summary of APA Moisture Damage Susceptibility Testing

The analysis conducted on rut depth obtained from APA testing was outlined in Chapter 7 summarizing ANOVA table results and mean comparison results. Interestingly for the majority of comparisons where there were differences between the condition effect levels, the unconditioned and condition state 3, freeze/thaw conditioned and tested in water, specimens were usually deemed statistically equivalent while condition state 2, freeze/thaw conditioned and tested in air, was deemed statistically different from both. However, only 8 mixes were considered statistically different by the condition state. The majority of mixes yielded statistically equivalent rut depths for all three condition states. A second observation that is intriguing is that there is no statistical difference between the rut depths of coarse-graded and fine-graded mixes.

The moisture damage criterion used was based on rutting knowledge. The criterion is based on calculating the ratio between a conditioned specimen and a control specimen. If the ratio yields a value less than 0.95, the mix did not lose stiffness therefore it is moisture resistant, If the ratio is greater than 1.05, the mix lost stiffness and is considered moisture damage prone. The final criteria states that if the rut depth is greater than 9.1mm and the ratio between the conditioned specimen tested in water divided by the control specimen rut depth values is greater than 1 then the mix is deemed moisture damage prone.

Further testing should be conducted to determine if there is a strong direct relationship between aggregate type and wet strength. Both the APA and TSR results indicated that further investigation relating aggregate type effect on wet strength would be a worthwhile investigation.

The criterion developed to determine whether or not a mix is moisture susceptible indicated that 14 of the 21 mixes were moisture susceptible. Further analysis revealed that there is a strong relationship between water absorbed data and APA test data. There, however is not a strong relationship between DSR and APA test results, nor is there a strong relationship between TSR results and APA test results. It is recommended that if a loaded wheel tester is to be used for moisture susceptibility testing that more than three

specimens be tested. The variability of the rut depth data was rather high and it is believed that additional specimens tested would yield data less affected by outliers.

## 9.5 Summary of Comparison between AASHTO T-283 and APA for Moisture Damage Susceptibility Testing

Comparing factors that affect moisture damage test results and mixes deemed moisture prone for TSR and APA testing resulted in finding no relationship between the two. Very few of the mixes were considered moisture damage susceptible by both test procedures. The same factors were considered for regression analysis with the exception of compaction and diameter, which were only accounted for in the TSR analysis. There were no similar factors affecting the results of these two tests. When the TSR values were grouped by compaction method and diameter it could be seen that high temperature binder PG was the one shared factor that may be affecting the test results.

## 9.6 Contribution to Material Science and State of Practice

The research presented in this dissertation presents a new method to evaluate how binders react to moisture saturation. The modification to a DSR enabled specimens to be evaluated in a truly moisture saturated environment to determine the change in the performance measurement $G^*/\sin(\delta)$. Prior to the modification to the DSR, moisture could only access the perimeter of an asphalt specimen during testing with a DSR. The perimeter of a specimen is a small fraction of the surface area, thus true moisture susceptibility testing could not be conducted with the traditional DSR configuration.

The test procedures and criteria outlined in this dissertation can be used to identify moisture prone HMA pavement materials. If moisture prone materials are identified prior to pavement construction, a better quality pavement can be substituted to prevent premature reconstruction and maintenance. The AASHTO T-283 analysis indicated that three freeze thaw/cycles would be required to test a Superpave specimen following the same standard. It was revealed that one freeze/thaw cycle could be used for APA testing and identify the same mixes as moisture prone or moisture resistant as three freeze/thaw cycles following the AASHTO T-283 procedure.

## 9.7 Summary of Theoretical Stochastic Finite Element Model of Rutting Induced by Moisture Damage

The theoretical stochastic finite element framework will be a conglomeration of previous models with adaptations to account for material variability and asphalt properties. The material properties will be obtained from laboratory testing. Material distribution will be conducted using the method employed by Wang et al. (Wang et al., 1999) for portland cement concrete. The imaging process used by Masad et al. (Masad et al., 2002)will also be used to determine aggregate settlement and asphalt film thickness trends. Since the random aggregate structure will be based on a job mix formula for each mix, material property distributions will be used to account for variability. It is suggested that OpenSEES be used to define material probability distributions for both properties and locations. OpenSEES has been used successfully in other stochastic finite element models.

## 9.8 Asphalt Binder Recommendations

This test criterion is based on data obtainable from dynamic shear rheometer testing software and water absorption. As previously mentioned, this criterion is based on theory and has been applied to laboratory results, but still needs to be verified with field results. It is recommended that binders are tested with a dynamic shear rheometer using a modified spindle and base plate. The binder that should be tested is original binder and binder with a filler. A binder with filler should be tested to allow for breaks in an asphalt binder specimen membrane surface, which enables water to permeate a specimen faster than a specimen without surface breaks. Surface breaks occur in pavements; therefore inducing breaks by adding a filler simulates, to an extent, reality.

Both of the original binder and binder with filler should be tested as unsaturated and saturated. The saturation should occur for a minimum of 24 hours in a 25˚C water bath. An evaluation of the change in viscous and elastic components should be conducted, as outline in Chapter 5. Confidence ellipsoids should be developed to account for noise associated with data readings. The rating used in Chapter 5 should be followed.

In conjunction with DSR testing results, specimens should be evaluated to determine water absorbing tendencies, following steps outlined in Chapter 5. If a binder exhibits an confidence ellipsoid that is close to crossing over into another quadrant, the water absorption test results should be consulted. This method should be validated with field data once the pavements where the material was collected from have aged properly.

## 9.9 HMA Testing Recommendations

If the APA is to be used for moisture damage susceptibility testing an increased number of specimens should be tested. Testing just three specimens yielded very high variances in many of the mixes. The moisture criterion developed in this dissertation should be compared with field data to establish limits.

# Chapter 10 References


1. @Risk™ Advanced Risk Analysis for Spreadsheets. Version 4; Newfield, NY, 2001
2. AASHTO TP48. "Standard Test Procedure for Viscosity Determination of Asphalt Binders Using Rotational Viscometer", Standard Specifications for Transportation Materials and Methods and Sampling and Testing Part II: Tests. Washington D.C., 1997
3. AASHTO T165-55. "Effect of Water on Cohesion of Compacted Bituminous Mixtures", Standard Specifications for Transportation Materials and Methods and Sampling and Testing Part II: Tests. Washington D.C., 1997.
4. AASHTO T166-93. "Bulk Specific Gravity of Compacted Bituminous Mixtures Using Saturated Surface-Dry Specimens", Standard Specifications for Transportation Materials and Methods and Sampling and Testing Part II: Tests. Washington D.C., 1997.
5. AASHTO T182-84. "Coating and Stripping of Bitumen-Aggregate Mixtures", Standard Specifications for Transportation Materials and Methods and Sampling and Testing Part II: Tests. Washington D.C., 1997.
6. AASHTO T209-94. "Theoretical Maximum Specific Gravity and Density of Bituminous Paving Mixtures", Standard Specifications for Transportation Materials and Methods and Sampling and Testing Part II: Tests. Washington D.C., 1997.
7. AASHTO T269-94. "Percent Air Voids in Compacted Dense and Open Bituminous Paving Mixtures", Standard Specifications for Transportation Materials and Methods and Sampling and Testing Part II: Tests. Washington D.C., 1997.
8. AASHTO T283-89. "Resistance of Compacted Bituminous Mixture to Moisture Induced Damage", Standard Specifications for Transportation

Materials and Methods and Sampling and Testing Part II: Tests. Washington D.C., 1993.

9. APA User's Manual 5.11.01. Pavement Technology, Inc., 2003.
10. Archilla, A.R. and S. Madanat, "Development of a Rutting Model from Experimental Data," Journal of Transportation Engineering, Volume 26, Number 4, American Society of Civil Engineers, Restin, VA., 2000.
11. ASTM D2041. "Standard Test Method for Theoretical Maximum Specific Gravity and Density of Bituminous Paving Mixtures" Annual Book of ASTM Standards 4.03. West Conshohocken, PA: ASTM International, 2004.
12. ASTM D2726. "Standard Test Method for Bulk Specific Gravity and Density of Non-Absorptive Compacted Bituminous Mixures", Annual Book of ASTM Standards 4.03. West Conshohocken, PA: ASTM International, 2004.
13. ASTM D3625. "Effect of Water on Bituminous-Coated Aggregate Using Boiling Water", Annual Book of ASTM Standards 4.03. West Conshohocken, PA: ASTM International, 2004.
14. ASTM D4867. "Standard Test Method for Effect of Moisture on Asphalt Concrete Paving Mixtures", Annual Book of ASTM Standards 4.03. West Conshohocken, PA: ASTM International, 2004.
15. Barcena, R., Epps Martin, A., and D. Hazlett. "Performance-Graded binder Specification for Surface Treatments." Transportation Research Record 1810, Transportation Research Board, National Highway Research Council, Washington, D.C., 2002.
16. Bausano, J. AutoCAD Drawing, 2005.
17. Bazant, Z.P., Tabbara, M.R., Kazemi, M.T., and G. Pijaudier-Cabot, "Random Particle Model for Fracture of Aggregate or Fiber Composites," Journal of Engineering Mechanics, 116, American Society of Civil Engineers, Restin, VA., 1990.

18. Cheng, D., Little, D.N., Lytton, R.L, and J.C. Holste, "Moisture Damage Evaluation of Asphalt Mixtures by Considering Both Moisture Diffusion and Repeated-Load Conditions", Transportation Research Record 1832, Transportation Research Board, National Highway Research Council, Washington, D.C., 2003.
19. Chengbin, D. and R. Chaojun, "Numerical Simulation of the Uniaxial Failure of Three-Grading Concrete Based on Micro Damage," Earth & Space 2006 Engineering, Construction, and Operations in Challenging Environments Proceedings of the Tenth Biennial ASCE Aerospace Division International Conference on Engineering, Construction, and Operations in Challenging Environments, CD, 2006.
20. Chappat, M. and J. Bilal, "The Environmental Road of the Future, Life Cycle Analysis," Colas Group, 2003.
21. Claessen, A.I.M, Edwards, J.M., Somme, P., and P. Uge, "Asphalt Pavement Design, the Shell Method," Procedure of 4th International Conference on the Structural Design of Asphalt Pavmeent, University of Michigan, Ann Arbor, MI, 1977.
22. Cooley, L.A., P.S. Kandhal, M.S. Buchanan, F. Fee, and A. Epps, "Loaded Wheel Testers in the United States: State of the Practice," Transportation Research E-Circular, Number E-C016, Transportation Research Board, Washington, D.C., July 2000.
23. Der Kiureghian, A., and J-B Ke. The Stochastic Finite Element Method in Structural Reliability. Probabilistic Engineering Mechanics Volume 3, Number 2, Computational Mechanics Publication, Ashurst, England, 1985.
24. Deshpande, V.S. and D. Cebon, "Micromechanical Modeling of Steady State Deformation in Asphalt," Journal of Materials in Civil Engineering, Volume 16, Number 2, American Society of Civil Engineers, Restin, VA., 2004.

25. Dienes, G.J. and H.F. Klemm, "Theory and Application of the Parallel Plate Plastometer", Journal of Applied Physics, Volume17, June 1946.
26. Dongre, Raj. Personal Communication on June 26, 2006.
27. Epps, J., Sebaaly, P., Penaranda, J., Maher, M., McCann, M., and A. Hand. NCHRP 444: Compatibility of a Test for Moisture-Induced Damage with Superpave Volumetric Mix Design. Transportation Research Board, National Highway Research Council, Washington, D.C. 2000.
28. Ghanem, R.G. and P.D. Spanos. Stochastic Finite Elements A Spectral Approach. Dover Publications, Inc., Mineola, NY, 1991.
29. Haukaas,T. A. and A. Der Kiureghian, "A Computer Program for Nonlinear Finite Element Reliability Analysis," ICOSSAR '01, 8th International Conference on Structural Safety and Reliability. June 17-21, 2001 at Newport Beach, California, USA, 2001.
30. HKS, ABAQUS Theory and Users Manual – Version 6.3, Hibbit, Karlsson, & Sorenson, Inc., Pawtucket, Rhode Island, 2002.
31. Huang, S.-C., Robertson, R.E., Branthaver, J.F., and J. C. Petersen, "Impact of Lime Modification of Asphalt-Aggregate Interaction and Moisture Resistance to Moisture Damage," Journal of Materials in Civil Engineering, Volume 17, Number 6, American Society of Civil Engineers, Restin, VA., 2005.
32. Ishikawa, M., Yoshikawa, H., and T. Tanube, "The Constitutive Model in Terms of Damage Tensor," Proceedings of Finite Element Analysis of Reinforced Concrete Structures, American Society of Civil Engineers, Restin, VA., 1986.
33. Jackson, N.M. and C.D. Baldwin, "Evaluation of the Asphalt Pavement Analyzer to Predict the Relative Rutting Susceptibility of HMA in Tennessee," International Conference on Accelerated Pavement Testing October 18-20, 1999 Dissertation Number CS6-3, 1999.

34. Kenis, W.J., "Predictive Design Procedures – A Design Method for Flexible Pavements Using the VESYS Structural Subsystem," Proceedings of 4th International Conference on the Structural Design of Asphalt Pavements, University of Michigan, Ann Arbor, MI, 1977.
35. Kulkarni, R.B., "Rational Approach in Applying Reliability Theory to Pavement Structural Design," Transportation Research Record 1449, Transportation Research Board, National Research Council, Washington, D.C., 1994.
36. Kvasnak, A.N. Development of an Integrated Transportation Management System for Chittenden County. MS Thesis, University of Vermont, Burlington, Vermont. 2002.
37. Kvasnak, A.N. and R.C Williams, "Use of Ridge Regression to Estimate Rutting in Asphalt Pavement Analyzer Samples," Mairepav4 - The Fourth International Conference on Maintenance and Rehabilitation of Pavements and Technological Control, Belfast, Northern Ireland, 2005.
38. Lai, J.S. and W.L. Hufferd, "Predicting Permanent Deformation of Asphalt Concrete From Creep Tests," Transportation Research Record 616, Transportation Research Board, National Research Council, Washington, D.C., 1976.
39. Lee, Y.-C., "Application of Viscoelastic Theory and Finite Element Analysis to Determine Effective Temperature of Asphalt Concrete Layer in Flexible Pavement," Transportation Research Board 2004 Annual Meeting CD-Rom, Transportation Research Board, Washington, D.C., 2004.
40. Lottman, R.P. NCHRP 192: Predicting Moisture-Inducted Damage to Asphaltic Concrete. Transportation Research Board, National Highway Research Council, Washington, D.C., 1978.
41. Lottman, R.P. NCHRP 246: Predicting Moisture-Inducted Damage to Asphaltic Concrete – Field Evaluation. Transportation Research Board, National Highway Research Council, Washington, D.C., 1982.

42. Lua, Y.J. and R.H. Sues, "Probabilistic Finite-Element Analysis of Airfield Pavements," Transportation Research Record, Transportation Research Board, National Research Council, Washington, D.C., 1996.
43. Liu, W.K., Belytschko, T. and Y.J. Lua. Probabilistic Finite Element Method. Probabilistic Structural Mechanics Handbook -- Theory and Industrial Applications. Chapman & Hall, New York, 1995.
44. Liu, P-L. and A. Der Kiureghian, "Finite Element Reliability of Two Dimensional Continua with Geometrical Nonlinearity," 5th International Conference on Structural Safety and Reliability, San Francisco, CA., 1989.
45. Lytton, R.L., "Characterizing Asphalt Pavements for Performance," Transportation Research Record 1723, Transportation Research Board, National Highway Research Council, Washington, D.C., 2000.
46. Lytton, R.L., J. Uzan, E.G. Fernando, R. Roque, D. Hilturnen, and S.M. Stoffels, "Development and Validation of Performance Prediction Models and Specifications for Asphalt Binders and Paving Mixes SHRP A-357 Rep.", National Research Council, Washington, D.C., 1993.
47. Maina, J.W. and K. Matsui, "Development of Software for Elastic Analysis of Pavement Structures Due to Vertical and Horizontal Surface Loading," 83rd Transportation Research Board 2004 Annual meeting CD-ROM, Transportation Research Board, 2004.
48. McCann, M. and P.E. Sebaaly, "Evaluation of Moisture Sensitivity and Performance of Lime in Hot-Mix Asphalt: Resilient Modulus, Tensile Strength, and Simple Shear Tests", Transportation Research Record 1832, Transportation Research Board, National Highway Research Council, Washington, D.C., 2003.
49. Monismith, C.L. K. Inkabit, C.R. Freerne, and D.B. Mclean, "A Subsystem to Predict Rutting in Asphalt Concrete Pavement Structures," Proceedings of 4th International Conference on the Structural Design of Asphalt Pavements, University of Michigan, Ann Arbor, MI, 1977.

50. Olsson, J. Computational Road Mechanics-With Emphasis on FE-Analysis of Rutting. Chalmers Tekniska Hogskolo, 2004.
51. Parvini, M. and D.F.E. Stolle, "Application of Stochastic Finite-Element Method to Deflection Analysis of Pavement Structures," Transportation Research Record 1540, Transportation Research Record, National Research Council, Washington, D.C., 1996.
52. Pendelton, O.J., "Reliability in Pavement Design: Issues, Concepts, and Significance," Transportation Research Record 1449, Transportation Research Board, National Research Council, Washington, D.C., 1994.
53. Petersen, J.C., Robertson, R.E., Branthaver, J.F, Harnsberger, P.M., Duvall, J.J., Kim, S.S., Anderson, D.A., Christiansen, D.W., and H.U. Bahia. "Binder Characterization and Evaluation Volume 1 SHRP-A-367", Strategic Highway Research Program, 1994.
54. Rauhut, J.B., Kenis, W.J., and W.R. Hudson, "Improved Techniques for Prediction of Fatigue Life for Asphalt Concrete Pavements," Transportation Research Record 602, Transportation Research Board, National Highway Research Council, Washington, D.C., 1976.
55. Roberts, F.L., P.S. Kandhal, E.R. Brown, D.Y. Lee, and T.W. Kennedy. Hot Mix Asphalt Materials, Mixture Design, and Construction Second Edition. NAPA Education Foundation, Lanham, MA, 1996.
56. Robertson R.E., "Chemical Properties of Asphalt and Their Relationship to Pavement Performance SHRP-A/UWP-91-510", Strategic Highway Research Program, 1991.
57. Rottermond, M.P., "Development of a Prototype Moisture Sensitivity Test for Asphalt Binder." M.S. Thesis Michigan Technological University, 2004.
58. Sadd, M.H., Dai, Q., Parameswaran, V., and A. Ashukla, "Microstructural Simulation of Asphalt Materials: Modeling and Experimental Studies," Journal of Materials in Civil Engineering, Volume 16, Number 2, American Society of Civil Engineers, Restin, VA.,March/April 2004.

59. Sanad, A. and M.P. Saka, "Prediction of Ultimate Shear Strength of Reinforced-Concrete Deep Beams Using Neural Networks," Journal of Structural Engineering, Volume 127, Number 7, 2001.
60. Scarpas, A., Van Gurp, C.A.P.M., Al-Khoury, R., and S.M.J.G. Erkens, "Finite Element Simulation of Damage Development in Asphalt Concrete Pavements," Eighth International Conference on Asphalt Pavements, August 10-14, 1997, Seattle, Washington: Proceedings,1997.
61. Scholz, T.V. and S.F. Brown, "Rheological Characteristics of Bitumen in Contact with Mineral Aggregate (With Discussion)," Journal of the Association of Asphalt Paving Technologists, Volume 65, Bookcrafters Inc., Chelsea, MI, 1996.
62. Shook, J.F., Finn, F.N., Witczack, M.W., and C.L. Monismith, "Thickness Design of Asphalt Pavements – The Asphalt Institute Method," Procedure of the 5th International Conference on the Structural Design of Asphalt Pavements, Delft University of Technology, The Netherlands, 1982.
63. Thompson, M.R. and D. Nauman. Rutting Rate Analyses of the AASHO Road Test Flexible Pavements. Transportation Research Record 1384, Transportation Research Board, National Highway Research Council, Washington, D.C., 1993.
64. Tunnicliff, D.G. and R.E. Root. NCHRP 274: Use of Antistripping Additives in Asphalt Concrete Mixtures – Laboratory Phase. Transportation Research Board, National Highway Research Council, Washington, D.C., 1984.
65. Tunnicliff, D.G. and R.E. Root. NCHRP 373: Use of Antistripping Additives in Asphalt Concrete Mixtures – Field Evaluation. Transportation Research Board, National Highway Research Council, Washington, D.C., 1995.
66. Uzan, J., "Permanent Deflection in Flexible Pavements," Journal of Transportation Engineering, Volume 130, Number 1, American Society of Civil Engineers, Restin, VA., 2004.

67. Wang, Z.M., Kwan, A.K.H, and H.C. Chan, "Mesocopic Study of Concrete I: Generation of Random Aggregate Structure and Finite Element Mesh," Computers and Structures, Volume 70, American Society of Civil Engineers, Restin, VA., 1999.
68. Weismann, S.L., Harvey, J., Sckman, J.L., and F. Long, "Selection of Laboratory Test Specimen Dimension for Permanent Deformation of Asphalt Concrete Pavements," Transportation Research Record 1681, Transportation Research Board, National Research Council, Washington, D.C., 1999.
69. Williams, R.C. and B.D. Prowell, "Comparison of Laboratory Wheel-Tracking Test Results with WesTrack Performance," Transportation Research Record 1681, Transportation Research Board, National Research Council, Washington, D.C., 1999.
70. Williams, R.C. A. Kvasnak, and V. Aurilio, "Properties of Recovered Binder Samples and Their Relationship to Tank Binders," 2002 Canadian Technical Asphalt Association Proceedings, Bookcrafters Inc., Chelsea, MI, 2002.
71. Willaims, R.C., Kvasnak, A.N., and K. Hofmann, "Analysis of Three Methods of Sampling Hot-Mix Asphalt From Behind the Paver," 83rd Transportation Research Board 2004 Annual meeting CD-ROM, Transportation Research Board, 2004.
72. Williams, T.M. and F.P. Miknis, "Use of Environmental SEM to Study Asphalt-Water Interactions," Journal of Materials in Civil Engineering, Volume 10, Number 2, American Society of Civil Engineers, Restin, VA., 1998.
73. Zaghloul, S. and T. White, "Use of a Three-Dimensional, Dynamic Finite Element Program for Analysis of Flexible Pavement," Transportation Research Record 1388, Transportation Research Board, National Research Council, Washington, D.C., 1993.

74. White, T.D., "Application of Finite Element Analysis to Pavement Problems", Proc., First National Symposium on 3D Finite Element Modeling for Pavement Analysis and Design, Charleston, W.Va., 1998.
75. Youtcheff, J. and V. Aurilio, "Moisture Sensitivity of Asphalt Binders: Evaluation and Modeling of the Pneumatic Adhesion Test Results." 1997 Canadian Technical Asphalt Association Proceedings, 1997.
76.

# Appendix A: Definitions

Rutting=Longitudinal depression in pavement

HMA=Hot Mix Asphalt

APA=Asphalt Pavement Analyzer

FEM=Finite Element Model

SFEM=Stochastic Finite Element Model

RVE=Representative Volume Element

DSR=Dynamic Shear Rheometer

MRL=Materials Reference Library

SHRP=Strategic Highway Research Program

PG=Performance Grade; It is a measure of the temperature range that the binder performs well in.

Neat=Binder that is not polymer modified

Original Binder=Binder collected without any modifications

G*=Complex shear modulus for binder

δ=Phase angle for binders

E*=Complex modulus for HMA

φ=Phase angle for HMA

ANOVA=Analysis of Variance

# Appendix B: Confidence Ellipsoids

**Multivariate Site=1, Filler (None=0, Silica=1, Hydrated Lime=2)=0, Percent=0**
Freq: Run

**Correlations**

| | Viscous Difference | Elastic Difference |
|---|---|---|
| Viscous Difference | 1.0000 | -0.9136 |
| Elastic Difference | -0.9136 | 1.0000 |

**Scatterplot Matrix**

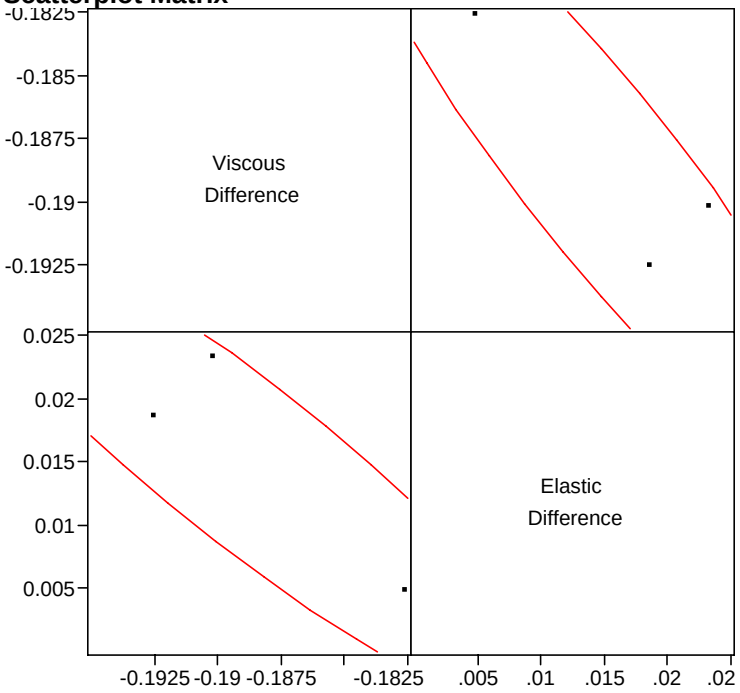


**Multivariate Site=1, Filler (None=0, Silica=1, Hydrated Lime=2)=1, Percent=5**
Freq: Run

**Correlations**

| | Viscous Difference | Elastic Difference |
|---|---|---|
| Viscous Difference | 1.0000 | 0.9829 |
| Elastic Difference | 0.9829 | 1.0000 |

**Scatterplot Matrix**

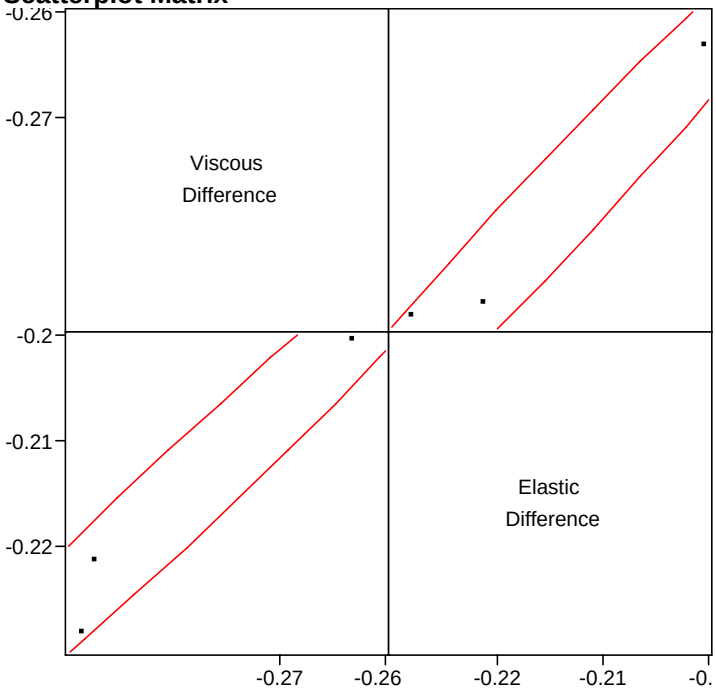


**Multivariate Site=1, Filler (None=0, Silica=1, Hydrated Lime=2)=1, Percent=10**

Freq: Run

**Correlations**

| | Viscous Difference | Elastic Difference |
|---|---|---|
| Viscous Difference | 1.0000 | 0.9976 |
| Elastic Difference | 0.9976 | 1.0000 |

**Scatterplot Matrix**

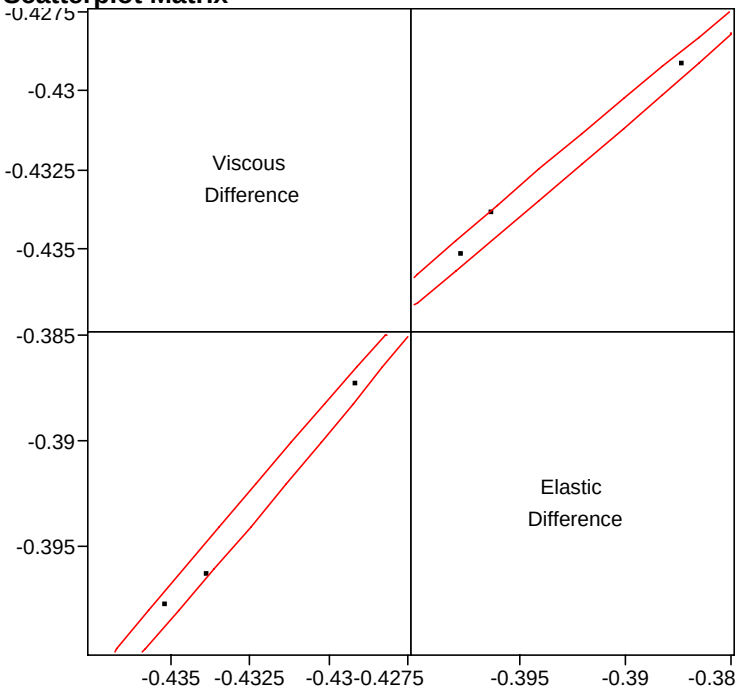


**Multivariate Site=1, Filler (None=0, Silica=1, Hydrated Lime=2)=1, Percent=20**

Freq: Run

**Correlations**

| | Viscous Difference | Elastic Difference |
|---|---|---|
| Viscous Difference | 1.0000 | 0.8402 |
| Elastic Difference | 0.8402 | 1.0000 |

**Scatterplot Matrix**

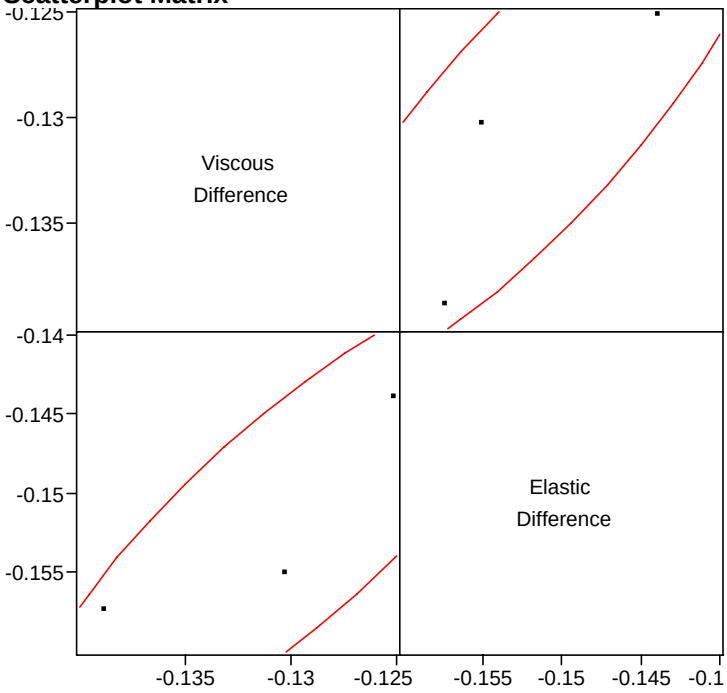


**Multivariate Site=1, Filler (None=0, Silica=1, Hydrated Lime=2)=2, Percent=5**

Freq: Run

**Correlations**

| | Viscous Difference | Elastic Difference |
|---|---|---|
| Viscous Difference | 1.0000 | 0.9908 |
| Elastic Difference | 0.9908 | 1.0000 |

**Scatterplot Matrix**

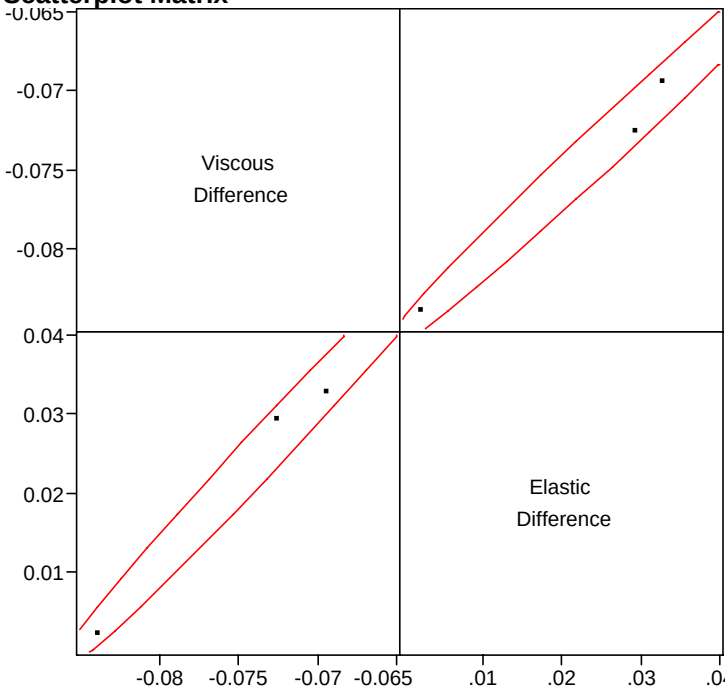


**Multivariate Site=1, Filler (None=0, Silica=1, Hydrated Lime=2)=2, Percent=10**

Freq: Run

**Correlations**

| | Viscous Difference | Elastic Difference |
|---|---|---|
| Viscous Difference | 1.0000 | 0.9389 |
| Elastic Difference | 0.9389 | 1.0000 |

**Scatterplot Matrix**

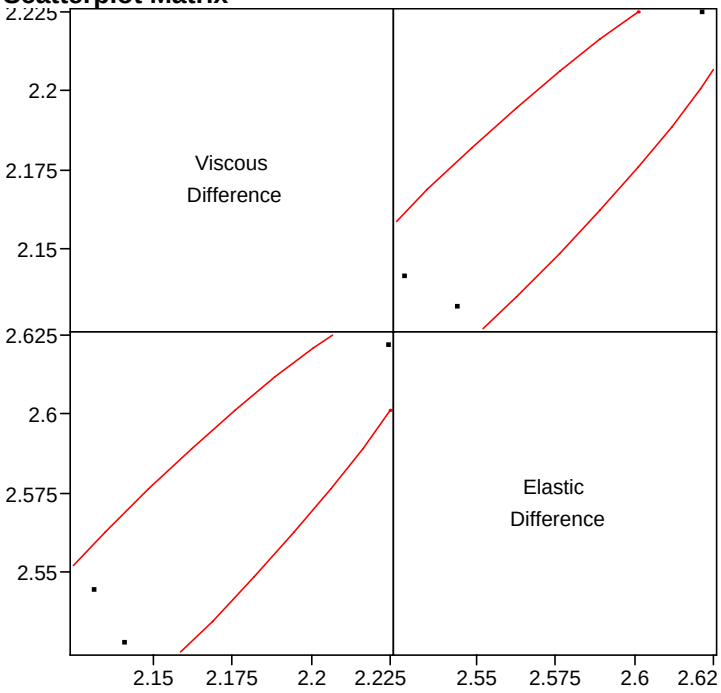


**Multivariate Site=1, Filler (None=0, Silica=1, Hydrated Lime=2)=2, Percent=20**

Freq: Run

**Correlations**

| | Viscous Difference | Elastic Difference |
|---|---|---|
| Viscous Difference | 1.0000 | 0.6337 |
| Elastic Difference | 0.6337 | 1.0000 |

**Scatterplot Matrix**

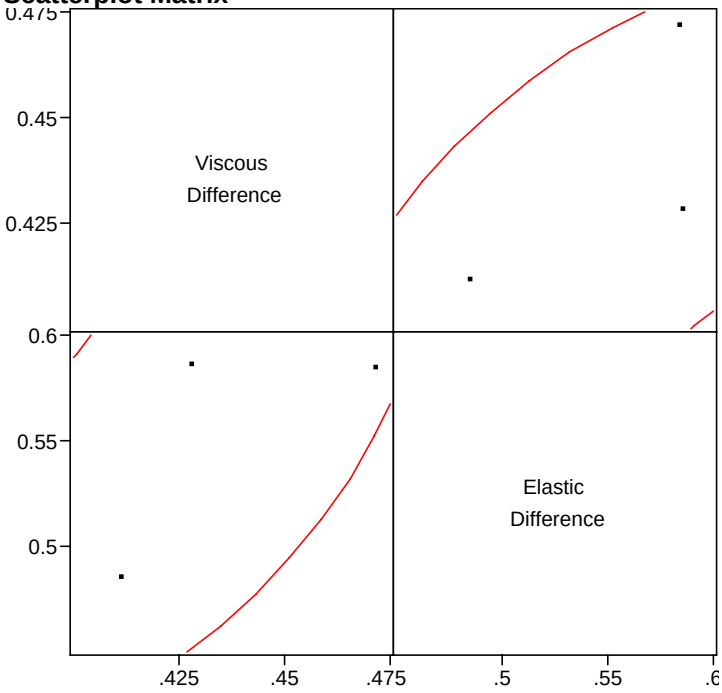


**Multivariate Site=2, Filler (None=0, Silica=1, Hydrated Lime=2)=0, Percent=0**

Freq: Run

**Correlations**

| | Viscous Difference | Elastic Difference |
|---|---|---|
| Viscous Difference | 1.0000 | -0.9887 |
| Elastic Difference | -0.9887 | 1.0000 |

**Scatterplot Matrix**

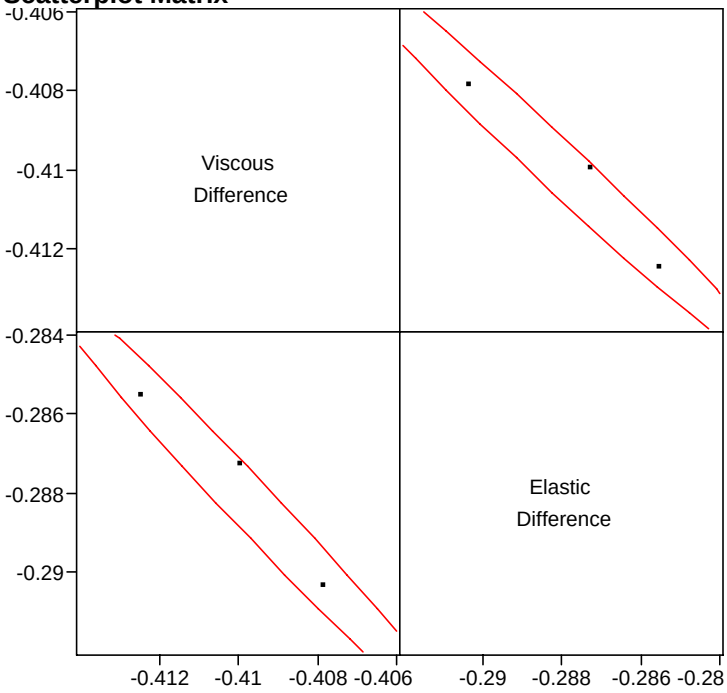


**Multivariate Site=2, Filler (None=0, Silica=1, Hydrated Lime=2)=1, Percent=5**

Freq: Run

**Correlations**

| | Viscous Difference | Elastic Difference |
|---|---|---|
| Viscous Difference | 1.0000 | 0.7805 |
| Elastic Difference | 0.7805 | 1.0000 |

**Scatterplot Matrix**

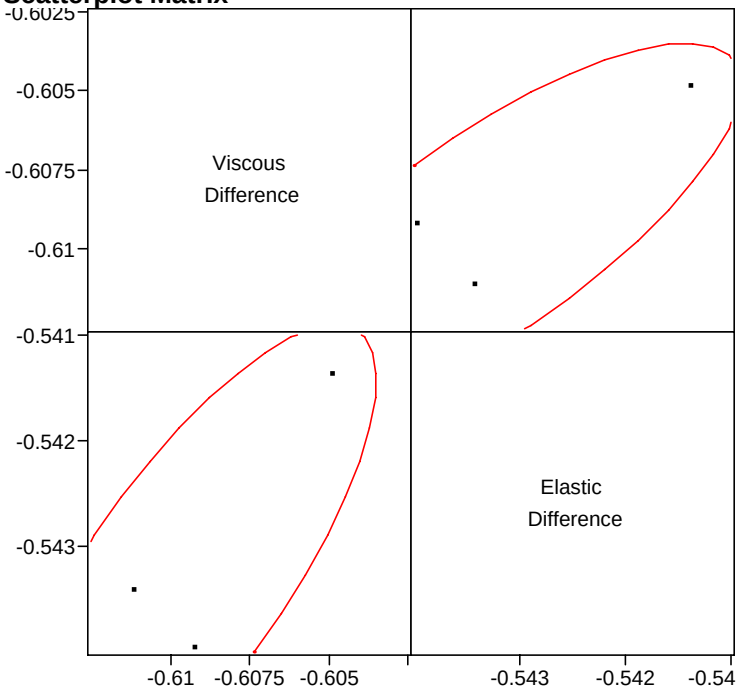


**Multivariate Site=2, Filler (None=0, Silica=1, Hydrated Lime=2)=1, Percent=10**

Freq: Run

**Correlations**

| | Viscous Difference | Elastic Difference |
|---|---|---|
| Viscous Difference | 1.0000 | 0.9829 |
| Elastic Difference | 0.9829 | 1.0000 |

**Scatterplot Matrix**

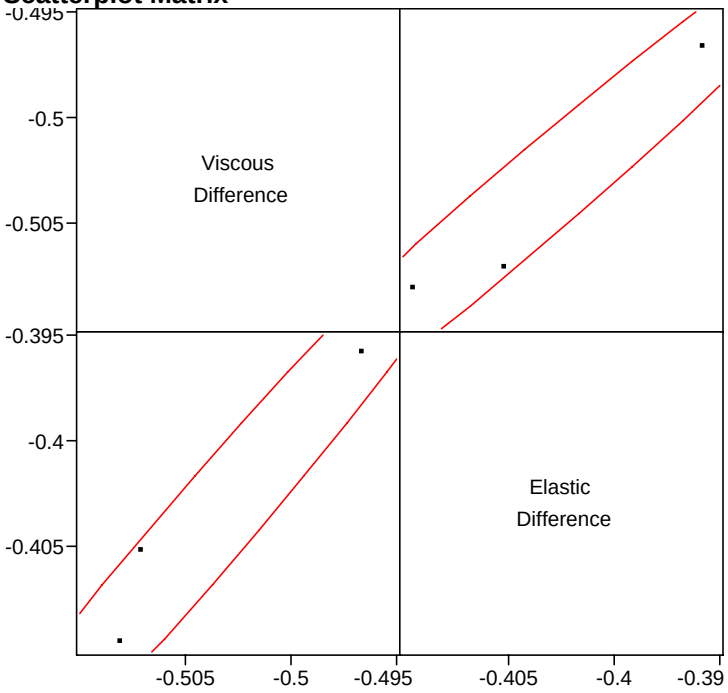


**Multivariate Site=2, Filler (None=0, Silica=1, Hydrated Lime=2)=1, Percent=20**

Freq: Run

**Correlations**

| | Viscous Difference | Elastic Difference |
|---|---|---|
| Viscous Difference | 1.0000 | 0.9999 |
| Elastic Difference | 0.9999 | 1.0000 |

**Scatterplot Matrix**

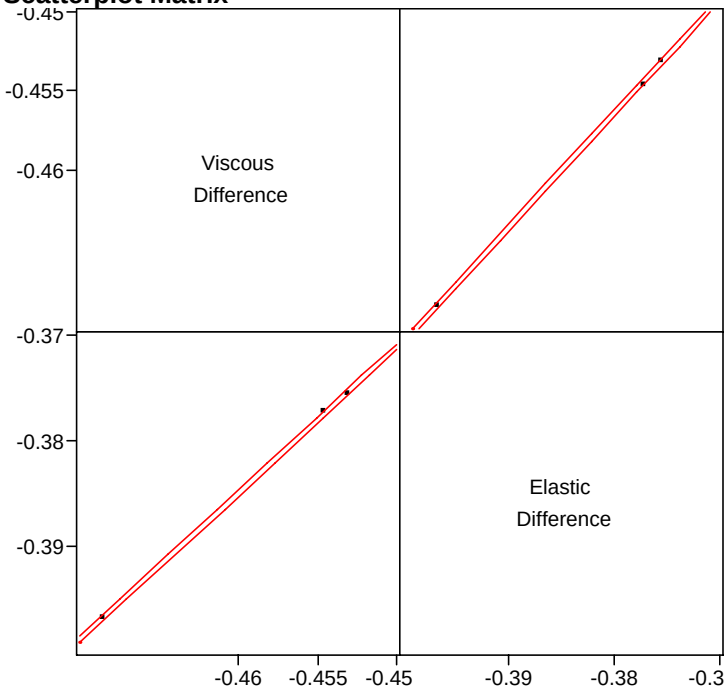


**Multivariate Site=2, Filler (None=0, Silica=1, Hydrated Lime=2)=2, Percent=5**

Freq: Run

**Correlations**

| | Viscous Difference | Elastic Difference |
|---|---|---|
| Viscous Difference | 1.0000 | 0.9476 |
| Elastic Difference | 0.9476 | 1.0000 |

**Scatterplot Matrix**

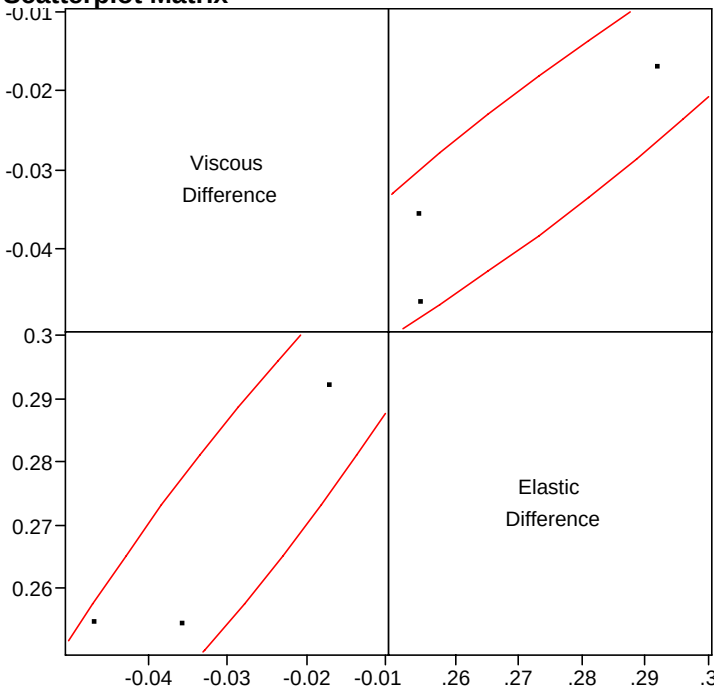


**Multivariate Site=2, Filler (None=0, Silica=1, Hydrated Lime=2)=2, Percent=10**

Freq: Run

**Correlations**

| | Viscous Difference | Elastic Difference |
|---|---|---|
| Viscous Difference | 1.0000 | 0.1970 |
| Elastic Difference | 0.1970 | 1.0000 |

**Scatterplot Matrix**

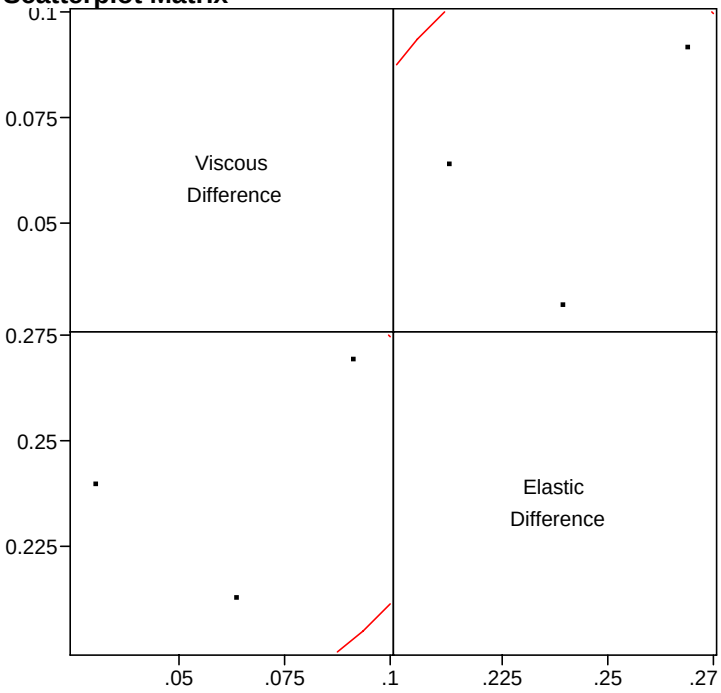


**Multivariate Site=2, Filler (None=0, Silica=1, Hydrated Lime=2)=2, Percent=20**

Freq: Run

**Correlations**

| | Viscous Difference | Elastic Difference |
|---|---|---|
| Viscous Difference | 1.0000 | 0.8339 |
| Elastic Difference | 0.8339 | 1.0000 |

**Scatterplot Matrix**

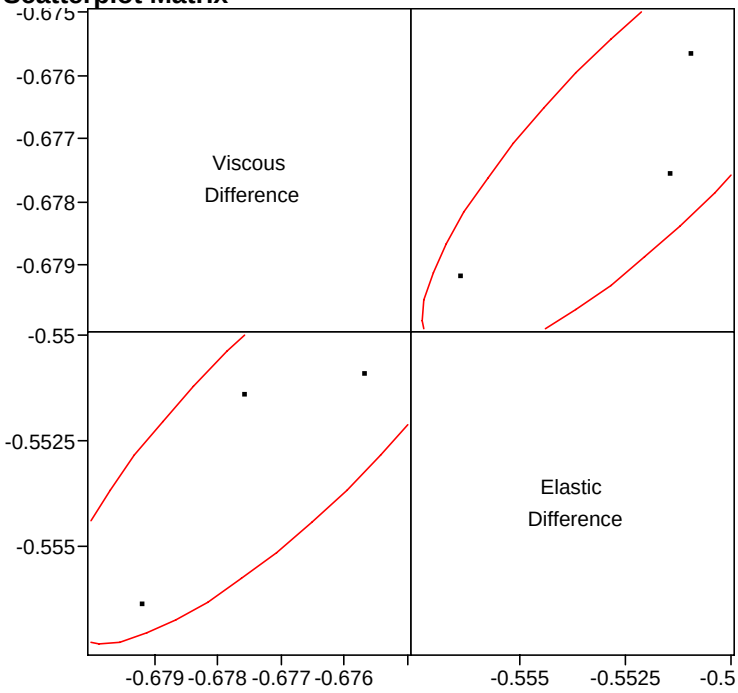


**Multivariate Site=3, Filler (None=0, Silica=1, Hydrated Lime=2)=0, Percent=0**

Freq: Run

**Correlations**

| | Viscous Difference | Elastic Difference |
|---|---|---|
| Viscous Difference | 1.0000 | 0.9901 |
| Elastic Difference | 0.9901 | 1.0000 |

**Scatterplot Matrix**

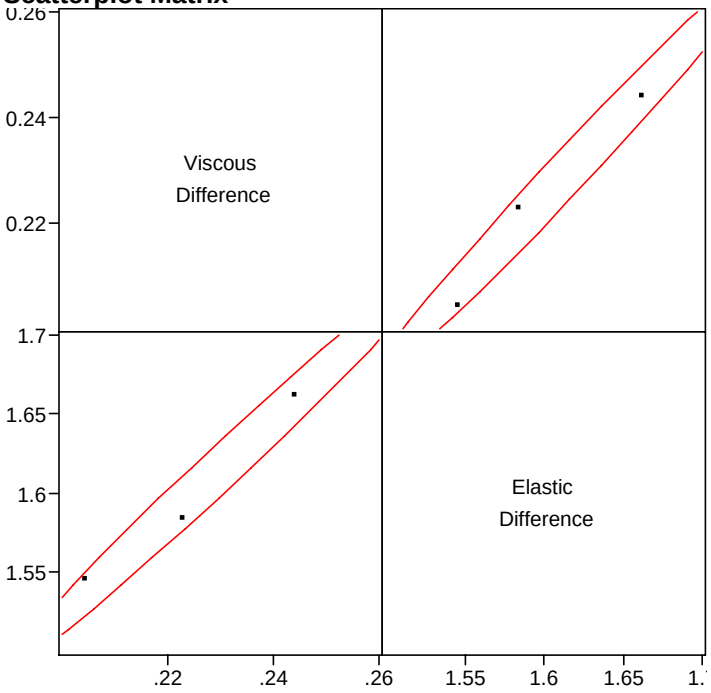


**Multivariate Site=3, Filler (None=0, Silica=1, Hydrated Lime=2)=1, Percent=5**

Freq: Run

**Correlations**

| | Viscous Difference | Elastic Difference |
|---|---|---|
| Viscous Difference | 1.0000 | 0.9613 |
| Elastic Difference | 0.9613 | 1.0000 |

**Scatterplot Matrix**

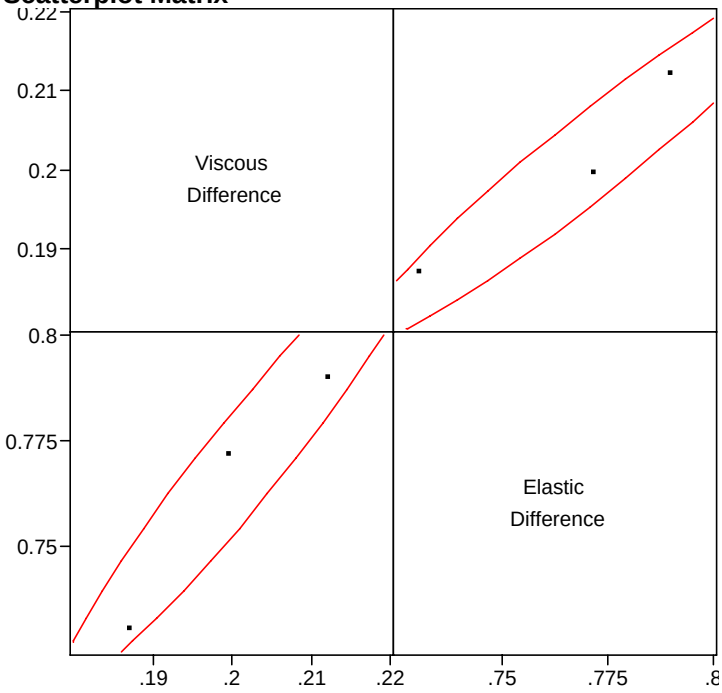


**Multivariate Site=3, Filler (None=0, Silica=1, Hydrated Lime=2)=1, Percent=10**

Freq: Run

**Correlations**

| | Viscous Difference | Elastic Difference |
|---|---|---|
| Viscous Difference | 1.0000 | -0.2282 |
| Elastic Difference | -0.2282 | 1.0000 |

**Scatterplot Matrix**

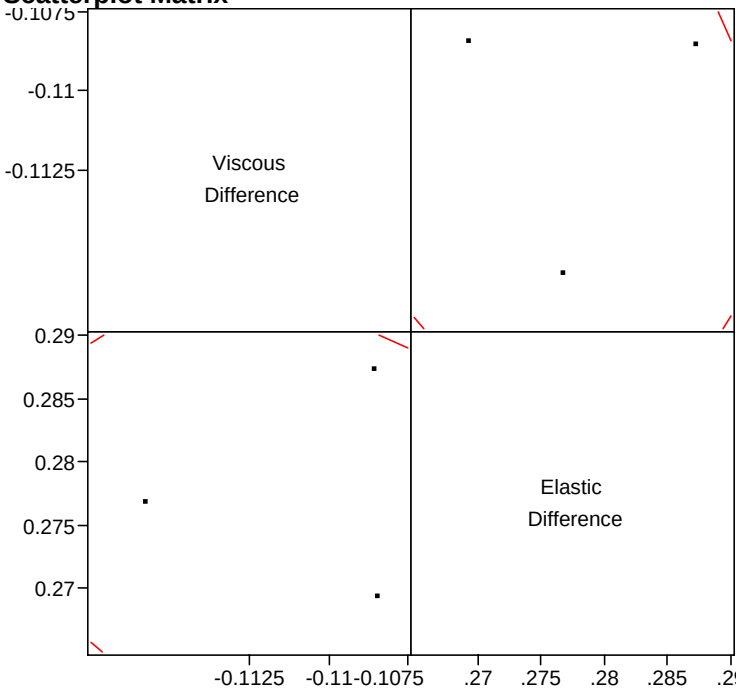


**Multivariate Site=3, Filler (None=0, Silica=1, Hydrated Lime=2)=1, Percent=20**

Freq: Run

**Correlations**

| | Viscous Difference | Elastic Difference |
|---|---|---|
| Viscous Difference | 1.0000 | 0.3578 |
| Elastic Difference | 0.3578 | 1.0000 |

**Scatterplot Matrix**

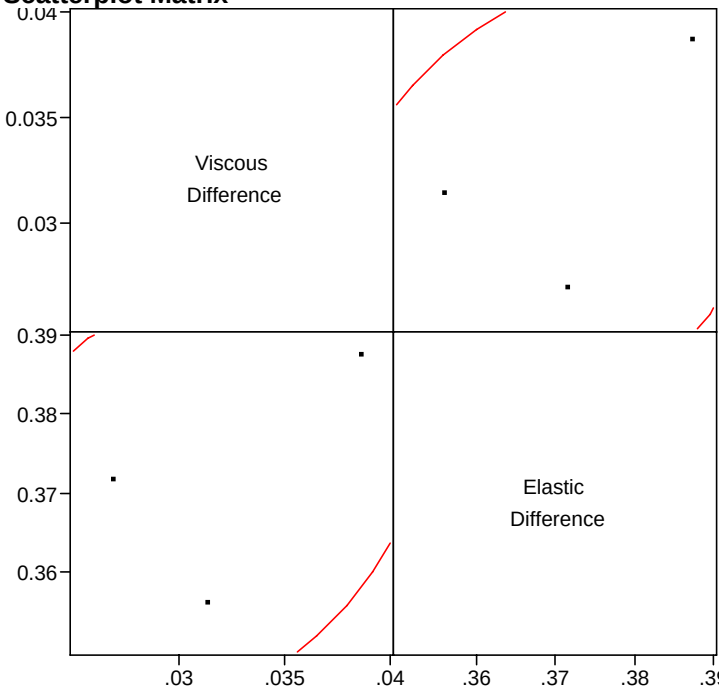


**Multivariate Site=3, Filler (None=0, Silica=1, Hydrated Lime=2)=2, Percent=5**

Freq: Run

**Correlations**

| | Viscous Difference | Elastic Difference |
|---|---|---|
| Viscous Difference | 1.0000 | 1.0000 |
| Elastic Difference | 1.0000 | 1.0000 |

**Scatterplot Matrix**

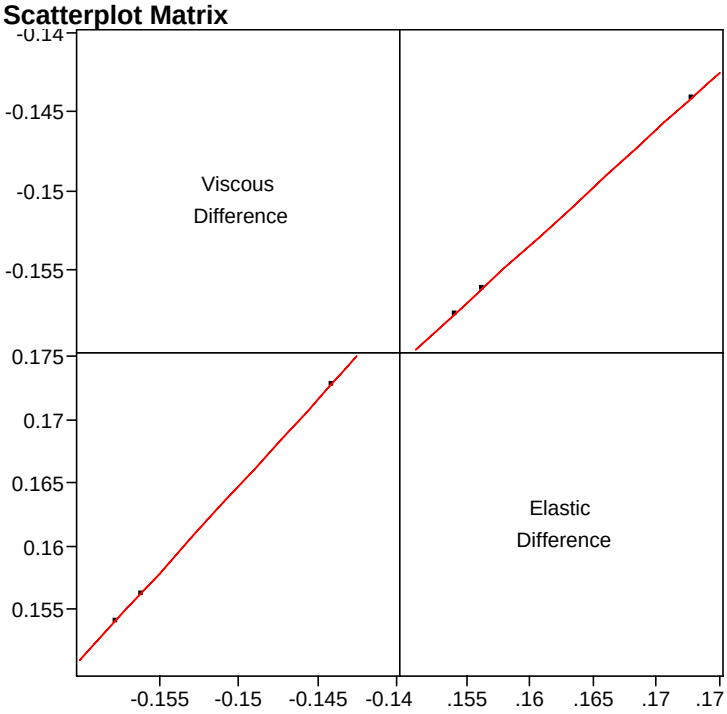


**Multivariate Site=3, Filler (None=0, Silica=1, Hydrated Lime=2)=2, Percent=10**

Freq: Run

**Correlations**

| | Viscous Difference | Elastic Difference |
|---|---|---|
| Viscous Difference | 1.0000 | 1.0000 |
| Elastic Difference | 1.0000 | 1.0000 |

**Scatterplot Matrix**

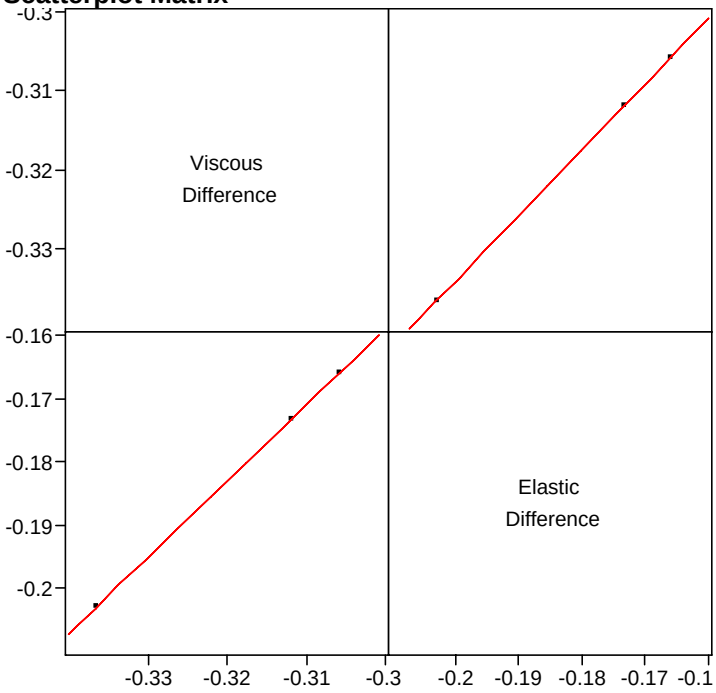


**Multivariate Site=3, Filler (None=0, Silica=1, Hydrated Lime=2)=2, Percent=20**

Freq: Run

**Correlations**

| | Viscous Difference | Elastic Difference |
|---|---|---|
| Viscous Difference | 1.0000 | -0.5035 |
| Elastic Difference | -0.5035 | 1.0000 |

**Scatterplot Matrix**

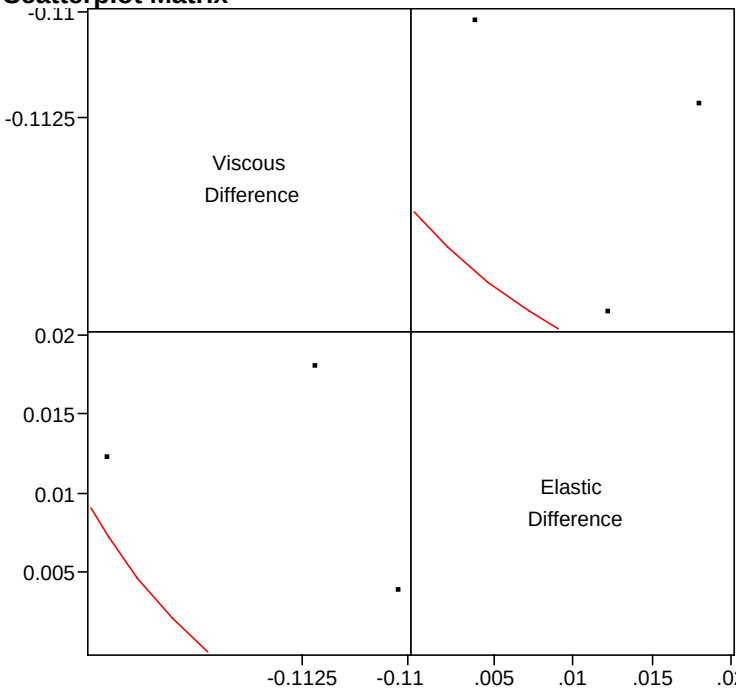


**Multivariate Site=4, Filler (None=0, Silica=1, Hydrated Lime=2)=0, Percent=0**

Freq: Run

**Correlations**

| | Viscous Difference | Elastic Difference |
|---|---|---|
| Viscous Difference | 1.0000 | -0.9783 |
| Elastic Difference | -0.9783 | 1.0000 |

**Scatterplot Matrix**

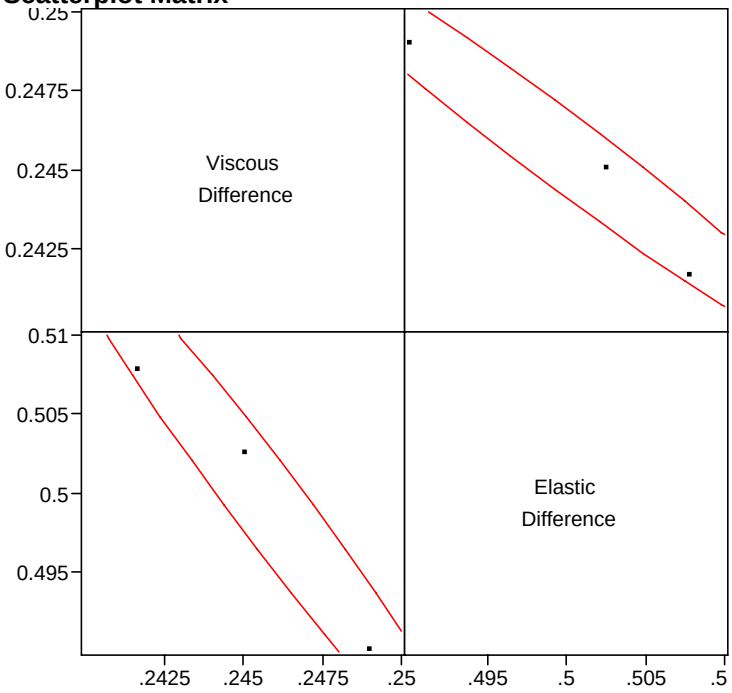


**Multivariate Site=4, Filler (None=0, Silica=1, Hydrated Lime=2)=1, Percent=5**

Freq: Run

**Correlations**

| | Viscous Difference | Elastic Difference |
|---|---|---|
| Viscous Difference | 1.0000 | 0.9542 |
| Elastic Difference | 0.9542 | 1.0000 |

**Scatterplot Matrix**

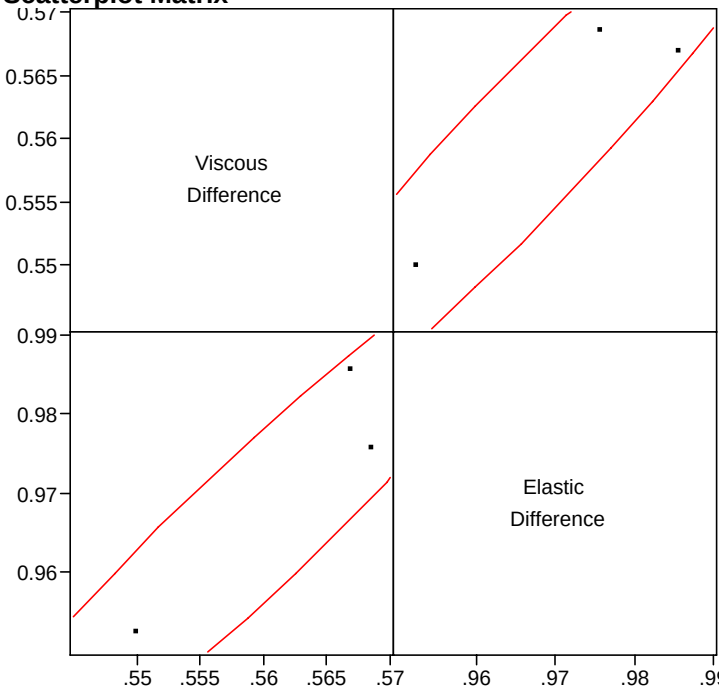


**Multivariate Site=4, Filler (None=0, Silica=1, Hydrated Lime=2)=1, Percent=10**

Freq: Run

**Correlations**

| | Viscous Difference | Elastic Difference |
|---|---|---|
| Viscous Difference | 1.0000 | 0.9975 |
| Elastic Difference | 0.9975 | 1.0000 |

**Scatterplot Matrix**

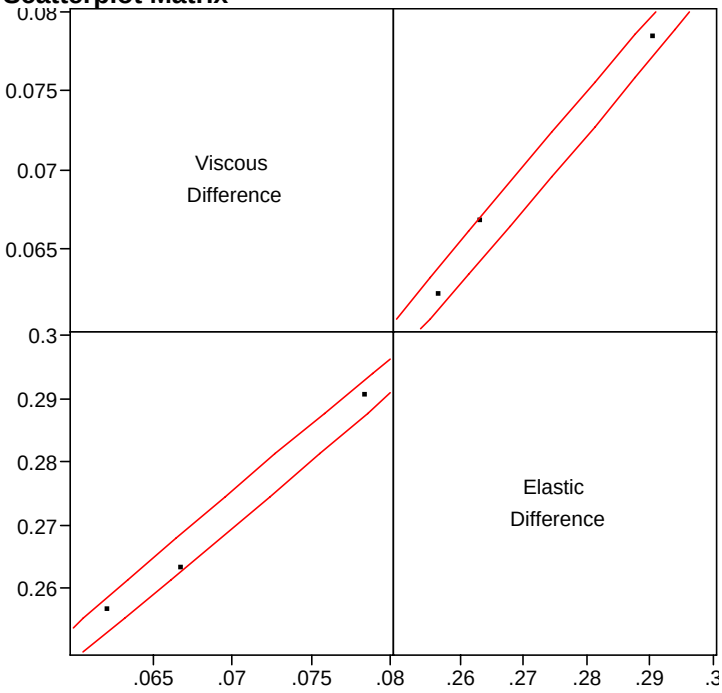


**Multivariate Site=4, Filler (None=0, Silica=1, Hydrated Lime=2)=1, Percent=20**

Freq: Run

**Correlations**

| | Viscous Difference | Elastic Difference |
|---|---|---|
| Viscous Difference | 1.0000 | 1.0000 |
| Elastic Difference | 1.0000 | 1.0000 |

**Scatterplot Matrix**

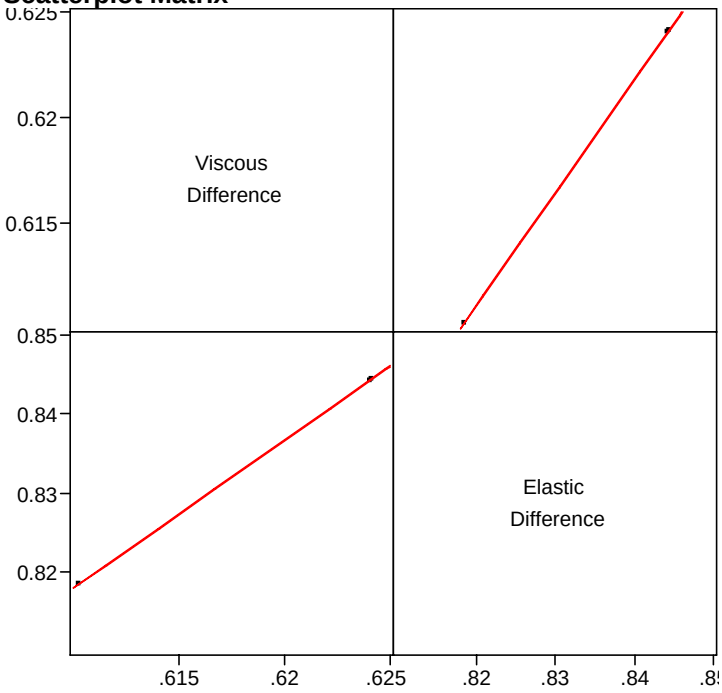


**Multivariate Site=4, Filler (None=0, Silica=1, Hydrated Lime=2)=2, Percent=5**

Freq: Run

**Correlations**

| | Viscous Difference | Elastic Difference |
|---|---|---|
| Viscous Difference | 1.0000 | -0.1203 |
| Elastic Difference | -0.1203 | 1.0000 |

**Scatterplot Matrix**

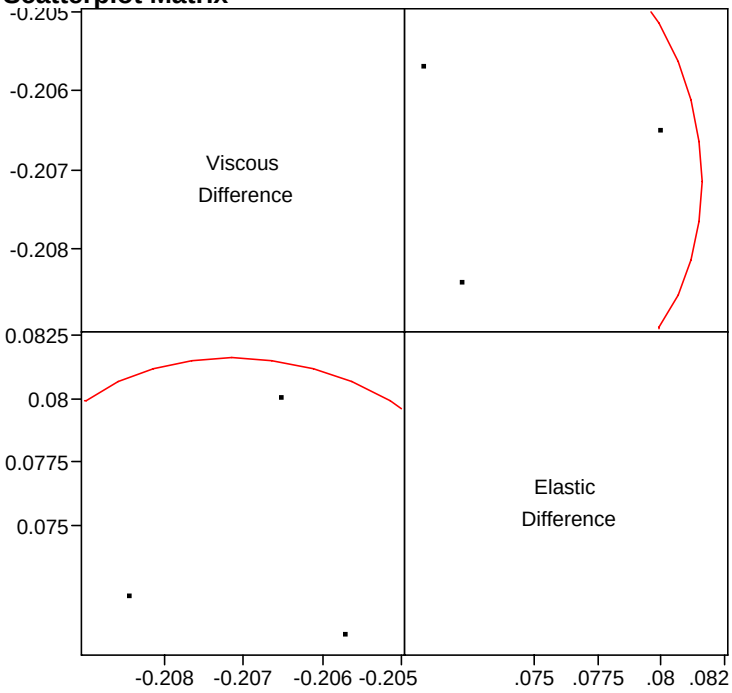


**Multivariate Site=4, Filler (None=0, Silica=1, Hydrated Lime=2)=2, Percent=10**

Freq: Run

**Correlations**

| | Viscous Difference | Elastic Difference |
|---|---|---|
| Viscous Difference | 1.0000 | 0.9458 |
| Elastic Difference | 0.9458 | 1.0000 |

**Scatterplot Matrix**

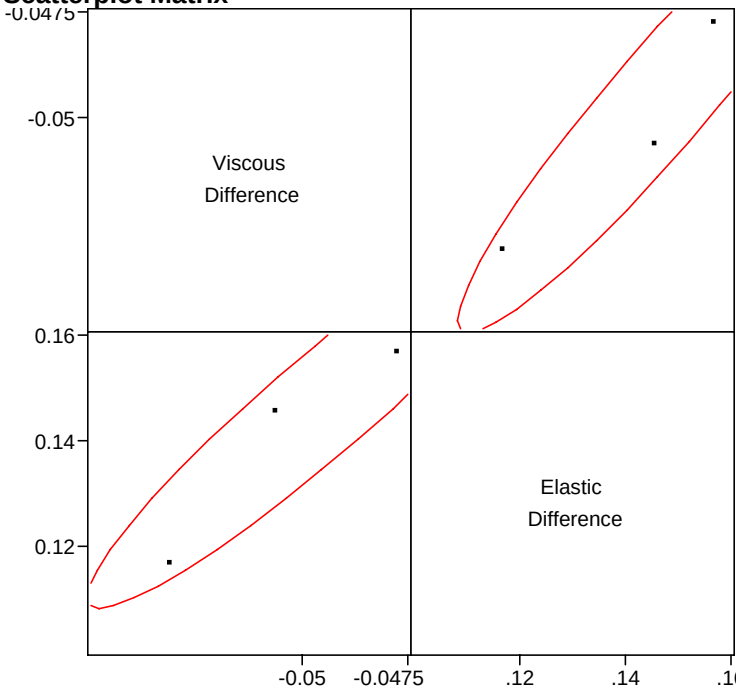


**Multivariate Site=4, Filler (None=0, Silica=1, Hydrated Lime=2)=2, Percent=20**

Freq: Run

**Correlations**

| | Viscous Difference | Elastic Difference |
|---|---|---|
| Viscous Difference | 1.0000 | 0.6129 |
| Elastic Difference | 0.6129 | 1.0000 |

**Scatterplot Matrix**

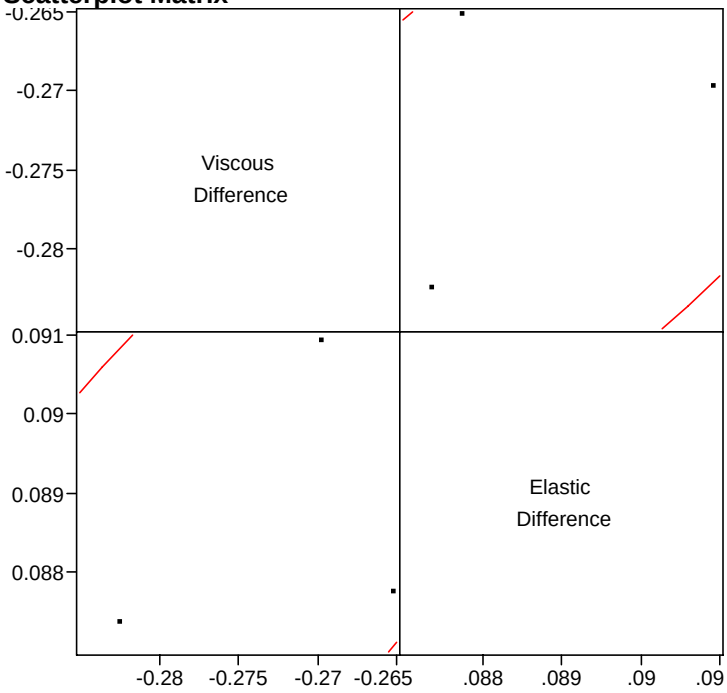


**Multivariate Site=5, Filler (None=0, Silica=1, Hydrated Lime=2)=0, Percent=0**

Freq: Run

**Correlations**

| | Viscous Difference | Elastic Difference |
|---|---|---|
| Viscous Difference | 1.0000 | 0.3257 |
| Elastic Difference | 0.3257 | 1.0000 |

**Scatterplot Matrix**

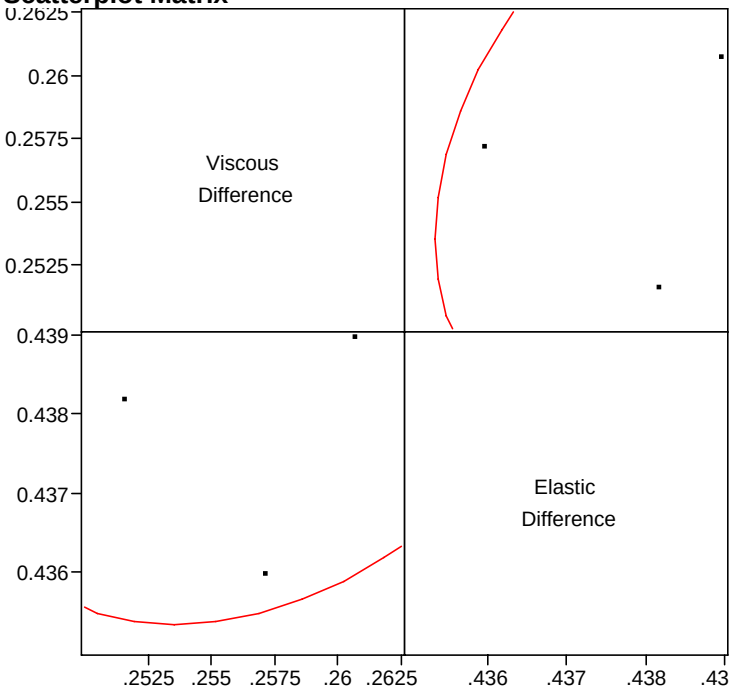


**Multivariate Site=5, Filler (None=0, Silica=1, Hydrated Lime=2)=1, Percent=5**

Freq: Run

**Correlations**

| | Viscous Difference | Elastic Difference |
|---|---|---|
| Viscous Difference | 1.0000 | 0.0913 |
| Elastic Difference | 0.0913 | 1.0000 |

**Scatterplot Matrix**

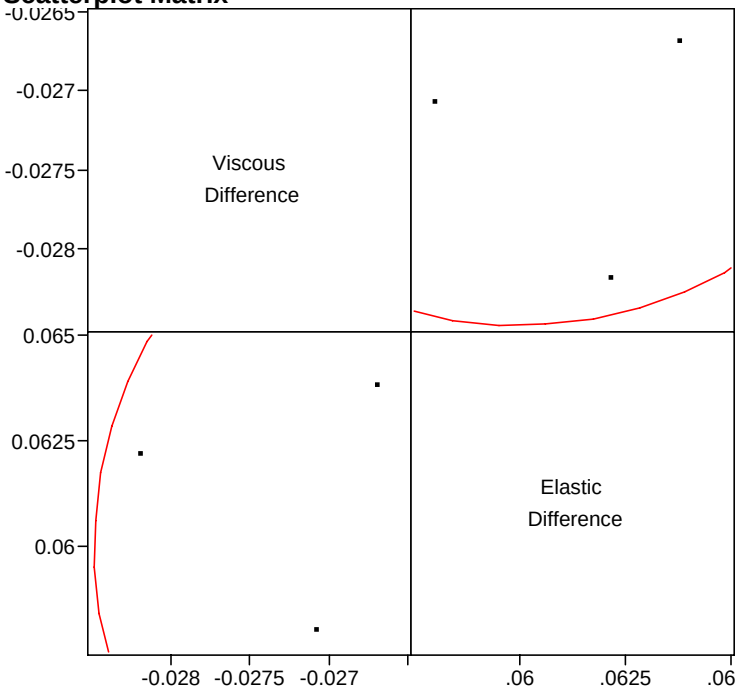


**Multivariate Site=5, Filler (None=0, Silica=1, Hydrated Lime=2)=1, Percent=10**

Freq: Run

**Correlations**

| | Viscous Difference | Elastic Difference |
|---|---|---|
| Viscous Difference | 1.0000 | 0.9949 |
| Elastic Difference | 0.9949 | 1.0000 |

**Scatterplot Matrix**

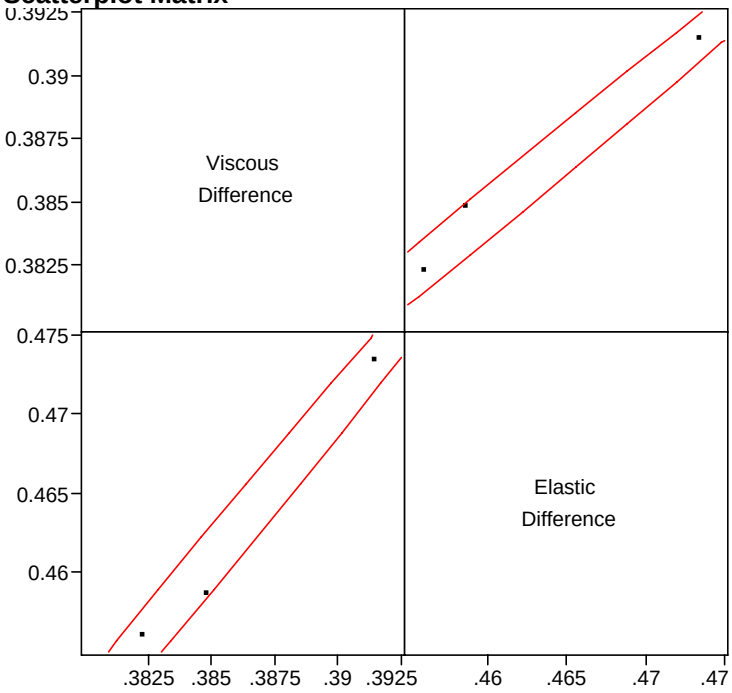


**Multivariate Site=5, Filler (None=0, Silica=1, Hydrated Lime=2)=1, Percent=20**

Freq: Run

**Correlations**

| | Viscous Difference | Elastic Difference |
|---|---|---|
| Viscous Difference | 1.0000 | 0.0129 |
| Elastic Difference | 0.0129 | 1.0000 |

**Scatterplot Matrix**

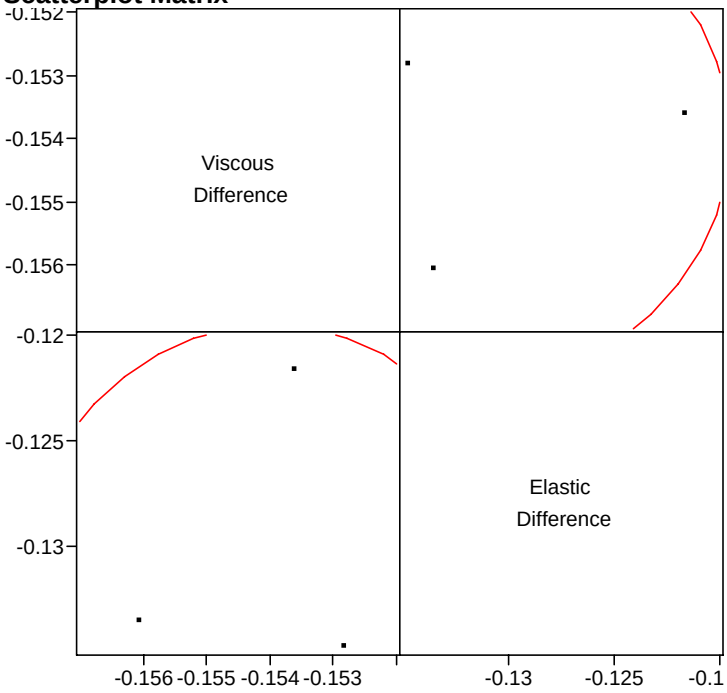


**Multivariate Site=5, Filler (None=0, Silica=1, Hydrated Lime=2)=2, Percent=5**

Freq: Run

**Correlations**

| | Viscous Difference | Elastic Difference |
|---|---|---|
| Viscous Difference | 1.0000 | 0.9242 |
| Elastic Difference | 0.9242 | 1.0000 |

**Scatterplot Matrix**

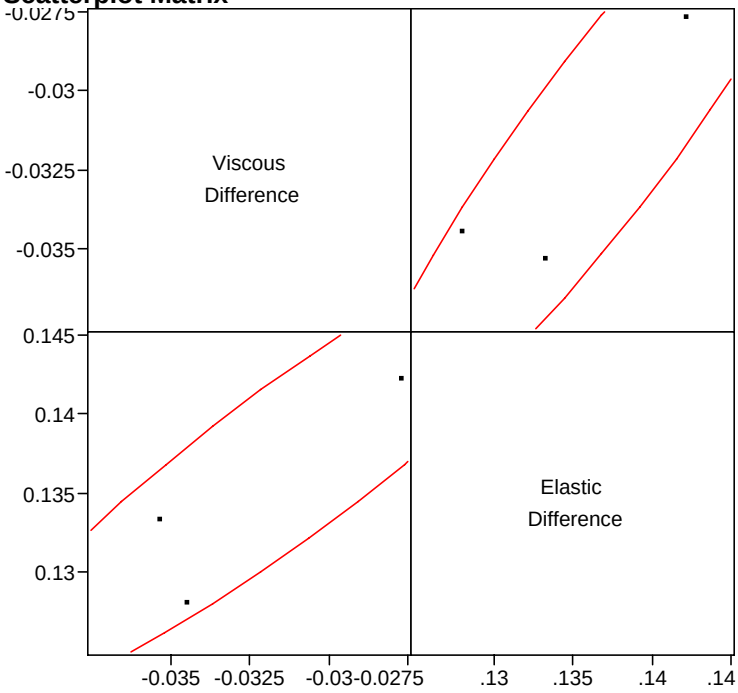


**Multivariate Site=5, Filler (None=0, Silica=1, Hydrated Lime=2)=2, Percent=10**

Freq: Run

**Correlations**

| | Viscous Difference | Elastic Difference |
|---|---|---|
| Viscous Difference | 1.0000 | 0.9993 |
| Elastic Difference | 0.9993 | 1.0000 |

**Scatterplot Matrix**

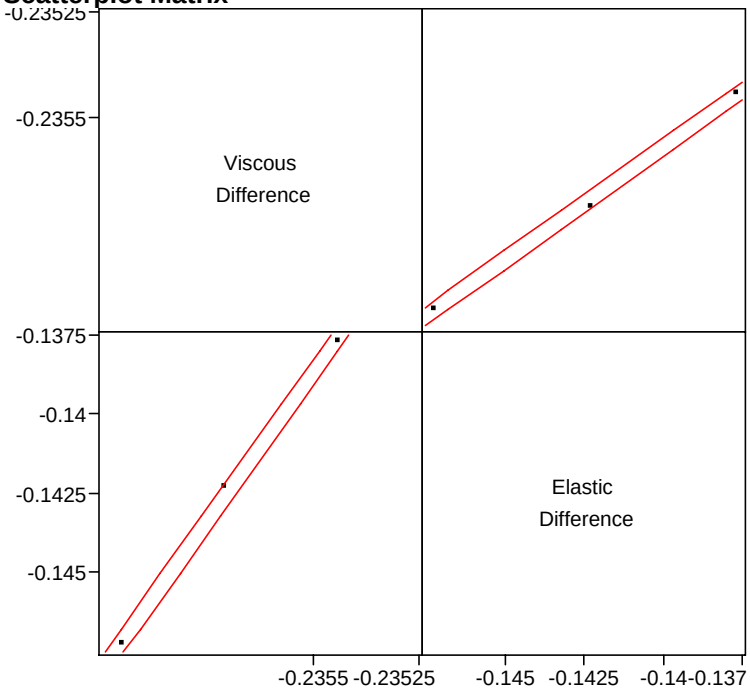


**Multivariate Site=5, Filler (None=0, Silica=1, Hydrated Lime=2)=2, Percent=20**

Freq: Run

**Correlations**

| | Viscous Difference | Elastic Difference |
|---|---|---|
| Viscous Difference | 1.0000 | 0.9127 |
| Elastic Difference | 0.9127 | 1.0000 |

**Scatterplot Matrix**

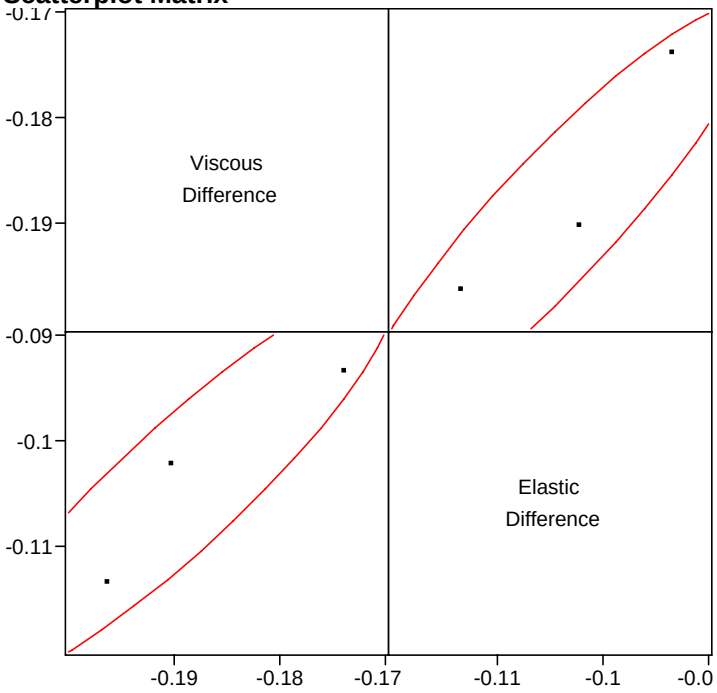


**Multivariate Site=6, Filler (None=0, Silica=1, Hydrated Lime=2)=0, Percent=0**

Freq: Run

**Correlations**

| | Viscous Difference | Elastic Difference |
|---|---|---|
| Viscous Difference | 1.0000 | 0.9805 |
| Elastic Difference | 0.9805 | 1.0000 |

**Scatterplot Matrix**

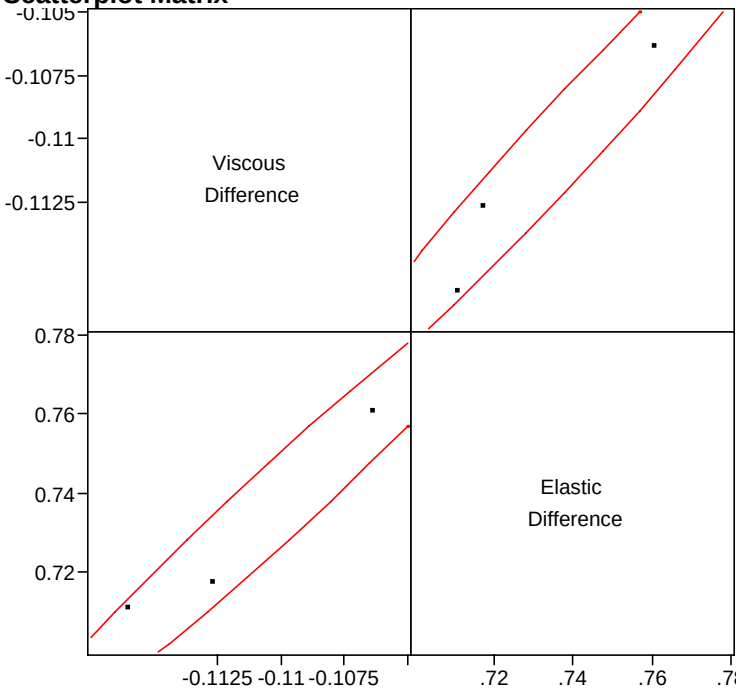


**Multivariate Site=6, Filler (None=0, Silica=1, Hydrated Lime=2)=1, Percent=5**

Freq: Run

**Correlations**

| | Viscous Difference | Elastic Difference |
|---|---|---|
| Viscous Difference | 1.0000 | 0.3331 |
| Elastic Difference | 0.3331 | 1.0000 |

**Scatterplot Matrix**

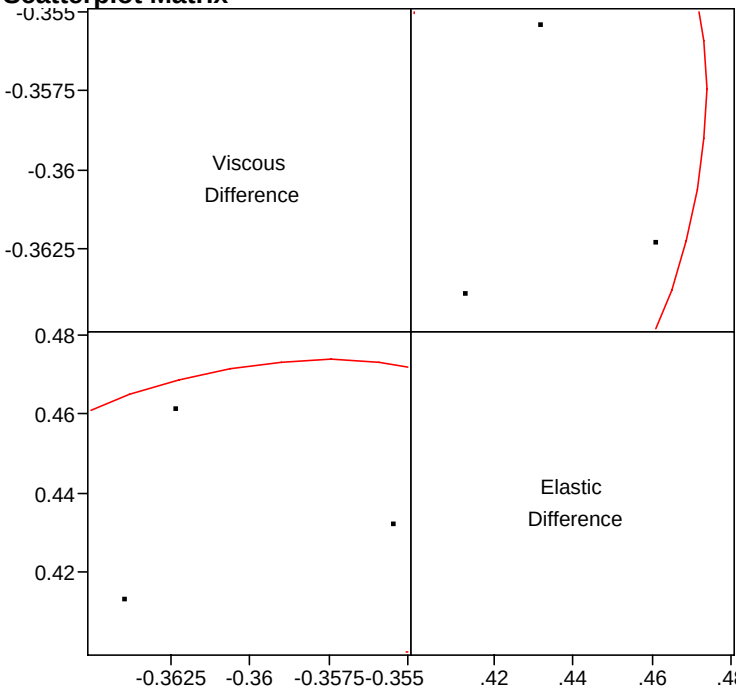


**Multivariate Site=6, Filler (None=0, Silica=1, Hydrated Lime=2)=1, Percent=10**

Freq: Run

**Correlations**

| | Viscous Difference | Elastic Difference |
|---|---|---|
| Viscous Difference | 1.0000 | 0.5455 |
| Elastic Difference | 0.5455 | 1.0000 |

**Scatterplot Matrix**

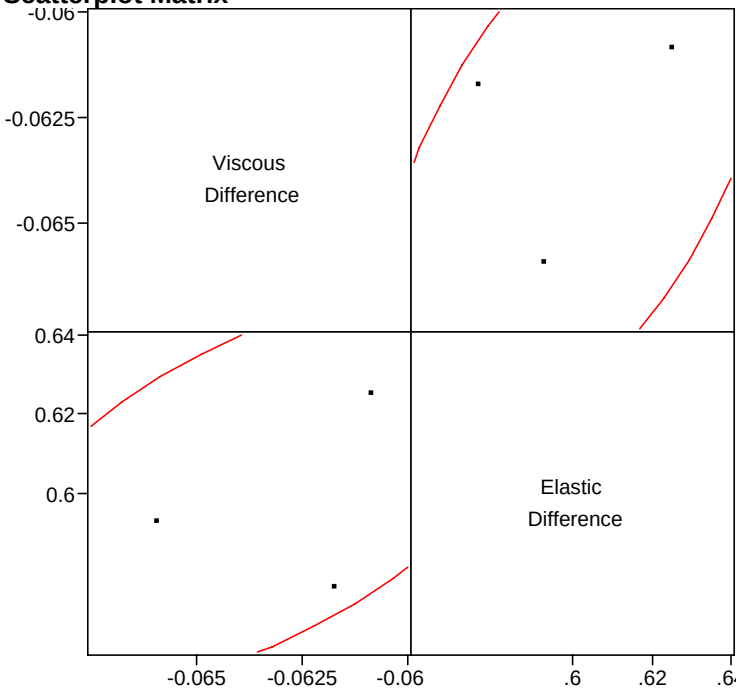


**Multivariate Site=6, Filler (None=0, Silica=1, Hydrated Lime=2)=1, Percent=20**

Freq: Run

**Correlations**

| | Viscous Difference | Elastic Difference |
|---|---|---|
| Viscous Difference | 1.0000 | 0.5934 |
| Elastic Difference | 0.5934 | 1.0000 |

**Scatterplot Matrix**

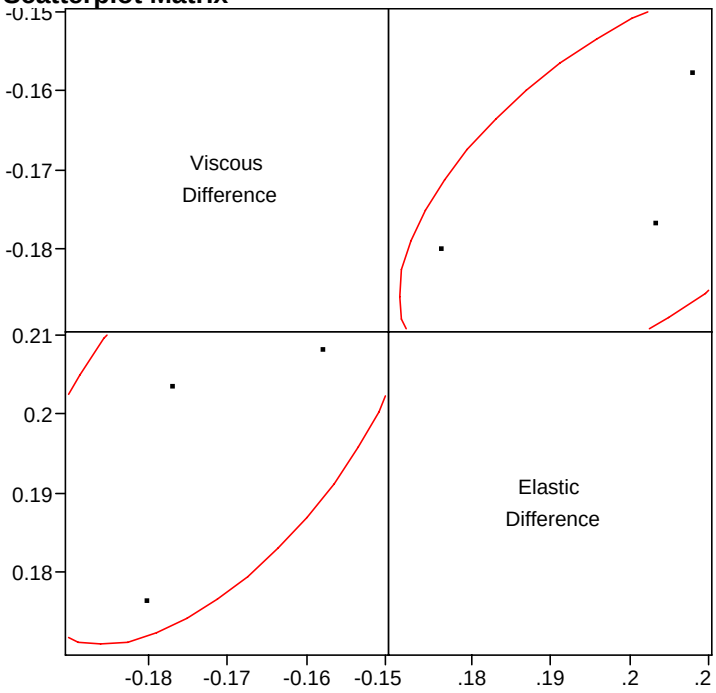


**Multivariate Site=6, Filler (None=0, Silica=1, Hydrated Lime=2)=2, Percent=5**

Freq: Run

**Correlations**

| | Viscous Difference | Elastic Difference |
|---|---|---|
| Viscous Difference | 1.0000 | 0.8897 |
| Elastic Difference | 0.8897 | 1.0000 |

**Scatterplot Matrix**

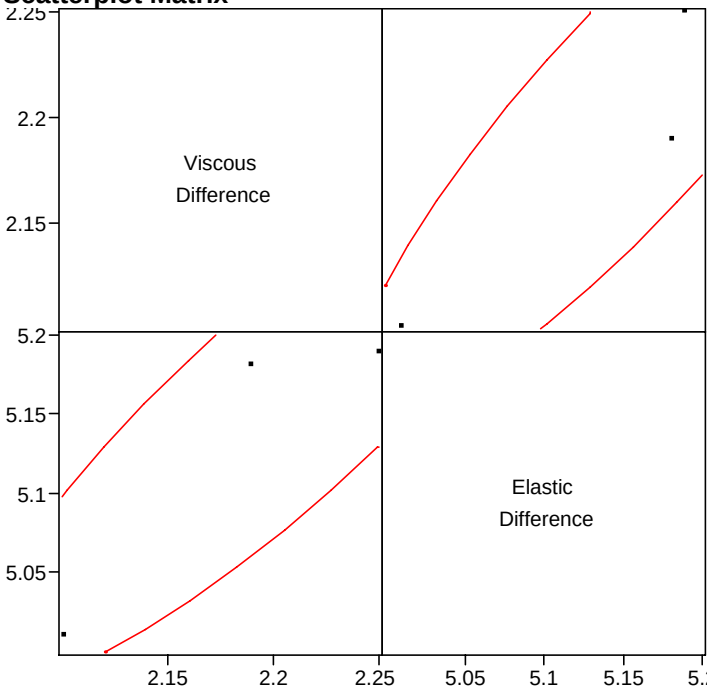


**Multivariate Site=6, Filler (None=0, Silica=1, Hydrated Lime=2)=2, Percent=10**

Freq: Run

**Correlations**

| | Viscous Difference | Elastic Difference |
|---|---|---|
| Viscous Difference | 1.0000 | 0.7389 |
| Elastic Difference | 0.7389 | 1.0000 |

**Scatterplot Matrix**

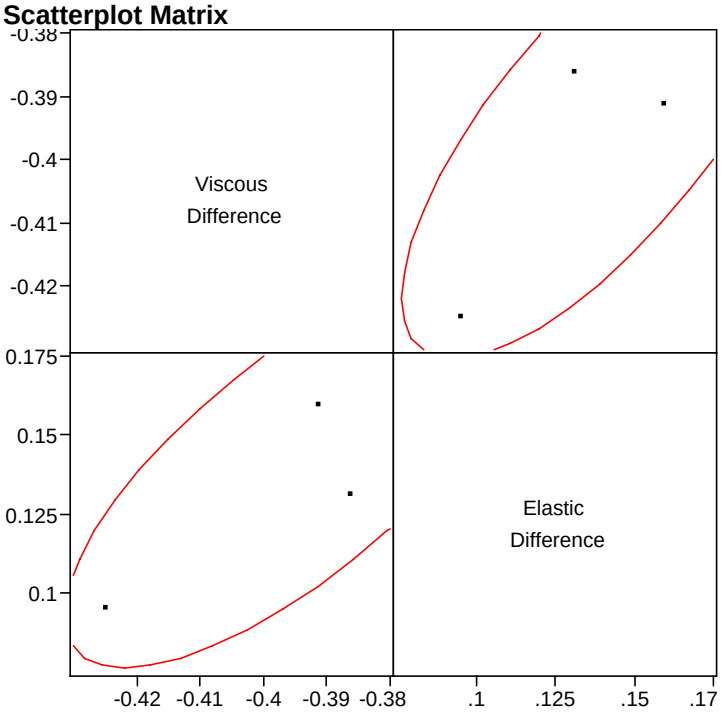


**Multivariate Site=6, Filler (None=0, Silica=1, Hydrated Lime=2)=2, Percent=20**

Freq: Run

**Correlations**

| | Viscous Difference | Elastic Difference |
|---|---|---|
| Viscous Difference | 1.0000 | 0.9579 |
| Elastic Difference | 0.9579 | 1.0000 |

**Scatterplot Matrix**

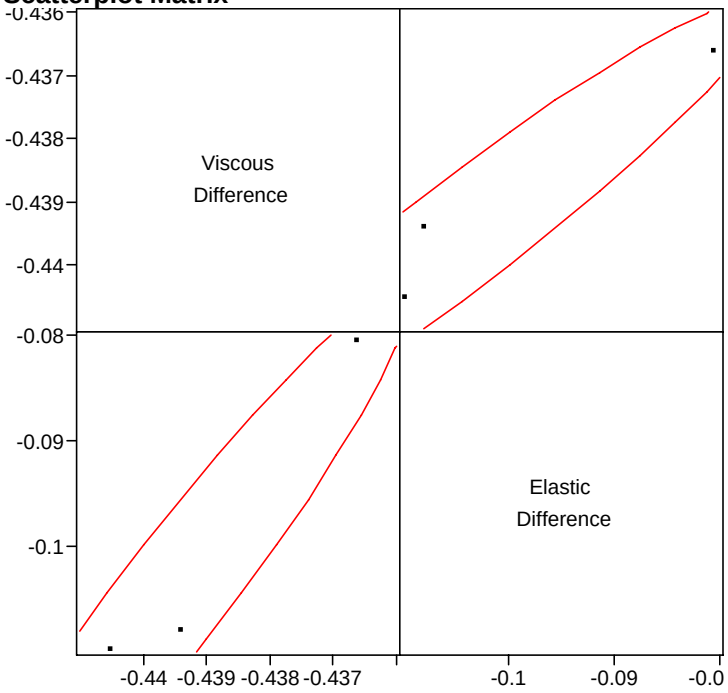


**Multivariate Site=7, Filler (None=0, Silica=1, Hydrated Lime=2)=0, Percent=0**

Freq: Run

**Correlations**

| | Viscous Difference | Elastic Difference |
|---|---|---|
| Viscous Difference | 1.0000 | 0.0437 |
| Elastic Difference | 0.0437 | 1.0000 |

**Scatterplot Matrix**

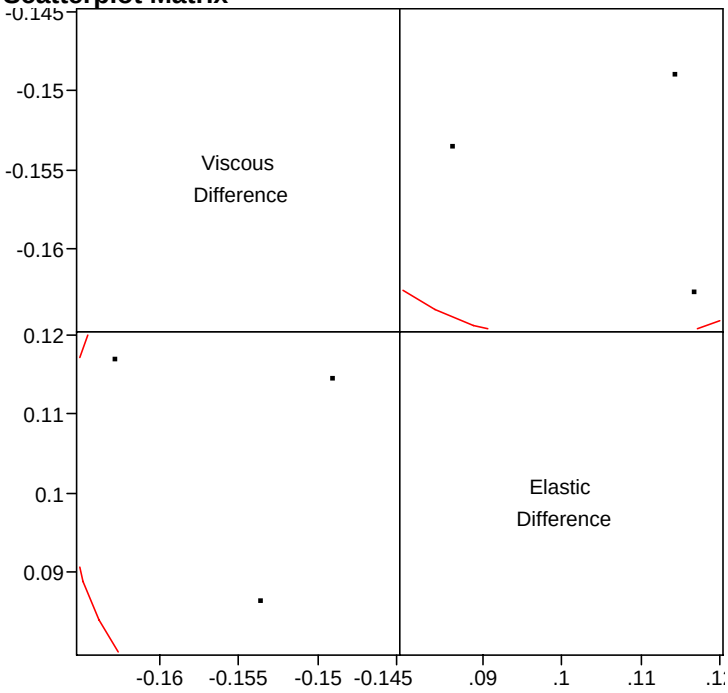


**Multivariate Site=7, Filler (None=0, Silica=1, Hydrated Lime=2)=1, Percent=5**

Freq: Run

**Correlations**

| | Viscous Difference | Elastic Difference |
|---|---|---|
| Viscous Difference | 1.0000 | 1.0000 |
| Elastic Difference | 1.0000 | 1.0000 |

**Scatterplot Matrix**

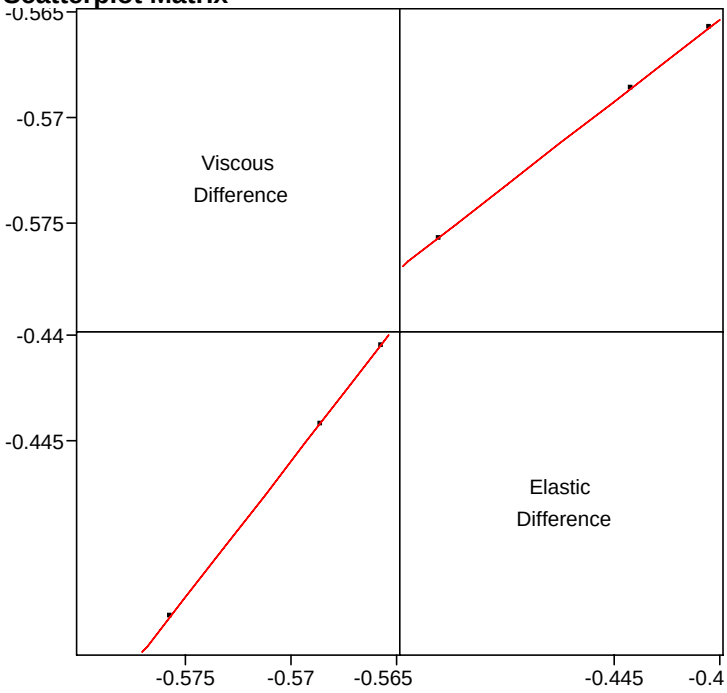


**Multivariate Site=7, Filler (None=0, Silica=1, Hydrated Lime=2)=1, Percent=10**

Freq: Run

**Correlations**

| | Viscous Difference | Elastic Difference |
|---|---|---|
| Viscous Difference | 1.0000 | 0.9955 |
| Elastic Difference | 0.9955 | 1.0000 |

**Scatterplot Matrix**

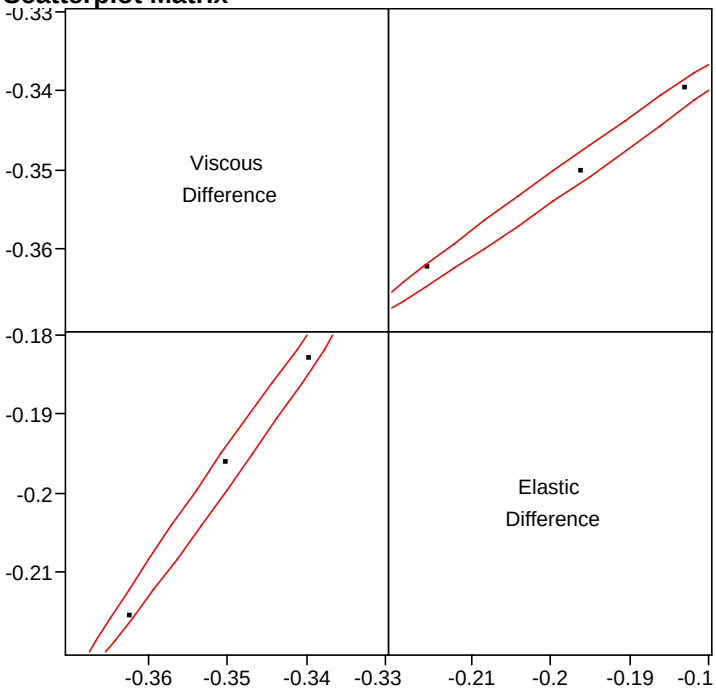


**Multivariate Site=7, Filler (None=0, Silica=1, Hydrated Lime=2)=1, Percent=20**

Freq: Run

**Correlations**

| | Viscous Difference | Elastic Difference |
|---|---|---|
| Viscous Difference | 1.0000 | 1.0000 |
| Elastic Difference | 1.0000 | 1.0000 |

**Scatterplot Matrix**

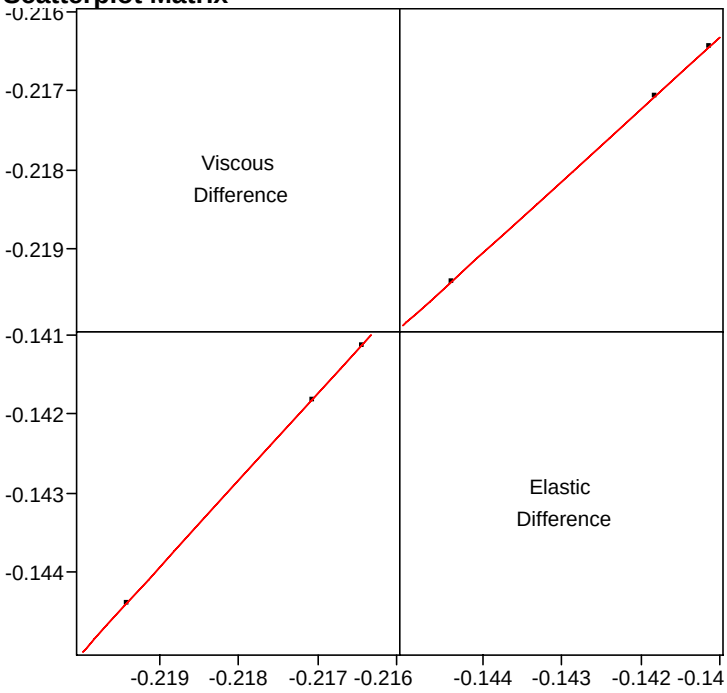


**Multivariate Site=7, Filler (None=0, Silica=1, Hydrated Lime=2)=2, Percent=5**

Freq: Run

**Correlations**

| | Viscous Difference | Elastic Difference |
|---|---|---|
| Viscous Difference | 1.0000 | 0.2461 |
| Elastic Difference | 0.2461 | 1.0000 |

**Scatterplot Matrix**

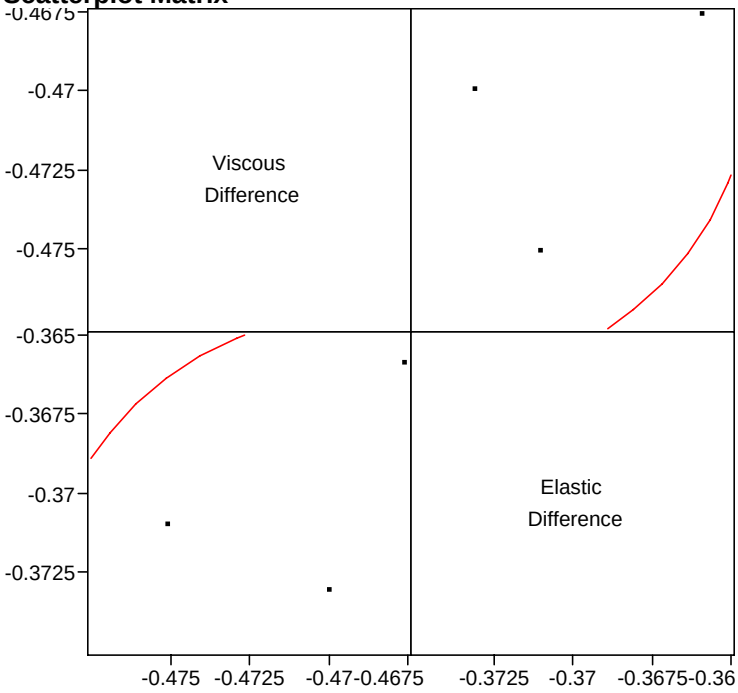


**Multivariate Site=7, Filler (None=0, Silica=1, Hydrated Lime=2)=2, Percent=10**

Freq: Run

**Correlations**

| | Viscous Difference | Elastic Difference |
|---|---|---|
| Viscous Difference | 1.0000 | 0.7321 |
| Elastic Difference | 0.7321 | 1.0000 |

**Scatterplot Matrix**

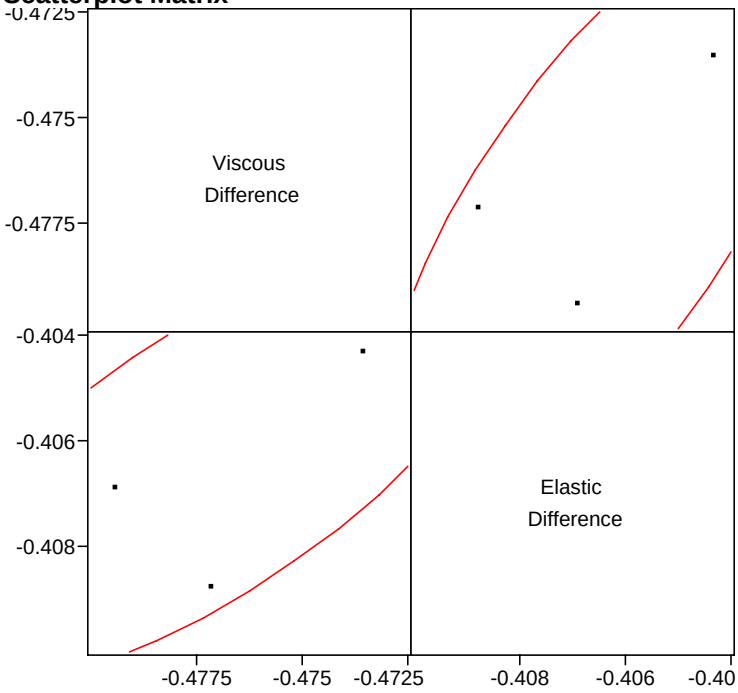


**Multivariate Site=7, Filler (None=0, Silica=1, Hydrated Lime=2)=2, Percent=20**

Freq: Run

**Correlations**

| | Viscous Difference | Elastic Difference |
|---|---|---|
| Viscous Difference | 1.0000 | 0.6169 |
| Elastic Difference | 0.6169 | 1.0000 |

**Scatterplot Matrix**

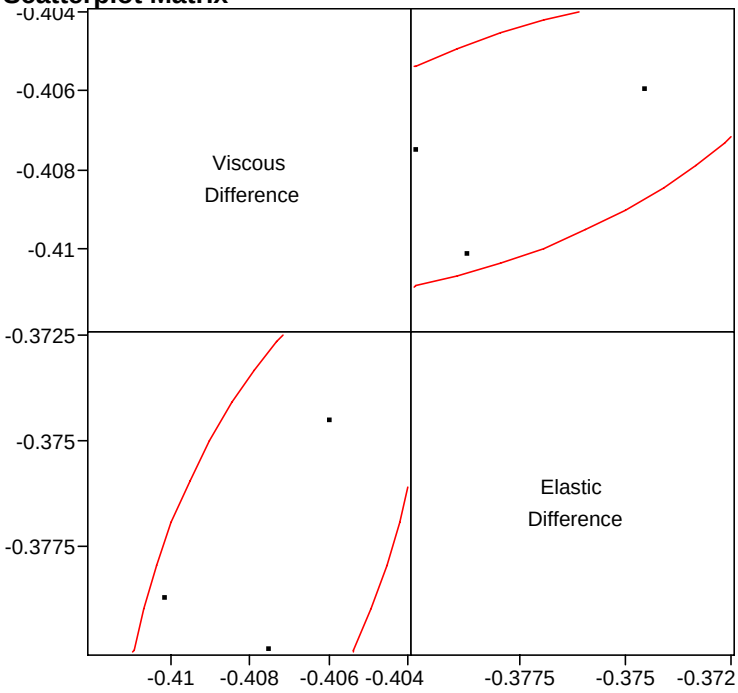


**Multivariate Site=8, Filler (None=0, Silica=1, Hydrated Lime=2)=0, Percent=0**

Freq: Run

**Correlations**

| | Viscous Difference | Elastic Difference |
|---|---|---|
| Viscous Difference | 1.0000 | 1.0000 |
| Elastic Difference | 1.0000 | 1.0000 |

**Scatterplot Matrix**

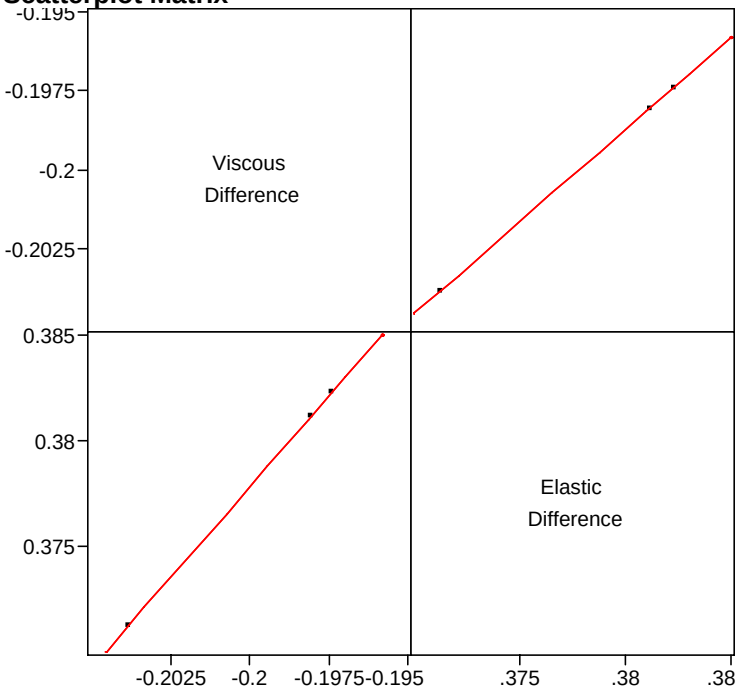


**Multivariate Site=8, Filler (None=0, Silica=1, Hydrated Lime=2)=1, Percent=5**

Freq: Run

**Correlations**

| | Viscous Difference | Elastic Difference |
|---|---|---|
| Viscous Difference | 1.0000 | 0.8152 |
| Elastic Difference | 0.8152 | 1.0000 |

**Scatterplot Matrix**

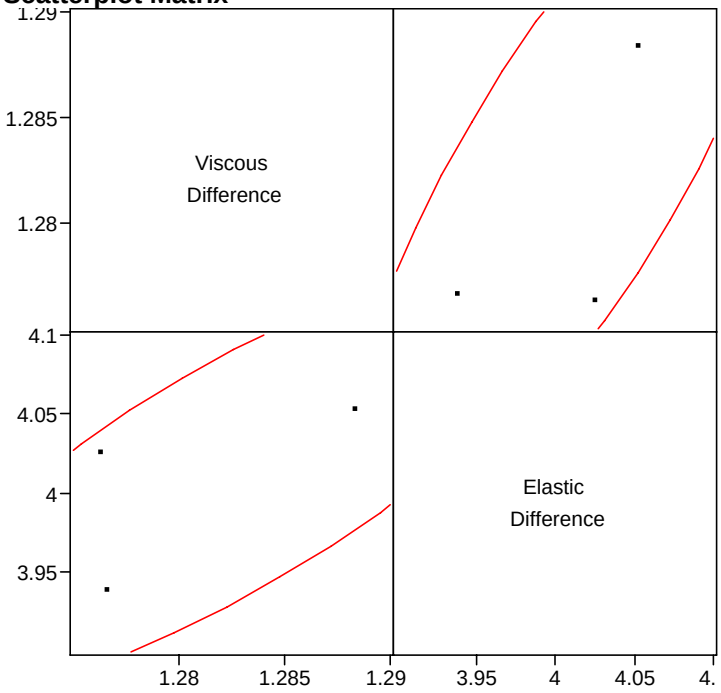


**Multivariate Site=8, Filler (None=0, Silica=1, Hydrated Lime=2)=1, Percent=10**

Freq: Run

**Correlations**

| | Viscous Difference | Elastic Difference |
|---|---|---|
| Viscous Difference | 1.0000 | 0.8813 |
| Elastic Difference | 0.8813 | 1.0000 |

**Scatterplot Matrix**

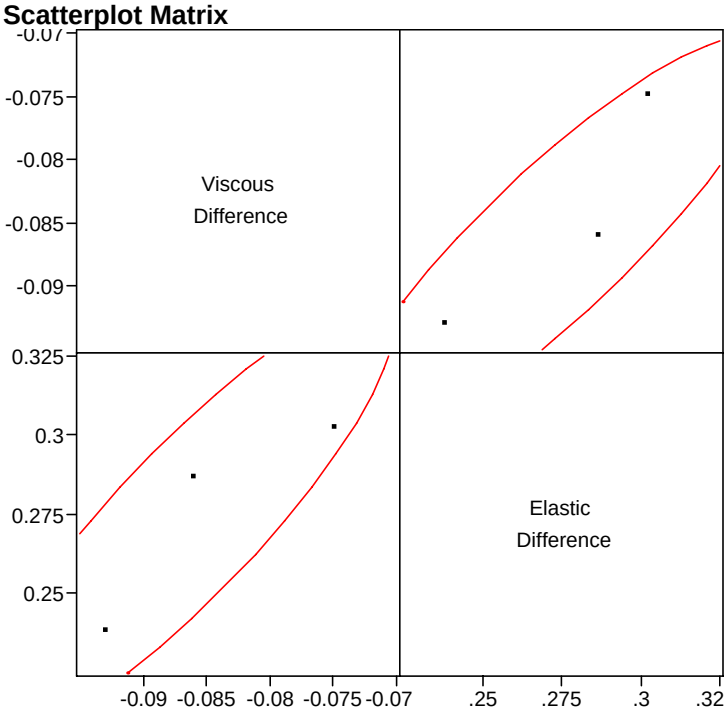


**Multivariate Site=8, Filler (None=0, Silica=1, Hydrated Lime=2)=1, Percent=20**

Freq: Run

**Correlations**

| | Viscous Difference | Elastic Difference |
|---|---|---|
| Viscous Difference | 1.0000 | 0.7893 |
| Elastic Difference | 0.7893 | 1.0000 |

**Scatterplot Matrix**

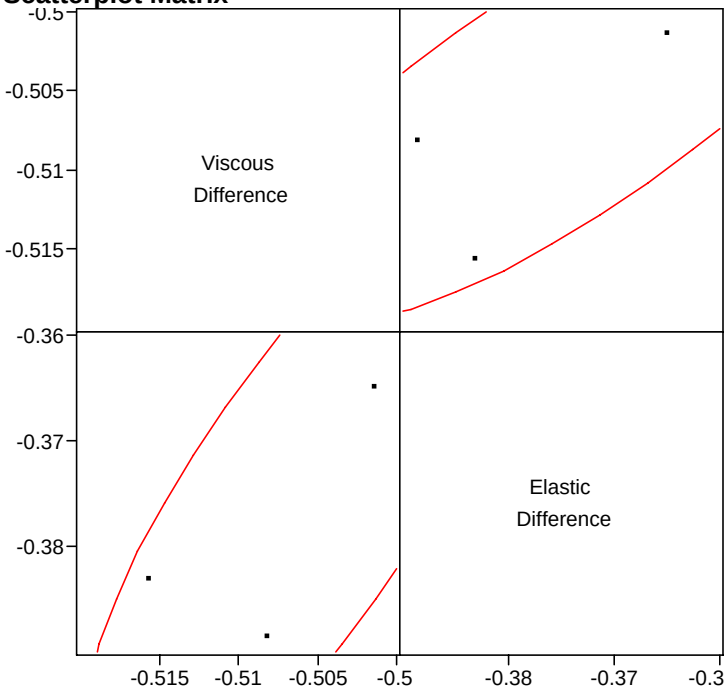


**Multivariate Site=8, Filler (None=0, Silica=1, Hydrated Lime=2)=2, Percent=5**

Freq: Run

**Correlations**

| | Viscous Difference | Elastic Difference |
|---|---|---|
| Viscous Difference | 1.0000 | 0.0750 |
| Elastic Difference | 0.0750 | 1.0000 |

**Scatterplot Matrix**

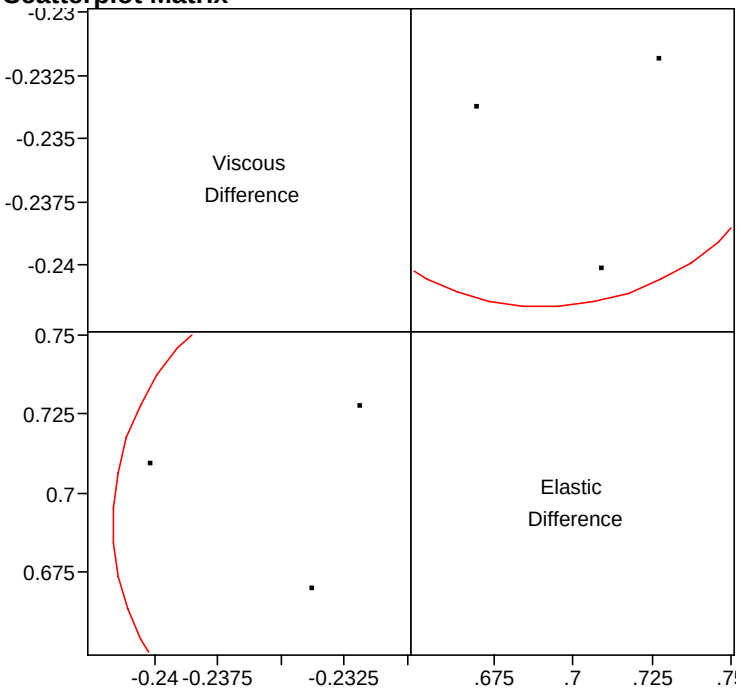


**Multivariate Site=8, Filler (None=0, Silica=1, Hydrated Lime=2)=2, Percent=10**

Freq: Run

**Correlations**

| | Viscous Difference | Elastic Difference |
|---|---|---|
| Viscous Difference | 1.0000 | 1.0000 |
| Elastic Difference | 1.0000 | 1.0000 |

**Scatterplot Matrix**

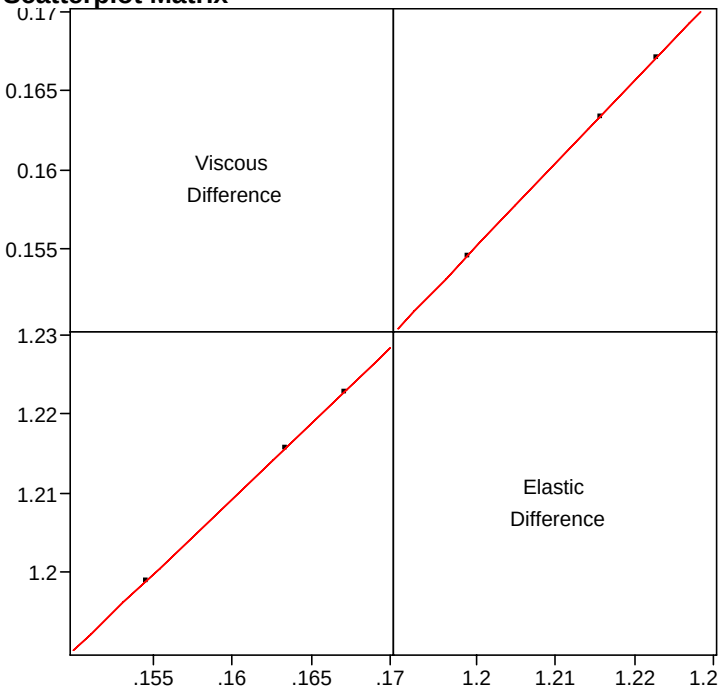


**Multivariate Site=8, Filler (None=0, Silica=1, Hydrated Lime=2)=2, Percent=20**

Freq: Run

**Correlations**

| | Viscous Difference | Elastic Difference |
|---|---|---|
| Viscous Difference | 1.0000 | -0.9609 |
| Elastic Difference | -0.9609 | 1.0000 |

**Scatterplot Matrix**

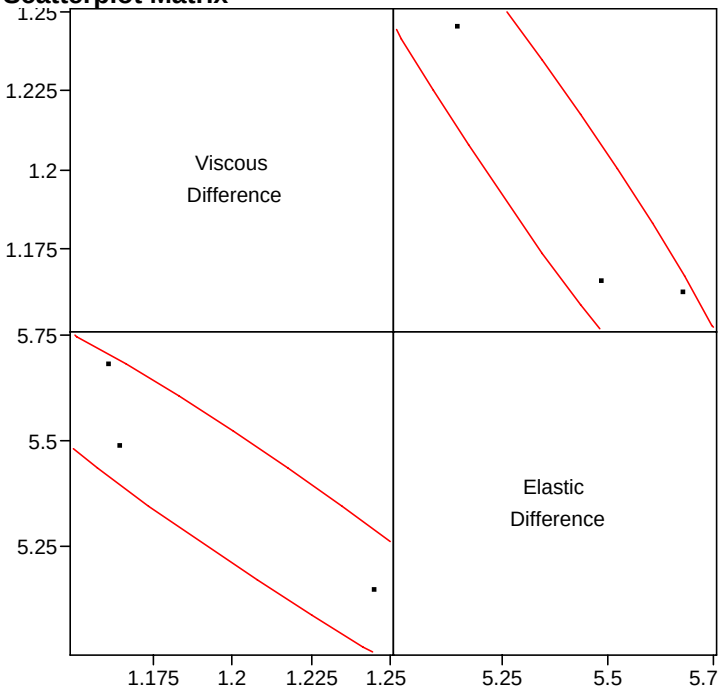


**Multivariate Site=9, Filler (None=0, Silica=1, Hydrated Lime=2)=0, Percent=0**

Freq: Run

**Correlations**

| | Viscous Difference | Elastic Difference |
|---|---|---|
| Viscous Difference | 1.0000 | -0.2424 |
| Elastic Difference | -0.2424 | 1.0000 |

**Scatterplot Matrix**

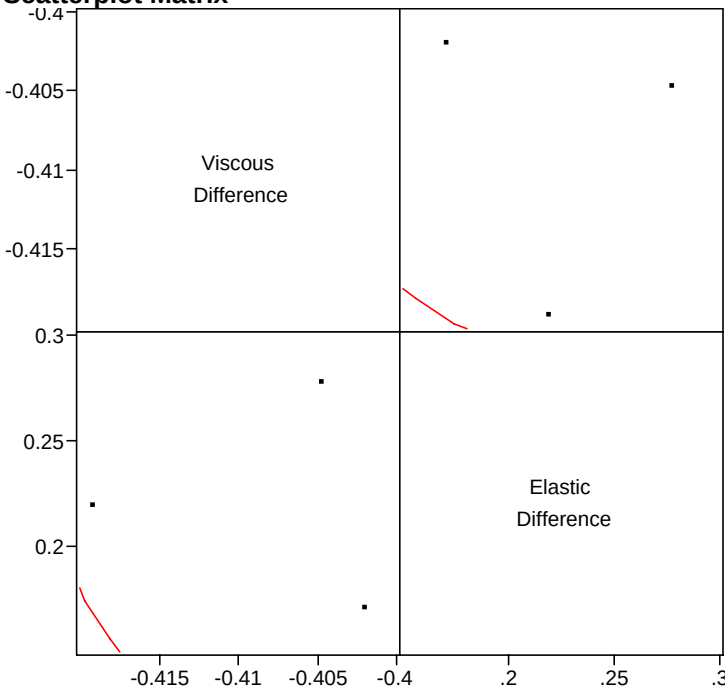


**Multivariate Site=9, Filler (None=0, Silica=1, Hydrated Lime=2)=1, Percent=5**

Freq: Run

**Correlations**

| | Viscous Difference | Elastic Difference |
|---|---|---|
| Viscous Difference | 1.0000 | 0.8678 |
| Elastic Difference | 0.8678 | 1.0000 |

**Scatterplot Matrix**

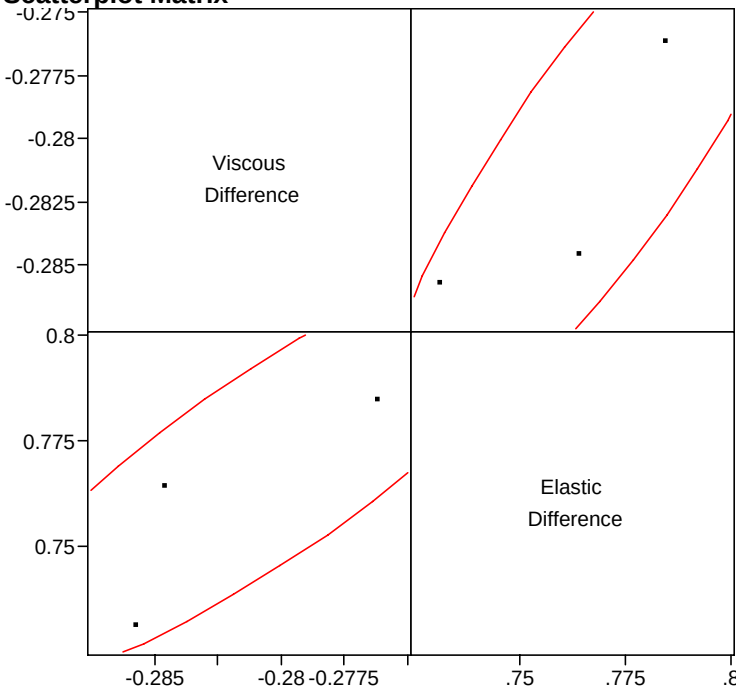


**Multivariate Site=9, Filler (None=0, Silica=1, Hydrated Lime=2)=1, Percent=10**

Freq: Run

**Correlations**

| | Viscous Difference | Elastic Difference |
|---|---|---|
| Viscous Difference | 1.0000 | 0.7081 |
| Elastic Difference | 0.7081 | 1.0000 |

**Scatterplot Matrix**

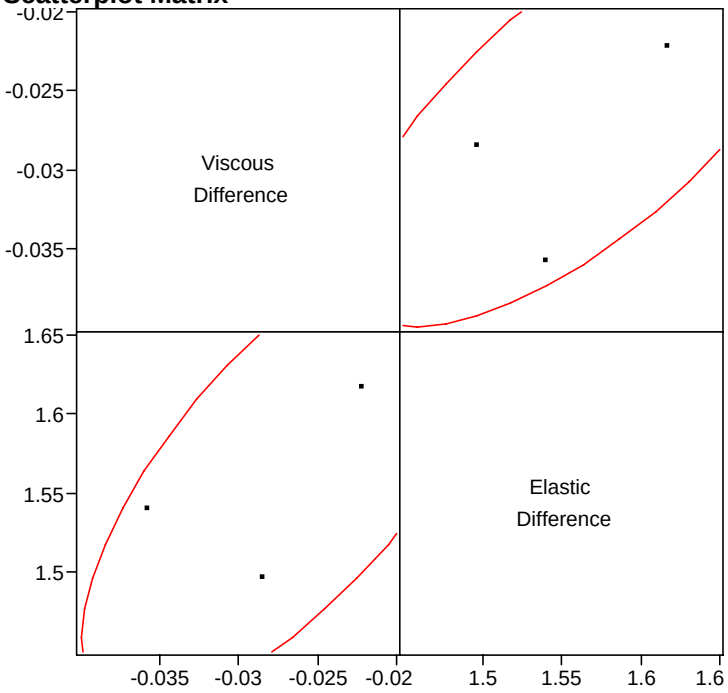


**Multivariate Site=9, Filler (None=0, Silica=1, Hydrated Lime=2)=1, Percent=20**

Freq: Run

**Correlations**

| | Viscous Difference | Elastic Difference |
|---|---|---|
| Viscous Difference | 1.0000 | 0.2385 |
| Elastic Difference | 0.2385 | 1.0000 |

**Scatterplot Matrix**

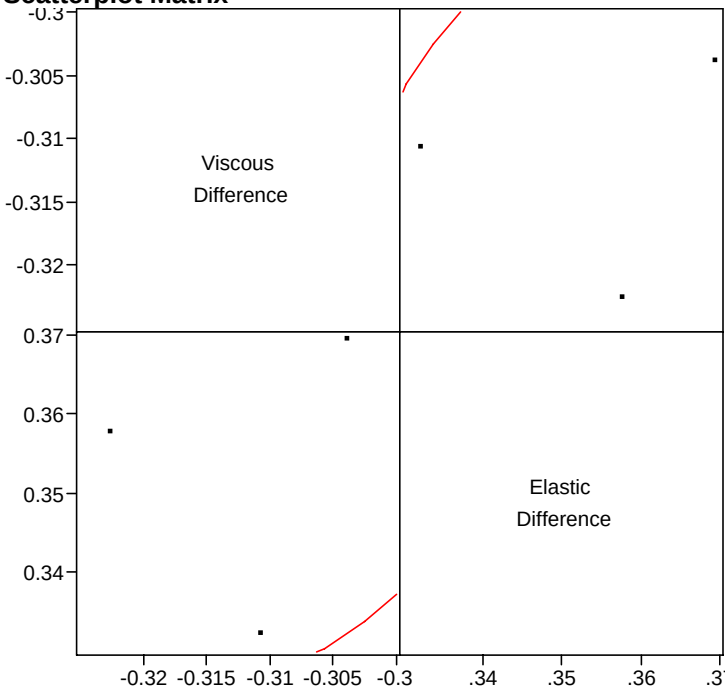


**Multivariate Site=9, Filler (None=0, Silica=1, Hydrated Lime=2)=2, Percent=5**

Freq: Run

**Correlations**

| | Viscous Difference | Elastic Difference |
|---|---|---|
| Viscous Difference | 1.0000 | -0.9914 |
| Elastic Difference | -0.9914 | 1.0000 |

**Scatterplot Matrix**

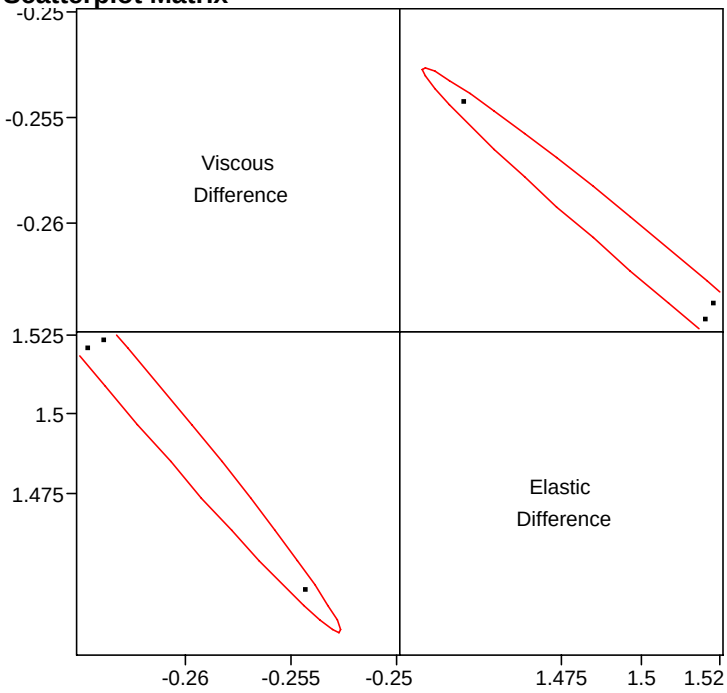


**Multivariate Site=9, Filler (None=0, Silica=1, Hydrated Lime=2)=2, Percent=10**

Freq: Run

**Correlations**

| | Viscous Difference | Elastic Difference |
|---|---|---|
| Viscous Difference | 1.0000 | 0.9883 |
| Elastic Difference | 0.9883 | 1.0000 |

**Scatterplot Matrix**

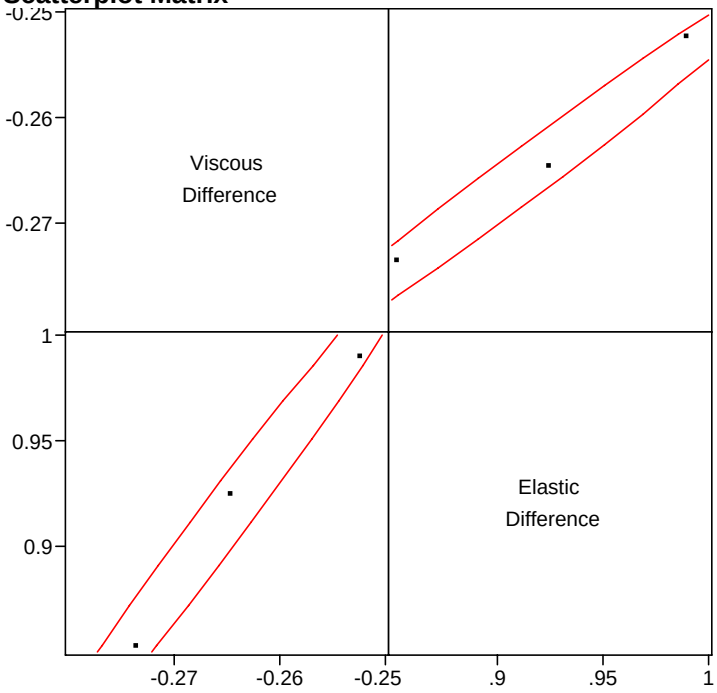


**Multivariate Site=9, Filler (None=0, Silica=1, Hydrated Lime=2)=2, Percent=20**

Freq: Run

**Correlations**

| | Viscous Difference | Elastic Difference |
|---|---|---|
| Viscous Difference | 1.0000 | -0.9991 |
| Elastic Difference | -0.9991 | 1.0000 |

**Scatterplot Matrix**

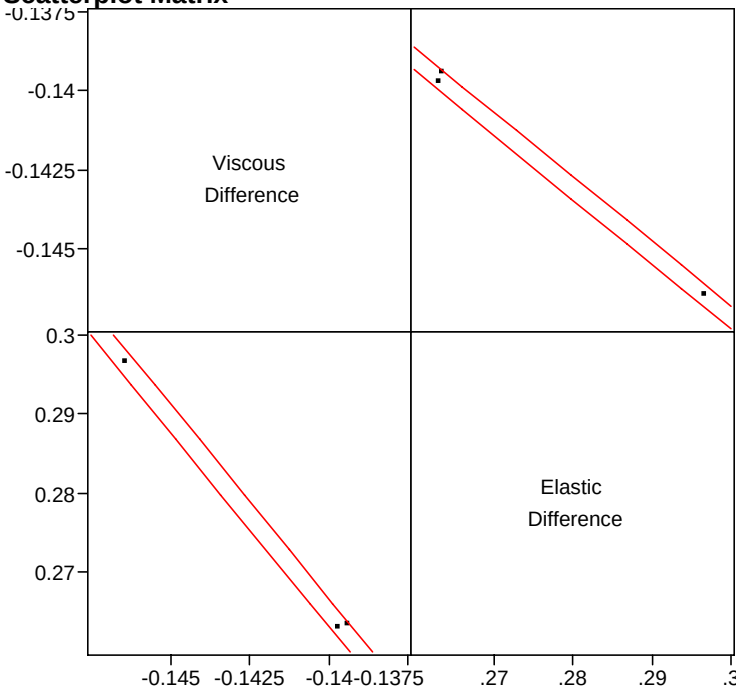


**Multivariate Site=10, Filler (None=0, Silica=1, Hydrated Lime=2)=0, Percent=0**

Freq: Run

**Correlations**

| | Viscous Difference | Elastic Difference |
|---|---|---|
| Viscous Difference | 1.0000 | 0.6500 |
| Elastic Difference | 0.6500 | 1.0000 |

**Scatterplot Matrix**

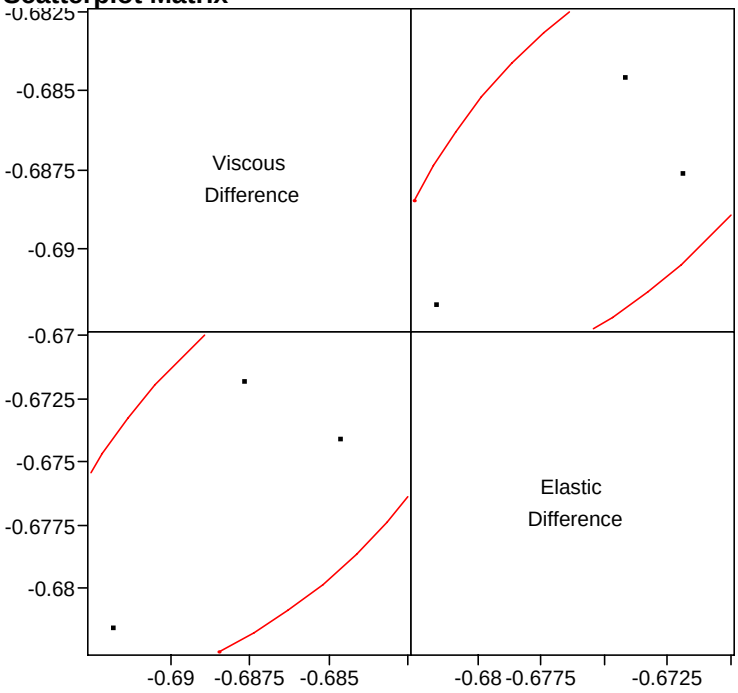


**Multivariate Site=10, Filler (None=0, Silica=1, Hydrated Lime=2)=1, Percent=5**

Freq: Run

**Correlations**

| | Viscous Difference | Elastic Difference |
|---|---|---|
| Viscous Difference | 1.0000 | 0.3685 |
| Elastic Difference | 0.3685 | 1.0000 |

**Scatterplot Matrix**

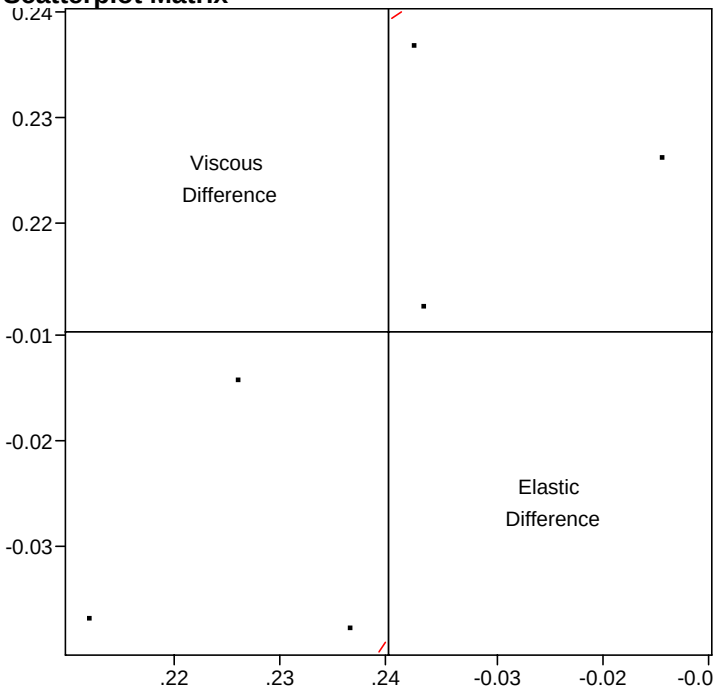


**Multivariate Site=10, Filler (None=0, Silica=1, Hydrated Lime=2)=1, Percent=10**

Freq: Run

**Correlations**

| | Viscous Difference | Elastic Difference |
|---|---|---|
| Viscous Difference | 1.0000 | 0.9769 |
| Elastic Difference | 0.9769 | 1.0000 |

**Scatterplot Matrix**

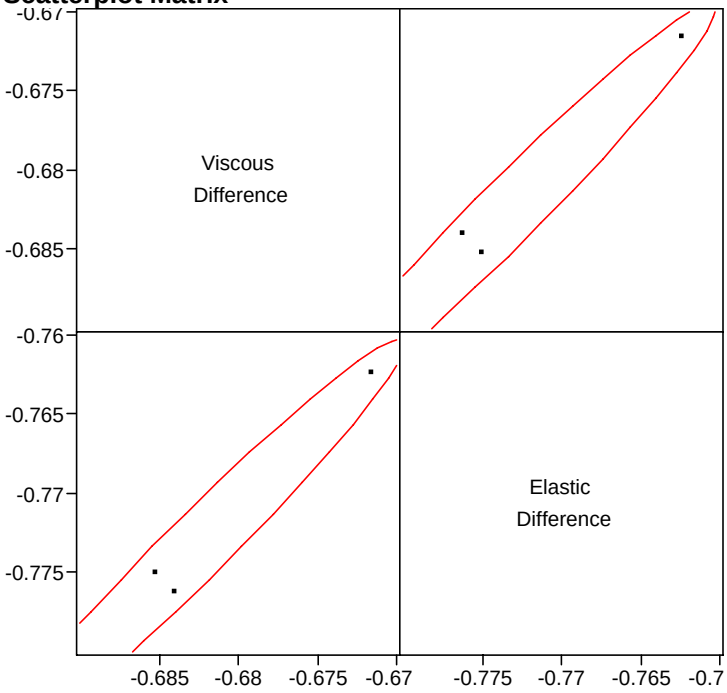


**Multivariate Site=10, Filler (None=0, Silica=1, Hydrated Lime=2)=1, Percent=20**

Freq: Run

**Correlations**

| | Viscous Difference | Elastic Difference |
|---|---|---|
| Viscous Difference | 1.0000 | -0.7703 |
| Elastic Difference | -0.7703 | 1.0000 |

**Scatterplot Matrix**

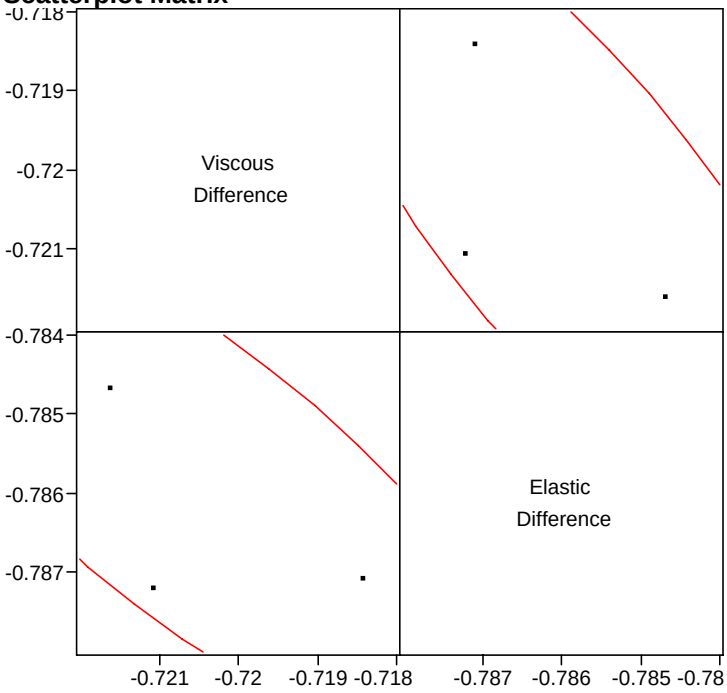


**Multivariate Site=10, Filler (None=0, Silica=1, Hydrated Lime=2)=2, Percent=5**

Freq: Run

**Correlations**

| | Viscous Difference | Elastic Difference |
|---|---|---|
| Viscous Difference | 1.0000 | 1.0000 |
| Elastic Difference | 1.0000 | 1.0000 |

**Scatterplot Matrix**

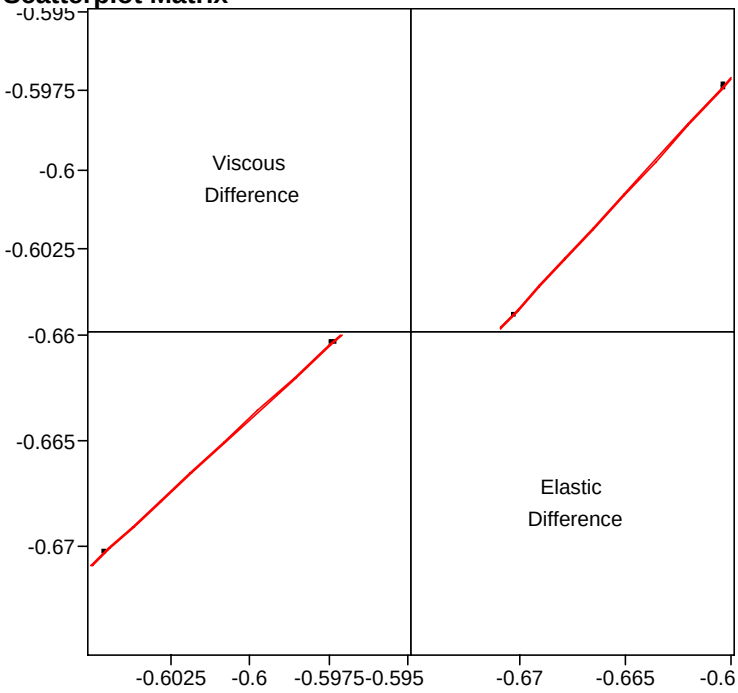


**Multivariate Site=10, Filler (None=0, Silica=1, Hydrated Lime=2)=2, Percent=10**

Freq: Run

**Correlations**

| | Viscous Difference | Elastic Difference |
|---|---|---|
| Viscous Difference | 1.0000 | 0.9999 |
| Elastic Difference | 0.9999 | 1.0000 |

**Scatterplot Matrix**

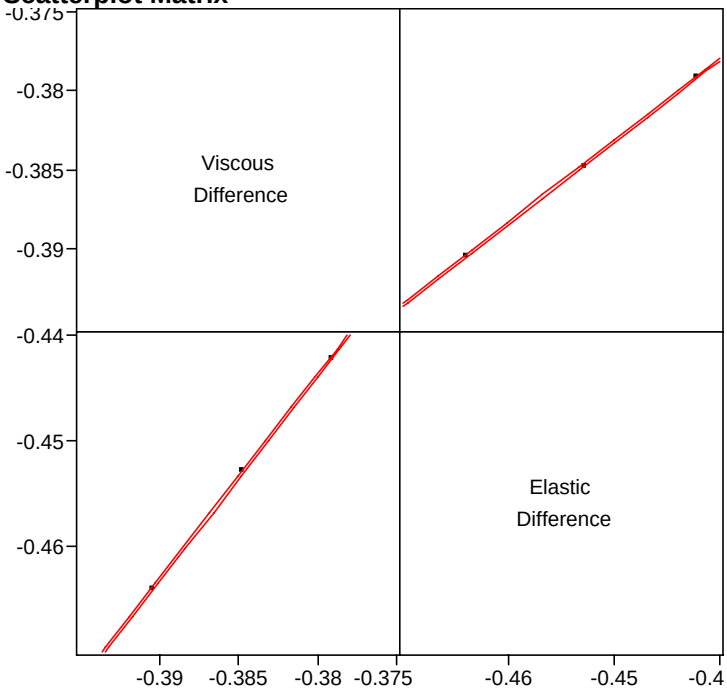


**Multivariate Site=10, Filler (None=0, Silica=1, Hydrated Lime=2)=2, Percent=20**

Freq: Run

**Correlations**

| | Viscous Difference | Elastic Difference |
|---|---|---|
| Viscous Difference | 1.0000 | 0.9986 |
| Elastic Difference | 0.9986 | 1.0000 |

**Scatterplot Matrix**

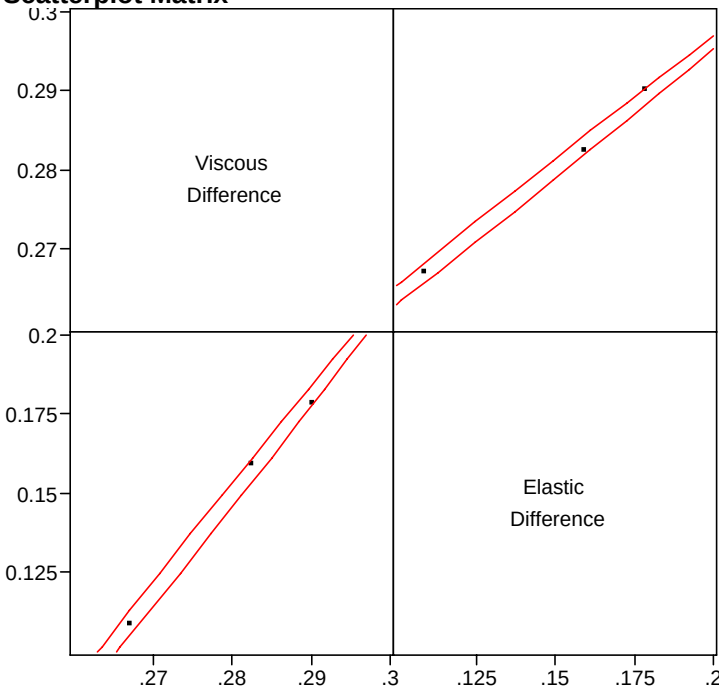


**Multivariate Site=11, Filler (None=0, Silica=1, Hydrated Lime=2)=0, Percent=0**

Freq: Run

**Correlations**

| | Viscous Difference | Elastic Difference |
|---|---|---|
| Viscous Difference | 1.0000 | 0.7935 |
| Elastic Difference | 0.7935 | 1.0000 |

**Scatterplot Matrix**

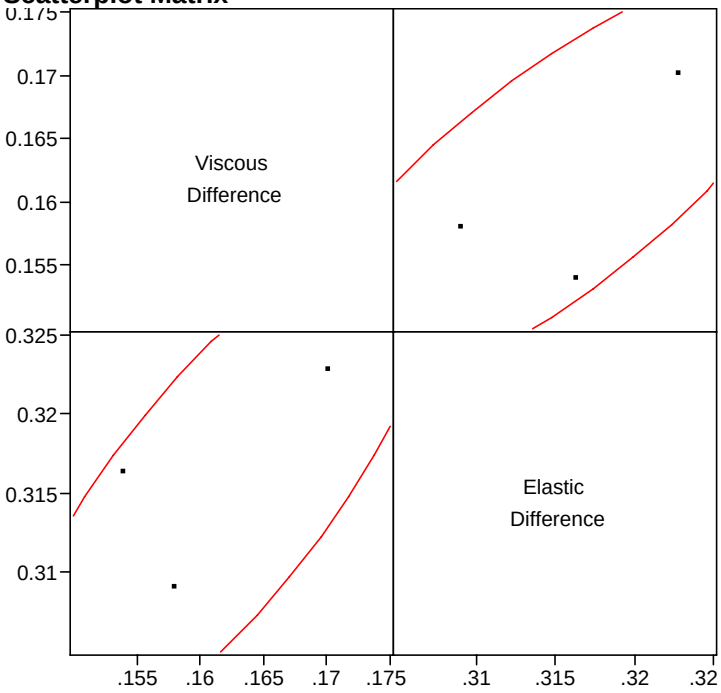


**Multivariate Site=11, Filler (None=0, Silica=1, Hydrated Lime=2)=1, Percent=5**

Freq: Run

**Correlations**

| | Viscous Difference | Elastic Difference |
|---|---|---|
| Viscous Difference | 1.0000 | 0.9998 |
| Elastic Difference | 0.9998 | 1.0000 |

**Scatterplot Matrix**

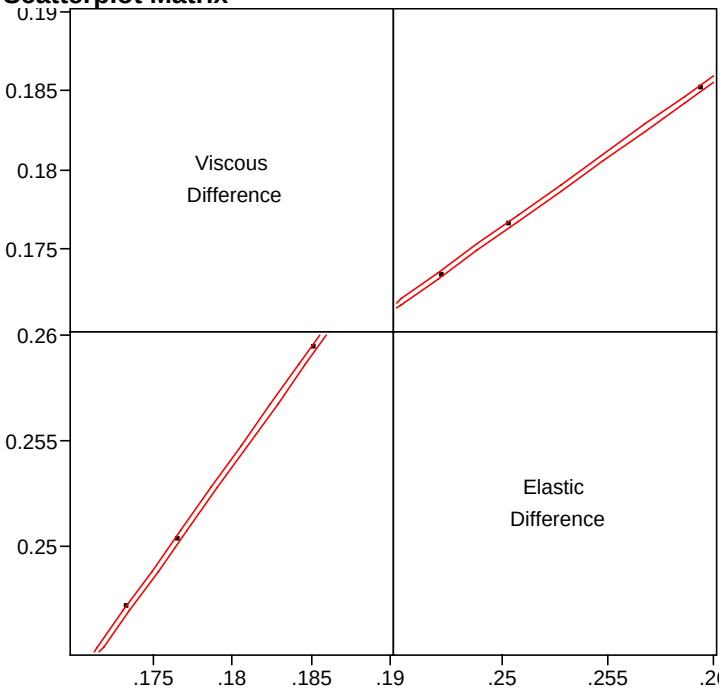


**Multivariate Site=11, Filler (None=0, Silica=1, Hydrated Lime=2)=1, Percent=10**

Freq: Run

**Correlations**

| | Viscous Difference | Elastic Difference |
|---|---|---|
| Viscous Difference | 1.0000 | 1.0000 |
| Elastic Difference | 1.0000 | 1.0000 |

**Scatterplot Matrix**

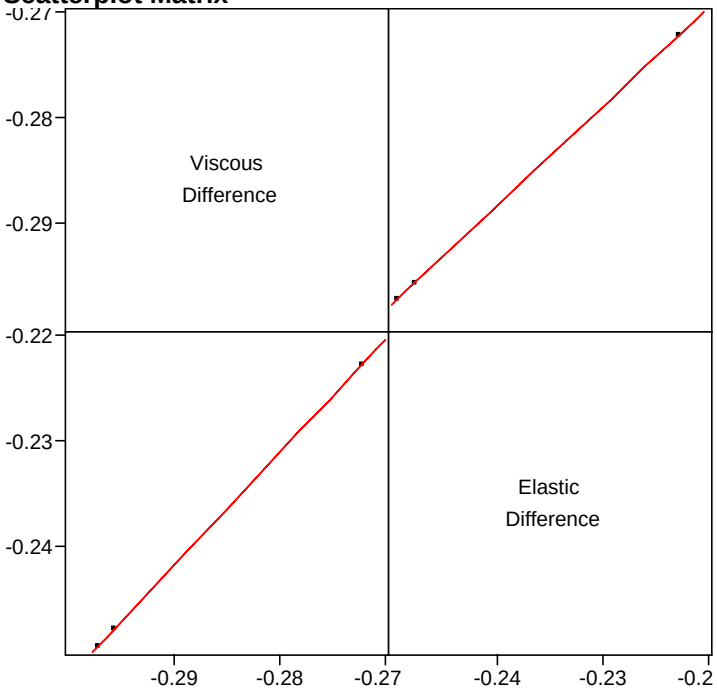


**Multivariate Site=11, Filler (None=0, Silica=1, Hydrated Lime=2)=1, Percent=20**

Freq: Run

**Correlations**

| | Viscous Difference | Elastic Difference |
|---|---|---|
| Viscous Difference | 1.0000 | 0.9305 |
| Elastic Difference | 0.9305 | 1.0000 |

**Scatterplot Matrix**

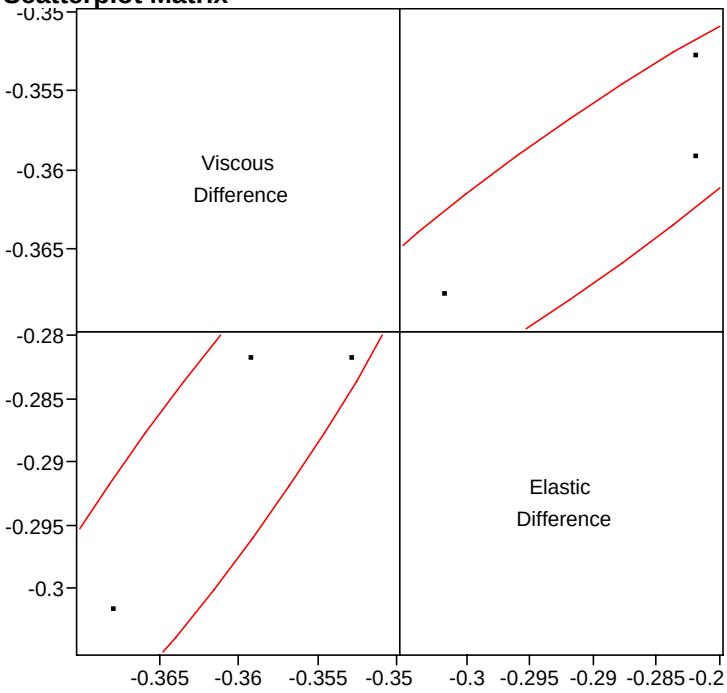


**Multivariate Site=11, Filler (None=0, Silica=1, Hydrated Lime=2)=2, Percent=5**

Freq: Run

**Correlations**

| | Viscous Difference | Elastic Difference |
|---|---|---|
| Viscous Difference | 1.0000 | 0.9248 |
| Elastic Difference | 0.9248 | 1.0000 |

**Scatterplot Matrix**

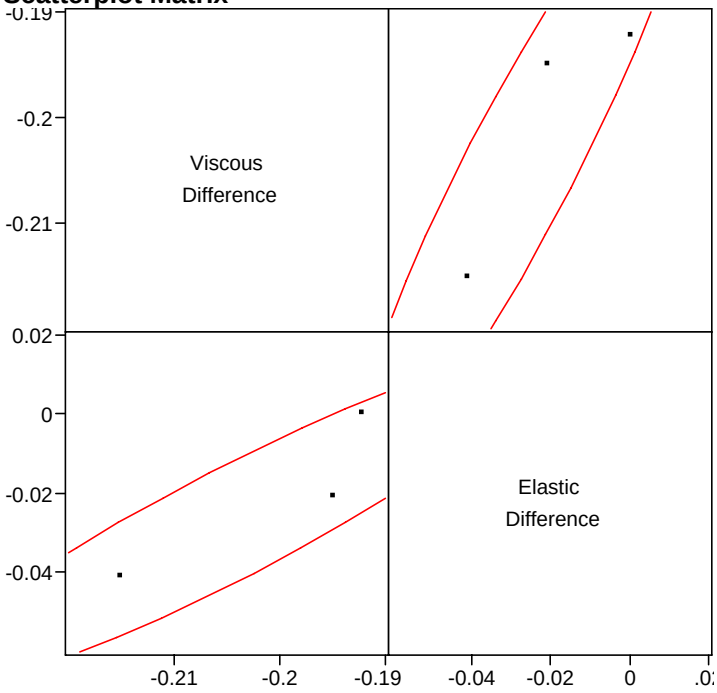


**Multivariate Site=11, Filler (None=0, Silica=1, Hydrated Lime=2)=2, Percent=10**

Freq: Run

**Correlations**

| | Viscous Difference | Elastic Difference |
|---|---|---|
| Viscous Difference | 1.0000 | 0.9645 |
| Elastic Difference | 0.9645 | 1.0000 |

**Scatterplot Matrix**

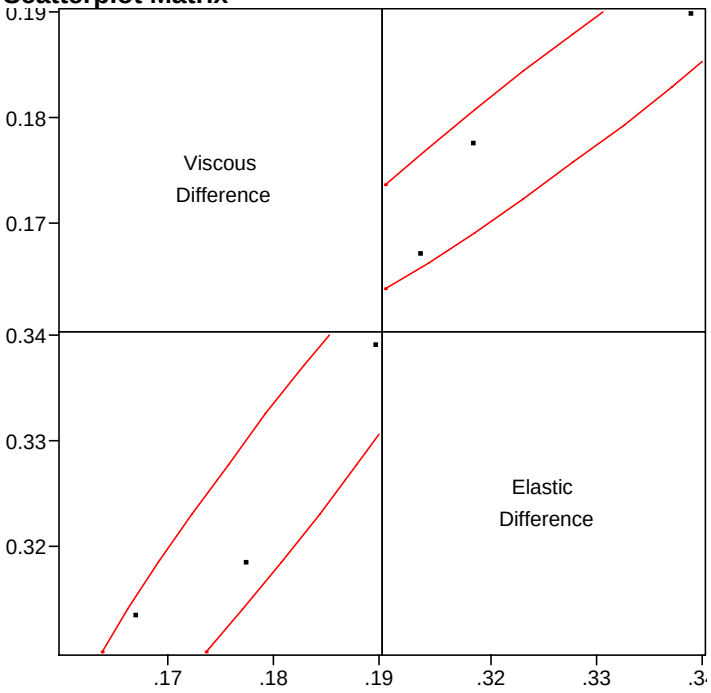


**Multivariate Site=11, Filler (None=0, Silica=1, Hydrated Lime=2)=2, Percent=20**

Freq: Run

**Correlations**

| | Viscous Difference | Elastic Difference |
|---|---|---|
| Viscous Difference | 1.0000 | 0.9395 |
| Elastic Difference | 0.9395 | 1.0000 |

**Scatterplot Matrix**

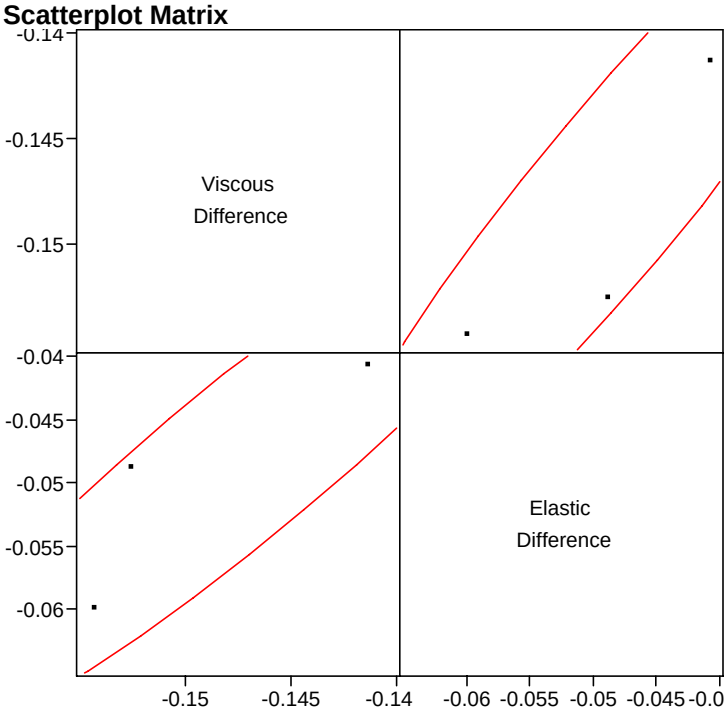


**Multivariate Site=12, Filler (None=0, Silica=1, Hydrated Lime=2)=0, Percent=0**

Freq: Run

**Correlations**

| | Viscous Difference | Elastic Difference |
|---|---|---|
| Viscous Difference | 1.0000 | 1.0000 |
| Elastic Difference | 1.0000 | 1.0000 |

**Scatterplot Matrix**

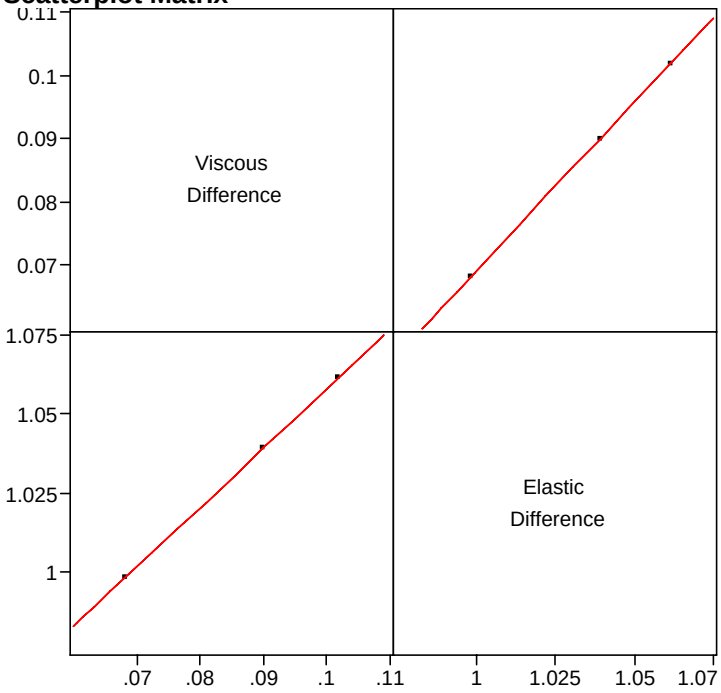


**Multivariate Site=12, Filler (None=0, Silica=1, Hydrated Lime=2)=1, Percent=5**

Freq: Run

**Correlations**

| | Viscous Difference | Elastic Difference |
|---|---|---|
| Viscous Difference | 1.0000 | -0.1250 |
| Elastic Difference | -0.1250 | 1.0000 |

**Scatterplot Matrix**

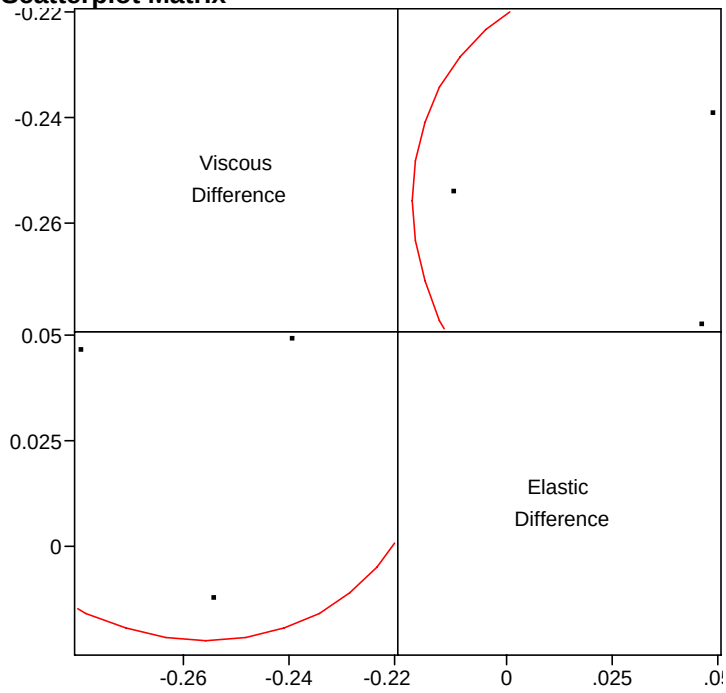


**Multivariate Site=12, Filler (None=0, Silica=1, Hydrated Lime=2)=1, Percent=10**

Freq: Run

**Correlations**

| | Viscous Difference | Elastic Difference |
|---|---|---|
| Viscous Difference | 1.0000 | 0.5737 |
| Elastic Difference | 0.5737 | 1.0000 |

**Scatterplot Matrix**

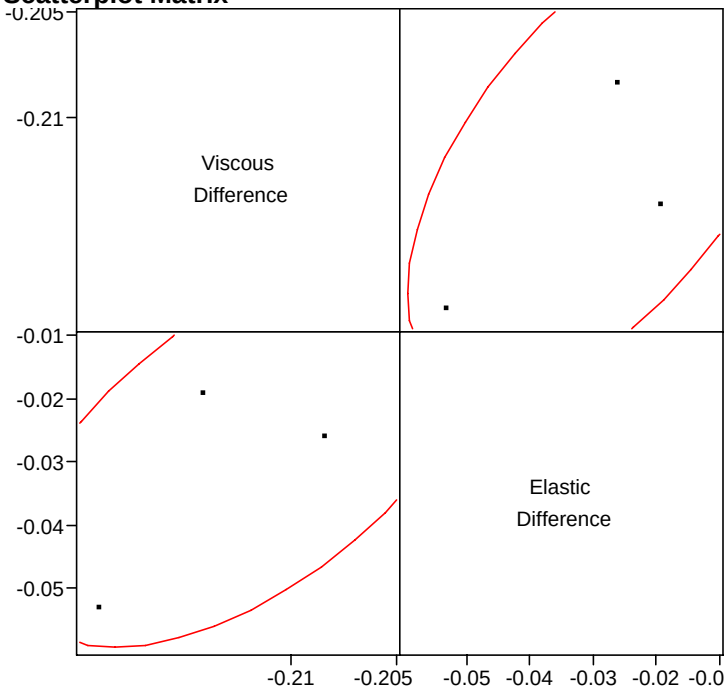


**Multivariate Site=12, Filler (None=0, Silica=1, Hydrated Lime=2)=1, Percent=20**

Freq: Run

**Correlations**

| | Viscous Difference | Elastic Difference |
|---|---|---|
| Viscous Difference | 1.0000 | 0.7693 |
| Elastic Difference | 0.7693 | 1.0000 |

**Scatterplot Matrix**

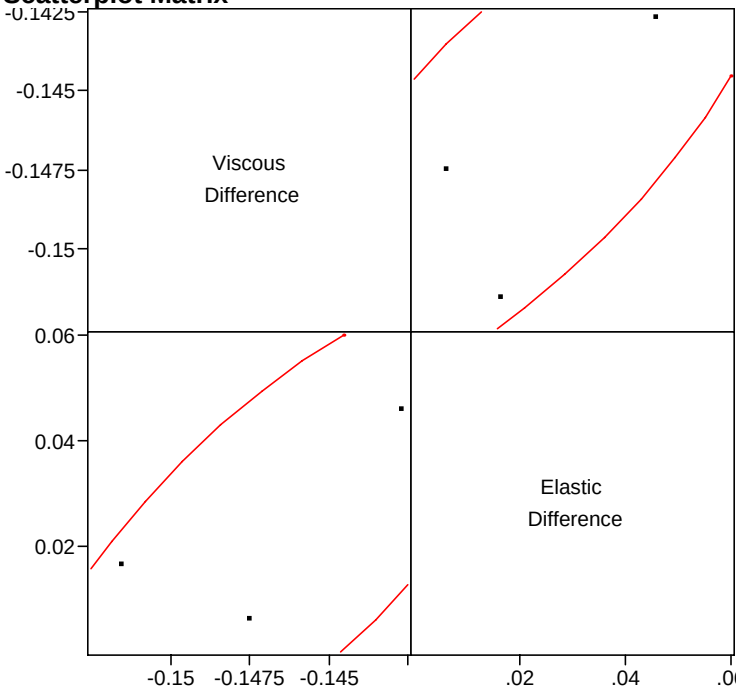


**Multivariate Site=12, Filler (None=0, Silica=1, Hydrated Lime=2)=2, Percent=5**

Freq: Run

**Correlations**

| | Viscous Difference | Elastic Difference |
|---|---|---|
| Viscous Difference | 1.0000 | -0.1138 |
| Elastic Difference | -0.1138 | 1.0000 |

**Scatterplot Matrix**

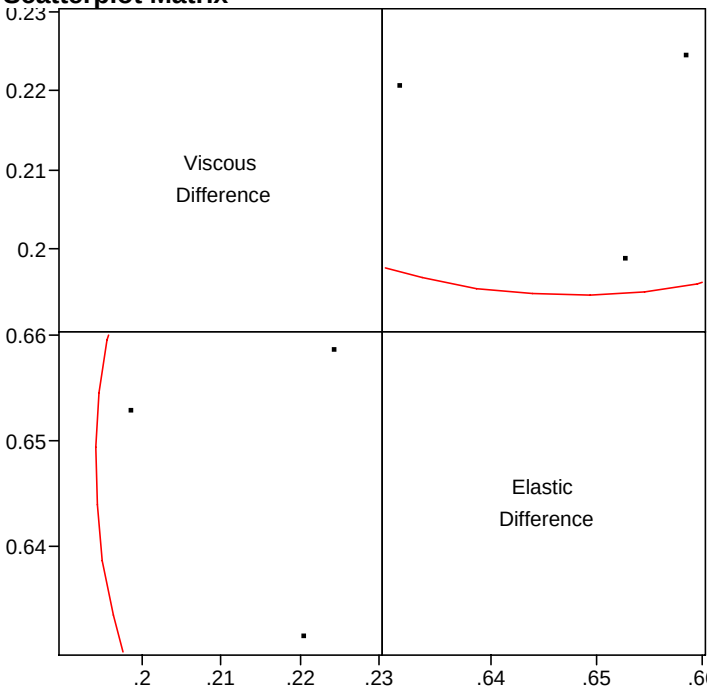


**Multivariate Site=12, Filler (None=0, Silica=1, Hydrated Lime=2)=2, Percent=10**

Freq: Run

**Correlations**

| | Viscous Difference | Elastic Difference |
|---|---|---|
| Viscous Difference | 1.0000 | 1.0000 |
| Elastic Difference | 1.0000 | 1.0000 |

**Scatterplot Matrix**

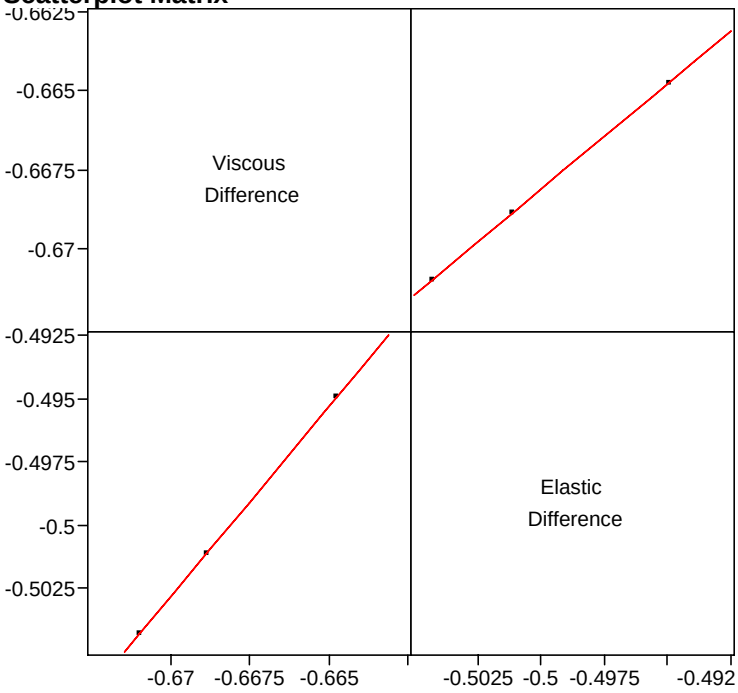


**Multivariate Site=12, Filler (None=0, Silica=1, Hydrated Lime=2)=2, Percent=20**

Freq: Run

**Correlations**

| | Viscous Difference | Elastic Difference |
|---|---|---|
| Viscous Difference | 1.0000 | 0.7860 |
| Elastic Difference | 0.7860 | 1.0000 |

**Scatterplot Matrix**

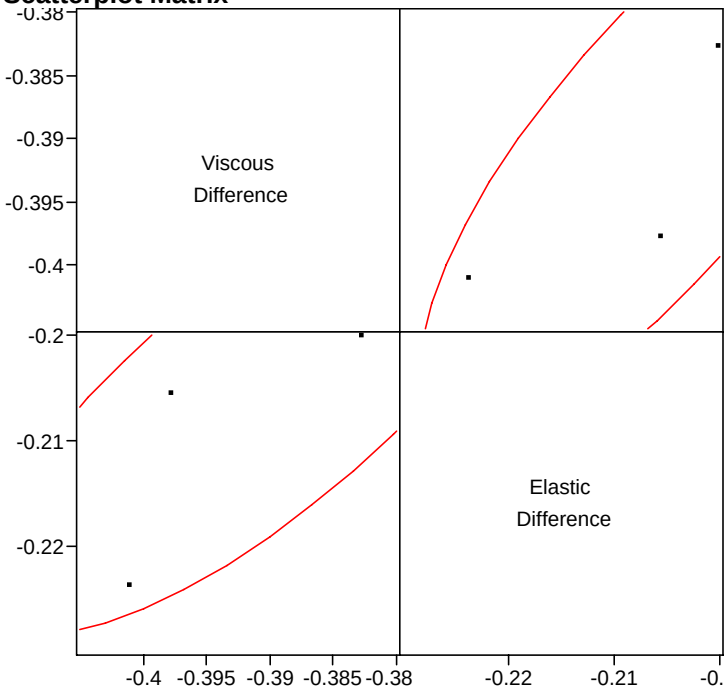


**Multivariate Site=13, Filler (None=0, Silica=1, Hydrated Lime=2)=0, Percent=0**

Freq: Run

**Correlations**

| | Viscous Difference | Elastic Difference |
|---|---|---|
| Viscous Difference | 1.0000 | 0.5286 |
| Elastic Difference | 0.5286 | 1.0000 |

**Scatterplot Matrix**

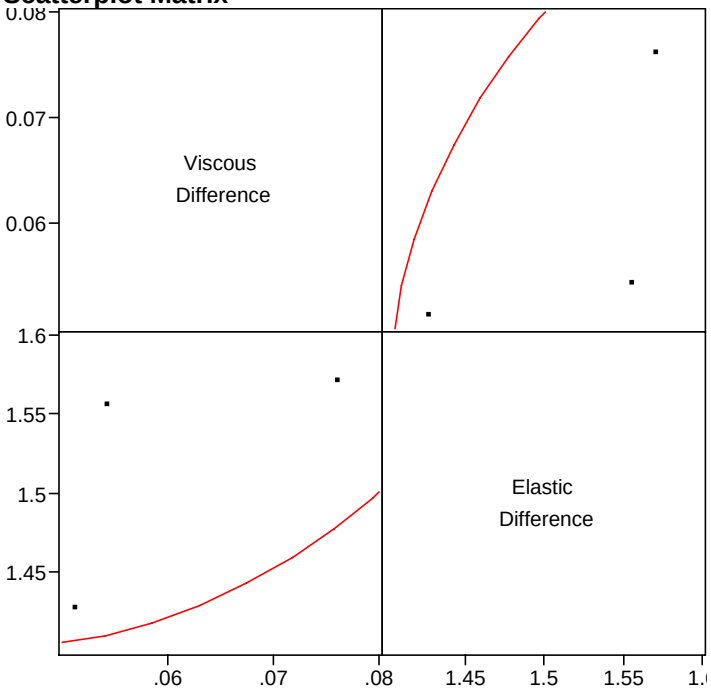


**Multivariate Site=13, Filler (None=0, Silica=1, Hydrated Lime=2)=1, Percent=5**

Freq: Run

**Correlations**

| | Viscous Difference | Elastic Difference |
|---|---|---|
| Viscous Difference | 1.0000 | 0.9387 |
| Elastic Difference | 0.9387 | 1.0000 |

**Scatterplot Matrix**

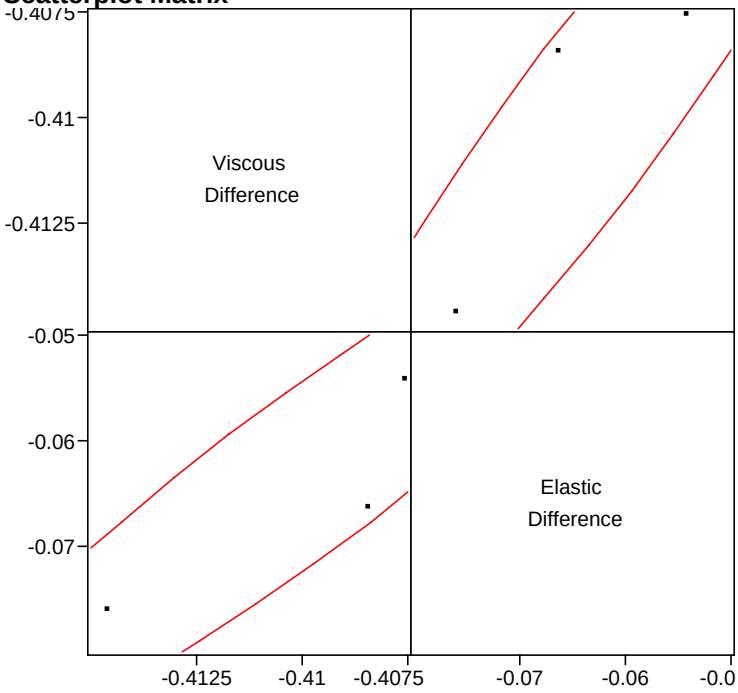


**Multivariate Site=13, Filler (None=0, Silica=1, Hydrated Lime=2)=1, Percent=10**

Freq: Run

**Correlations**

| | Viscous Difference | Elastic Difference |
|---|---|---|
| Viscous Difference | 1.0000 | 0.9967 |
| Elastic Difference | 0.9967 | 1.0000 |

**Scatterplot Matrix**

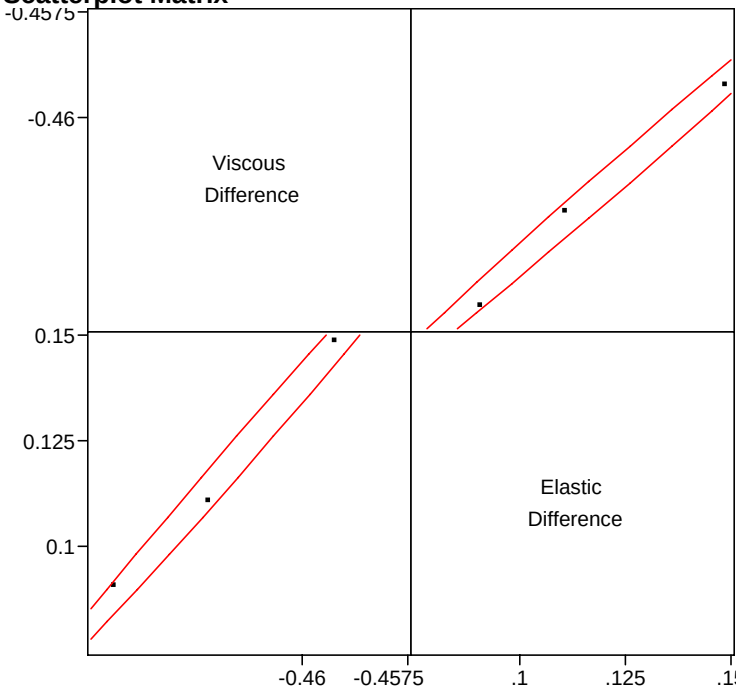


**Multivariate Site=13, Filler (None=0, Silica=1, Hydrated Lime=2)=1, Percent=20**

Freq: Run

**Correlations**

| | Viscous Difference | Elastic Difference |
|---|---|---|
| Viscous Difference | 1.0000 | 0.5441 |
| Elastic Difference | 0.5441 | 1.0000 |

**Scatterplot Matrix**

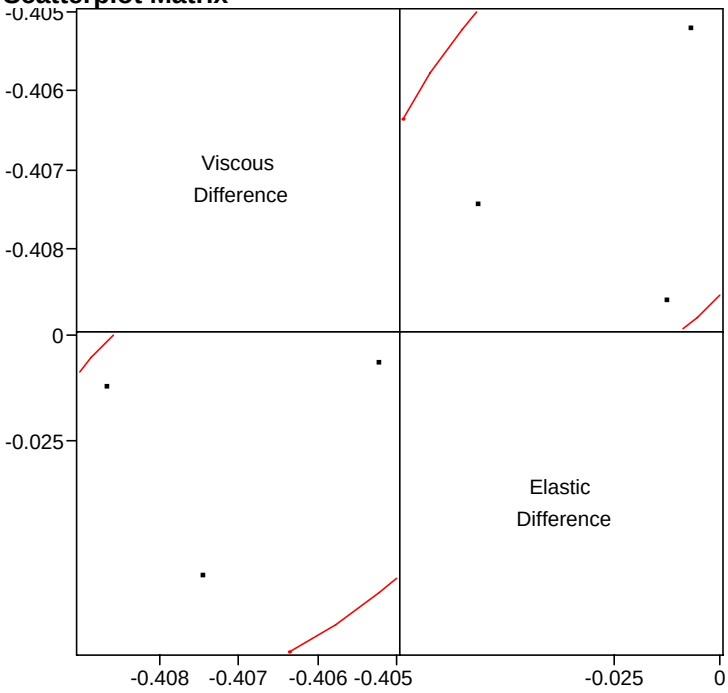


**Multivariate Site=13, Filler (None=0, Silica=1, Hydrated Lime=2)=2, Percent=5**

Freq: Run

**Correlations**

| | Viscous Difference | Elastic Difference |
|---|---|---|
| Viscous Difference | 1.0000 | 0.6909 |
| Elastic Difference | 0.6909 | 1.0000 |

**Scatterplot Matrix**

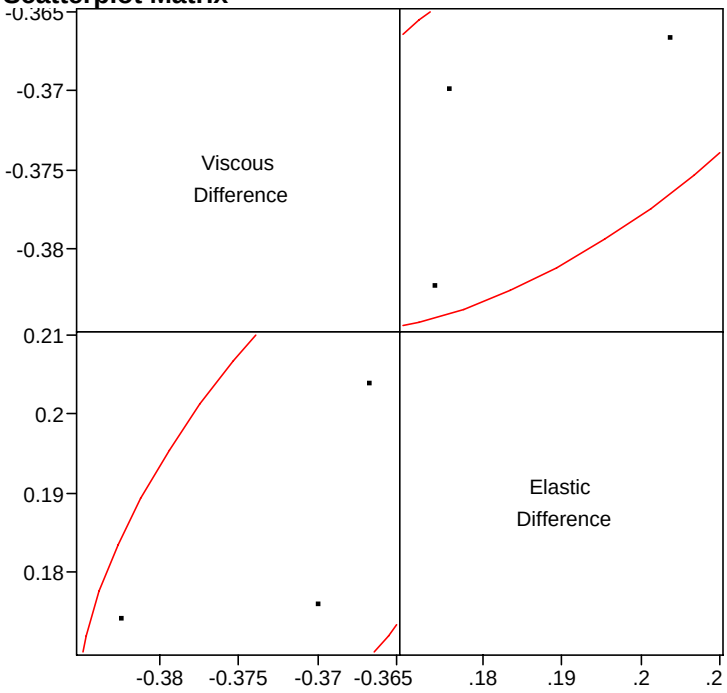


**Multivariate Site=13, Filler (None=0, Silica=1, Hydrated Lime=2)=2, Percent=10**

Freq: Run

**Correlations**

| | Viscous Difference | Elastic Difference |
|---|---|---|
| Viscous Difference | 1.0000 | 0.6503 |
| Elastic Difference | 0.6503 | 1.0000 |

**Scatterplot Matrix**

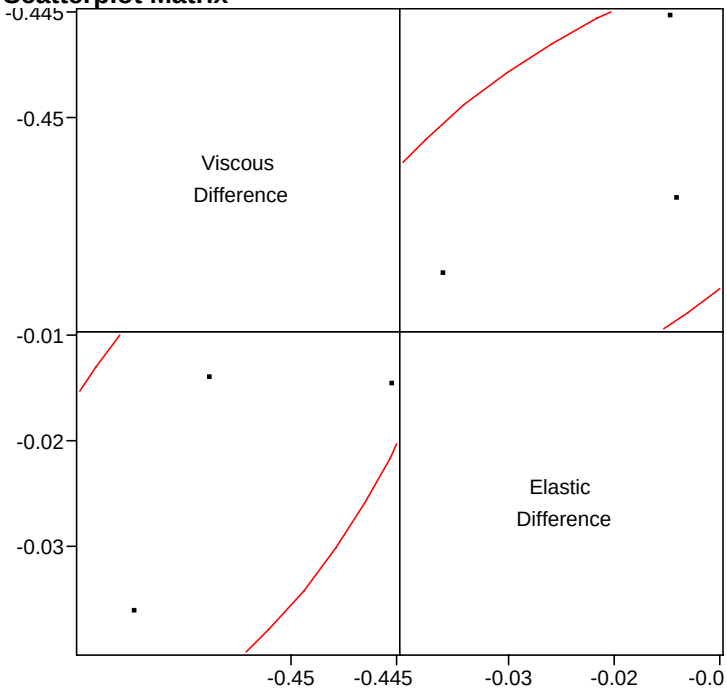


**Multivariate Site=13, Filler (None=0, Silica=1, Hydrated Lime=2)=2, Percent=20**

Freq: Run

**Correlations**

| | Viscous Difference | Elastic Difference |
|---|---|---|
| Viscous Difference | 1.0000 | -0.9001 |
| Elastic Difference | -0.9001 | 1.0000 |

**Scatterplot Matrix**

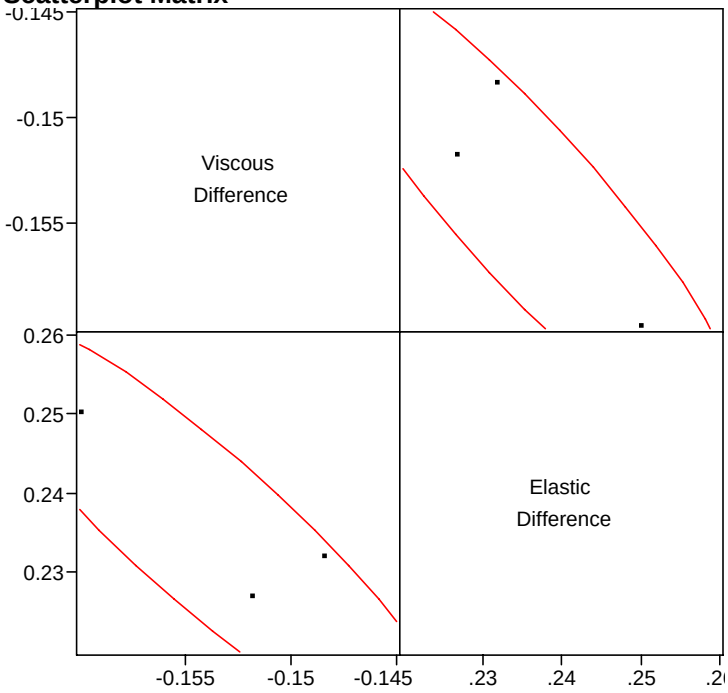


**Multivariate Site=14, Filler (None=0, Silica=1, Hydrated Lime=2)=0, Percent=0**

Freq: Run

**Correlations**

| | Viscous Difference | Elastic Difference |
|---|---|---|
| Viscous Difference | 1.0000 | -0.9094 |
| Elastic Difference | -0.9094 | 1.0000 |

**Scatterplot Matrix**

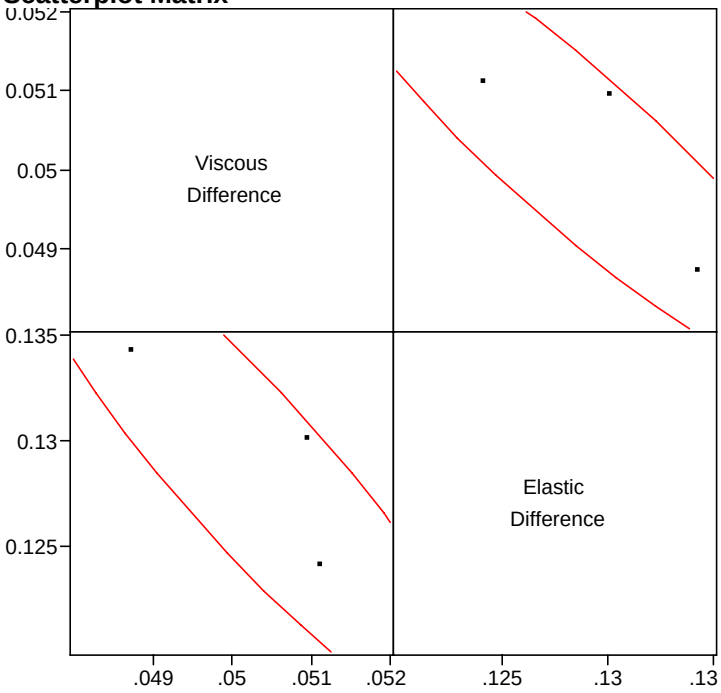


**Multivariate Site=14, Filler (None=0, Silica=1, Hydrated Lime=2)=1, Percent=5**

Freq: Run

**Correlations**

| | Viscous Difference | Elastic Difference |
|---|---|---|
| Viscous Difference | 1.0000 | 1.0000 |
| Elastic Difference | 1.0000 | 1.0000 |

**Scatterplot Matrix**

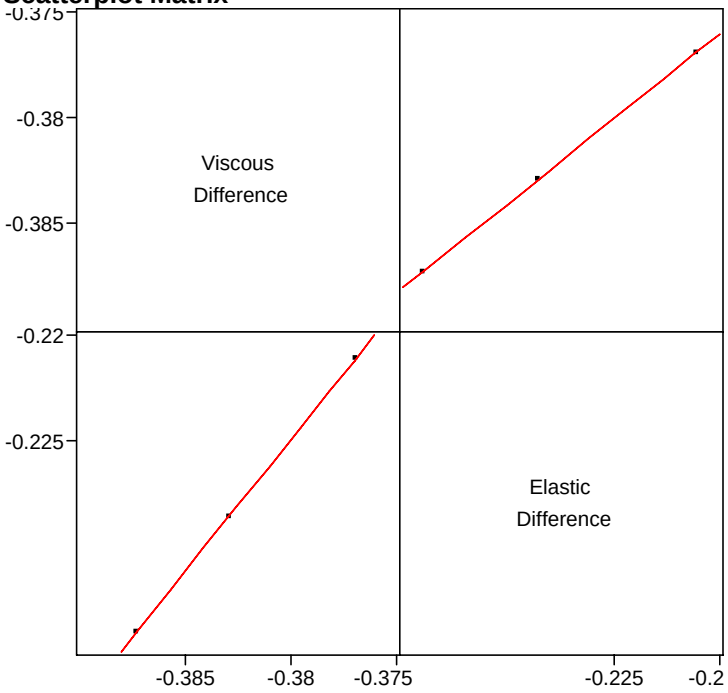


**Multivariate Site=14, Filler (None=0, Silica=1, Hydrated Lime=2)=1, Percent=10**

Freq: Run

**Correlations**

| | Viscous Difference | Elastic Difference |
|---|---|---|
| Viscous Difference | 1.0000 | 1.0000 |
| Elastic Difference | 1.0000 | 1.0000 |

**Scatterplot Matrix**

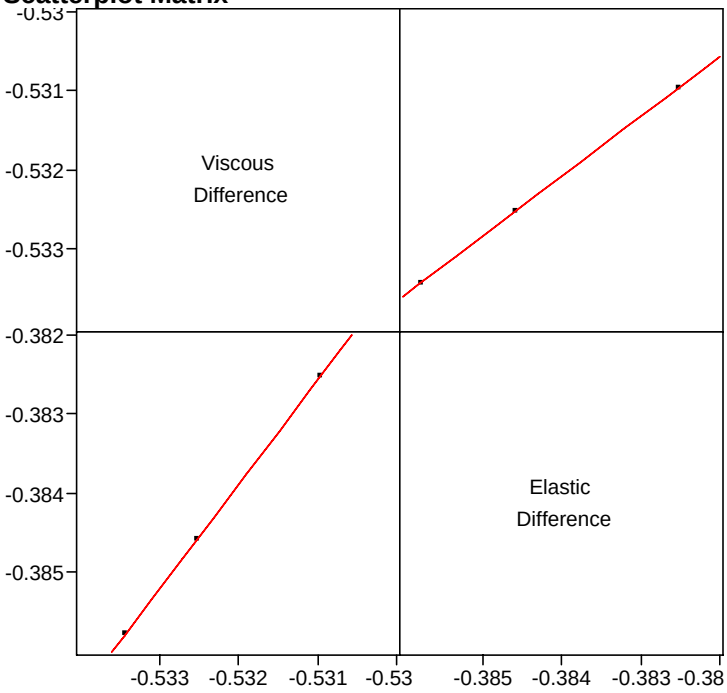


**Multivariate Site=14, Filler (None=0, Silica=1, Hydrated Lime=2)=1, Percent=20**

Freq: Run

**Correlations**

| | Viscous Difference | Elastic Difference |
|---|---|---|
| Viscous Difference | 1.0000 | 0.9995 |
| Elastic Difference | 0.9995 | 1.0000 |

**Scatterplot Matrix**

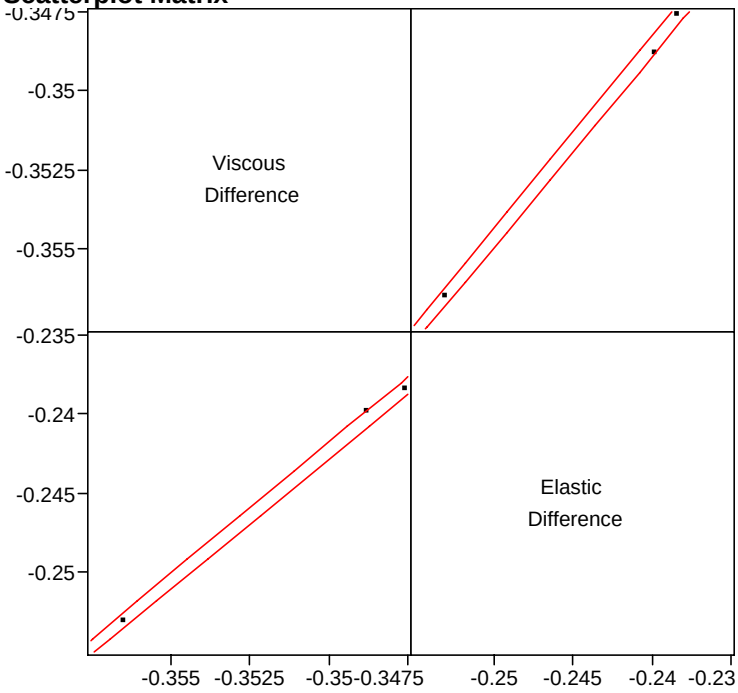


**Multivariate Site=14, Filler (None=0, Silica=1, Hydrated Lime=2)=2, Percent=5**

Freq: Run

**Correlations**

| | Viscous Difference | Elastic Difference |
|---|---|---|
| Viscous Difference | 1.0000 | 0.9916 |
| Elastic Difference | 0.9916 | 1.0000 |

**Scatterplot Matrix**

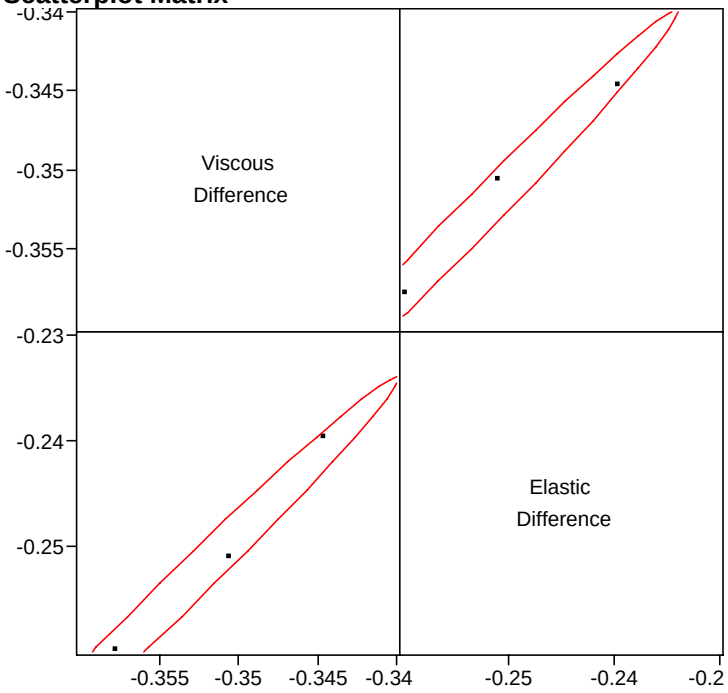


**Multivariate Site=14, Filler (None=0, Silica=1, Hydrated Lime=2)=2, Percent=10**

Freq: Run

**Correlations**

| | Viscous Difference | Elastic Difference |
|---|---|---|
| Viscous Difference | 1.0000 | 0.9855 |
| Elastic Difference | 0.9855 | 1.0000 |

**Scatterplot Matrix**

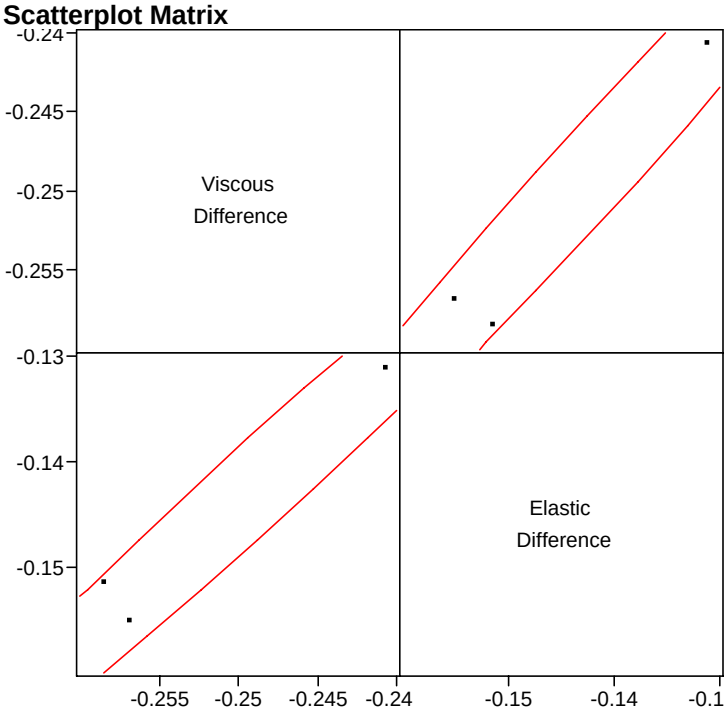


**Multivariate Site=14, Filler (None=0, Silica=1, Hydrated Lime=2)=2, Percent=20**

Freq: Run

**Correlations**

| | Viscous Difference | Elastic Difference |
|---|---|---|
| Viscous Difference | 1.0000 | 0.9900 |
| Elastic Difference | 0.9900 | 1.0000 |

**Scatterplot Matrix**

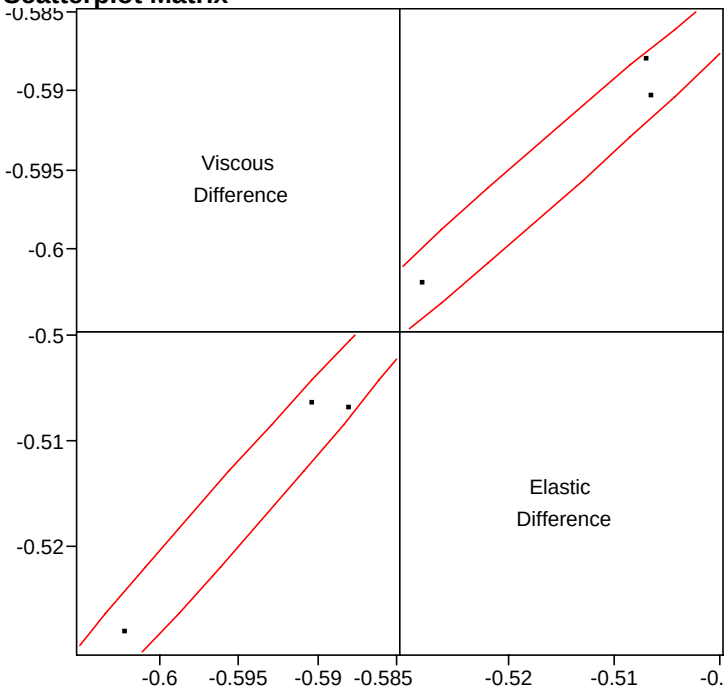


**Multivariate Site=15, Filler (None=0, Silica=1, Hydrated Lime=2)=0, Percent=0**

Freq: Run

**Correlations**

| | Viscous Difference | Elastic Difference |
|---|---|---|
| Viscous Difference | 1.0000 | 0.5837 |
| Elastic Difference | 0.5837 | 1.0000 |

**Scatterplot Matrix**

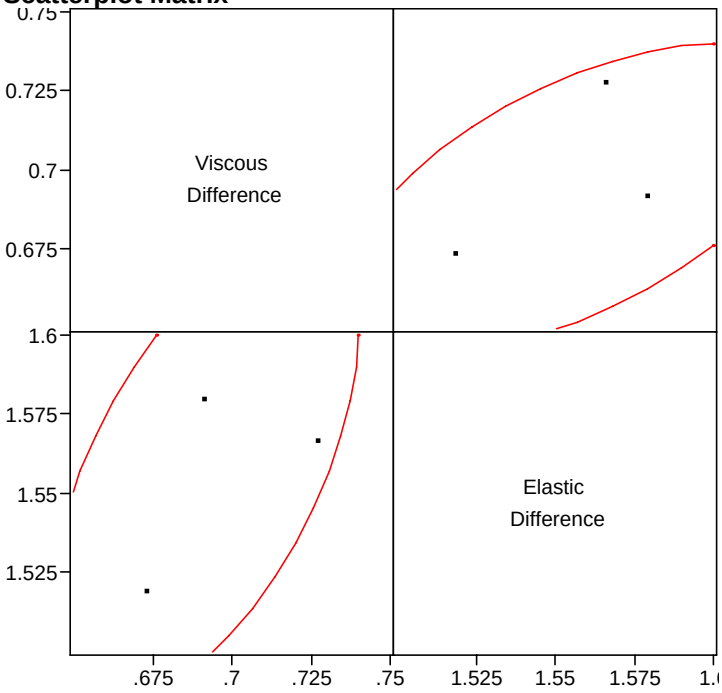


**Multivariate Site=15, Filler (None=0, Silica=1, Hydrated Lime=2)=1, Percent=5**

Freq: Run

**Correlations**

| | Viscous Difference | Elastic Difference |
|---|---|---|
| Viscous Difference | 1.0000 | 0.9501 |
| Elastic Difference | 0.9501 | 1.0000 |

**Scatterplot Matrix**

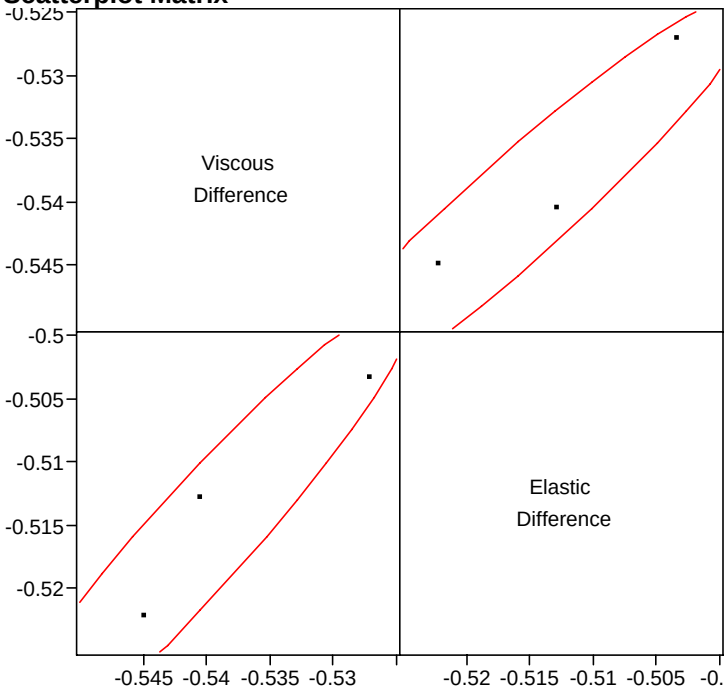


**Multivariate Site=15, Filler (None=0, Silica=1, Hydrated Lime=2)=1, Percent=10**

Freq: Run

**Correlations**

| | Viscous Difference | Elastic Difference |
|---|---|---|
| Viscous Difference | 1.0000 | 0.8213 |
| Elastic Difference | 0.8213 | 1.0000 |

**Scatterplot Matrix**

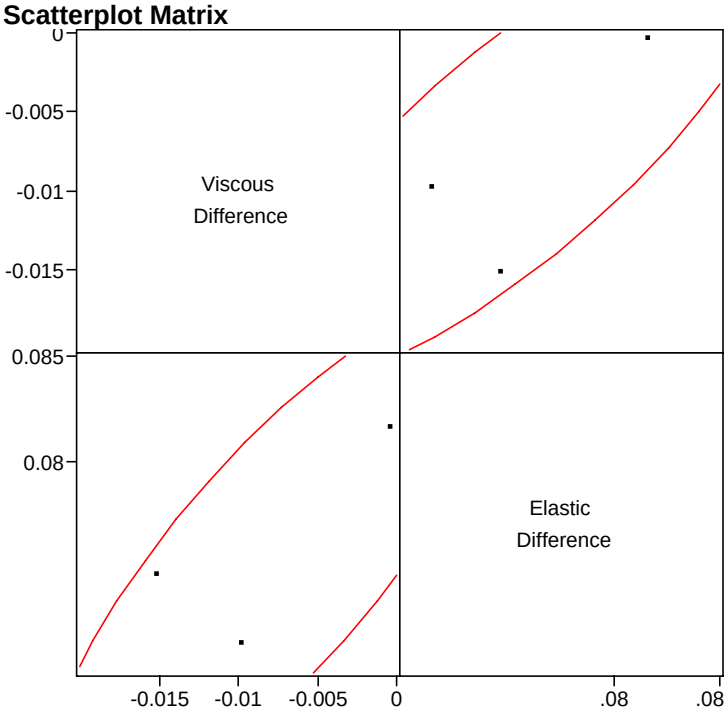


**Multivariate Site=15, Filler (None=0, Silica=1, Hydrated Lime=2)=1, Percent=20**

Freq: Run

**Correlations**

| | Viscous Difference | Elastic Difference |
|---|---|---|
| Viscous Difference | 1.0000 | 0.9601 |
| Elastic Difference | 0.9601 | 1.0000 |

**Scatterplot Matrix**

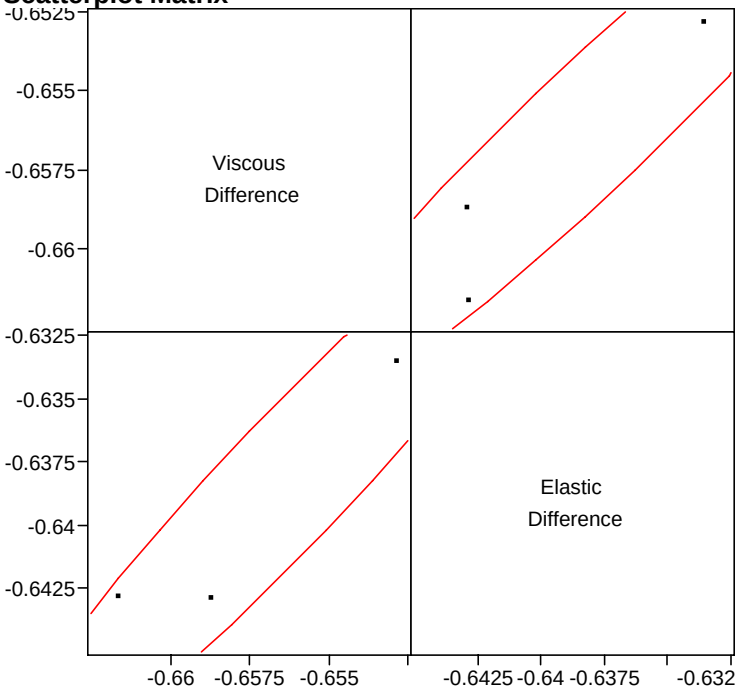


**Multivariate Site=15, Filler (None=0, Silica=1, Hydrated Lime=2)=2, Percent=5**

Freq: Run

**Correlations**

| | Viscous Difference | Elastic Difference |
|---|---|---|
| Viscous Difference | 1.0000 | 0.1273 |
| Elastic Difference | 0.1273 | 1.0000 |

**Scatterplot Matrix**

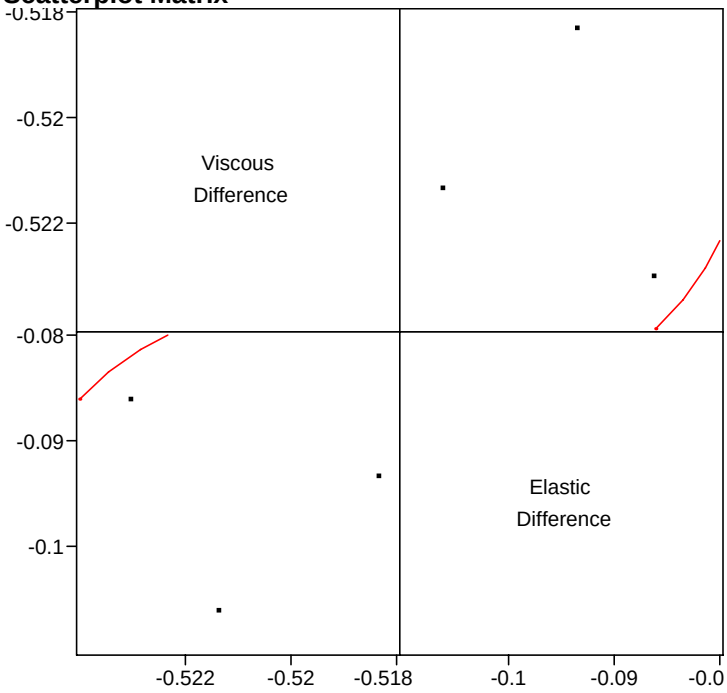


**Multivariate Site=15, Filler (None=0, Silica=1, Hydrated Lime=2)=2, Percent=10**

Freq: Run

**Correlations**

| | Viscous Difference | Elastic Difference |
|---|---|---|
| Viscous Difference | 1.0000 | 0.5147 |
| Elastic Difference | 0.5147 | 1.0000 |

**Scatterplot Matrix**

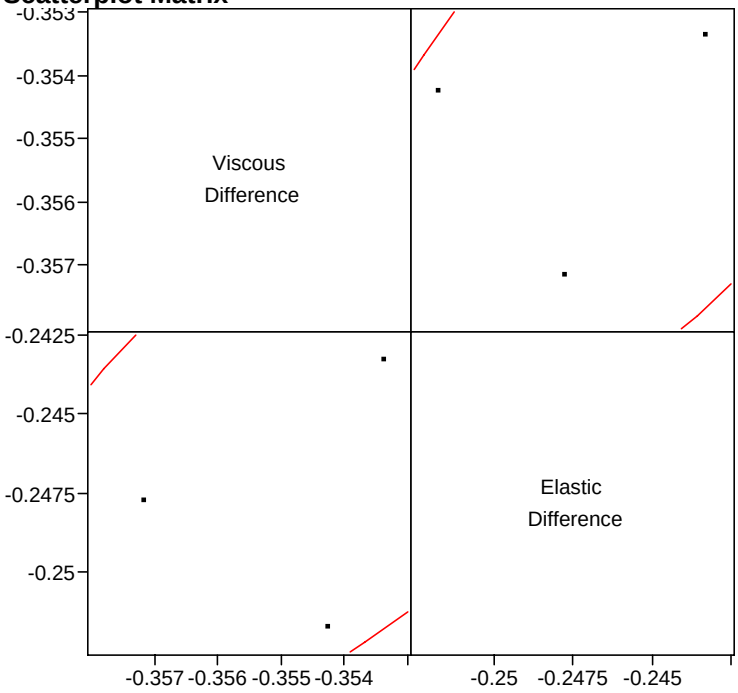


**Multivariate Site=15, Filler (None=0, Silica=1, Hydrated Lime=2)=2, Percent=20**

Freq: Run

**Correlations**

| | Viscous Difference | Elastic Difference |
|---|---|---|
| Viscous Difference | 1.0000 | 0.9581 |
| Elastic Difference | 0.9581 | 1.0000 |

**Scatterplot Matrix**

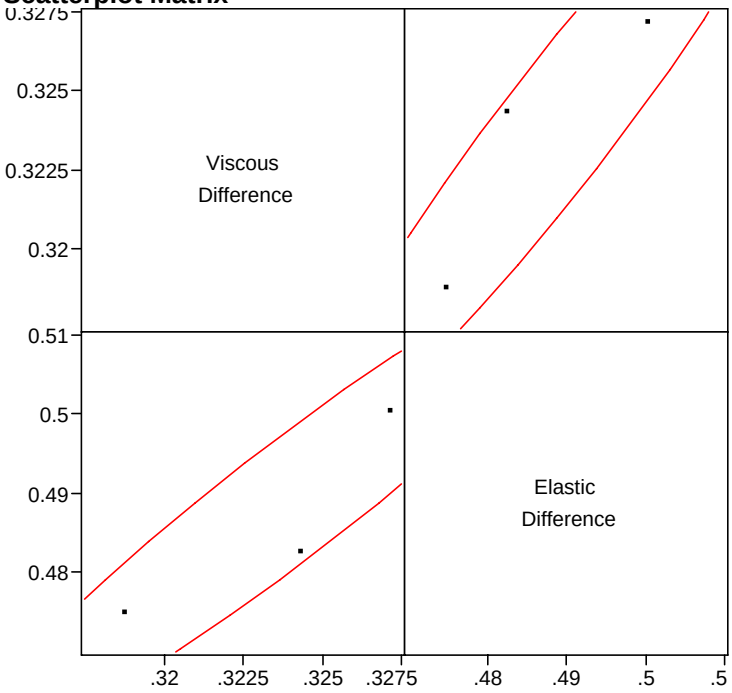


**Multivariate Site=16, Filler (None=0, Silica=1, Hydrated Lime=2)=0, Percent=0**

Freq: Run

**Correlations**

| | Viscous Difference | Elastic Difference |
|---|---|---|
| Viscous Difference | 1.0000 | 0.8678 |
| Elastic Difference | 0.8678 | 1.0000 |

**Scatterplot Matrix**

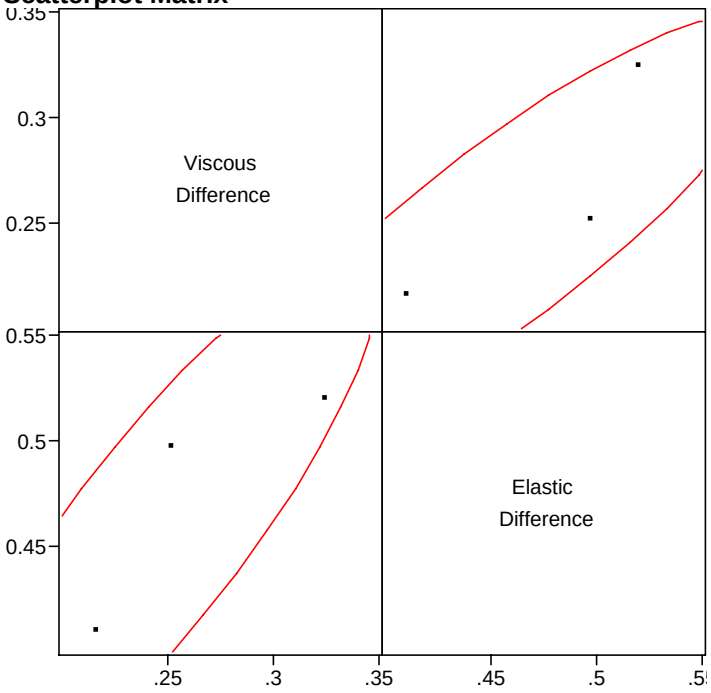


**Multivariate Site=16, Filler (None=0, Silica=1, Hydrated Lime=2)=1, Percent=5**

Freq: Run

**Correlations**

| | Viscous Difference | Elastic Difference |
|---|---|---|
| Viscous Difference | 1.0000 | 0.9953 |
| Elastic Difference | 0.9953 | 1.0000 |

**Scatterplot Matrix**

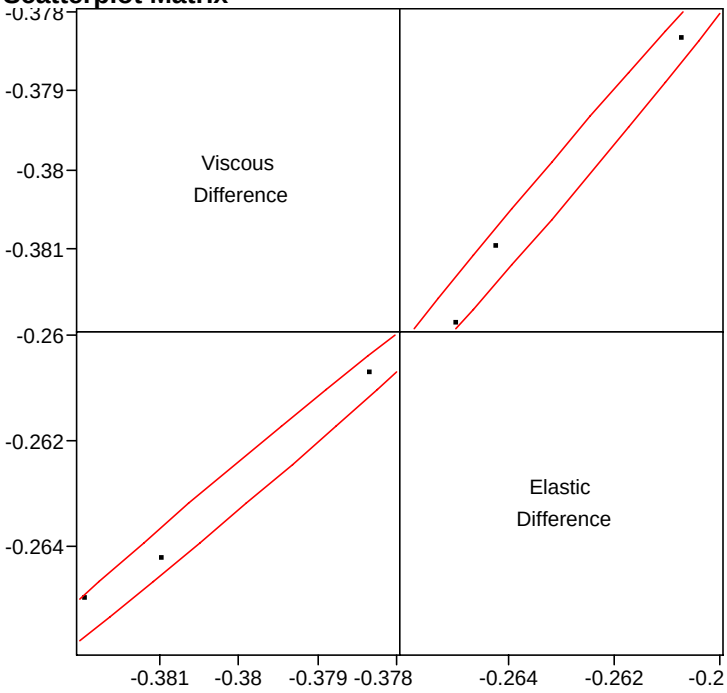


**Multivariate Site=16, Filler (None=0, Silica=1, Hydrated Lime=2)=1, Percent=10**

Freq: Run

**Correlations**

| | Viscous Difference | Elastic Difference |
|---|---|---|
| Viscous Difference | 1.0000 | 0.3408 |
| Elastic Difference | 0.3408 | 1.0000 |

**Scatterplot Matrix**

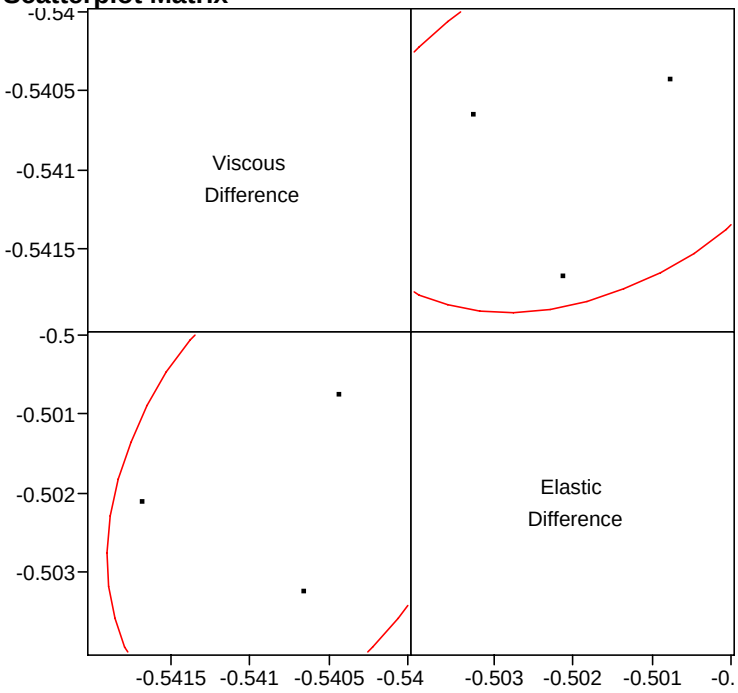


**Multivariate Site=16, Filler (None=0, Silica=1, Hydrated Lime=2)=1, Percent=20**

Freq: Run

**Correlations**

| | Viscous Difference | Elastic Difference |
|---|---|---|
| Viscous Difference | 1.0000 | 0.9891 |
| Elastic Difference | 0.9891 | 1.0000 |

**Scatterplot Matrix**

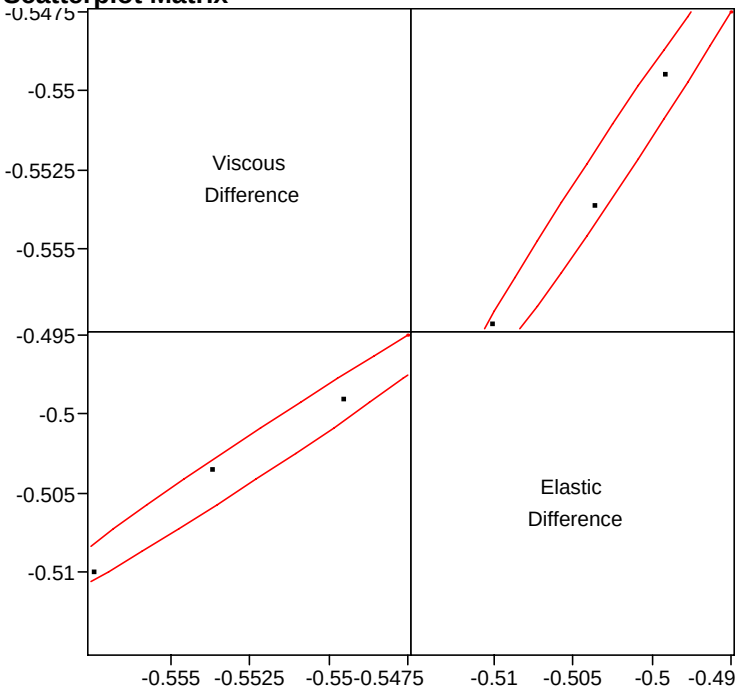


**Multivariate Site=16, Filler (None=0, Silica=1, Hydrated Lime=2)=2, Percent=5**

Freq: Run

**Correlations**

| | Viscous Difference | Elastic Difference |
|---|---|---|
| Viscous Difference | 1.0000 | -0.5385 |
| Elastic Difference | -0.5385 | 1.0000 |

**Scatterplot Matrix**

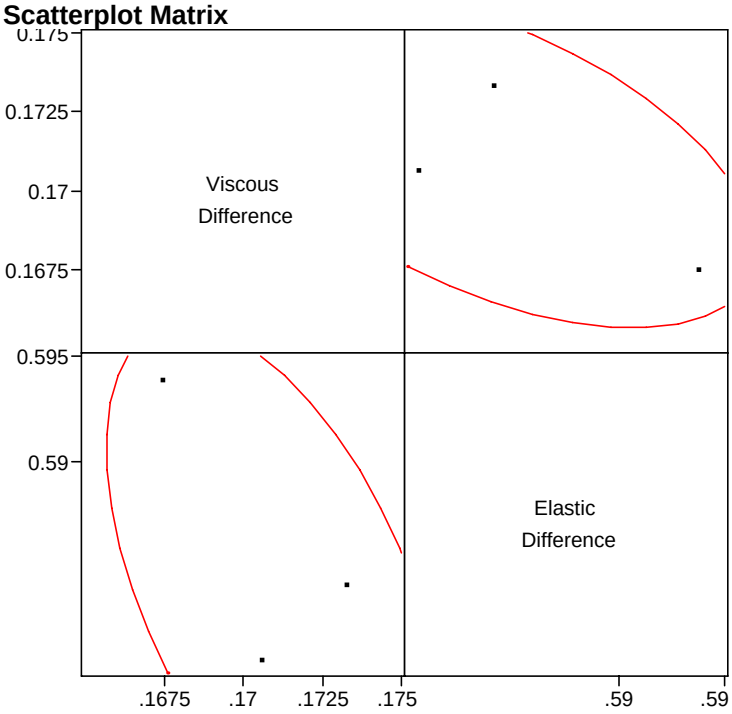


**Multivariate Site=16, Filler (None=0, Silica=1, Hydrated Lime=2)=2, Percent=10**

Freq: Run

**Correlations**

| | Viscous Difference | Elastic Difference |
|---|---|---|
| Viscous Difference | 1.0000 | 0.9729 |
| Elastic Difference | 0.9729 | 1.0000 |

**Scatterplot Matrix**

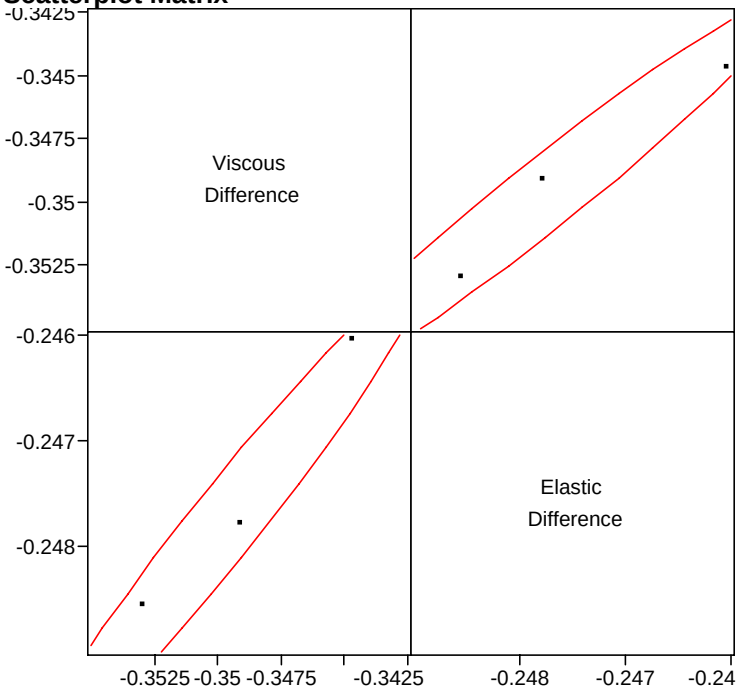


**Multivariate Site=16, Filler (None=0, Silica=1, Hydrated Lime=2)=2, Percent=20**

Freq: Run

**Correlations**

| | Viscous Difference | Elastic Difference |
|---|---|---|
| Viscous Difference | 1.0000 | 0.9828 |
| Elastic Difference | 0.9828 | 1.0000 |

**Scatterplot Matrix**

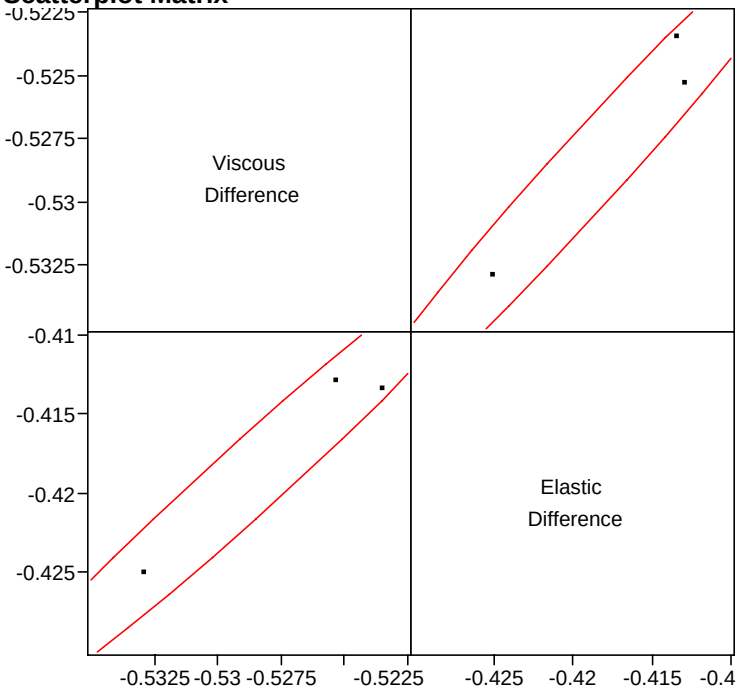


**Multivariate Site=17, Filler (None=0, Silica=1, Hydrated Lime=2)=0, Percent=0**

Freq: Run

**Correlations**

| | Viscous Difference | Elastic Difference |
|---|---|---|
| Viscous Difference | 1.0000 | -0.8641 |
| Elastic Difference | -0.8641 | 1.0000 |

**Scatterplot Matrix**

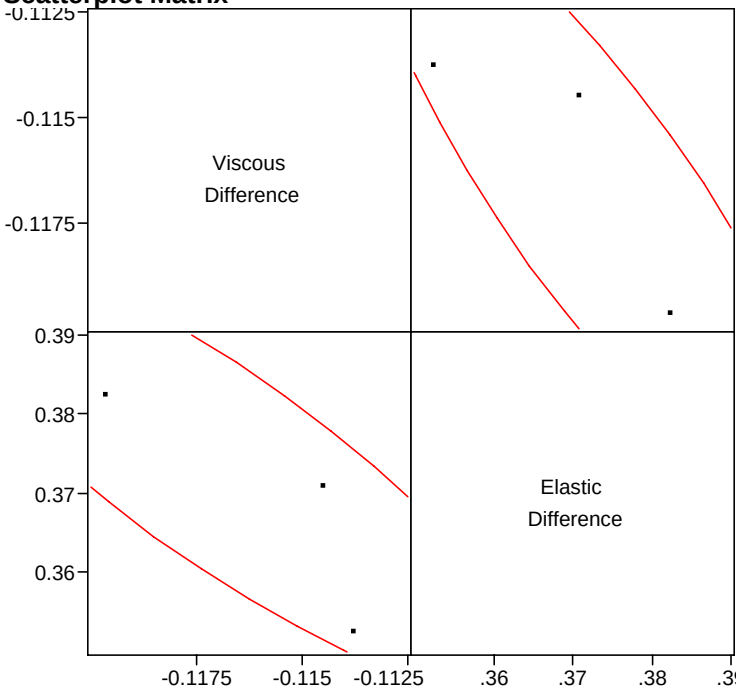


**Multivariate Site=17, Filler (None=0, Silica=1, Hydrated Lime=2)=1, Percent=5**

Freq: Run

**Correlations**

| | Viscous Difference | Elastic Difference |
|---|---|---|
| Viscous Difference | 1.0000 | 0.9853 |
| Elastic Difference | 0.9853 | 1.0000 |

**Scatterplot Matrix**

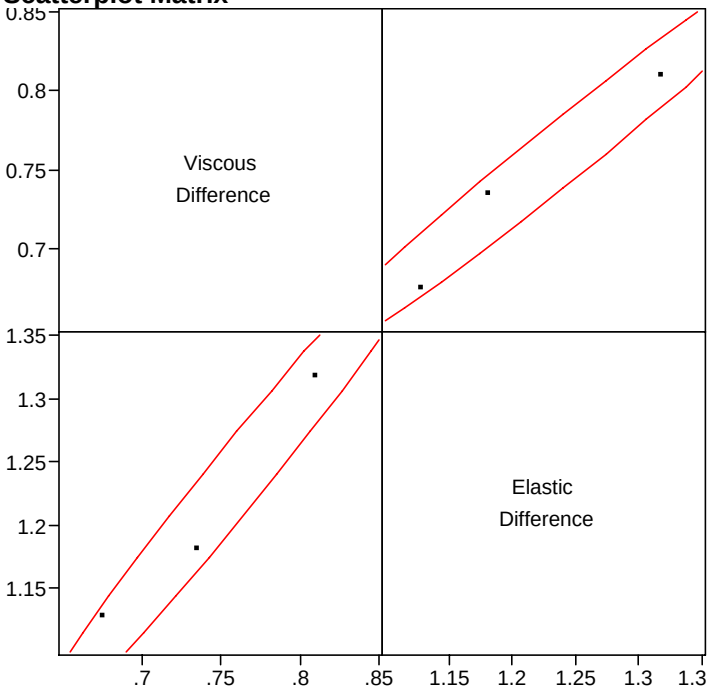


**Multivariate Site=17, Filler (None=0, Silica=1, Hydrated Lime=2)=1, Percent=10**

Freq: Run

**Correlations**

| | Viscous Difference | Elastic Difference |
|---|---|---|
| Viscous Difference | 1.0000 | 0.8851 |
| Elastic Difference | 0.8851 | 1.0000 |

**Scatterplot Matrix**

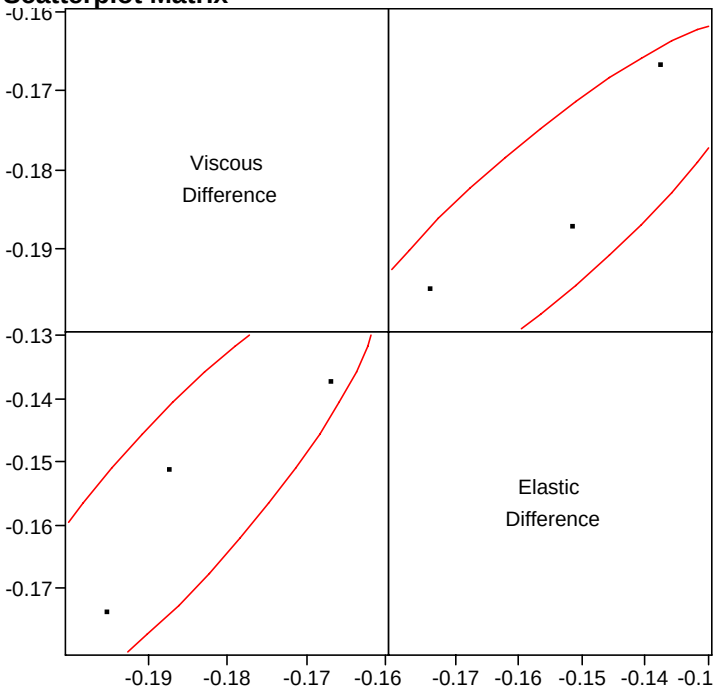


**Multivariate Site=17, Filler (None=0, Silica=1, Hydrated Lime=2)=1, Percent=20**

Freq: Run

**Correlations**

| | Viscous Difference | Elastic Difference |
|---|---|---|
| Viscous Difference | 1.0000 | 1.0000 |
| Elastic Difference | 1.0000 | 1.0000 |

**Scatterplot Matrix**

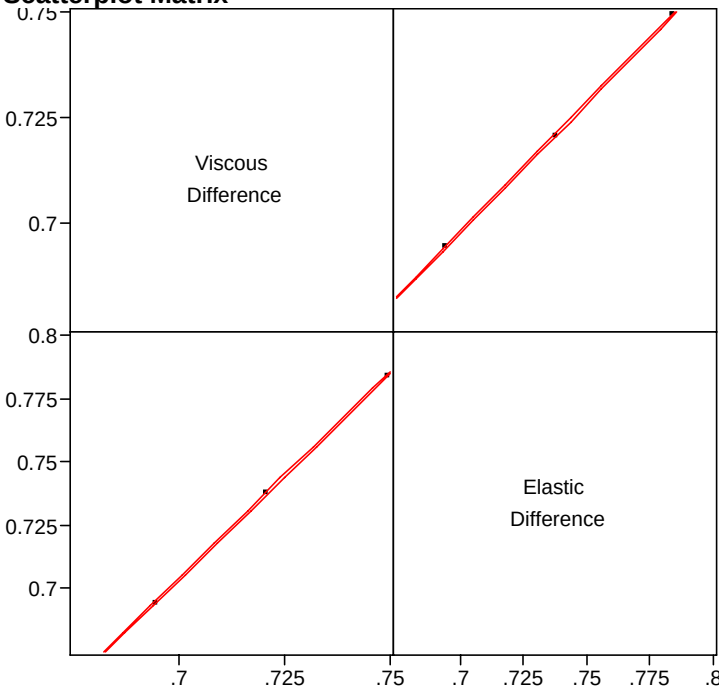


**Multivariate Site=17, Filler (None=0, Silica=1, Hydrated Lime=2)=2, Percent=5**

Freq: Run

**Correlations**

| | Viscous Difference | Elastic Difference |
|---|---|---|
| Viscous Difference | 1.0000 | -0.0622 |
| Elastic Difference | -0.0622 | 1.0000 |

**Scatterplot Matrix**

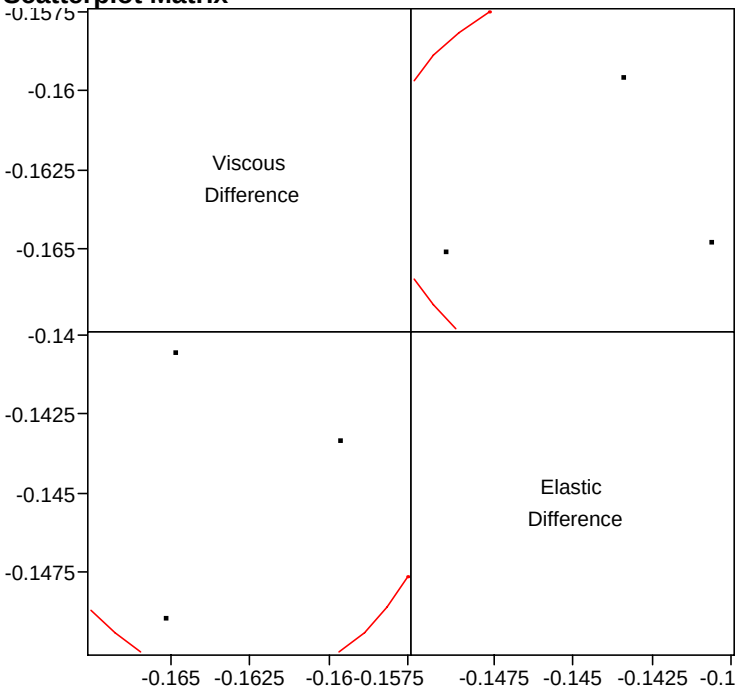


**Multivariate Site=17, Filler (None=0, Silica=1, Hydrated Lime=2)=2, Percent=10**

Freq: Run

**Correlations**

| | Viscous Difference | Elastic Difference |
|---|---|---|
| Viscous Difference | 1.0000 | 0.9812 |
| Elastic Difference | 0.9812 | 1.0000 |

**Scatterplot Matrix**

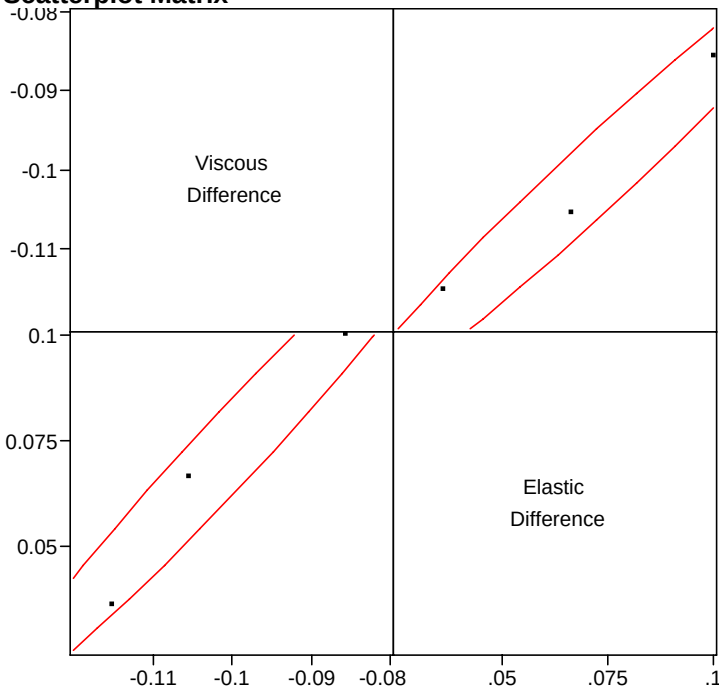


**Multivariate Site=17, Filler (None=0, Silica=1, Hydrated Lime=2)=2, Percent=20**
Freq: Run

**Correlations**

| | Viscous Difference | Elastic Difference |
|---|---|---|
| Viscous Difference | 1.0000 | 0.9980 |
| Elastic Difference | 0.9980 | 1.0000 |

**Scatterplot Matrix**

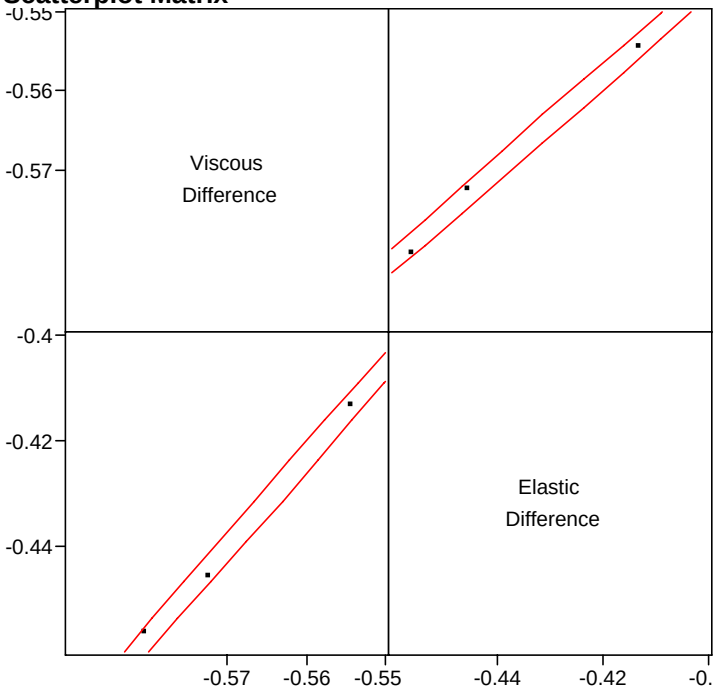


**Multivariate Site=18, Filler (None=0, Silica=1, Hydrated Lime=2)=0, Percent=0**

Freq: Run

**Correlations**

| | Viscous Difference | Elastic Difference |
|---|---|---|
| Viscous Difference | 1.0000 | 0.7836 |
| Elastic Difference | 0.7836 | 1.0000 |

**Scatterplot Matrix**

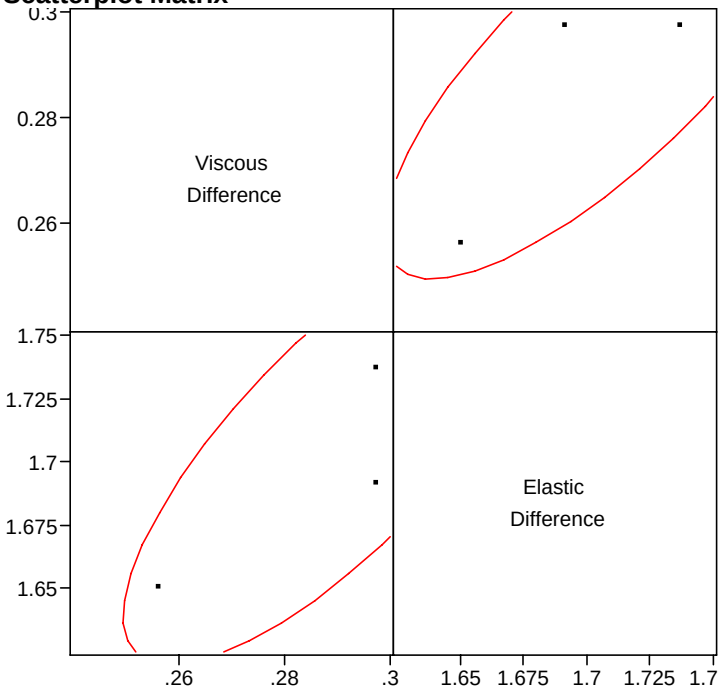


**Multivariate Site=18, Filler (None=0, Silica=1, Hydrated Lime=2)=1, Percent=5**

Freq: Run

**Correlations**

| | Viscous Difference | Elastic Difference |
|---|---|---|
| Viscous Difference | 1.0000 | 0.8094 |
| Elastic Difference | 0.8094 | 1.0000 |

**Scatterplot Matrix**

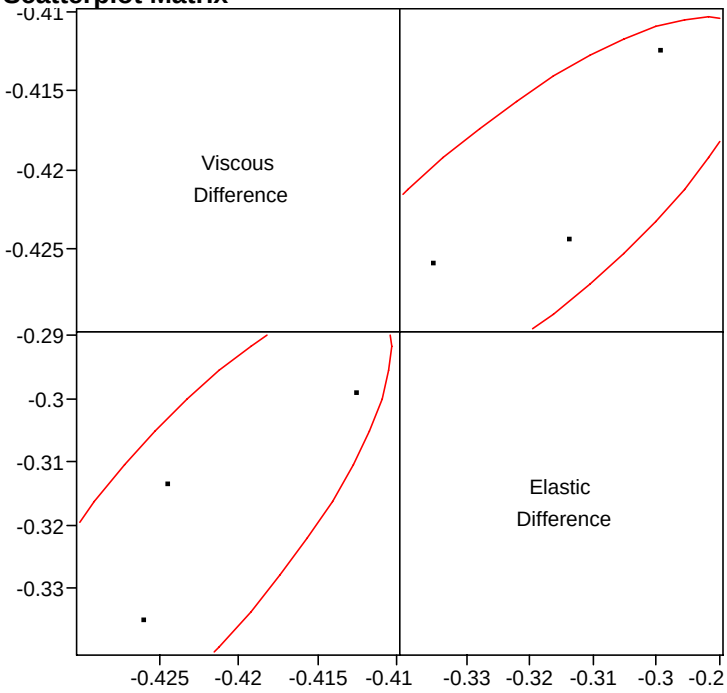


**Multivariate Site=18, Filler (None=0, Silica=1, Hydrated Lime=2)=1, Percent=10**

Freq: Run

**Correlations**

| | Viscous Difference | Elastic Difference |
|---|---|---|
| Viscous Difference | 1.0000 | -0.6820 |
| Elastic Difference | -0.6820 | 1.0000 |

**Scatterplot Matrix**

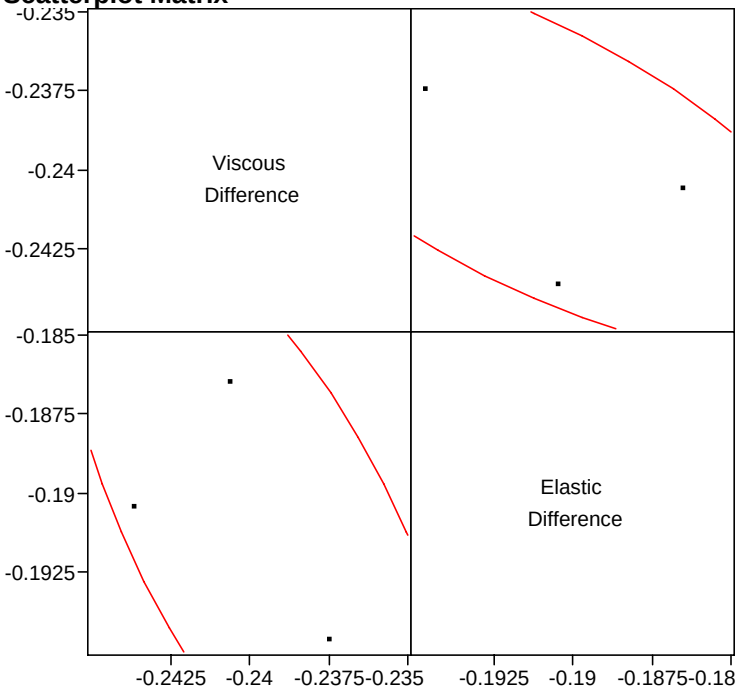


**Multivariate Site=18, Filler (None=0, Silica=1, Hydrated Lime=2)=1, Percent=20**

Freq: Run

**Correlations**

| | Viscous Difference | Elastic Difference |
|---|---|---|
| Viscous Difference | 1.0000 | 0.7714 |
| Elastic Difference | 0.7714 | 1.0000 |

**Scatterplot Matrix**

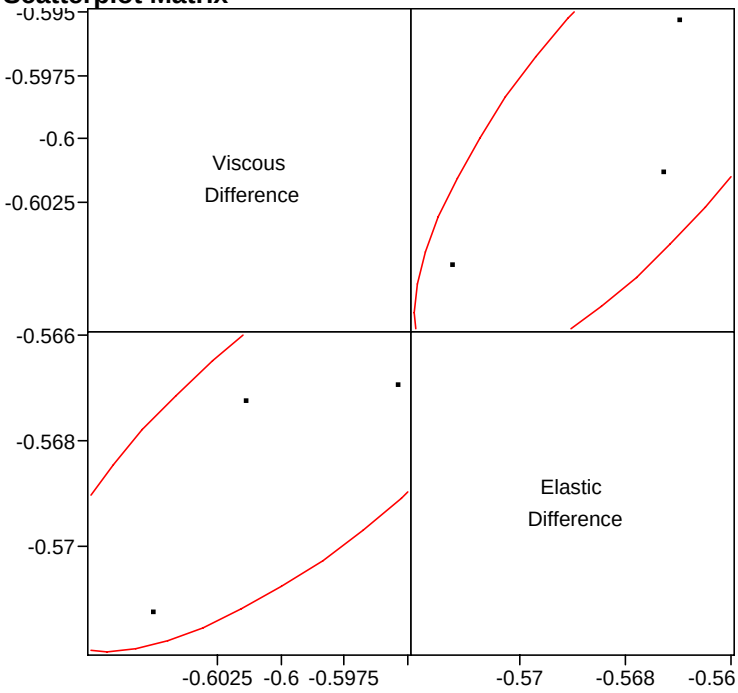


**Multivariate Site=18, Filler (None=0, Silica=1, Hydrated Lime=2)=2, Percent=5**

Freq: Run

**Correlations**

| | Viscous Difference | Elastic Difference |
|---|---|---|
| Viscous Difference | 1.0000 | -0.9871 |
| Elastic Difference | -0.9871 | 1.0000 |

**Scatterplot Matrix**

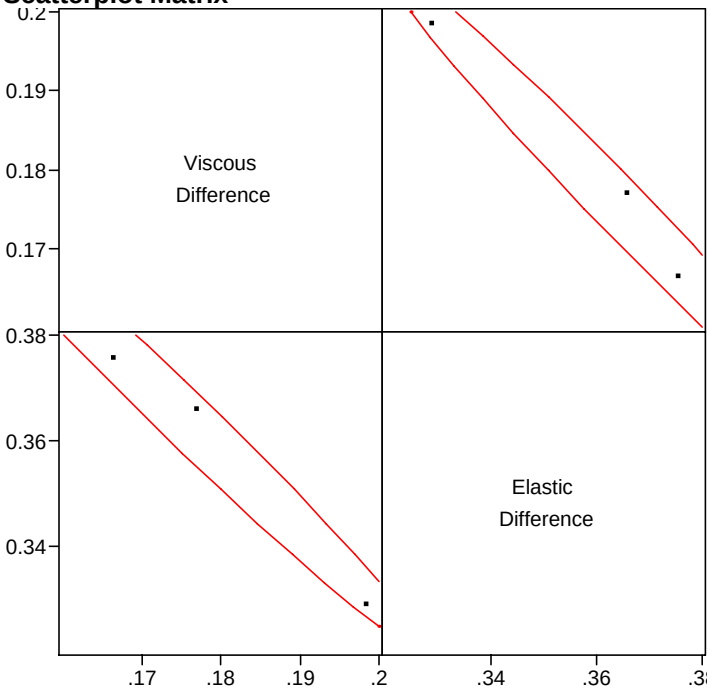


**Multivariate Site=18, Filler (None=0, Silica=1, Hydrated Lime=2)=2, Percent=10**

Freq: Run

**Correlations**

| | Viscous Difference | Elastic Difference |
|---|---|---|
| Viscous Difference | 1.0000 | 0.8701 |
| Elastic Difference | 0.8701 | 1.0000 |

**Scatterplot Matrix**

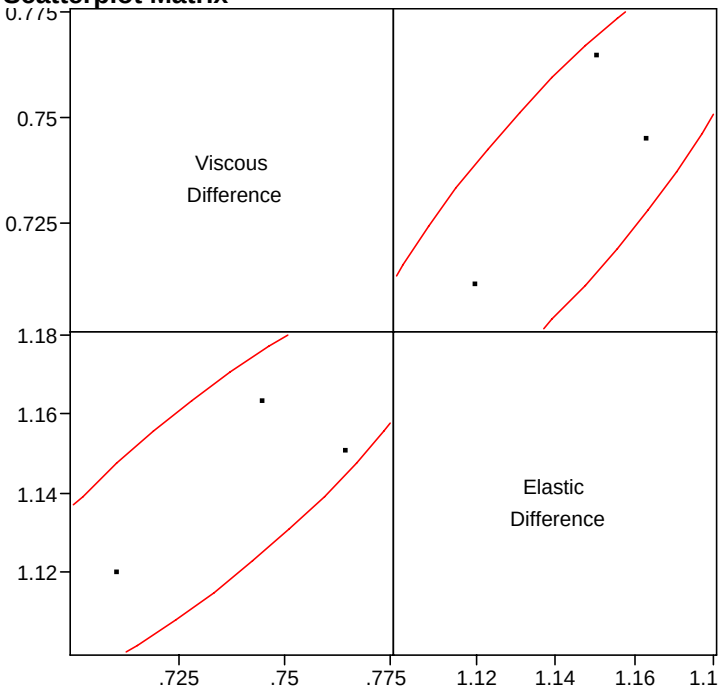


**Multivariate Site=18, Filler (None=0, Silica=1, Hydrated Lime=2)=2, Percent=20**

Freq: Run

**Correlations**

| | Viscous Difference | Elastic Difference |
|---|---|---|
| Viscous Difference | 1.0000 | -0.9274 |
| Elastic Difference | -0.9274 | 1.0000 |

**Scatterplot Matrix**

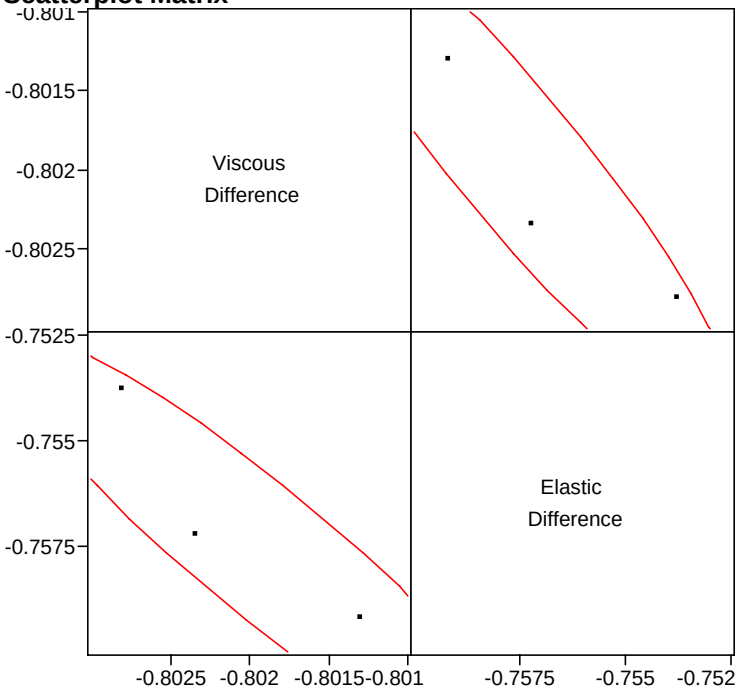


**Multivariate Site=19, Filler (None=0, Silica=1, Hydrated Lime=2)=0, Percent=0**

Freq: Run

**Correlations**

| | Viscous Difference | Elastic Difference |
|---|---|---|
| Viscous Difference | 1.0000 | -0.4292 |
| Elastic Difference | -0.4292 | 1.0000 |

**Scatterplot Matrix**

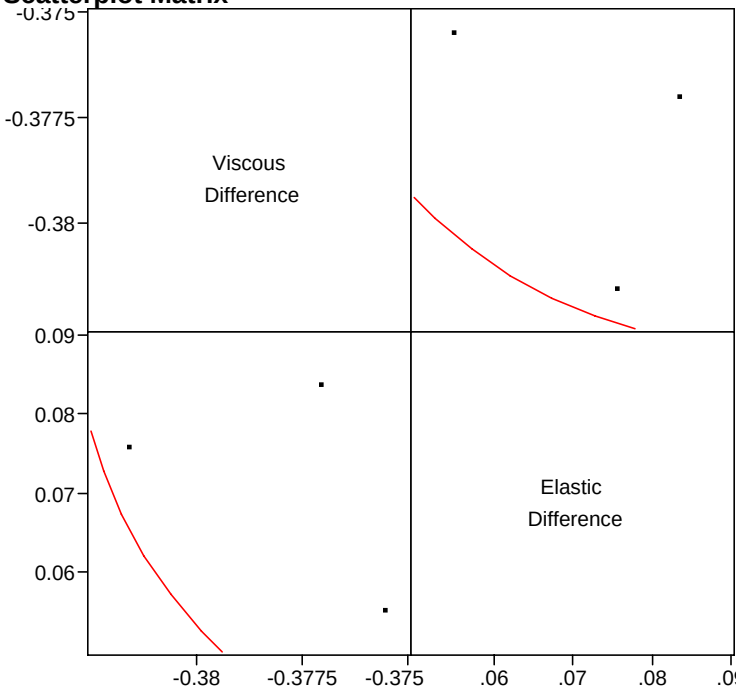


**Multivariate Site=19, Filler (None=0, Silica=1, Hydrated Lime=2)=1, Percent=5**

Freq: Run

**Correlations**

| | Viscous Difference | Elastic Difference |
|---|---|---|
| Viscous Difference | 1.0000 | -0.4387 |
| Elastic Difference | -0.4387 | 1.0000 |

**Scatterplot Matrix**

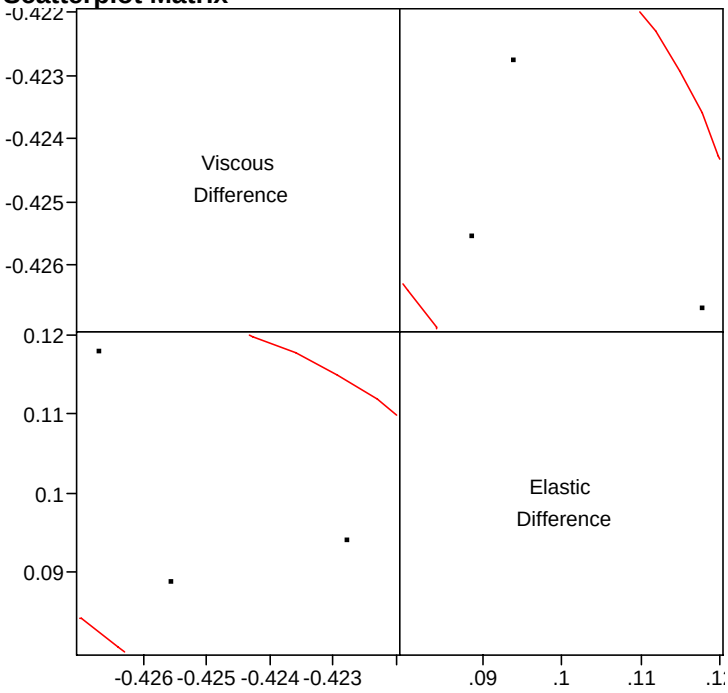


**Multivariate Site=19, Filler (None=0, Silica=1, Hydrated Lime=2)=1, Percent=10**

Freq: Run

**Correlations**

| | Viscous Difference | Elastic Difference |
|---|---|---|
| Viscous Difference | 1.0000 | 0.4882 |
| Elastic Difference | 0.4882 | 1.0000 |

**Scatterplot Matrix**

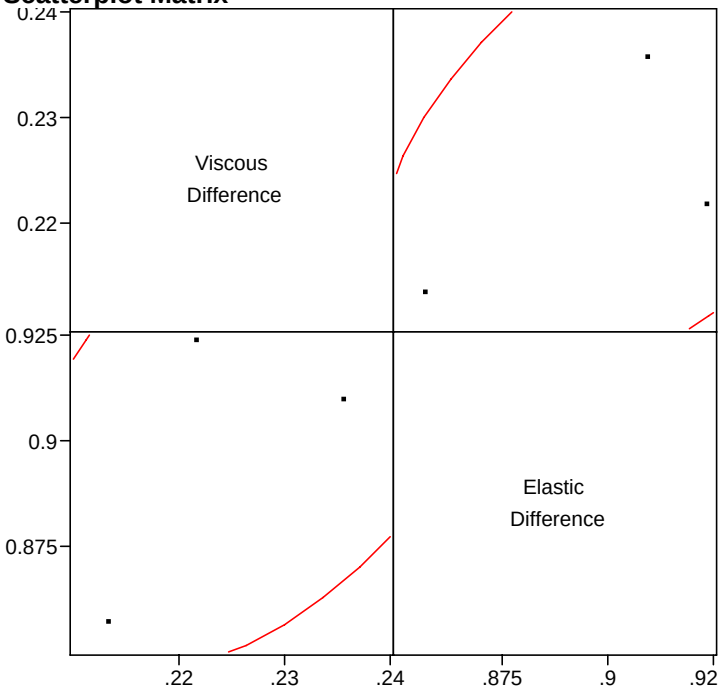


**Multivariate Site=19, Filler (None=0, Silica=1, Hydrated Lime=2)=1, Percent=20**

Freq: Run

**Correlations**

| | Viscous Difference | Elastic Difference |
|---|---|---|
| Viscous Difference | 1.0000 | -0.5050 |
| Elastic Difference | -0.5050 | 1.0000 |

**Scatterplot Matrix**

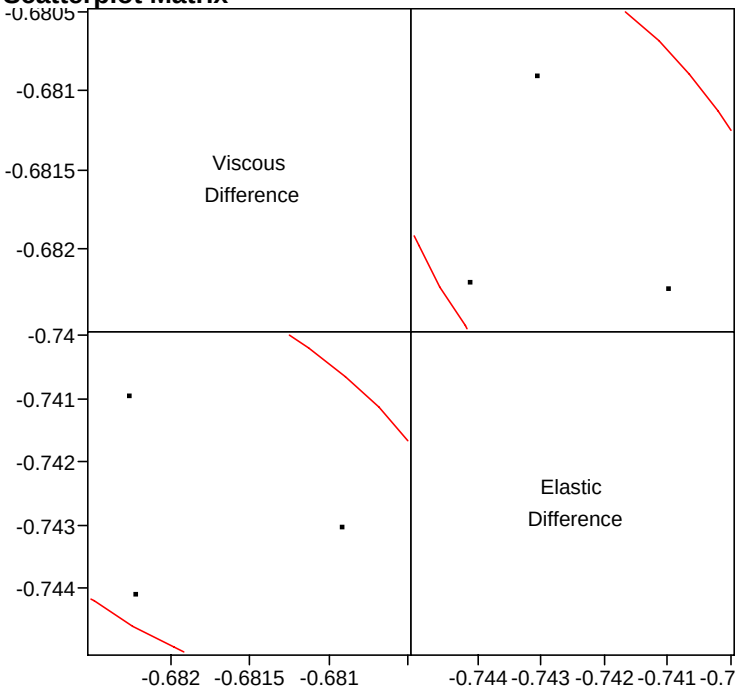


**Multivariate Site=19, Filler (None=0, Silica=1, Hydrated Lime=2)=2, Percent=5**

Freq: Run

**Correlations**

| | Viscous Difference | Elastic Difference |
|---|---|---|
| Viscous Difference | 1.0000 | -0.6673 |
| Elastic Difference | -0.6673 | 1.0000 |

**Scatterplot Matrix**

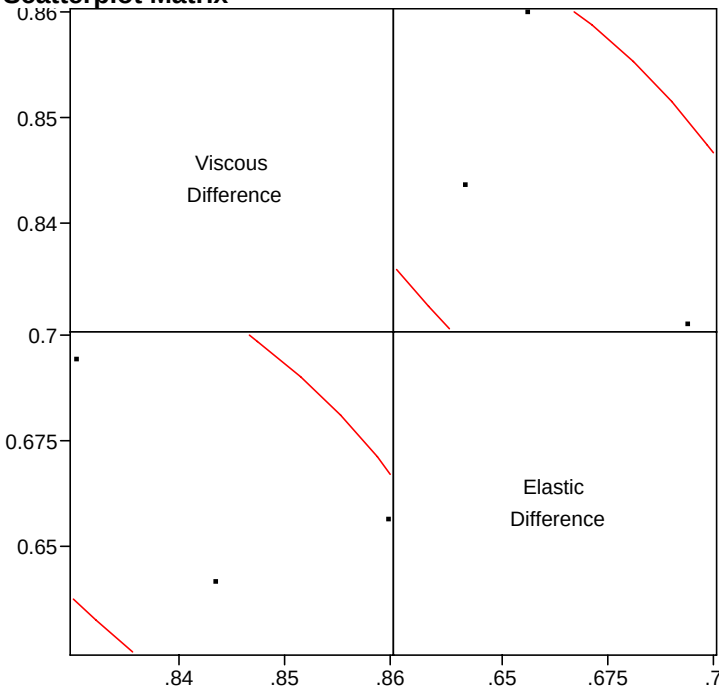


**Multivariate Site=19, Filler (None=0, Silica=1, Hydrated Lime=2)=2, Percent=10**

Freq: Run

**Correlations**

| | Viscous Difference | Elastic Difference |
|---|---|---|
| Viscous Difference | 1.0000 | 1.0000 |
| Elastic Difference | 1.0000 | 1.0000 |

**Scatterplot Matrix**

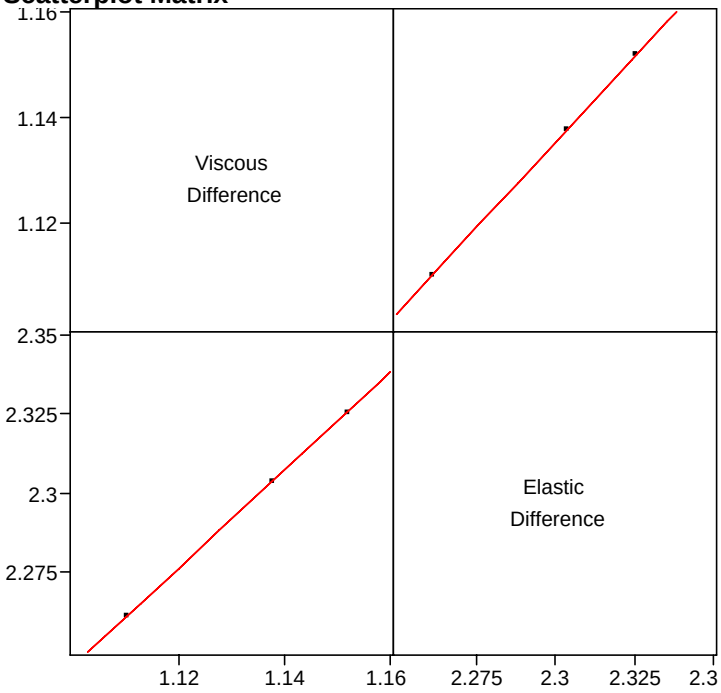


**Multivariate Site=19, Filler (None=0, Silica=1, Hydrated Lime=2)=2, Percent=20**

Freq: Run

**Correlations**

| | Viscous Difference | Elastic Difference |
|---|---|---|
| Viscous Difference | 1.0000 | 0.6375 |
| Elastic Difference | 0.6375 | 1.0000 |

**Scatterplot Matrix**

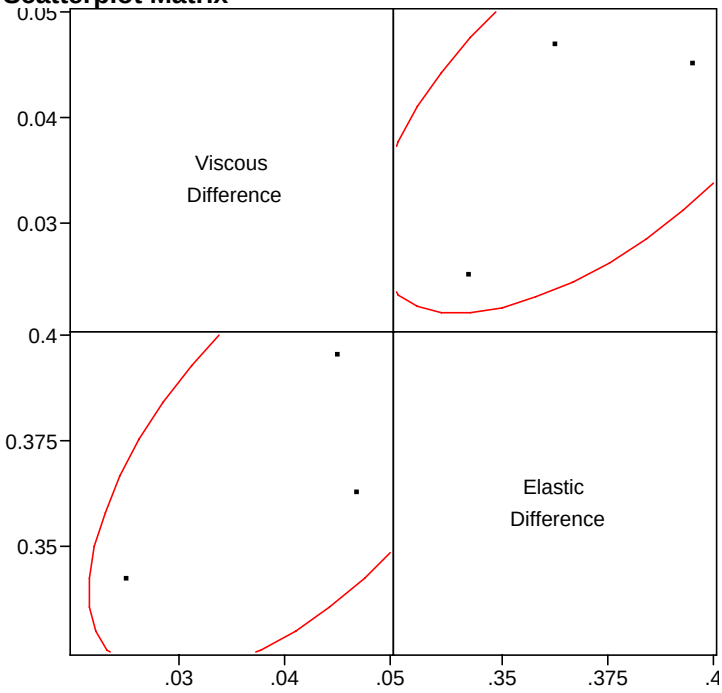


**Multivariate Site=20, Filler (None=0, Silica=1, Hydrated Lime=2)=0, Percent=0**

Freq: Run

**Correlations**

| | Viscous Difference | Elastic Difference |
|---|---|---|
| Viscous Difference | 1.0000 | 0.1032 |
| Elastic Difference | 0.1032 | 1.0000 |

**Scatterplot Matrix**

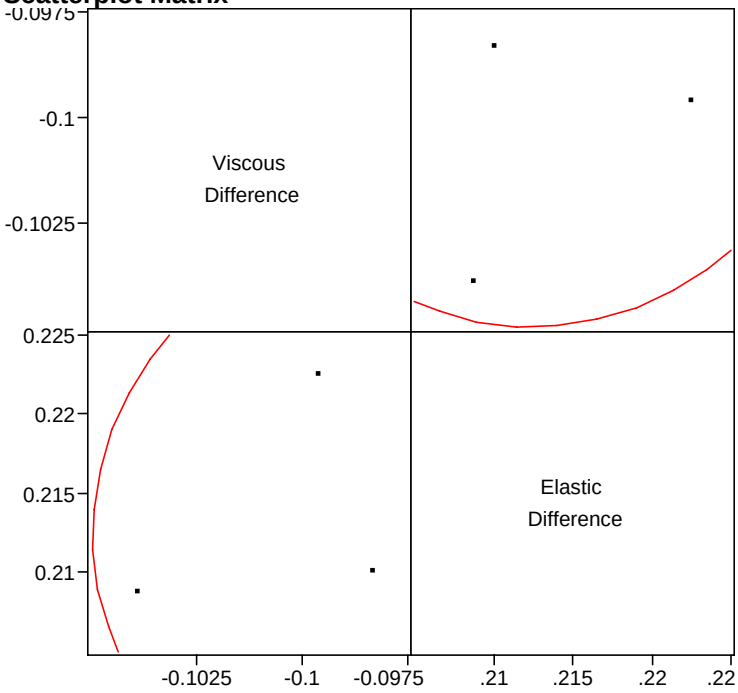


**Multivariate Site=20, Filler (None=0, Silica=1, Hydrated Lime=2)=1, Percent=5**

Freq: Run

**Correlations**

| | Viscous Difference | Elastic Difference |
|---|---|---|
| Viscous Difference | 1.0000 | 0.7445 |
| Elastic Difference | 0.7445 | 1.0000 |

**Scatterplot Matrix**

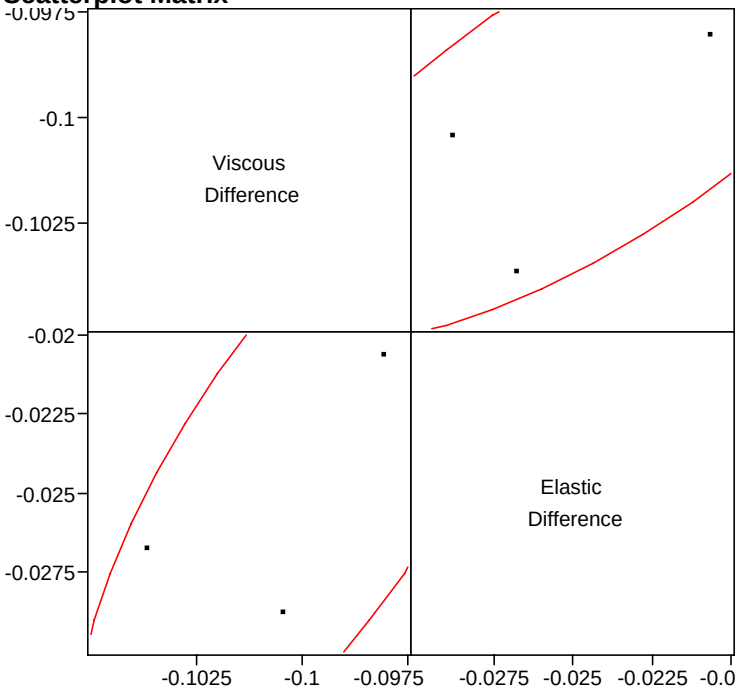


**Multivariate Site=20, Filler (None=0, Silica=1, Hydrated Lime=2)=1, Percent=10**

Freq: Run

**Correlations**

| | Viscous Difference | Elastic Difference |
|---|---|---|
| Viscous Difference | 1.0000 | 0.9347 |
| Elastic Difference | 0.9347 | 1.0000 |

**Scatterplot Matrix**

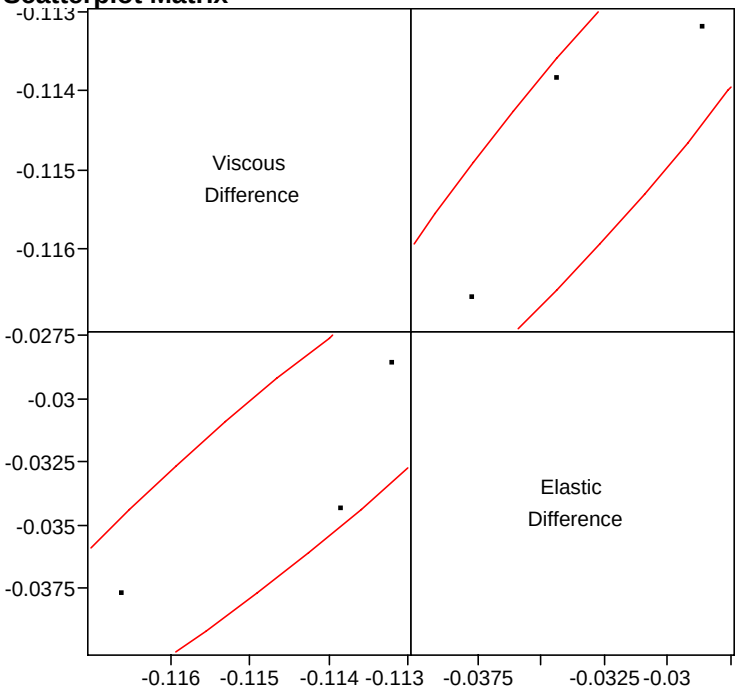


**Multivariate Site=20, Filler (None=0, Silica=1, Hydrated Lime=2)=1, Percent=20**

Freq: Run

**Correlations**

| | Viscous Difference | Elastic Difference |
|---|---|---|
| Viscous Difference | 1.0000 | 0.9557 |
| Elastic Difference | 0.9557 | 1.0000 |

**Scatterplot Matrix**

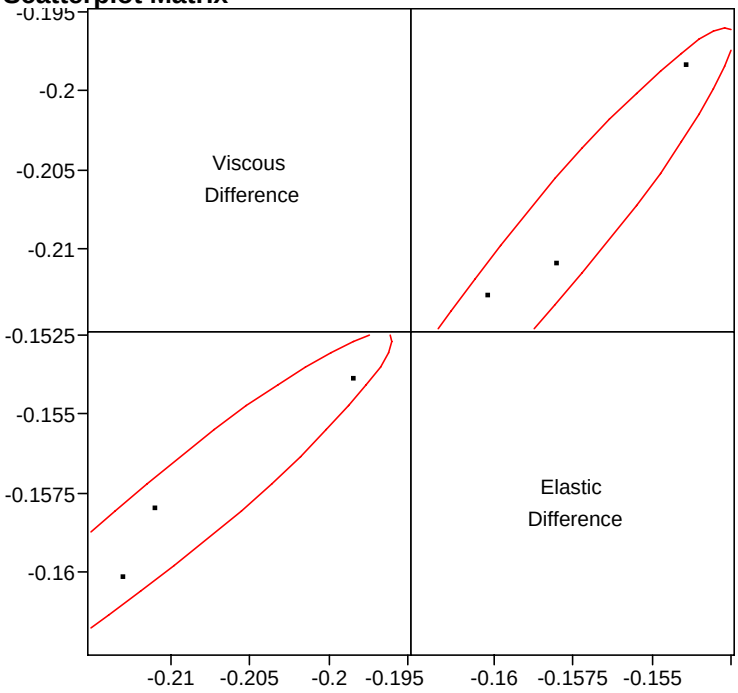


**Multivariate Site=20, Filler (None=0, Silica=1, Hydrated Lime=2)=2, Percent=5**

Freq: Run

**Correlations**

| | Viscous Difference | Elastic Difference |
|---|---|---|
| Viscous Difference | 1.0000 | 0.9851 |
| Elastic Difference | 0.9851 | 1.0000 |

**Scatterplot Matrix**

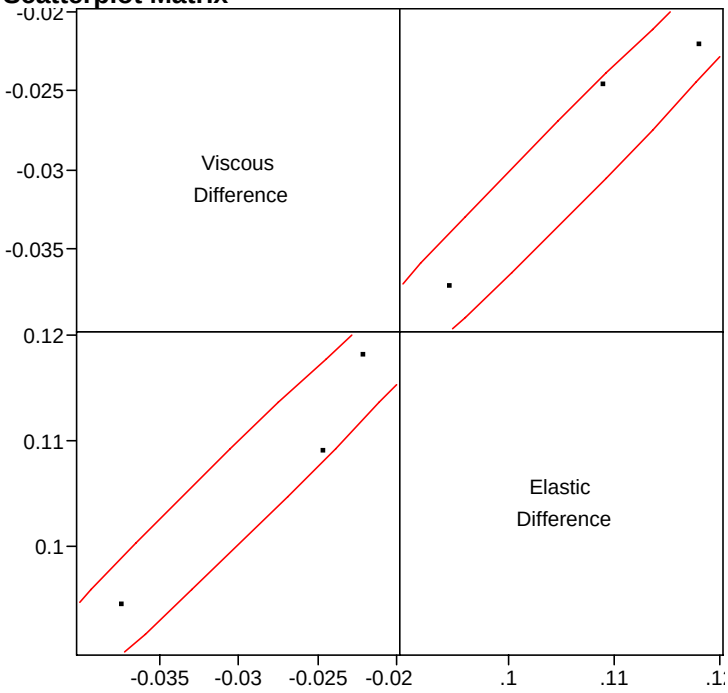


**Multivariate Site=20, Filler (None=0, Silica=1, Hydrated Lime=2)=2, Percent=10**

Freq: Run

**Correlations**

| | Viscous Difference | Elastic Difference |
|---|---|---|
| Viscous Difference | 1.0000 | 0.9997 |
| Elastic Difference | 0.9997 | 1.0000 |

**Scatterplot Matrix**

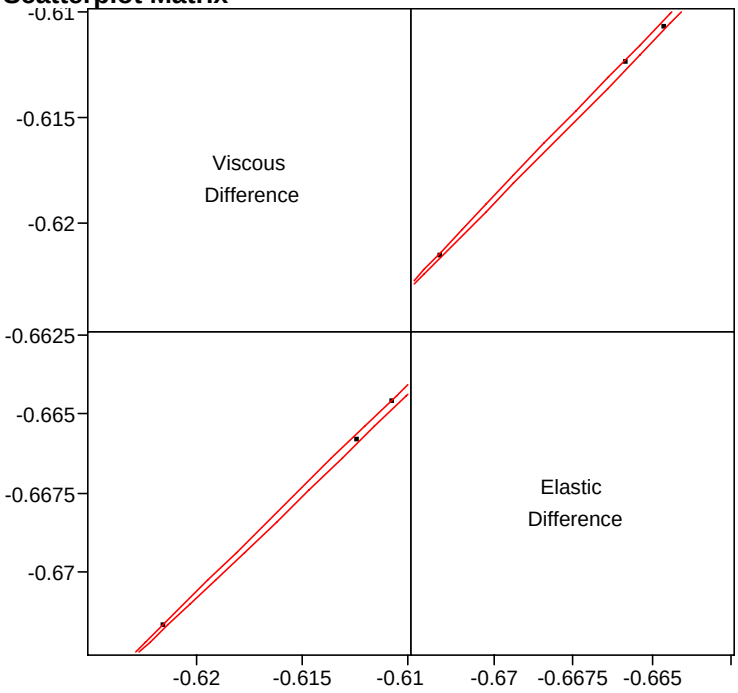


**Multivariate Site=20, Filler (None=0, Silica=1, Hydrated Lime=2)=2, Percent=20**

Freq: Run

**Correlations**

| | Viscous Difference | Elastic Difference |
|---|---|---|
| Viscous Difference | 1.0000 | -0.1676 |
| Elastic Difference | -0.1676 | 1.0000 |

**Scatterplot Matrix**

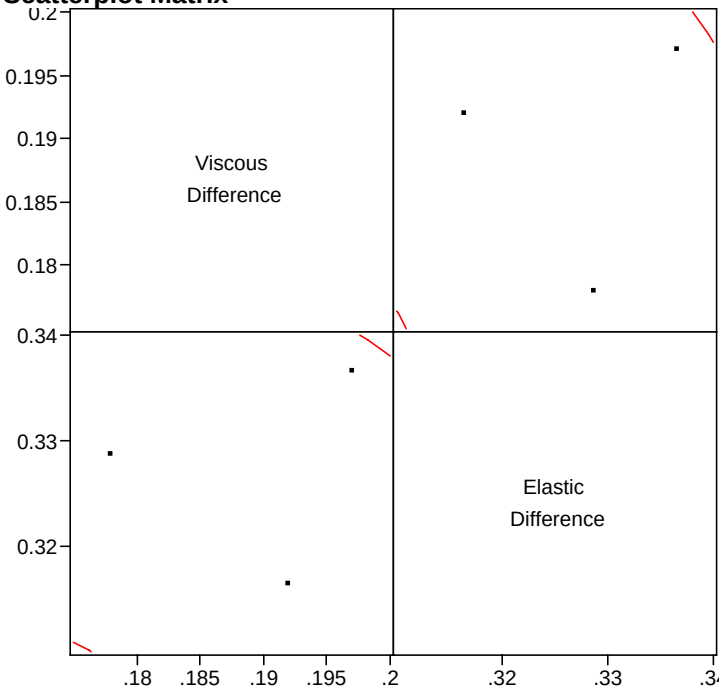


**Multivariate Site=21, Filler (None=0, Silica=1, Hydrated Lime=2)=0, Percent=0**

Freq: Run

**Correlations**

| | Viscous Difference | Elastic Difference |
|---|---|---|
| Viscous Difference | 1.0000 | -0.4549 |
| Elastic Difference | -0.4549 | 1.0000 |

**Scatterplot Matrix**

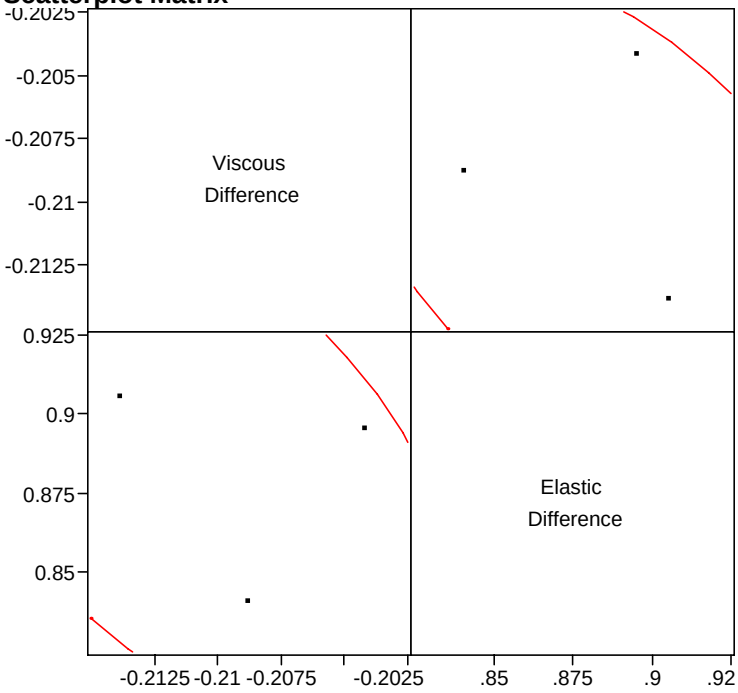


**Multivariate Site=21, Filler (None=0, Silica=1, Hydrated Lime=2)=1, Percent=5**

Freq: Run

**Correlations**

| | Viscous Difference | Elastic Difference |
|---|---|---|
| Viscous Difference | 1.0000 | 0.9885 |
| Elastic Difference | 0.9885 | 1.0000 |

**Scatterplot Matrix**

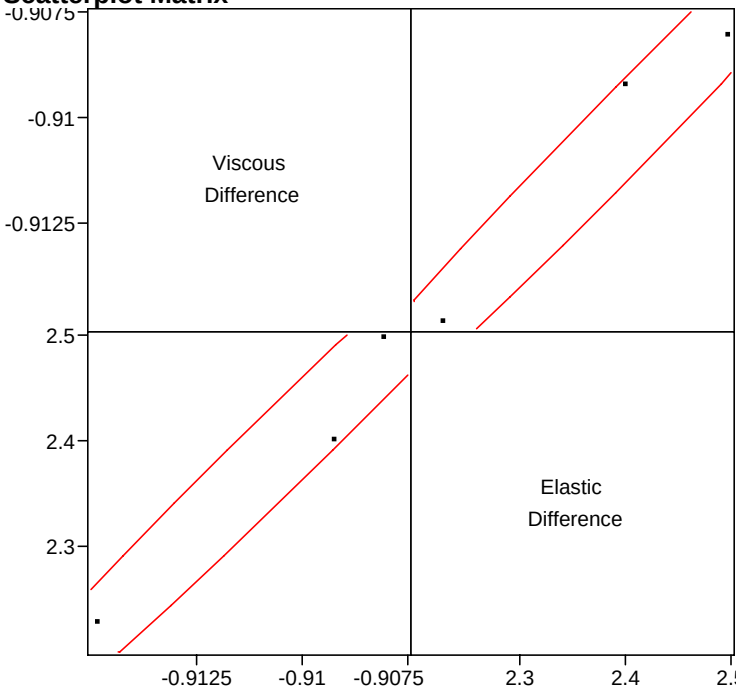


**Multivariate Site=21, Filler (None=0, Silica=1, Hydrated Lime=2)=1, Percent=10**

Freq: Run

**Correlations**

| | Viscous Difference | Elastic Difference |
|---|---|---|
| Viscous Difference | 1.0000 | 0.9700 |
| Elastic Difference | 0.9700 | 1.0000 |

**Scatterplot Matrix**

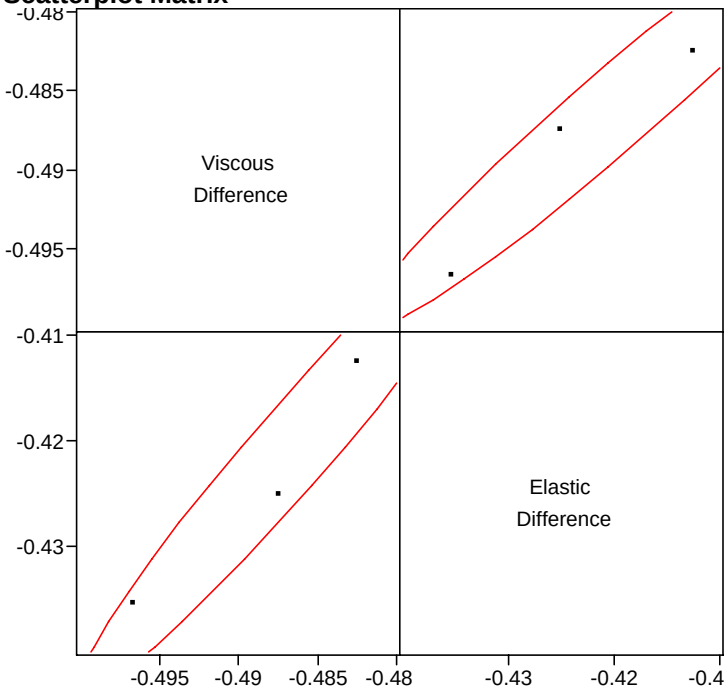


**Multivariate Site=21, Filler (None=0, Silica=1, Hydrated Lime=2)=1, Percent=20**

Freq: Run

**Correlations**

| | Viscous Difference | Elastic Difference |
|---|---|---|
| Viscous Difference | 1.0000 | 0.9845 |
| Elastic Difference | 0.9845 | 1.0000 |

**Scatterplot Matrix**

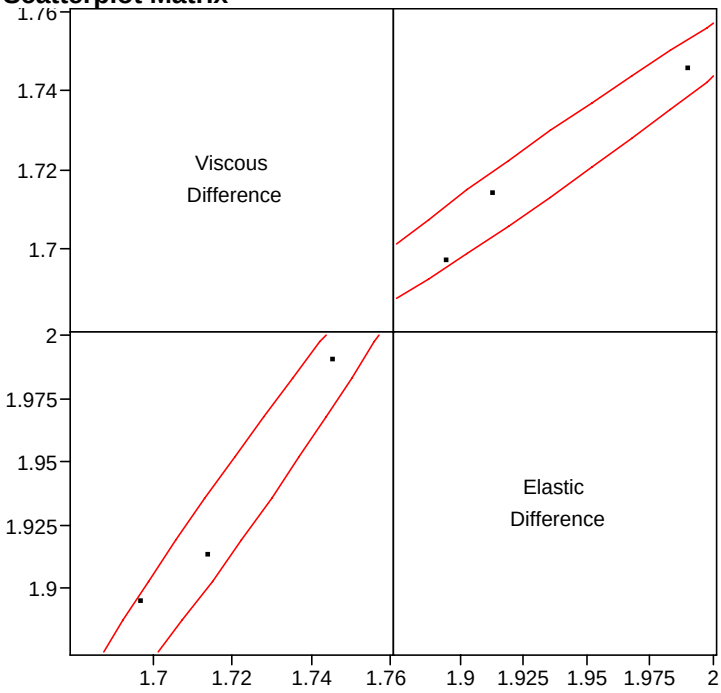


**Multivariate Site=21, Filler (None=0, Silica=1, Hydrated Lime=2)=2, Percent=5**

Freq: Run

**Correlations**

| | Viscous Difference | Elastic Difference |
|---|---|---|
| Viscous Difference | 1.0000 | 1.0000 |
| Elastic Difference | 1.0000 | 1.0000 |

**Scatterplot Matrix**

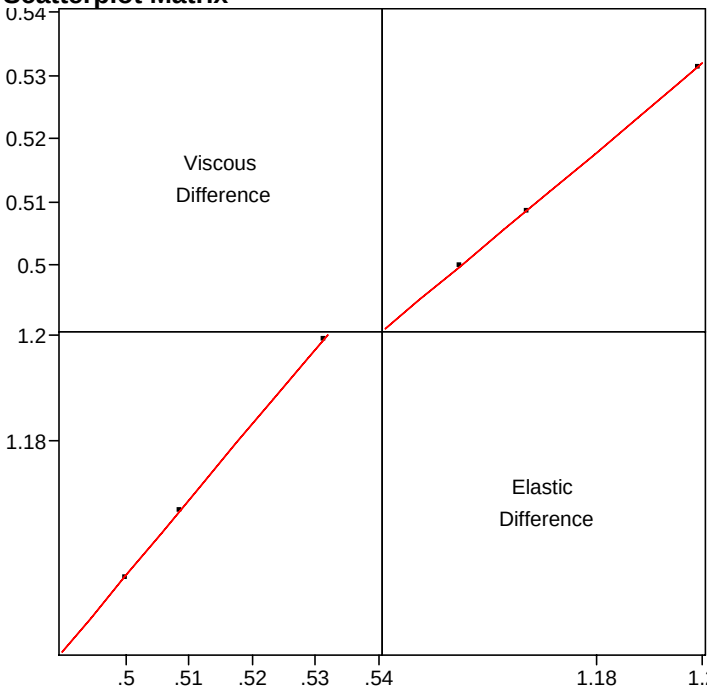


**Multivariate Site=21, Filler (None=0, Silica=1, Hydrated Lime=2)=2, Percent=10**

Freq: Run

**Correlations**

| | Viscous Difference | Elastic Difference |
|---|---|---|
| Viscous Difference | 1.0000 | -0.9862 |
| Elastic Difference | -0.9862 | 1.0000 |

**Scatterplot Matrix**

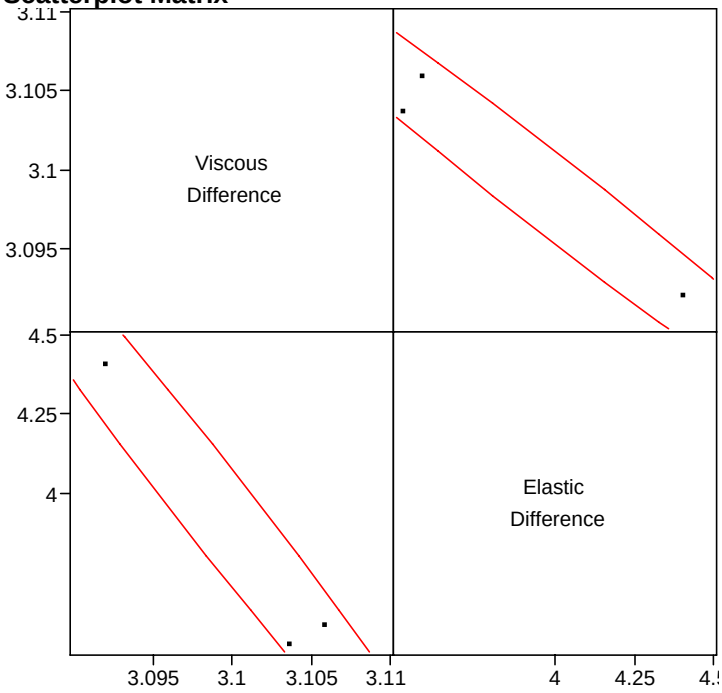


**Multivariate Site=21, Filler (None=0, Silica=1, Hydrated Lime=2)=2, Percent=20**

Freq: Run

**Correlations**

| | Viscous Difference | Elastic Difference |
|---|---|---|
| Viscous Difference | 1.0000 | 0.9982 |
| Elastic Difference | 0.9982 | 1.0000 |